Spring 1-1-2016

Carbon Dynamics of the Deglacial and Contemporary Ocean Inferred from Radiocarbon Measurements in Foraminifera, Seawater and Atmospheric Carbon Dioxide

Colin Metz Lindsay
University of Colorado at Boulder, Colin.Lindsay@colorado.edu

CARBON DYNAMICS OF THE DEGLACIAL AND CONTEMPORARY OCEAN INFERRED FROM RADIOCARBON MEASUREMENTS IN FORAMINIFERA, SEAWATER AND ATMOSPHERIC CARBON DIOXIDE

by

COLIN METZ LINDSAY

B.A., Amherst College, 2007

A thesis submitted to the
Faculty of the Graduate School of the
University of Colorado in partial fulfillment
of the requirement for the degree of
Doctor of Philosophy
Department of Geological Sciences
2016

This thesis entitled:
Carbon Dynamics of the Deglacial and Contemporary Ocean Inferred from Radiocarbon Measurements in Foraminifera, Seawater and Atmospheric Carbon Dioxide
written by Colin Metz Lindsay
has been approved for the Department of Geological Sciences

_____
Dr. Scott J. Lehman

_____
Dr. Thomas M. Marchitto

Date_____

The final copy of this thesis has been examined by the signatories, and we find that both the content and the form meet acceptable presentation standards of scholarly work in the above mentioned discipline.

Lindsay, Colin Metz (Ph.D., Geological Sciences)

Carbon Dynamics of the Deglacial and Contemporary Ocean Inferred from Radiocarbon Measurements in Foraminifera, Seawater and Atmospheric Carbon Dioxide

Thesis directed by Dr. Scott J. Lehman and Dr. Thomas M. Marchitto

Late Pleistocene atmospheric CO_2 concentrations varied by ~90 ppm, rising with Antarctic and global temperatures during deglaciations. These natural variations were smaller and slower than the present CO_2 increase, caused by anthropogenic emissions, which is driving the current transition to the warm Anthropocene. Because the ocean is the largest carbon reservoir that exchanges readily with the atmosphere, most explanations of the glacial-interglacial variations and predictions of future CO_2 concentrations involve mechanisms that mediate that exchange. A critical region for such exchange is the Southern Ocean (SO), where carbon-rich deep water is upwelled to the surface by westerly winds that may be responsive to past and present warming. In this dissertation, I use radiocarbon (^{14}C) measurements as a tracer to investigate the ocean's role in controlling atmospheric CO_2 during the last deglaciation and the past two decades.

Previously documented intervals of anomalously low ^{14}C activity ($\Delta^{14}C$) in the deglacial (18-11 ka BP) mid-depth ocean coincide with rising CO_2 and decreasing $\Delta^{14}C$ in the atmosphere, possibly tracing the re-emergence of aged carbon sequestered in the deep ocean during the preceding glacial period. I combined new ^{14}C measurements in foraminifera from marine sediment cores near Baja California with published data to reconstruct regional gradients of $\Delta^{14}C$ during deglaciation. The results appear to constrain the source of aged carbon to the SO, via the Equatorial Pacific. I also present new ^{14}C measurements in air sampled since 2006 from Drake

Passage in the SO. Transiently high CO_2 concentrations correlate with low $\Delta^{14}C$ and dominant modes of atmospheric variability, suggesting that increases in wind-driven upwelling drive more deep ocean carbon into the atmosphere, temporarily reducing the local net ocean carbon sink. Finally, I estimate rates of surface ocean $\Delta^{14}C$ change since the 1990s using published datasets. The results imply that anthropogenic carbon, previously absorbed at high southern latitudes, is now re-emerging in the low latitude ocean. In summary, evidence presented in this dissertation suggests that SO upwelling, during both deglacial and contemporary periods of global warming, can act as a positive feedback in the coupled climate-carbon system by shifting deep ocean carbon into the atmosphere.

Acknowledgements

I thank my advisors Scott Lehman and Tom Marchitto for their confidence in me, and for their teaching, encouragement, and help. I have also benefitted from the lectures, thoughtful questions and suggestions, and shared computer code of my committee members John Miller, Nicole Lovenduski and Jim White. Patrick Kappa, Chad Wolak and Stephen Morgan trained and helped me in the ^{14}C lab while also providing hours of conversation and Spotify playlists, and Derek Weller and Peter Rody assisted me by picking foraminifera. John Southon at UC Irvine provided all the new ^{14}C measurements presented in this thesis. Lex Van Geen at Columbia University provided all the core samples used in Chapters II and III, Jose Carriquiry at the Autonomous University of Baja California allowed me to use the stable oxygen isotope measurements from core PC08 in Chapter III, Joe Ortiz provided DSR measurements, and all provided thoughtful comments. Jess Adkins shared Matlab code used in Chapter II. Ann McNichol and Robert Key helped me compile the recent ocean $\Delta^{14}C$ data used in Chapter V, and the framing of Chapter V was inspired by an unpublished talk by Keith Rodgers. I am grateful to Baylor Fox-Kemper for his patience teaching Matlab to the first-year geology grad students in his physical oceanography course, and to Anne Jennings for advice on identifying and picking foraminifera.

Funding from a National Science Foundation grant to Drs. Lehman and Marchitto supported this work, as well as a Graduate Research Grant from the Geological Society of America.

I feel very lucky to have been a part of the INSTAAR community. My cohort of graduate students have been impressive, generous and fun companions, and I owe especial

thanks to Whitney Doss, Andy Wickert, Emily Zakem, Hannah Grist, Katy Barnhart, Ursula Quillman, Katie Hayo, Kate Zalzal and Phil Taylor for their help and good company. I also am grateful to Sylvia Michel, Bruce Vaughn and the rest of the Stable Isotope Lab for their friendship and open kitchen policy.

Thank you to my family, who have always supported me in my various endeavors; to Kim Hedberg, the den mother of Amherst Alumni in Boulder; and to my former housemates Adam Kaufman, Matt Seaberg, Will Kindel and Joe Britton for helping me stay sheltered, fed, and occasionally not at a computer. Thanks also to my friends at the Boulder Irish Session for their warm welcome and many hours of musical companionship, and to Peter and Laura Terpenning for sharing their home and garden with me during my last few months in Boulder.

Even with all this assistance and support, I could not have completed this thesis without the love, patience and enthusiasm of my wife Becky, who tolerated the distance and delays while tackling her own studies in New York.

Table of Contents

List of Tables

List of Figures

Chapter 1: Introduction

The ocean is by far the largest of Earth's readily-exchanging carbon reservoirs and therefore changes in ocean physics, biology and chemistry underlie most attempts to explain the large natural variations in atmospheric carbon dioxide (CO_2) between late Pleistocene glacial and interglacial periods and to predict the rate and magnitude of future CO_2 rise associated with anthropogenic emissions from combustion of fossil fuels and land use change. This dissertation uses precise radiocarbon (^{14}C) measurements in marine sediments and in contemporary seawater and atmospheric CO_2 as a geophysical and geochemical tracer to advance our understanding of the ocean's role in controlling atmospheric CO_2 concentration on two different time scales: the 10^3-10^4 yr transition to a more CO_2-rich and warmer atmosphere during the last deglaciation (~24-10 ka BP) and the 10^1-10^2 year transition marking the recent onset of the rapidly warming Anthropocene. Although the time scales are very different, results presented in this work strengthen the view that the Southern Ocean, in particular, may have played (and is playing) a similar role in the global climate-carbon system during both transitions, one of which is still very much underway.

Because of its chemical properties, the partitioning of carbon between different global reservoirs has significant consequences. In air, CO_2 is a well-known greenhouse gas that warms the atmosphere, and when dissolved in seawater it reduces the buffering capacity of the ocean (a measure of how much carbon can be stored for a given increase in the partial pressure of CO_2) and harms calcifying organisms by lowering pH and carbonate ion concentrations. Over the last few hundred years, CO_2 emissions from industrial activities have increased atmospheric CO_2 concentrations to levels higher than at any time in the past 800,000 years, and this transfer of carbon from terrestrial and fossil fuel reservoirs into the atmosphere is expected to cause

significant changes to global climate and ocean chemistry that will persist for thousands of years [*IPCC*, 2013].

Measurements on air trapped in Antarctic ice cores have revealed that CO_2 concentrations in the ancient atmosphere varied by ~90ppm in ~100 kyr cycles over the last 800 kyrs, with lower CO_2 during cold glacial periods and rapidly increasing concentrations during deglacial warming [*Petit et al.*, 1999; *Monnin et al.*, 2001]. Because the atmospheric carbon inventory exchanges quickly with the ocean, the concentration of atmospheric CO_2 on millennial timescales is set by the partial pressure of CO_2 in the surface ocean [*Broecker*, 1982]. Surface pCO_2 is, in turn, controlled by a balance between biological processes and physical circulation that maintains a concentration gradient between the surface ocean and the carbon-rich deep ocean: CO_2 is removed from the atmosphere by photosynthesis in the warm, sunlit surface ocean and is regenerated in deep waters, which eventually return to the surface via upwelling. Most exchange between the deep ocean and the surface occurs in low-temperature outcrop regions at high latitudes, particularly in the Southern Ocean where strong wind-driven upwelling exposes the densest ocean waters, and consequently the concentration of CO_2 in the atmosphere and shallow ocean is sensitive to changing conditions at high latitudes [*Knox and Mcelroy*, 1984; *Sarmiento and Toggweiler*, 1984; *Siegenthaler and Wenk*, 1984].

Following this logic, most attempts to explain the glacial-interglacial atmospheric CO_2 cycles involve mechanisms operating at high latitudes that can trap more carbon in the deep ocean, either through physical barriers to high-latitude air-sea gas exchange such as sea ice at the surface [*Stephens and Keeling*, 2000] or by varying the upward wind-driven flux of carbon and nutrients [*Francois et al.*, 1997; *Toggweiler*, 1999] or the proportion of upwelled carbon that is returned to the deep ocean by biological productivity [*Martin*, 1990; *Francois et al.*, 1997;

Martínez-Garcia et al., 2011]. Others have invoked combinations of all three of these mechanisms [e.g. *Sigman and Boyle*, 2000]. These theories focus on the Southern Ocean, in accordance with observed correlations between Southern Ocean climate and productivity proxies and atmospheric CO_2 concentrations (Figure 1.1).

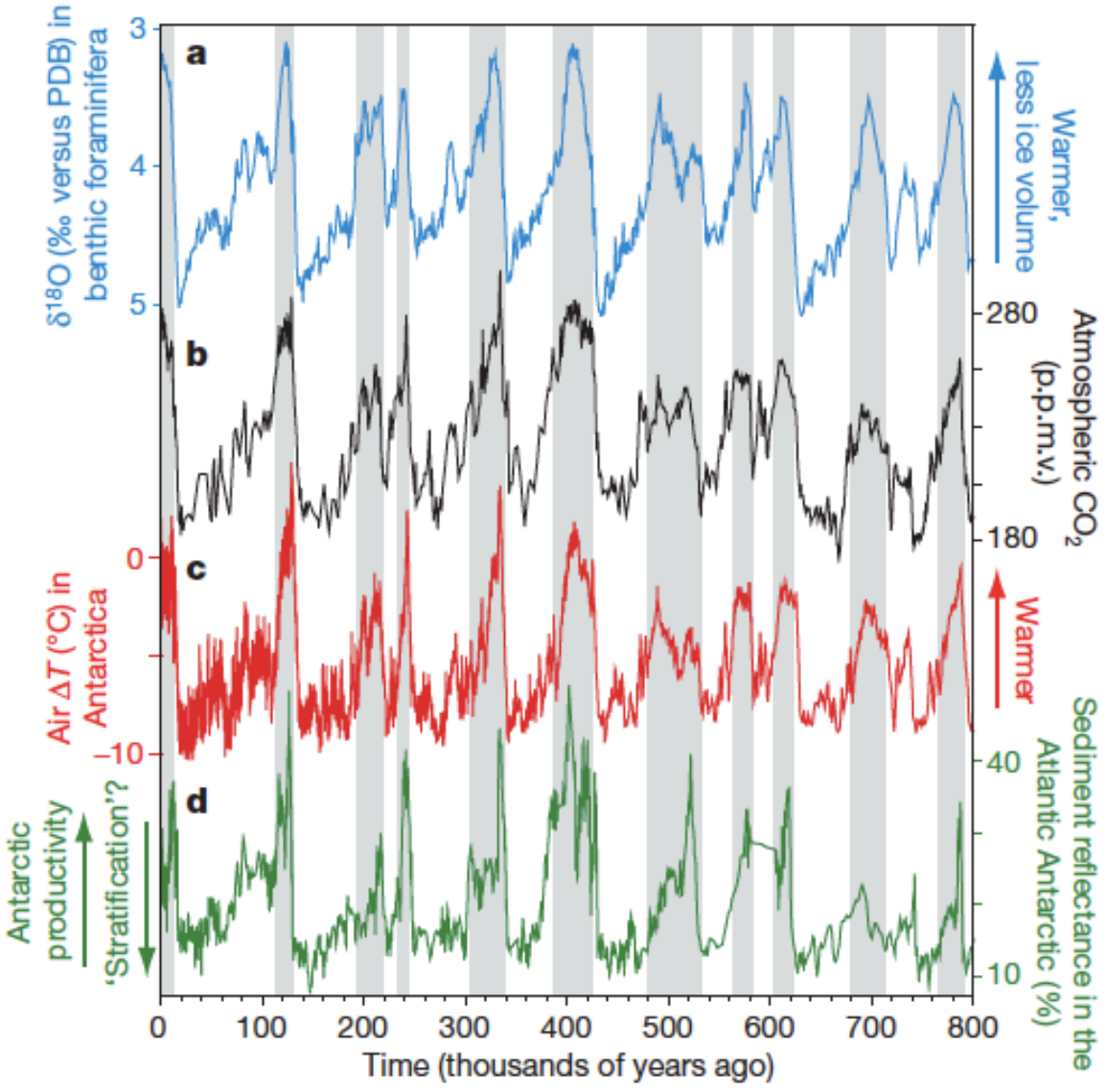

Figure 1.1: Times series of a measure of global ice volume (blue line), atmospheric CO_2 concentrations (black line), Antarctic temperature (red line), and surface ocean productivity in the Southern Ocean (green line) over the last 800 kyrs. Figure from Sigman *et al.* [2010].

1. Ocean Climate-Carbon Cycle Feedback

The net meridional flows of carbon within the ocean and atmosphere may be represented in a schematic section (Figure 1.2, after Toggweiler *et al.* [2006]) as two overturning cells, a "southern" (blue) loop which surfaces in the Southern Ocean and fills most of the deepest ocean, and a "northern" (red) loop which encompasses most of the shallow ocean and fills the mid-depths via sinking in the North Atlantic. The sinking flux of organic matter (brown arrows) removes carbon from the surface of the red loop to the deep parts of both loops, where it is temporarily isolated from the atmosphere and transferred southwards towards upwelling in the Southern Ocean. Regenerated carbon that is upwelled within the red loop is soon re-sequestered by efficient biological activity, but shorter residence times at the surface and an inadequate supply of micronutrients allow upwelled, regenerated CO_2 in the blue loop to escape to the atmosphere [*Siegenthaler and Wenk*, 1984; *Martin*, 1990; *Toggweiler et al.*, 2006]. In the unperturbed preindustrial case, the CO_2 escaping from the Southern Ocean was mixed between hemispheres in the atmosphere, causing a net carbon transport from south to north (cyan arrow in Figure 1.2A) that compensated for the north-to-south transport in the deep ocean. In the present case, CO_2 emissions from fossil fuel burning occur predominately in the northern hemisphere, and the resulting concentration gradients cause a net transfer of carbon north-to-south in the atmosphere. CO_2 is driven into the ocean in both hemispheres (represented by the downward-pointing magenta arrows in both hemispheres in Figure 1.2B), as the partial pressure of the atmosphere now generally exceeds the partial pressure of the surface ocean even in regions influenced by upwelling.

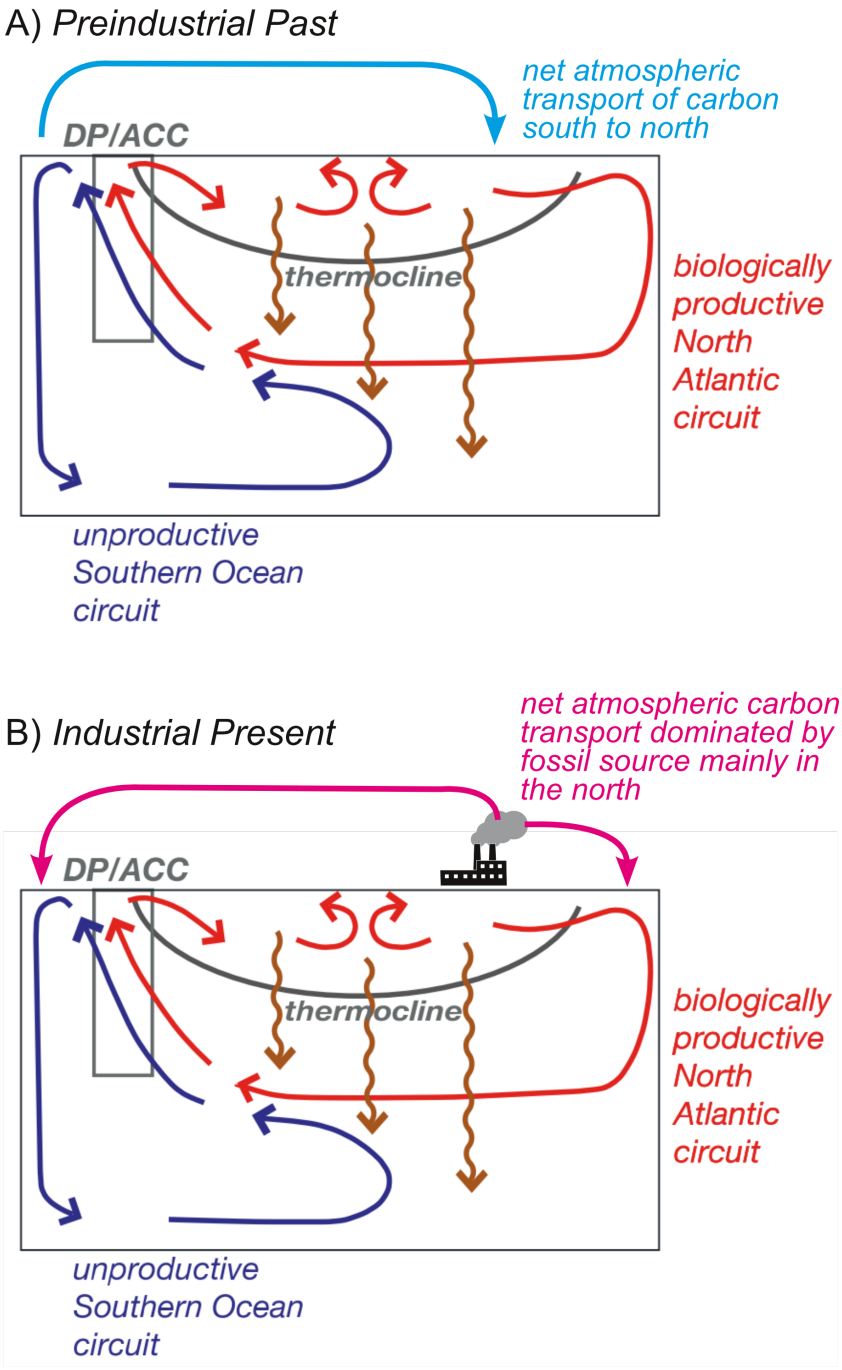

Figure 1.2: Schematic view of net meridional carbon transport in the ocean and atmosphere during A) the preindustrial past and B) the industrial present. Carbon dissolved in northern (red) and southern-sourced (blue) deep waters upwells into the Southern Ocean near the latitudes of Drake Passage and the Antarctic Circumpolar Current (indicated by the box labeled DP/ACC). Sinking organic carbon (brown arrows) moves carbon to the ocean interior. Net preindustrial interhemispheric carbon transport in the atmosphere was south to north (cyan arrow), but is reversed (north to south) in the industrial present (magenta arrows). Figure modified from Toggweiler *et al.* [2006]).

Although many details remain to be fleshed out, it is very likely that during late-Pleistocene glacial periods, some combination of weaker wind-driven upwelling, expanded sea ice and strengthened stratification in the Southern Ocean stemmed the escaping flux of carbon from the blue loop, trapping more carbon in the deep ocean. Warming during deglaciation likely reversed these mechanisms, releasing carbon back into the atmosphere and amplifying the warming [*Toggweiler et al.*, 2006].

A similar feedback may also react to contemporary anthropogenic warming by strengthening the westerly winds over the Southern Ocean and shifting them poleward [*Thompson and Solomon*, 2002; *Arblaster and Meehl*, 2006], causing more deep ocean carbon to be upwelled to the surface. The increased supply of carbon could raise surface ocean pCO_2, decreasing the net uptake of CO_2 from the atmosphere. Studies of atmospheric CO_2 concentrations over the Southern Ocean [*Butler et al.*, 2007; *Le Quéré et al.*, 2007] and hindcast ocean circulation models [*Le Quéré et al.*, 2007; *Lovenduski et al.*, 2007] suggest that in recent decades, periods with stronger westerly winds tended to have a relatively weaker Southern Ocean net carbon sink, consistent with this suspected mechanism, but evidence from surface pCO_2 observations is less clear [*Metzl*, 2009; *Takahashi et al.*, 2009; *Lenton et al.*, 2013; *Landschützer et al.*, 2015; *Munro et al.*, 2015].

2. Radiocarbon as a Carbon Cycle Tracer

Radiocarbon (^{14}C) is an excellent tracer of the hypothesized changes in Southern Ocean upwelling common to both the deglacial and contemporary scenarios. ^{14}C is a radioactive isotope of carbon that is naturally produced by cosmic rays interacting with nitrogen in the upper atmosphere. It is quickly oxidized to $^{14}CO_2$ and enters the global carbon cycle, decaying with a

half-life of 5700 years [*Godwin*, 1962; National Nuclear Data Center, Brookhaven National Laboratory, www.nndc.bnl.gov]. The prevalence of ^{14}C in a carbon sample is expressed as $\Delta^{14}C$, which is the ^{14}C:^{12}C ratio relative to a standard ratio, in units of per mil [*Stuiver and Polach*, 1977]. As described previously, dissolved inorganic carbon (DIC) accumulates in the deep ocean, while ^{14}C is lost quantitatively to decay, both as a function of residence time in the ocean interior. Thus high DIC concentrations in the deep ocean are accompanied by low $\Delta^{14}C$, and the return of deep water to the surface via upwelling in the Southern Ocean results in low surface $\Delta^{14}C$ and high DIC concentrations [Figure 1.3; *Key*, 2004]. Air-sea gas exchange at the surface reintroduces aged, low-$\Delta^{14}C$ CO_2 to the atmosphere, and high-$\Delta^{14}C$ CO_2 dissolves into the upwelled surface water. Exchange between aqueous CO_2 and the other chemical species of the DIC pool slowly restores the $\Delta^{14}C$ of surface water towards that of the atmosphere, with a characteristic equilibration timescale of about 10 years [*Ito*, 2004]. Deep water that is upwelled in the Southern Ocean is re-submerged well before its DIC pool reaches isotopic equilibrium with the atmosphere, and the remaining low-$\Delta^{14}C$ signature persists in Southern Ocean mode and intermediate waters that reach the low-latitude shallow ocean [*Toggweiler and Dixon*, 1991].

In the modern industrial era, atmospheric $\Delta^{14}C$ increased sharply in the 1950s and 1960s due to above-ground nuclear weapons testing [*Rafter and Fergusson*, 1957; *Levin et al.*, 1985]. This "bomb spike," and the ensuing rapid decline as excess ^{14}C was assimilated into the surface ocean and terrestrial biosphere, was superimposed on a negative secular trend caused by the addition of ^{14}C-free CO_2 from fossil fuel burning [*Revelle and Suess*, 1957]. Measurements of $\Delta^{14}C$ in the shallow and mid-depth ocean taken in the 1990s and 2000s reflect this recent atmospheric history, as convolved with the ventilation age distribution of the water and the preexisting natural gradients [*Jenkins et al.*, 2010; *Graven et al.*, 2012].

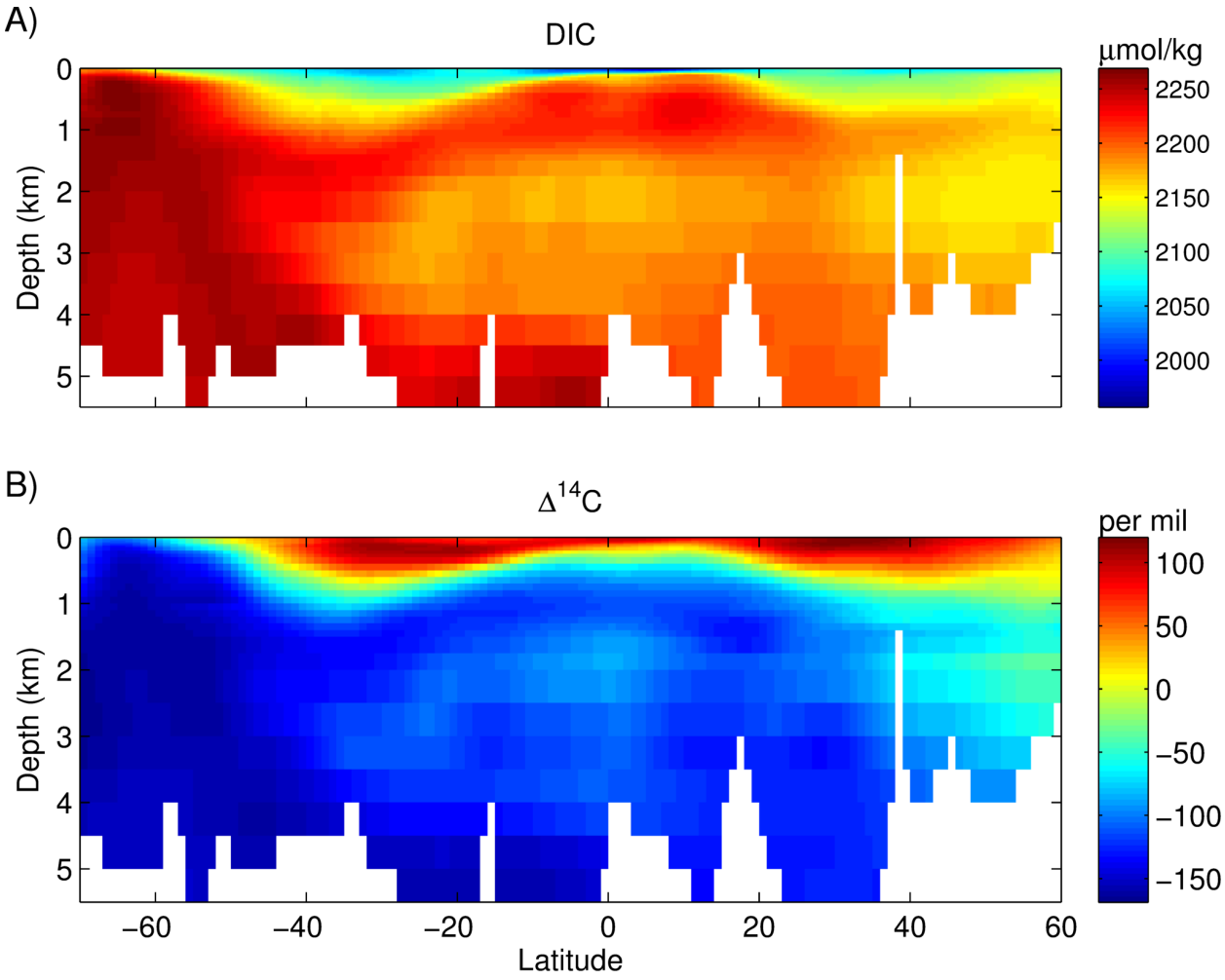

Figure 1.3: Meridional transects of A) DIC and B) $\Delta^{14}C$ in the Atlantic and Southern Oceans illustrate the association of low-$\Delta^{14}C$ with high DIC concentrations in deep water that upwells in the Southern Ocean. Data is from the GLODAP gridded climatology, which is based on ocean measurements made mostly in the 1990s [*Key*, 2004].

Any hypotheses calling for a weakening of Southern Ocean overturning or an otherwise isolated carbon pool in the deep ocean to explain low glacial atmospheric CO_2 concentrations necessarily require a decline in $\Delta^{14}C$ of the deep ocean relative to that of the atmosphere. The return of this aged carbon to the upper ocean and atmosphere during deglaciation should in turn have lowered $\Delta^{14}C$ in the surface ocean and atmosphere [*Broecker and Barker*, 2007; *Marchitto et al.*, 2007] and caused a transient pulse of low-$\Delta^{14}C$ carbon that propagated from the Southern Ocean surface into the mid-depth ocean via mode and intermediate water. Reconstructions of

$\Delta^{14}C$ in the deep ocean [*Sikes et al.*, 2000; *Skinner et al.*, 2010, 2014; *Burke and Robinson*, 2012; *de la Fuente et al.*, 2015; *Keigwin and Lehman*, 2015; *Tiedemann et al.*, 2015] and atmosphere [*Reimer et al.*, 2013] are roughly consistent with these predictions, but puzzling contradictions remain, particularly among $\Delta^{14}C$ reconstructions from intermediate and mode waters [*Marchitto et al.*, 2007; *Stott et al.*, 2009; *Bryan et al.*, 2010; *De Pol-Holz et al.*, 2010; *Rose et al.*, 2010; *Cléroux et al.*, 2011; *Sortor and Lund*, 2011; *Burke and Robinson*, 2012; *Siani et al.*, 2013].

The net carbon flux between the ocean and the atmosphere is the sum of two gross fluxes of CO_2 that are each proportional to the pCO_2 of the giving reservoir, and thus the net transfer can be said to be driven by the air-sea pCO_2 gradient. The potential for such two-way exchange to change the $\Delta^{14}C$ of the overlying atmosphere is driven by the isotopic disequilibrium between the two carbon reservoirs, weighted by the size of the one-way gross flux out of the ocean. This product is referred to as an isoflux.

In the contemporary Southern Ocean, short-term changes in wind-driven upwelling that influence surface ocean pCO_2 should also change surface ocean $\Delta^{14}C$. If, as hypothesized, greater upwelling releases more deep ocean carbon to the atmosphere and decreases the net carbon sink, this should also lower surface ocean $\Delta^{14}C$ (increasing the isotopic disequilibrium with the atmosphere) and raise surface pCO_2 (increasing the gross sea-air CO_2 flux and decreasing the pCO_2 gradient), causing a more negative isoflux and a smaller net carbon sink. These changes should be observable in local air as transiently lower $\Delta^{14}C$ of CO_2 and higher CO_2 concentrations.

On the other side of the exchange, Southern Ocean surface $\Delta^{14}C$ is affected by the isoflux caused by the gross flux from the atmosphere. In the mid 20th century, the atmosphere-ocean isoflux became sharply more positive as bomb ^{14}C accumulated in the atmosphere, injecting a

pulse of ^{14}C into mode waters formed at the Southern Ocean surface. As this pulse returns to the surface after decades in transit, it contrasts with the currently declining $\Delta^{14}C$ of the atmosphere and the shallow ocean, providing an opportunity to trace the transport of 20th-century industrial-age carbon from the Southern Ocean to its reemergence in low-latitude upwelling regions,

3. Dissertation Organization

The chapters that follow this introduction are written in the form of journal papers that will be read in isolation from the rest of this dissertation. This results in some repetition in the introduction and methods sections of each chapter. Chapter II builds on a study by Marchitto et al. [2007] that found evidence of a mid-depth deglacial pulse of low-$\Delta^{14}C$ carbon in a marine sediment core near Baja California, Mexico, which was interpreted to be the return of aged carbon from the deep ocean, via intermediate water from the Southern Ocean. Marchitto et al. [2007] used sediment color to relate core depth to the layer-counted absolute age model of a Greenland ice core, allowing ^{14}C measurements on benthic foraminifer from the core to be corrected for decay since deposition. In chapter II, measurements of ^{14}C in the shells of three different species of planktic foramifera from the same core allow us to reconstruct the deglacial evolution of $\Delta^{14}C$ at the surface, including seasonal offsets that provide information on the horizontal $\Delta^{14}C$ gradients present in the deglacial eastern tropical Pacific surface ocean. This chapter was published in the July 15, 2015 issue of *Earth and Planetary Science Letters*.

Chapter III uses some of the planktic ^{14}C measurements presented in Chapter II and new planktic ^{14}C measurements from two other nearby cores to align them with the Marchitto et al., [2007] age model. This common calendar age model allows benthic ^{14}C measurements from the three cores, which span depths of ~400-1300 meters modern water depth, to be used in a

reconstruction of the vertical $\Delta^{14}C$ gradient during deglaciation. This depth transect reconstruction, along with a new stable oxygen isotope record from one of the cores, provides information on the proximal source of the pulse of low-$\Delta^{14}C$ carbon first observed by Marchitto et al., [2007]. This chapter has been submitted for publication in *Paleoceanography*.

Chapter IV presents time series of $\Delta^{14}C$ and CO_2 concentrations measured in air over Drake Passage (Southern Ocean) since 2006, enabling us to constrain the source of CO_2 concentration anomalies observed during periods of stronger westerly winds. We find that samples with higher CO_2 concentrations have anomalously low $\Delta^{14}C$, which in the remote Southern Ocean region identifies the ocean as the carbon source. Chapter V demonstrates that $\Delta^{14}C$ observations from the surface ocean in the 1990s and early 2000s contain information on the low-latitude reemergence of anthropogenic carbon, previously absorbed by the ocean at high latitudes in the decades following the bomb spike. Chapter VI summarizes the main findings of each chapter and comments on their implications and some remaining questions that future work should address. Following Chapter VI is a list of cited references and appendices containing data and supplementary material for the chapters.

Chapter II: The surface expression of radiocarbon anomalies near Baja California during deglaciation

Abstract:

Periods of declining atmospheric radiocarbon activity ($\Delta^{14}C$) during the Heinrich 1 (~17.8-14.6 ka) and Younger Dryas (~12.8 -11.5 ka) stadials of the last deglaciation coincide with intervals of rising atmospheric CO_2, as well as evidence of ^{14}C-depleted carbon at intermediate ocean depths near Baja California, Mexico and in the Arabian Sea. The latter has been interpreted as the signature of aged carbon emerging through the intermediate ocean to the atmosphere from a previously isolated deep ocean reservoir. Here we report on measurements from near Baja California that enable us to reconstruct the $\Delta^{14}C$ of surface waters as recorded by three different species of planktonic foraminifera. We find that surface ocean $\Delta^{14}C$ recorded by planktonic foraminifera was anomalously low relative to the coeval atmosphere during previously documented periods of low benthic $\Delta^{14}C$, consistent with upwelling and subsequent mixing and/or partial atmospheric equilibration of the intermediate-depth benthic signal. We also propose an oceanographic explanation for observed $\Delta^{14}C$ differences between individual planktonic species during deglaciation at this location, based on seasonal growth habitats and a seasonal change in the source of coastal upwelling waters: from northern in the spring to southern in late summer, as the shelf-trapped poleward California Undercurrent strengthens. An analysis of the contemporary hydrography and planktic habitat preferences suggests that *G. bulloides* and *G. sacculifer* record primarily springtime conditions off Baja California, when the local influence of waters sourced from the surface of the North Pacific is greatest. This is supported by strong resemblance of the $\Delta^{14}C$ of those species and a recent record of planktic $\Delta^{14}C$ from the Northeast Pacific during deglaciation. Lower $\Delta^{14}C$ recorded by the late-summer

species *G. ruber* suggests that locally upwelling waters carried ^{14}C-depleted carbon that was proximately sourced from equatorial subsurface waters entrained by the California Undercurrent. Together with the benthic record, these observations are consistent with transport of an anomalous ^{14}C-depletion signal carried primarily by Antarctic Intermediate Water from an ultimate source in the Southern Ocean.

1. Introduction

Radiocarbon (^{14}C) is a rare isotope of carbon that is produced by cosmic ray interactions in the upper atmosphere, and radioactively decays in global carbon pools with a half-life of ~5700 years [Godwin, 1962; National Nuclear Data Center, Brookhaven National Laboratory, www.nndc.bnl.gov]. Atmospheric ^{14}C activity (expressed as $\Delta^{14}C$) decreased markedly during the most recent deglaciation [*Reimer et al.*, 2004], at rates greater than can be explained by changes in the strength of geomagnetic field shielding alone [*Hughen et al.*, 2004]. A 2007 study including three of the present authors [*Marchitto et al.*, 2007] observed that the pace of atmospheric $\Delta^{14}C$ decline coincided with that of the deglacial atmospheric CO_2 rise, suggesting dilution of atmospheric CO_2 by addition of aged, ^{14}C-depleted carbon that could only have been sourced from the deep ocean. The same study [*Marchitto et al.*, 2007] also presented evidence of extreme ^{14}C-depletion in deglacial-age intermediate-depth sediments near Baja California in the eastern tropical Pacific, which they suggested was the signature of aged, sequestered dissolved inorganic carbon upwelled in the Southern Ocean and advected to the Baja California Margin by Antarctic Intermediate Water (AAIW). Other studies have since found evidence of pronounced deglacial ^{14}C depletion at intermediate-depth locations in the eastern equatorial Pacific [*Stott et al*., 2009] and the Arabian Sea [*Bryan et al*., 2010], and there is also evidence that the deep Southern Ocean was substantially less well ventilated during the last glacial maximum and early

deglacial period than today [*Burke & Robinson*, 2012; *Sikes et al.*, 2000; *Skinner et al.*, 2010]. However, despite several attempts, no study has yet found evidence of substantial deglacial ^{14}C depletion near the present-day sources of AAIW in the southern hemisphere [*Burke & Robinson*, 2012; *De Pol-Holz et al.*, 2010; *Rose et al.*, 2010; *Siani et al.,* 2013; *Sortor & Lund*, 2011].

Here we present new ^{14}C measurements in foraminifera tests from the same sediment core studied by Marchitto *et al*. [2007) that increase the resolution of the intermediate-depth $\Delta^{14}C$ record off Baja California and reveal that surface waters at the site were also depleted in ^{14}C during deglaciation. Observed $\Delta^{14}C$ differences between planktic species are consistent with seasonal changes in the source of locally-upwelled waters today, and point to the equatorial Pacific as the proximate source of aged carbon to intermediate and surface waters near Baja California during deglaciation.

2. Study Site

Composite core MV99-MC19/GC31/PC08 was raised from 705 m water depth at a location about 85 km west of Baja California Sur [Fig. 2.1; *van Geen et al*., 2003]. At the seafloor, the core location lies near the present boundary between North Pacific Intermediate Water (NPIW) and Equatorial Pacific Intermediate Water (EqPIW), which itself is a mixture of Antarctic Intermediate Water (AAIW) and Pacific Deep Water [*Bostock et al*., 2010]. The ocean surface near the core site is influenced by coastal upwelling throughout the year as a result of climatological mean northwesterly winds, with maximum upwelling during the spring [*Bakun and Nelson*, 1977]. The California Current (CC) brings relatively cold, fresh North Pacific sub-arctic water southward along the margin, visible in climatological salinity data from the 2009 World Ocean Atlas [*Antonov et al*., 2010] as a tongue of low salinity values about 100 km

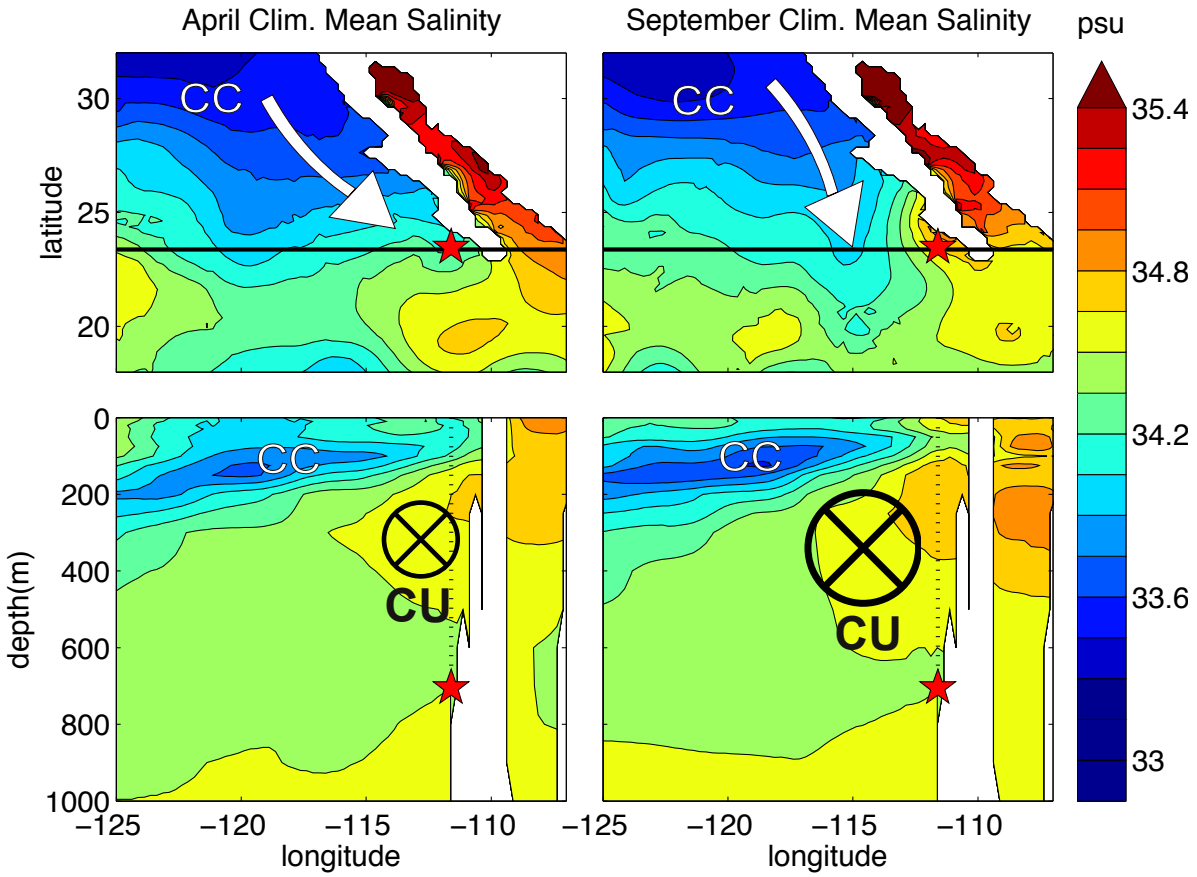

Figure 2.1: Map view (top panels) and zonal transect (lower panels) of contoured April and September climatological salinity near Baja California, from the World Ocean Atlas 2009 [*Antonov et al.*, 2010]. In the top panels, arrows marked CC indicate the California Current and the black line indicates the latitude of the zonal transect. In the lower panels, vector symbols marked CU indicate the California Undercurrent, and the salinity minimum associated with the California Current is labeled CC. The red star indicates the location of core PC08.

offshore (Fig. 2.1, upper panels). The CC can also be seen in ocean sections (Fig. 2.1, lower panels) as a shallow (50-150 m) salinity minimum near the southern Baja California coast [*Hickey*, 1979; *Lynn & Simpson*, 1987]. The CC is strongest near the shore during the spring [*Hickey,* 1979; *Lynn & Simpson*, 1987], coinciding with the time of maximum upwelling. The California Undercurrent (CU) flows at a depth of ~250 m, carrying relatively warm, salty equatorial subsurface water (ESSW) from the Eastern Equatorial Pacific northward along the

edge of the shelf break [*Hickey*, 1979; *Lynn & Simpson*, 1987]. The physical forcing of the CU is not fully understood, but is thought to arise from a combination of the along-shore pressure gradient and the positive curl of the wind stress field near the coast [*Connolly et al*., 2014; *Hickey*, 1979, 1998]. In response to seasonal wind stress and changes in dynamic height of the sea surface, the CU gains strength in the summer and fall, expanding into shallower depths [*Hickey*, 1979; *Lynn and Simpson*, 1987; *Connolly et al.*, 2014]. The seasonal shift is characterized by greater extent and shoaling of salty CU water in section and an increase in surface salinity near the coast in September relative to April (Fig. 2.1).

Elevated surface salinity near Southern Baja is caused primarily by regional and localized upwelling of high-salinity ESSW from the CU [*Durazo*, 2009]. ESSW carried by the CU appears to be sourced from the deeper portions of the Northern Subsurface Countercurrent (NSCC), also known as the northern Tsuchiya jet, a sub-thermocline eastward current that shoals as it crosses the Pacific at about 5° N [*Fiedler and Talley*, 2006; *Kessler*, 2006]. The NSCC originates near the western boundary of the Equatorial Pacific carrying AAIW from near Papua New Guinea [*Rowe et al*., 2000; *Tsuchiya*, 1991] that mixes with high salinity North Pacific Eastern Subtropical Mode Water (NPESTMW) and, possibly, North Pacific Intermediate Water (NPIW) as it is carried in the jet [*Fiedler and Talley*, 2006].

3. Methods

Foraminifera samples were picked from the >250 μm size fraction of washed sediment samples from the deglacial sections of core MV99-PC08. In some cases, samples that were too small for radiocarbon measurement were brought up to weight by adding foraminifera from the 150-250 μm size fraction. Monospecific samples of the planktic foraminifera *Globigerinoides*

ruber, *Globigerinoides sacculifer* and *Globigerina bulloides* were picked and analyzed separately. Additional samples of the benthic foraminifera *Uvigerina* spp. (mainly *U. peregrina*) were also picked to increase the resolution of the previously published MV99-MC19/GC31/PC08 benthic record [*Marchitto et al.*, 2007]. In the Holocene sections of the composite core (i.e., sediments <11.5 ka), planktic abundances were too low for ^{14}C measurement. All samples were prepared at the INSTAAR Laboratory for AMS Radiocarbon Preparation and Research at the University of Colorado before measurement at the Keck Carbon Cycle AMS Laboratory at the University of California, Irvine. Samples were leached for 5 minutes in a 0.001 N solution of HCl, reacted with H_3PO_4, and then cryogenically purified. The CO_2 was reduced to graphite over an Fe catalyst in the presence of H_2, and packed into AMS targets. The decay-corrected initial radiocarbon activity [$\Delta^{14}C$; *Stuiver & Polach*, 1977] of the samples was calculated from the measured ^{14}C age results using the previously published calendrical age model for the cores, based on correlation of diffuse spectral reflectance of the core sediments to the layer-counted GISP2 oxygen isotope record [*Marchitto et al.*, 2007], and a geophysical ^{14}C half-life of 5730±40 years [*Godwin*, 1962].

Estimated errors in initial $\Delta^{14}C$ include contributions from both ^{14}C measurement error and calendar age uncertainty. Because the latter dominate, error bars will generally have slopes that approximate age-decay trajectories when plotting $\Delta^{14}C$ with respect to age. Propagated estimates of calendar age uncertainty are based on estimated uncertainties of correlation associated with individual tie-points from Marchitto *et al*. [2007] and, for the present study, additional age uncertainties between tie-points from Monte-Carlo simulations that permitted sedimentation rates to vary by ±20%. We do not incorporate additional uncertainties associated with the underlying GISP2 age model, which may include biases of up to 100-200 years during our study

interval [*Svensson et al.*, 2008]. Importantly, estimated $\Delta^{14}C$ differences between different species sampled at or near the same stratigraphic level or between neighboring samples would not be significantly influenced by plausible adjustments to tie point age (from either correlation error or ice core event age bias), since affected samples would move up and down age decay trajectories (and related error bars) together. For reference, plausible tie-point age errors of a few hundred years would correspond to systematic $\Delta^{14}C$ biases of a few tens of per mil.

A recent study suggested that previously documented benthic $\Delta^{14}C$ anomalies in core PC08 might be an artifact of tuning the sediment age model to GISP2 age [*Davies-Walczak et al.*, 2014]. Following Davies-Walczak *et al*. [2014] we therefore constructed an alternative age model based on an assumption of constant reservoir age in the better equilibrated (younger) planktonic species as measured in the present study. The alternative age model only slightly affects the timing and magnitude of the estimated $\Delta^{14}C$ anomalies in the benthic and other planktic species, while imposing an unlikely sedimentation rate history (see Appendix A for details). We therefore base the results and discussion that follow on the original PC08 age model, with uncertainties as described above.

Measured Fractions Modern and resultant ^{14}C ages include a $\delta^{13}C$ normalization to account for sources of mass-dependent fractionation, based here on $\delta^{13}C$ acquired in-line on the AMS. These $\delta^{13}C$ results are, however, not precise enough for meaningful paleo-environmental interpretation and are not presented. All other results are available in tabulated form in Appendix B.

4. Results

4.1 New benthic radiocarbon measurements

The additional benthic foraminiferal measurements (Fig. 2.2) fill gaps in the previously

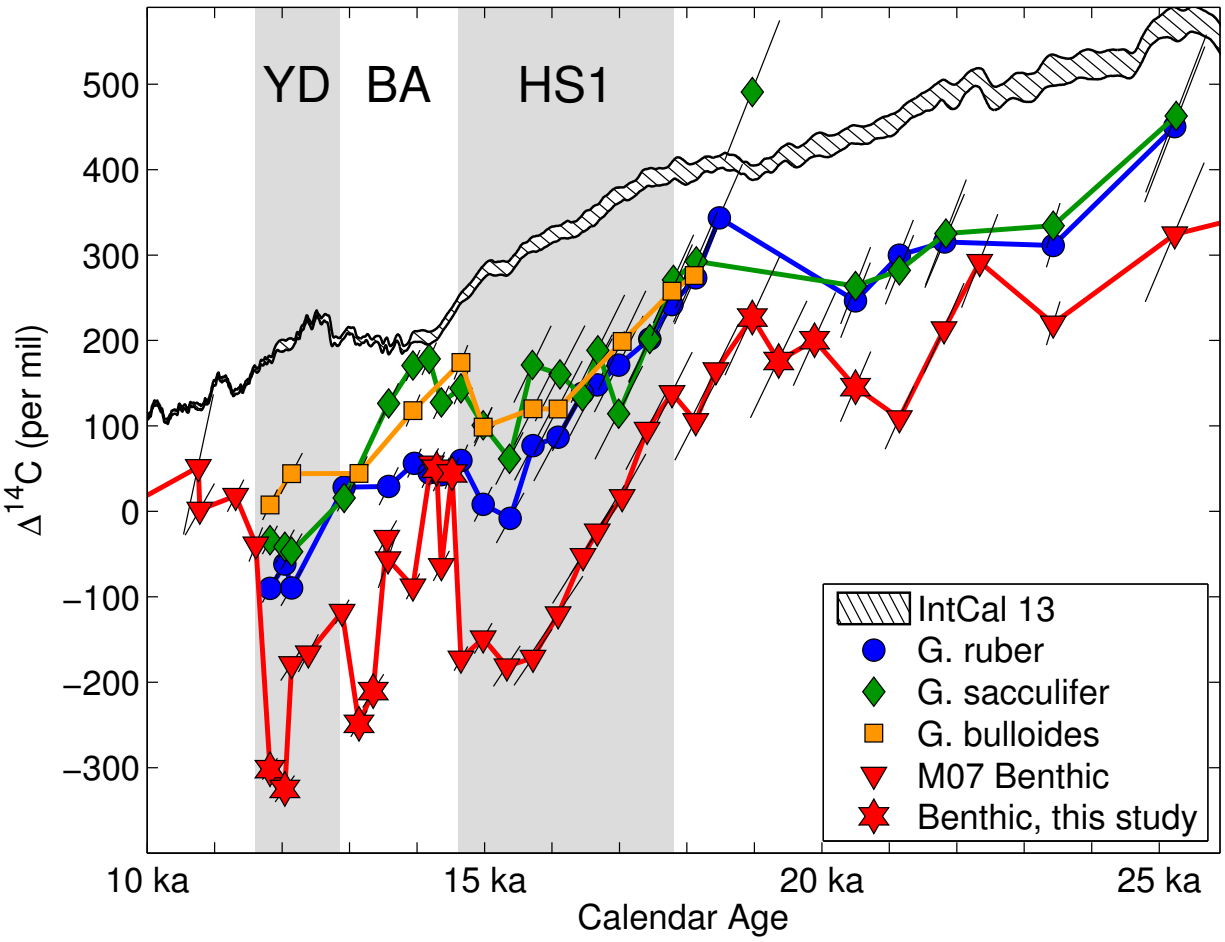

Figure 2.2: Benthic and planktic PC08 $\Delta^{14}C$ from this study and Marchitto *et al*. (2007) plotted with IntCal13 atmospheric $\Delta^{14}C$ [*Reimer et al.*, 2013]. Grey fields indicate the Heinrich 1 (HS1) and Younger Dryas (YD) stadials bracketing the Bølling-Allerød period (BA). Error bars connect the values calculated from the combined 1-sigma calendar age and measurement uncertainty bounds.

published $\Delta^{14}C$ record and document greater $\Delta^{14}C$ variability in the middle to latter part of the deglaciation than reported earlier by Marchitto *et al*. [2007]. In the ~21-18 ka interval, the measurements are consistent with previous evidence that prior to the Heinrich stadial 1 (HS1) intermediate water $\Delta^{14}C$ tracked the atmosphere with an average offset of approximately 200‰, which is approximately twice the average offset observed for the last 10 ka but similar to both the near-modern core top offset of ~160‰ [*Marchitto et al.*, 2007] and the ~170‰ estimated from a nearby GEOSECS profile [*Ostlund et al.*, 1987].

The larger offset during the glacial interval can be attributed primarily to the greater glacial atmospheric ^{14}C inventory, as opposed to differences in physical ventilation. During the early part of the Bølling-Allerød/Antarctic Climate Reversal (BA/ACR) the new measurements reveal an offset from the coeval atmosphere of ~150‰, which lies between the average Holocene and Last Glacial Maximum values. Relatively short, multi-century excursions to ~450-500‰ less than the coeval atmosphere are seen during the late BA and late in the Younger Dryas stadial (YD), greater than in the original record for this interval but similar to the largest offsets from atmosphere seen during HS1.

The new data add to the similarity previously apparent between the Baja California benthic record and records of intermediate water $\Delta^{14}C$ from the Arabian Sea prior to ~13 ka (Fig. 2.3a), providing further evidence that the records have a common oceanographic origin [*Bryan et al.*, 2010]. We also note that the very high rates of sedimentation that characterize PC08 (30 cm/ka) substantially limit the likelihood that structural features of the $\Delta^{14}C$ record could have arisen from bioturbation and changes in carrier species abundance [i.e. *Bard et al.*, 1987].

4.2 Planktic radiocarbon measurements

The $\Delta^{14}C$ results from planktic foraminifera show coherent trends with relatively little point-to-point scatter (Fig. 2.2). Estimated uncertainty, which includes contributions from measurement error and calendar age uncertainty, is relatively small and dominated by the calendar age uncertainty, leading to error bars that are oriented approximately along a decay trajectory. A single *G. sacculifer* measurement at 18.9 ka is higher than estimated coeval atmospheric $\Delta^{14}C$, a result that is highly unlikely in a region of upwelling and under pre-nuclear conditions (because positive surface ocean ^{14}C disequilibrium with respect to the atmosphere

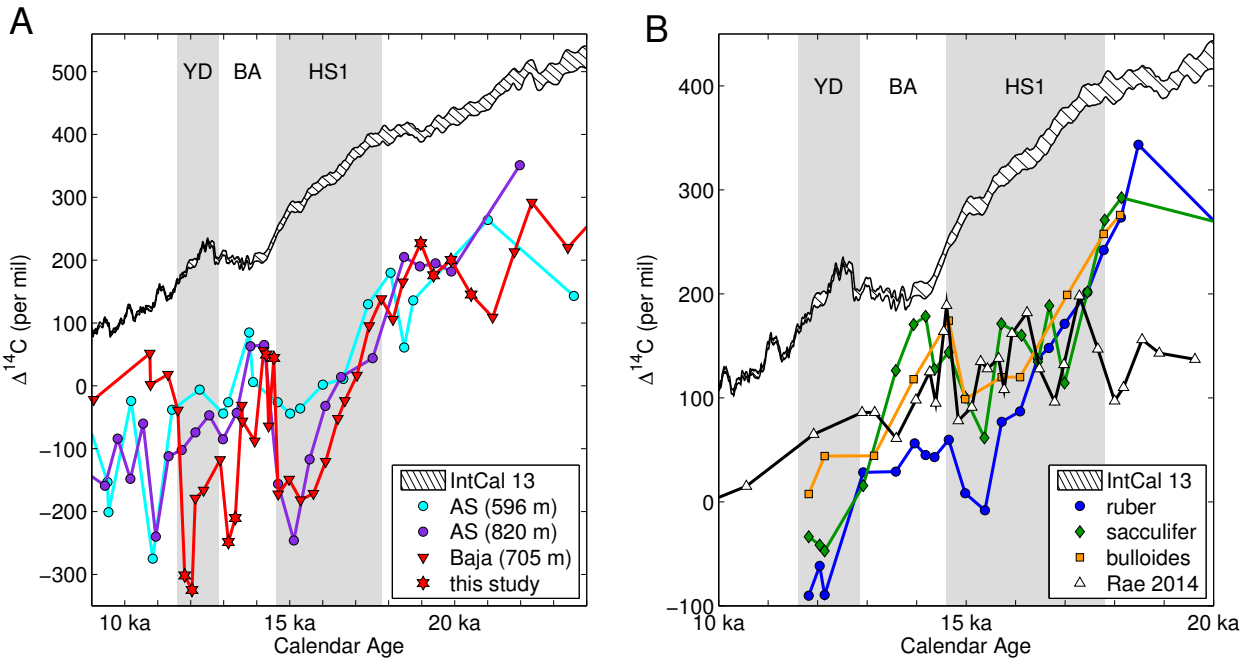

Figure 2.3: A) Reconstructed intermediate-depth benthic $\Delta^{14}C$ from Baja California plotted with similar benthic results from the Arabian Sea (AS, Bryan *et al.*, 2010) and the IntCal 2013 atmospheric $\Delta^{14}C$ reconstruction [*Reimer et al.*, 2013]. **B)** Baja California planktic $\Delta^{14}C$ plotted with similar planktic results from the Northeast Pacific [*Rae et al.*, 2014] and the IntCal 2013 atmospheric $\Delta^{14}C$ reconstruction [*Reimer et al.*, 2013]. Grey fields indicate the Heinrich 1 (HS1) and Younger Dryas (YD) stadials bracketing the Bølling-Allerød period (BA).

requires a very rapid transient decline in atmospheric $\Delta^{14}C$). We surmise this result is either an analytical outlier (source unknown) or due to downward transfer of *G. sacculifer* tests by lumpy mixing, such as in a deep burrow. We note, however, that this would require the bulk of the dated tests to have been transported downward about 30 centimeters, which seems unlikely. There were too few *G. ruber* for ^{14}C measurement at the level of the anomalous *G. sacculifer* result, so no additional analytical constraints are available. Due to these issues this sample will be excluded from further discussion.

The remainder of the planktic $\Delta^{14}C$ results follow a temporal pattern similar to that of the benthic record, but with smaller amplitude (Fig. 2.2). Prior to the HS1 interval, average planktic

$\Delta^{14}C$ was about 100‰ lower than the atmosphere. Average planktic $\Delta^{14}C$ decreased faster than the atmosphere during HS1, reaching a maximum offset from the atmosphere of ~150-250‰ at about 15 ka. Planktic $\Delta^{14}C$ rebounded to ~50-150‰ below atmosphere during the early BA, and decreased again to ~150-250‰ less than the atmosphere during the late BA and YD. After ~ 16.5 ka, *G. ruber* $\Delta^{14}C$ tends to be lower than *G. sacculifer* and *G. bulloides* $\Delta^{14}C$, with the difference increasing to about 90‰ during the BA. There does not appear to be a systematic $\Delta^{14}C$ offset between *G. sacculifer* and *G. bulloides*.

5. Discussion

The general pattern of the planktic results is similar to the benthic results, but characterized by lower amplitude and higher absolute values that are closer to those of the coeval atmosphere. These characteristics suggest that the composition of waters at both intermediate depths and at the surface were influenced by a common source (or sources), with some attenuation of the surface signal arising from mixing with better-equilibrated surface waters and exchange with the atmosphere. The observed inter-species planktic $\Delta^{14}C$ differences are not readily explained in terms of preferential depth habitat, since, of the three species analyzed here, *G. ruber* is generally regarded as preferring the warmest and presumably shallowest waters [*Ortiz et al.,* 1995; *Spero et al.*, 2003] and yet typically displays lower $\Delta^{14}C$ than the other species. There is also little evidence that differences in dissolution resistance amongst species, combined with residence time in the sediment mixed layer, caused the observed $\Delta^{14}C$ offsets, since dissolution in the sediment mixed layer would be expected to produce a young (high initial $\Delta^{14}C$) bias in the more dissolution prone *G. ruber* relative to the other measured species [e.g. *Barker et al.*, 2007], opposite to what we observe here. High rates of sedimentation in core PC08 also limit the

likelihood that systematic inter-species $\Delta^{14}C$ offsets have arisen from bioturbation and changes in carrier species abundance [e.g. *Bard et al*., 1987]. These arguments lead us to posit that the inter-species planktic $\Delta^{14}C$ differences reflect primarily seasonal habitat preferences combined with seasonal changes in the source and composition of waters upwelling at the Baja California Margin.

5.1 Interspecies offsets and inferred $\Delta^{14}C$ seasonal cycle

G. bulloides is an asymbiotic planktonic foraminifera that tolerates relatively low light and cool temperatures. Thus, when present at low latitudes, this species is commonly associated with cool, turbid conditions in areas of upwelling [*Sautter and Sancetta*, 1992; *Ortiz et al.*, 1995]. Seasonality in the source of upwelling water near Baja California should cause *G. bulloides* to preferentially record spring conditions, when more cool high-nutrient northern-sourced water from the CC is at the surface [*Lynn and Simpson*, 1987]. As noted above, *G. ruber* is the most temperature-sensitive of the measured planktic species [*Ortiz et al.*, 1995], favoring the warmest temperatures at shallow depths within the mixed layer [*Spero et al*., 2003]. Near Baja California, *G. ruber* is expected to record late summer/fall surface water properties, when temperatures are highest [*Mortyn et al*., 2011; *Sautter & Sancetta*, 1992]. The local seasonal preferences of *G. sacculifer* are not well known, but this species seems to be more tolerant of cooler temperatures than *G. ruber*, migrating across a wide range of depths in the mixed layer and thermocline during calcification [*Spero et al*., 2003 and references therein].

Although modern ^{14}C data is not available near Baja California in sufficient temporal or spatial resolution to resolve seasonal changes at the scale shown by the salinity maps and sections in Figure 2.1, an estimate of the expected sense of $\Delta^{14}C$ seasonality in local surface

waters can be obtained by comparing estimated pre-nuclear $\Delta^{14}C$ from the Global Ocean Data Analysis Project [GLODAP, *Key et al.* 2004] with annual mean surface salinity from the 2009 World Ocean Atlas [*Antonov et al.*, 2010](Figure 2.4). Pre-nuclear ("natural") $\Delta^{14}C$ in the GLODAP dataset is a calculated quantity derived from the empirical relationship between $\Delta^{14}C$ and salinity-normalized potential alkalinity in the deep ocean, where measured $\Delta^{14}C$ had not yet been affected by the addition of bomb radiocarbon at the time of measurement [*Rubin and Key*,

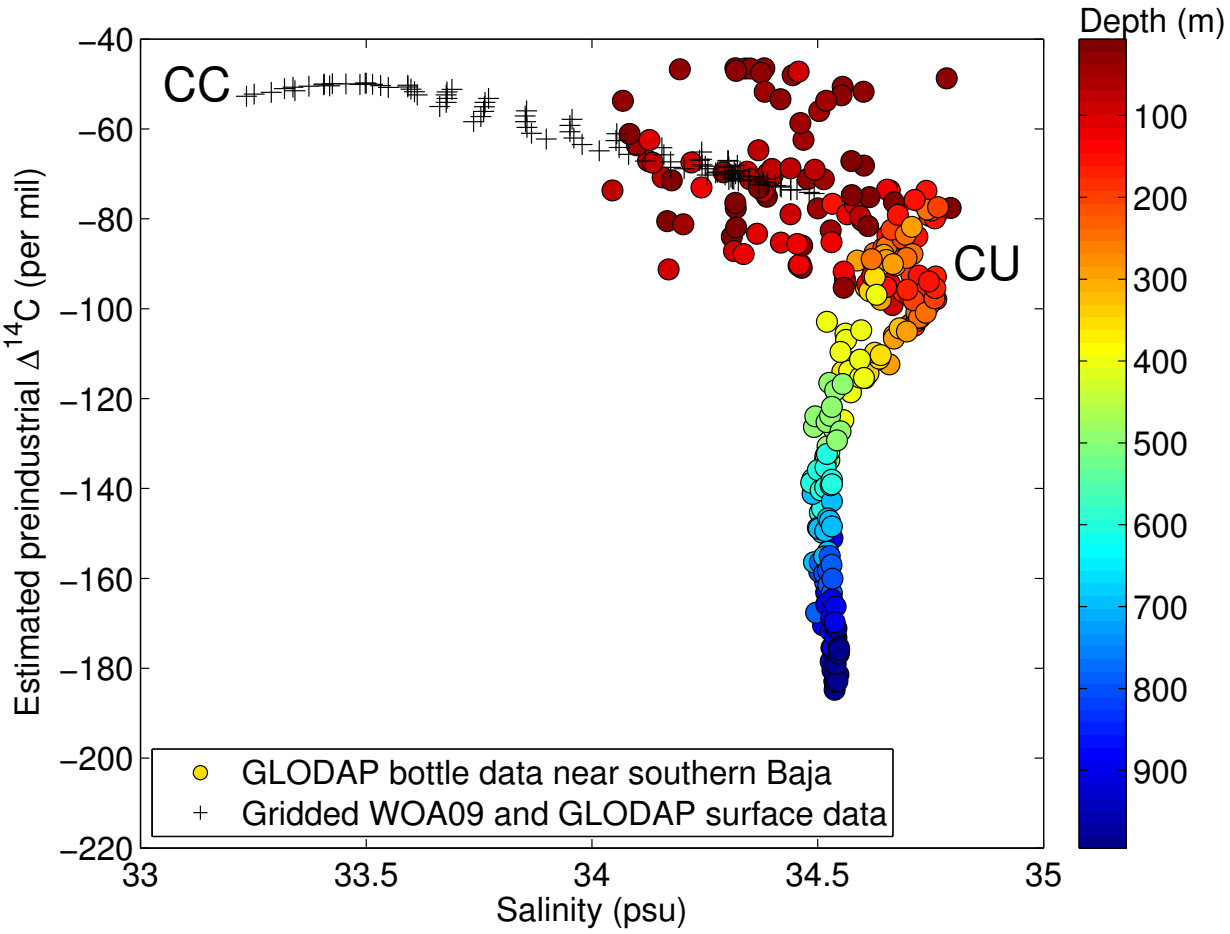

Figure 2.4: Estimated natural $\Delta^{14}C$ in surface waters between 17 and 32°N along the west coast of Baja California from the gridded GLODAP product [*Key*, 2004] plotted versus WOA09 gridded surface salinity data [*Antonov et al.*, 2010] (black crosses). GLODAP bottle data from the same region is plotted as filled circles and colored by depths corresponding to the right-hand scale. Labels indicate approximate California Current (CC) and California Undercurrent (CU) end-member values.

2002]. The method relies on the correlated decay of ^{14}C and accumulation of alkalinity in the deep ocean and the reverse of those processes at the surface and, in theory, should present no salinity-related biases. As can be seen in Figure 2.4, $\Delta^{14}C$ and salinity of surface and near-surface waters near Baja California appear to be inversely related.

The influence of the CU is visible in paired pre-industrial $\Delta^{14}C$ and salinity data from individual GLODAP bottle casts (filled circles in Fig. 2.4) as a salinity maximum at about 250 m water depth. Shallower observations scatter around a mixing line between relatively low $\Delta^{14}C$ and high salinity values of the CU and those of northern-sourced waters in the CC, characterized by higher $\Delta^{14}C$ and lower salinity. The slope of the salinity-$\Delta^{14}C$ relationship above ~250 m, combined with the average seasonal cycle in salinity at the surface (~0.4 psu, see Fig. 2.1), suggests that pre-nuclear $\Delta^{14}C$ of surface waters at the location of PC08 might decline seasonally by ~10‰ between April and September if the salinity change were due solely to changes in the mixture of source waters. This would result in *G. ruber* recording lower $\Delta^{14}C$ (i.e., more CU) than *G. bulloides* (i.e., more CC), as is generally observed in our sediment record. On the basis of similar $\Delta^{14}C$ signatures in the sediment record, we would also infer that *G. sacculifer* had a local seasonal habitat broadly similar to that of *G. bulloides*, perhaps because it can tolerate cooler spring conditions.

As already noted, the overall temporal pattern of planktic $\Delta^{14}C$ variation is similar to that observed in the benthic record, but from about 15-14 ka the planktic inter-species $\Delta^{14}C$ offsets increase markedly, with $\Delta^{14}C$ in both *G. bulloides* and *G. sacculifer* increasing more than in *G. ruber*. This is most readily explained by a transient increase in $\Delta^{14}C$ of northern surface waters entrained in the CC and upwelled locally in springtime when *G. bulloides* and *G. sacculifer* are thought to be most abundant. Recent ^{14}C results from the NE Pacific provide strong support for

this view, with clear evidence of a sudden younging of NE Pacific surface waters beginning ~15 ka [*Rae et al.*, 2014]. Indeed, the new results greatly reinforce the impression of a northern influence on the "springtime" ^{14}C signal at Baja California, consistent with expectation based on our analysis of the contemporary hydrography. To illustrate this, we show the new NE Pacific planktic $\Delta^{14}C$ results of Rae *et al*. [2014] along with those from the Baja California Margin in Figure 2.3b. After ~17 ka there is much greater similarity between the northern planktic record and $\Delta^{14}C$ in both *G. bulloides* and *G. sacculifer* than in *G. ruber* from the Baja California margin. As argued above, the latter species appears to sample more depleted waters with a proximate source in the eastern equatorial Pacific. The suggested geographic separation of signals coming alternately from northern and southern sources would permit the near surface $\Delta^{14}C$:salinity mixing line in Figure 2.4 to steepen or flatten over time in response to independent changes in the different source regions, increasing or decreasing the potential for measured inter-species $\Delta^{14}C$ differences near Baja California. The low $\Delta^{14}C$ values recorded by the NE Pacific planktics at ~18–20 ka are 200‰ lower than coeval planktic $\Delta^{14}C$ values at Baja California, and lower even than the coeval benthic values. This suggests either decoupling between the NE Pacific surface and Baja California at that time or, more likely, that correlation tiepoints to independent chronologies used to constrain the age of the pre-HS1 portion of the NE Pacific record [*Rae et al.*, 2014] are approximately 1300 years too young.

Despite evidence for substantial seasonal differences in northern- *vs.* southern-source contributions to local surface water admixtures, *G. ruber* $\Delta^{14}C$ increased at the end of HS1 and into the BA at the same time as *G. bulloides* and *G. sacculifer,* but to a much lesser degree. The common timing of the seasonal ^{14}C responses suggests a degree of common forcing. As outlined earlier, ESSW is thought to have both northern and southern sources, as NPESTMW and,

possibly, NPIW are entrained in the northern Tsuchiya jet as it carries AAIW to the shallow subsurface of the east equatorial Pacific [*Fiedler and Talley*, 2006]. Ventilation of NPESTMW may have improved along with that of NE Pacific surface waters in the latter part of HS1, which would have increased the $\Delta^{14}C$ of ESSW entrained in the CU (and recorded by *G. ruber* at the surface near Baja California), but to a lesser degree than in the NE Pacific due to mixing with other watermasses contributing to mode water itself and also to ESSW. Alternatively, the similarity in timing of the $\Delta^{14}C$ variations in *G. ruber* and the other two species in late HS1 and the early BA may reflect some local admixing of North Pacific surface waters continuing into late summer (when the upwelling component is otherwise dominated by waters of the ESSW-containing CU). Available ^{14}C reconstructions from the mid-depth North Pacific [Okazaki *et al*., 2010) depict a ventilation history opposite to what we observe at Baja California, suggesting that $\Delta^{14}C$ changes in NPIW did not exert a dominant influence on our observations.

5.2 Ultimate sources of aged carbon

All measured planktic and benthic species in PC08 record transient declines in initial $\Delta^{14}C$ relative to the atmosphere during HS1 and the latter parts of the BA and YD (Fig. 2.2), indicating addition of aged waters to both surface- and bottom-water mixtures at the site at those times. The most sustained decline is observed during HS1, where it is steadily progressive in both the benthics and in *G. ruber* (Fig. 2.2), while the other two planktic species display some additional time-dependent variability that can be traced to changes in age of surface waters of the NE Pacific (Fig. 2.3b). Comparable changes in *G. ruber* and the benthics suggest that some or all of the water masses presently influencing local bottom waters and late-summer surface waters, namely EqPIW and/or NPIW and ESSW, had similar ventilation histories. As already noted,

available reconstructions from the mid-depth North Pacific suggest that the ventilation history of NPIW was different than observed at Baja California, whereas the other two water masses have a common source in AAIW. While our observations obviously do not constrain the distal source directly, our analysis of the hydrographic influences on the study site today and compositional changes during deglaciation point to AAIW as a likely conduit of aged carbon during transient deglacial ^{14}C-depletion events, with a distal source of aged water in the deep Southern Ocean [*Anderson et al.*, 2009; *Basak et al.*, 2010; *Burke & Robinson*, 2012; *Sikes et al.*, 2000; *Skinner et al.*, 2010].

Although this scenario [*Marchitto et al.*, 2007] remains challenged by the absence of evidence (so far) for significant deglacial ^{14}C depletion in some present-day source areas of AAIW [*Burke & Robinson*, 2012; *De Pol-Holz et al.*, 2010; *Rose et al.*, 2010; *Siani et al.,* 2013; *Sortor & Lund*, 2011], there are few defensible alternatives. For example, the fraction of aged North Pacific deep water within EqPIW (the mixture of AAIW and Pacific Deep Water that bathes the core site today) may have increased at times, but available records of North Pacific ventilation fail to document changes that are coincident with depletion events at Baja California [*Galbraith et al.*, 2007; *Rae et al.*, 2014] and cannot explain nearly simultaneous changes in the Arabian Sea [*Bryan et al.*, 2010]. Another alternative, which proposes the transient deglacial release of ^{14}C-dead volcanic CO_2 from shallow gas hydrates [*Stott and Timmermann*, 2011], would require very large amounts of pure CO_2 injection in order to reduce $\Delta^{14}C$ to observed values and, in consequence, very low carbonate ion concentrations. However, the record of planktic foraminiferal fragmentation in core PC08 [*Ortiz et al*., 2004] depicts a reduction in dissolution at times of anomalously low $\Delta^{14}C$, presumably in response to local controls on productivity and pore water chemistry (Fig. S5; see Appendix A for details). Lastly, box model

studies have questioned the physical plausibility of maintaining large negative gradients between the $\Delta^{14}C$ of intermediate waters and the atmosphere [*Hain et al.*, 2011], but the observed differences between benthics and the best-equilibrated planktic species recorded here provide evidence that such gradients existed.

5.3 Implications for deglacial marine radiocarbon chronologies

The single good estimate of the recent reservoir age for the southern Baja California region (631 ± 46 years) is based on ^{14}C measurement of a mollusk shell collected at Cabo San Lucas in 1932, prior to anthropogenic nuclear emissions [*Berger et al.*, 1966]. Our planktic results reveal several periods between 25 and 10 ka when the reservoir age near Baja appears to have been two to three times larger than the modern estimate, depending on the species (Figure 2.5).

These periods of large reservoir age, if sampled by a ^{14}C-based marine chronology that assumed a constant modern reservoir age correction, would cause the corrected radiocarbon age of the corresponding intervals to be too old by up to ~1300 years and would produce comparably large biases in estimated calendar age. The choice to date *G. ruber* instead of *G. bulloides* or *G. sacculifer* would, in this case, maximize those errors. Our results, along with a number of other previous studies documenting variable surface reservoir ages during deglaciation [e.g. *Sarnthein et al*., 2007; *Siani et al.*, 2013; *Stern & Lisiecki*, 2013; *Thornalley et al.*, 2011; *Voelker et al.*, 1998; *Waelbroeck et al.*, 2001), illustrate that conclusions regarding lead-lag relationships in deglacial marine records with radiocarbon-based calendar age models should be made cautiously, especially when the sites are located in or near regions influenced by upwelling.

Numerous studies have used planktic ^{14}C-based age models and the assumption of constant surface reservoir age to investigate the degree of benthic ^{14}C disequilibrium and deepwater

ventilation age with respect to the contemporaneous atmosphere, including many of the studies we have cited regarding AAIW and NPIW ventilation [e.g. *Ahagon*, 2003; *De Pol-Holz et al*., 2010; *Duplessy et al*., 1989; *Okazaki et al*., 2010; *Sortor & Lund*, 2011]. Underestimation of actual surface reservoir ages would lead to a high bias in the reconstructed bottom water $\Delta^{14}C$. In the absence of independent constraints on calendar age, one would need to apply very large

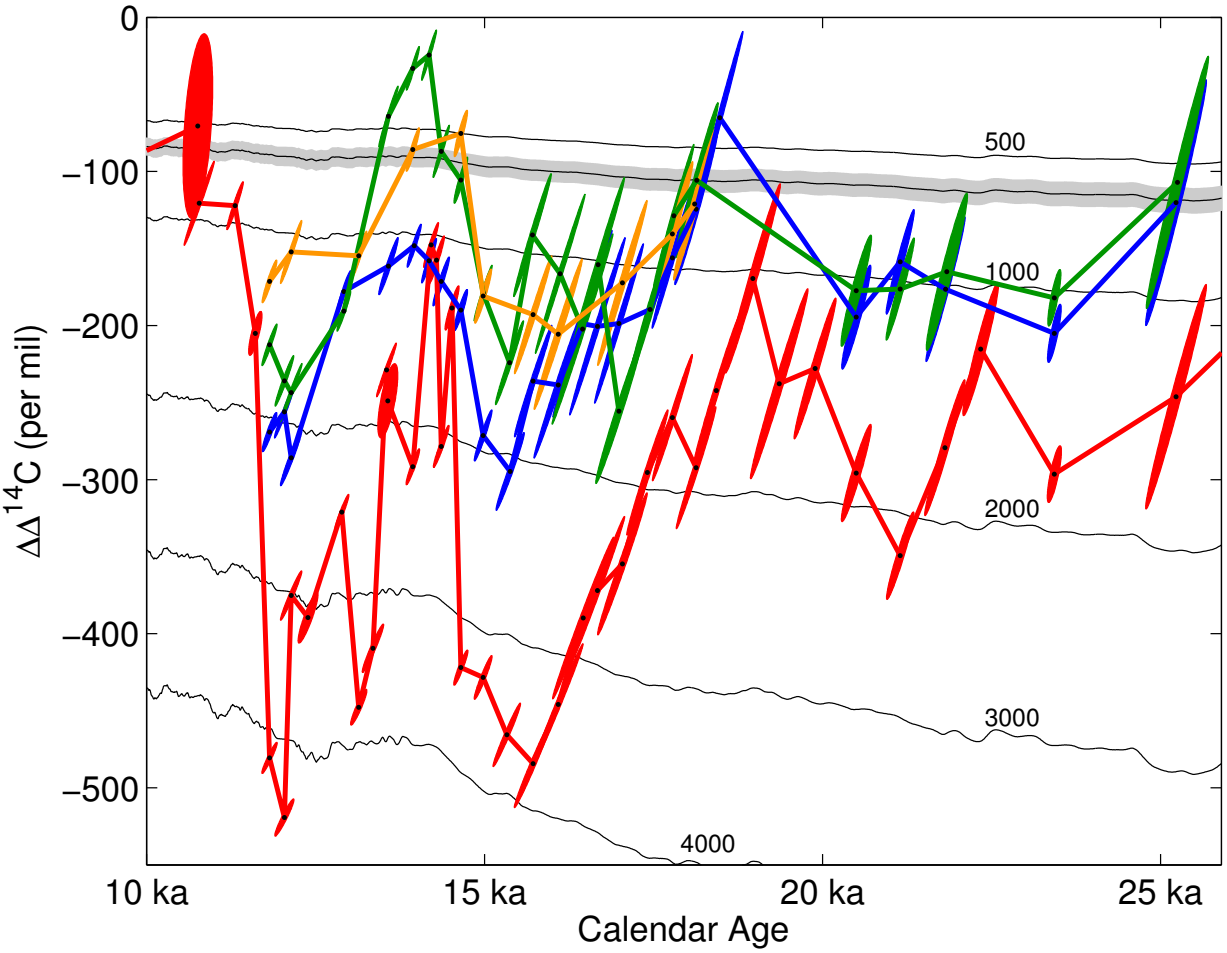

Figure 2.5: Baja California $\Delta\Delta^{14}C$ (foraminifera $\Delta^{14}C$ minus IntCal13 atmospheric $\Delta^{14}C$ [*Reimer et al.*, 2013]) plotted for all measured species (red: benthic, blue: *G. ruber*, green: *G. sacculifer*, orange: *G. bulloides*). Constant radiocarbon year offsets from the coeval atmosphere, converted to $\Delta\Delta^{14}C$, are plotted as thin black lines to illustrate equivalent reservoir ages. A constant offset based on the nearest measurement of preindustrial reservoir age (631 ± 46 years, mollusk shell collected at Cabo San Lucas (Berger, Taylor, & Libby, 1966)) is plotted as a thin black line with a shaded gray error envelope. Error ellipses are 1-sigma and incorporate both atmospheric and marine $\Delta^{14}C$ uncertainties.

uncertainties in surface reservoir age to account for the possibility of surface reservoir changes such as the ones we have reconstructed near Baja California. Siani *et al.* [2013] demonstrated the potential for underestimation of reservoir ages to bias the intermediate-depth ^{14}C record by using an independently dated ash-constrained chronology to resolve substantial changes in surface reservoir age near Chile. When applied to the Chilean margin core studied by De Pol Holz *et al.*, [2010], changes in the reconstructed surface reservoir age lowered the estimated benthic $\Delta^{14}C$ significantly [*Siani et al.*, 2013]. The Baja California benthic $\Delta^{14}C$ anomalies, however, are still as much as 200‰ lower than the adjusted Chilean records during HS1 and the YD.

5.4 Implications for the isolated reservoir hypothesis

In addition to our results and those from Siani *et al.,* [2013], negative planktic $\Delta^{14}C$ anomalies during deglaciation have been reported coinciding with low benthic $\Delta^{14}C$ in the East Equatorial Pacific [*Stott et al.*, 2009] and the Atlantic sector of the Southern Ocean [*Skinner et al.*, 2010]. The hypothesis that marine carbon from an isolated reservoir caused the deglacial decline in atmospheric $\Delta^{14}C$ and rise in CO_2 requires that it surfaced, and thus predicts anomalously old surface reservoir ages in at least some parts of the world ocean during the HS1 and YD atmospheric $\Delta^{14}C$ declines. This is important because the deglacial evolution of $\Delta^{14}C$ in the shallow and mid-depth ocean constrains the size and age of the hypothetical isolated deep reservoir required to produce the atmospheric $\Delta^{14}C$ decline. Broecker *et al.* [2007] assumed that the mid-depth and shallow ocean maintained a constant average offset (in ^{14}C years) from the glacial atmosphere (i.e. complete redistribution of ^{14}C atoms not in the deep ocean across all remaining reservoirs), and concluded that the implied size or age of any deep, isolated glacial reservoir was significantly greater than indicated by observations. Alternatively, Burke &

Robinson [2012] noted that if the Southern Ocean released old carbon directly to the atmosphere without affecting the $\Delta^{14}C$ of the rest of the ocean (i.e., transiently limited redistribution of ^{14}C atoms), the deglacial atmospheric decline is attainable with glacial deep ocean $\Delta^{14}C$ values that are consistent with observations. However, it is unlikely that ^{14}C-depleted carbon upwelling south of the Antarctic polar front could have fully equilibrated with the atmosphere before being subducted into the shallow and mid-depth ocean [*Bryan et al.*, 2010], because the residence time of upwelled deep water at the surface in the modern Southern Ocean is very short relative to the timescale of ^{14}C equilibration [*Ito*, 2004]. Our results would seem to require a scenario between these two limiting cases, in which some of the upwelled old carbon in the Southern Ocean was subducted before it could fully equilibrate with the atmosphere and was subsequently advected in AAIW to low-latitude upwelling locations. Once this water reemerged, continued gas exchange with the atmosphere would have played a secondary role in the atmospheric $\Delta^{14}C$ decline.

6. Conclusions

Hydrographic analysis indicates that present day surface waters near southern Baja California undergo significant seasonal changes in source water admixture, leading to $\Delta^{14}C$ offsets between planktic foraminiferal species with different seasonal habitat preferences, particularly when large $\Delta^{14}C$ differences existed between source waters during deglaciation. The general pattern of planktic $\Delta^{14}C$ and interspecies $\Delta^{14}C$ offsets during deglaciation are consistent with transmission of old carbon to the Baja California surface during HS1 and YD via the equatorial Northern Subsurface Countercurrent (northern Tsuchiya jet) and the California Undercurrent. This is also consistent with the interpretation of Marchitto *et al.* [2007], suggesting that old carbon was advected in AAIW from the Southern Ocean to the low latitude eastern Pacific during HS1 and

YD. We acknowledge that this conclusion remains challenged by the lack of evidence (so far) for significant deglacial ^{14}C depletion near present-day AAIW source areas in the Pacific and Atlantic sectors of the Southern Ocean, but we do not see strong evidence in support of other potential explanations for the ultimate source and routing of aged carbon during deglaciation. Whatever the cause, our observations of high and variable surface reservoir ages during deglaciation suggest that caution must be exercised when using planktic radiocarbon to derive age models and estimates of deep ocean ventilation age, especially in settings influenced by upwelling.

Chapter III: New constraints on deglacial marine radiocarbon variability from a depth transect near Baja California

Abstract:

Reconstructions of initial radiocarbon activity ($\Delta^{14}C$) from the low-latitude, mid-depth Pacific and Indian oceans are anomalously low during the Heinrich 1 (HS1, ~17.8-14.6 ka) and Younger Dryas (YD, ~12.8 -11.5 ka) stadials, coincident with intervals of rising atmospheric CO_2 concentration and declining atmospheric $\Delta^{14}C$. However, a full explanation of these events remains elusive due to sparse and sometimes conflicting data. Here we present new ^{14}C measurements on benthic and planktic foraminifera that, in combination with previously published measurements, enable us to reconstruct the $\Delta^{14}C$ depth gradient near Baja California. Vertical profiles were similar to present during the Last Glacial Maximum and Bolling/Allerod (14.6-12.8 ka), but display a pronounced mid-depth $\Delta^{14}C$ minimum during HS1 and the YD. The latter observation, along with a comparison to other regional reconstructions appear to rule out intermediate and deep waters originating in the North Pacific as the proximate source of aged ocean carbon during deglaciation and point instead to changes in composition of Equatorial Pacific intermediate waters. Simple mixing constraints require Equatorial Pacific intermediate waters to be only slightly lower than at Baja California, in contrast with previous observations of extremely low $\Delta^{14}C$ in at Galapagos Rise. While the latter may have been influenced by localized releases of geologic (^{14}C-dead) CO_2, other upper ocean $\Delta^{14}C$ records would seem to require a source of aged carbon in the deep Southern and Pacific Oceans, for which there is growing evidence.

1. Introduction

Radiocarbon (^{14}C) is a rare radioactive isotope of carbon that is naturally produced by cosmic ray interactions in the upper atmosphere, where it is rapidly oxidized to $^{14}CO_2$ and becomes available for incorporation within the global carbon cycle. The ^{14}C half-life of 5700 years [*Godwin*, 1962; National Nuclear Data Center, Brookhaven National Laboratory, www.nndc.bnl.gov] makes it especially useful for quantification of present and past residence times of carbon within global reservoirs that overturn on centennial to millennial timescales, such as the deep ocean. During the last deglaciation, the large fractional increase in atmospheric CO_2 concentration [*Monnin et al.*, 2001] and the complimentary decrease in its ^{14}C activity ($\Delta^{14}C$) [*Reimer et al.*, 2013] are both suggestive of a significant redistribution of carbon from an anomalously aged, ^{14}C-depleted, carbon-rich ocean reservoir to the atmosphere [*Broecker and Barker*, 2007; *Marchitto et al.*, 2007]. Sediment reconstructions indicating periods of very low initial radiocarbon activity at intermediate ocean depths near Baja California [*Marchitto et al.*, 2007], the Galapagos Archipelago [*Stott et al.*, 2009] and in the Arabian Sea [*Bryan et al.*, 2010] have been interpreted as evidence of this redistribution process, with aged, excess carbon upwelled from a presumed abyssal reservoir in the Southern Ocean and transported (at least in part) to low latitudes via Antarctic Intermediate Water (AAIW). Observational support for a ^{14}C-depleted reservoir of excess carbon in the deep glacial Southern and Pacific Oceans continues to mount [*Sikes et al.*, 2000; *Skinner et al.*, 2010, 2014; *Burke and Robinson*, 2012; *de la Fuente et al.*, 2015; *Keigwin and Lehman*, 2015; *Tiedemann et al.*, 2015] and there is also strong evidence for transiently high CO_2 and nutrient concentrations in intermediate waters originating from the Southern Ocean during deglaciation [*Spero and Lea*, 2002; *Anderson et al.*, 2009; *Allen et al.*, 2015; *Carriquiry et al.*, 2015; *Martínez-Botí et al.*, 2015]. However, complimentary evidence for

anomalously low $\Delta^{14}C$ near AAIW source areas in the Southern Hemisphere is still lacking [*De Pol-Holz et al.*, 2010; *Rose et al.*, 2010; *Cléroux et al.*, 2011; *Sortor and Lund*, 2011; *Burke and Robinson*, 2012; *Siani et al.*, 2013]. Adding to the problem is the growing suspicion that the ^{14}C signal from at least one intermediate-depth location off of the Galapagos Archipelago has been influenced by local sources of volcanic CO_2, leading to anomalously low $\Delta^{14}C$ values [*Stott and Timmermann*, 2011]. Consequently, our understanding of previously observed deglacial radiocarbon anomalies remains incomplete.

Here we present time series of ^{14}C measurements and estimated initial $\Delta^{14}C$ from cores near Baja California that, together with previous results from Marchitto et al. [2007] and Lindsay et al. [2015], constitute a depth transect from the surface to 1270 m modern water depth, enabling us to constrain the local vertical gradients of $\Delta^{14}C$ during deglaciation. We also present a high resolution benthic oxygen isotope record that, in the context of $\delta^{18}O$ and $\Delta^{14}C$ records from other regional cores, provides information on the lateral mixture of water masses near Baja California and likely regional end-member $\Delta^{14}C$ values, none of which would seem to require anomalous contributions from local geologic sources. Taken together, our analysis suggests that transient deglacial $\Delta^{14}C$ minima off Baja California were not caused by upward mixing of North Pacific Deep Water or lateral addition of North Pacific Intermediate Water, and were more likely influenced by waters coming from the Equatorial Pacific, with a probable origin in the deep Southern and Pacific Oceans.

1.1 Study Site and Regional Context

Cores MV99-PC10, MV99-PC08 and MV99-GC38 form a depth transect at modern water depths of 432, 705 and 1270 m, respectively, on the western margin of Southern Baja

California [*van Geen et al.*, 2003]. The core sites lie near the present-day mixing boundary of fresh, cold North Pacific Intermediate Water (NPIW) and salty, warmer Equatorial Pacific Intermediate Water (EqPIW). In an effort to characterize these two water masses (or their regional analogs) in the past, we also discuss published data from two sediment cores retrieved from intermediate water depths to the north and south of Baja California: Santa Barbara Basin core ODP893A [SBB, 34° N, modern sill depth 475 m, *Hendy & Kennett*, 2003] and Galapagos Rise core VM21-30 [1° S, 617 m, *Koutavas et al.*, 2006; *Stott et al.*, 2009].

Figure 3.1 shows the locations of these cores with respect to contoured salinity values and estimated "natural" (i.e., pre-industrial, pre-nuclear) $\Delta^{14}C$ of waters in the 27.1 kg/m^3 σ_θ density anomaly layer which occupies a mean depth of ~625 m along the eastern Pacific margin, close to that of the relevant core (and sill) depths. At this density level the deepest and densest NPIW circulates clockwise from its formation region in the northwest northern Pacific [*Talley*, 1993; *You*, 2003; *Bostock et al.*, 2010]. The saltier EqPIW south of Baja California is formed by mixing between Antarctic Intermediate Water (AAIW) and North Pacific Deep Water [NPDW; *Bostock et al.*, 2010] in narrow intermediate-depth zonal jets passing through the shadow zone within ~10° of the equator [*Firing et al.*, 1998; *Cravatte et al.*, 2012]. Both NPIW and EqPIW overlie NPDW with a transitional boundary between ~1000-1500 m [*Fiedler and Talley*, 2006; *Bostock et al.*, 2010]. Nearer the surface, the California Undercurrent (CU) carries warm, high-salinity Equatorial Subsurface Water (ESSW) north along the shelf break near Baja California [*Hickey*, 1979; *Lynn and Simpson*, 1987], raising subsurface temperatures and salinities in waters with densities ranging from ~25.5-27.2σ_θ and at depths of ~100-500 m (Figs. 3.2 and 3.3). The ESSW in the CU is probably sourced from the northern Tsuchiya jet (also know as the Northern Subsurface Countercurrent), an eastward-flowing jet just below the equatorial Pacific

thermocline that carries a mixture of AAIW, high-salinity North Pacific Eastern Subtropical Mode Water (NPESTMW) and, possibly, also NPIW [*Fiedler and Talley*, 2006].

Mixing between northern and equatorial source waters is clearly evident in climatological salinity and temperature profiles along the Pacific Margin [*Locarnini et al.*, 2013; *Zweng et al.*,

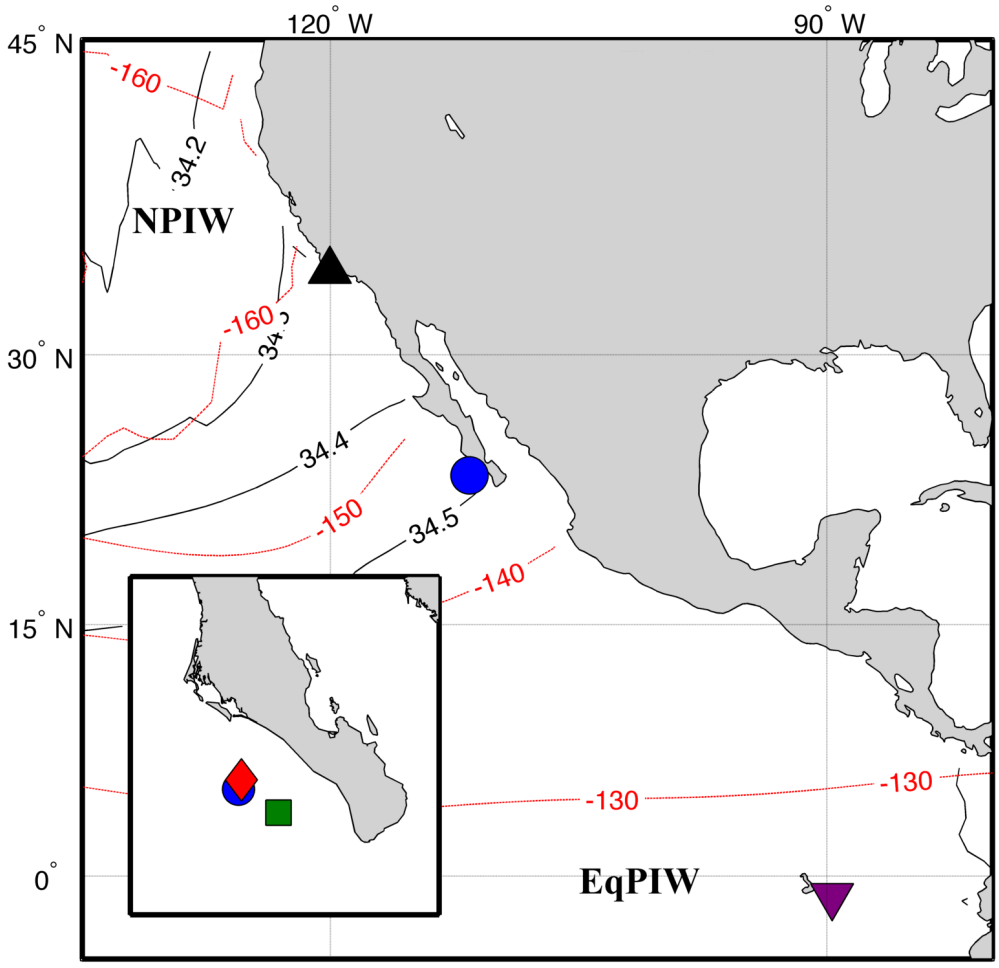

Figure 3.1: Symbols show the locations of cores with benthic records discussed in this paper, plotted with contoured mean salinity (psu, solid black lines, World Ocean Atlas 2013 [WOA13; *Zweng et al.*, 2013]) and estimated natural radiocarbon (‰, dashed red lines, GLODAP [*Key*, 2004]) of waters with density anomaly (σ_θ) values of 27.1 ± 0.05 kg/m^3. Inset shows a zoomed-in view of core locations near Baja California. Cores shown are Santa Barbara Basin core ODP893A (black triangle; *Hendy & Kennett*, 2003), Baja California cores MV99-MC19/GC31/PC08 (blue circle), MV99-PC10 (red diamond) and MV99-GC38 (green square) [*Van Geen et al.*, 2003], and Galapagos Rise core VM21-30 (purple inverted triangle; [*Koutavas et al.*, 2006]). Regions are labeled where North Pacific Intermediate Water (NPIW) and Equatorial Pacific Intermediate Water (EqPIW) occupy this density layer.

2013] (Figs. 3.2 and 3.3). At the location and depth of our Baja Margin transect, absolute S and T values suggest a greater contribution of EqPIW than NPIW, while ESSW carried by the CU dominates above to depths up to ~100 m. NPIW in its strict sense (defined by a salinity minimum at intermediate depth) is not observed this far east in the modern North Pacific [*Talley*, 1993; *You*, 2003], but we will follow other authors [e.g. *Hendy and Kennett*, 2003; *Bostock et al.*, 2010] and use the term NPIW for the fresher North Pacific water affecting the California margin at intermediate depths.

2. Methods

2.1 ^{14}C Methods and Derived Values

Monospecific samples of the planktic foraminifer *G. ruber*, as well as samples of the benthic foraminifera *Uvigerina spp*, were picked from the >250 μm size fraction of washed sediment from cores MV99-PC10 and MV99-GC38. In some cases, samples that were too small for radiocarbon measurement were brought up to weight by adding foraminifera from the 150-250 μm size-fraction. All ^{14}C samples were prepared at the INSTAAR Laboratory for AMS Radiocarbon Preparation and Research (NSRL) before measurement by Accelerator Mass Spectrometry at the Keck Carbon Cycle AMS Laboratory at the UC Irvine (KCCAMS). Picked foraminifera were leached for 5 minutes in a 0.001 M solution of HCl. Each sample was then reacted with H_3PO_4 and the CO_2 produced was cryogenically purified. The purified CO_2 was reduced with H_2 in the presence of a Fe catalyst and the resulting graphite was packed into AMS targets and sent to KCCAMS.

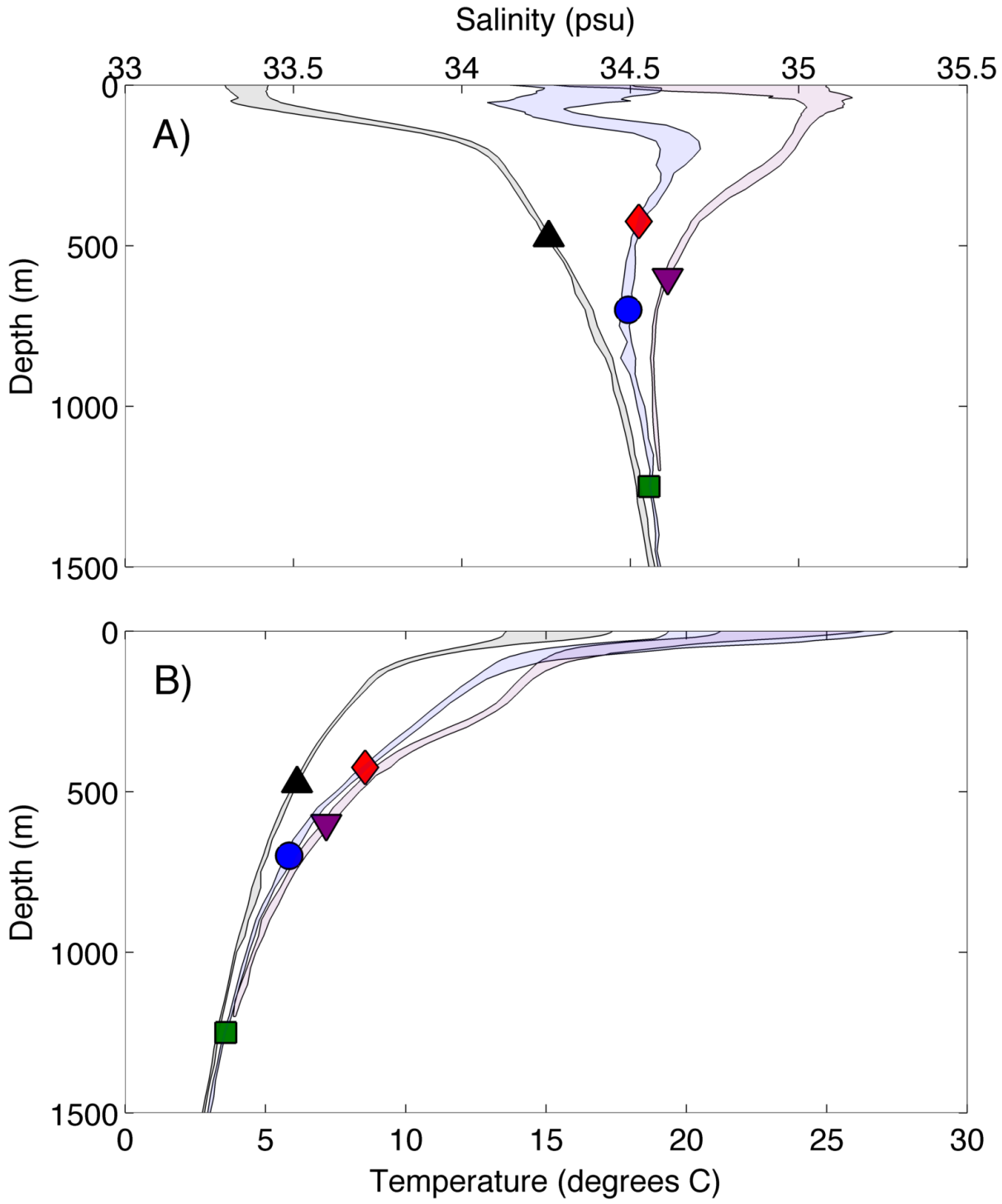

Figure 3.2: Shaded envelopes show the annual range of **A)** monthly mean salinity and **B)** temperature depth profiles from WOA13 grid cells closest to the three core locations shown in Figure 3.1. The water or sill depths of all marine cores discussed in this paper are indicated by filled symbols on the matching profiles. Symbols and colors are same as in Figure 3.1.

Benthic-Planktic (B-P) age differences were calculated by subtracting the conventional planktic ^{14}C age from the conventional benthic ^{14}C age in samples where both were measured. In cases where benthic and planktic measurements were not paired directly, B-P age differences were estimated by subtracting the linearly interpolated planktic ^{14}C age from the benthic ^{14}C age measured at a given level. Decay-corrected initial radiocarbon activities [$\Delta^{14}C$; *Stuiver & Polach*,

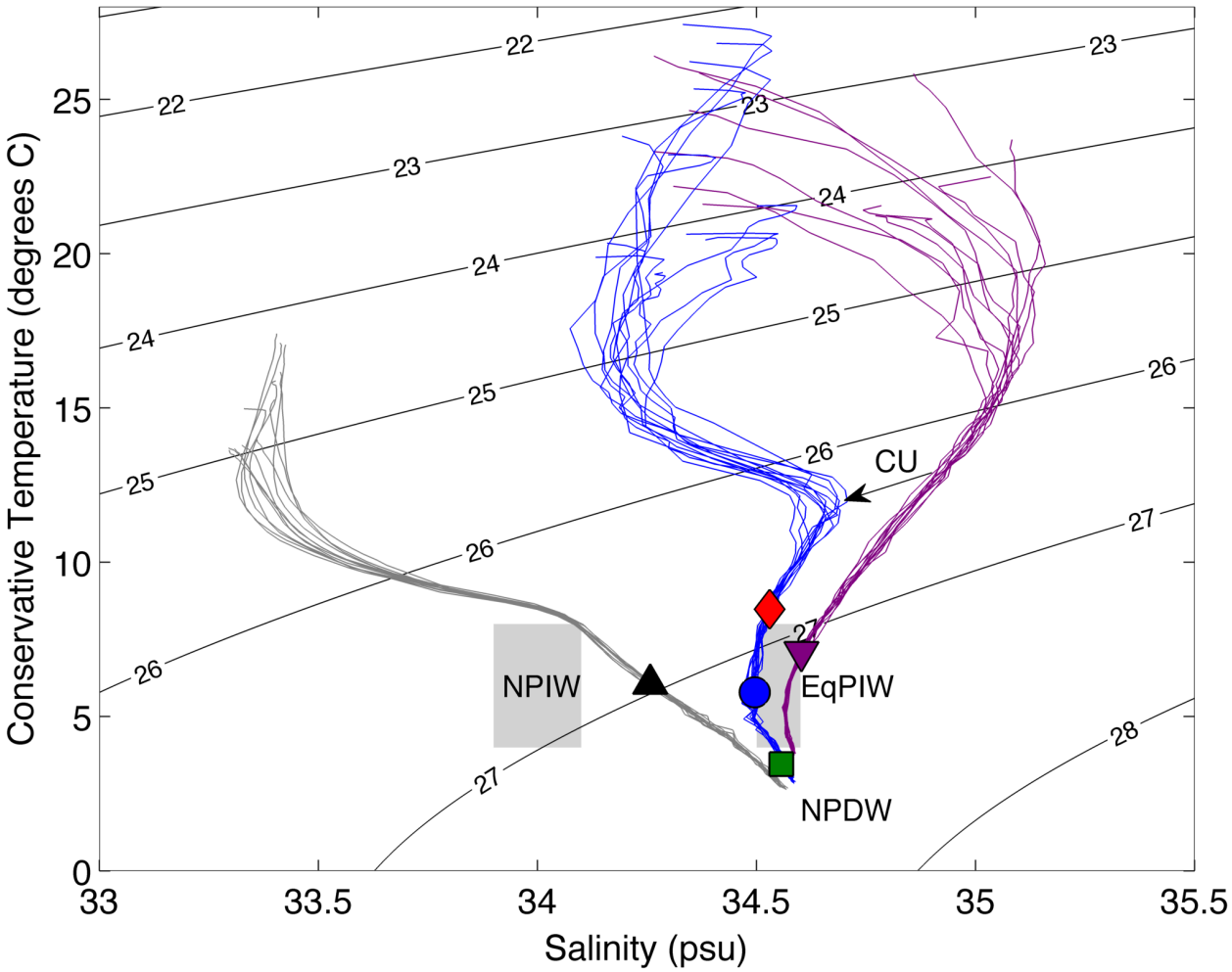

Figure 3.3: WOA13 monthly mean temperature profiles plotted vs. monthly mean salinity for the three core locations, with contoured density anomaly (σ_θ) values. Cores are plotted at their annual mean values according to the WOA13 grid cell closest to their location and water or sill depth, with the same symbols as in Figure 3.1. Grey rectangles and labels show salinity and temperature ranges of NPIW, EqPIW and NPDW from *Bostock et al.*, [2010] and the transport of ESSW by the CU is represented by an arrow. Density anomaly was estimated using the Gibbs Seawater Oceanographic Toolbox [*MacDougall and Barker*, 2011].

1977] were calculated for all deglacial ^{14}C results, using the measured conventional ^{14}C age and estimates of calendar age and its uncertainty from age-depth modeling described below (section 2.4).

2.2 Stable Isotope Methods

Stable isotope ratios of carbon and oxygen (‰ vs. PDB) were measured in monospecific samples of *Uvigerina peregrina* from core PC08 on an OPTIMA mass spectrometer interfaced to an automated common acid bath (ISOCARB) at the Instituto de Investigaciones Oceanológicas of the Universidad Autónoma de Baja California, Mexico. Sediment samples were washed and wet-sieved at 250, 125, and 63 μm. Foraminifera were picked manually under a stereoscopic microscope, oven-dried and stored in vials. Before analysis, foraminifera samples were heated to 350° C in order to eliminate hydrolyzable organic matter. Between 5 and 11 foraminifera tests within the 125-250 μm size fraction were used for each isotopic analysis. Samples were reacted at 90° C in orthophosphoric acid (specific gravity = 1.92 g cm^{-3}) to generate carbon dioxide and water. During each run sequence, an in-house standard MIIO Marble calibrated against NBS-19 (National Bureau of Standards) was used to correct the data, including a drift correction. Corrected delta values are expressed relative to PDB (PeeDee Belemnite) international standards for $\delta^{13}C$ and $\delta^{18}O$. The external precision of the isotopic measurements were <0.04‰ for both $\delta^{18}O$ and $\delta^{13}C$. A low-resolution version of this record has previously been published in a compilation of stable isotope measurements from near Baja California [*Carriquiry et al.*, 2015].

2.3 DSR Measurement Methods

Diffuse spectral reflectance (DSR) for all MV99 Baja California cores was measured

shipboard using a Minolta CM-2022 spectrophotometer with 1-cm resolution [*Ortiz et al.*, 2004]. Measurements were conducted on the wet, split surfaces of the sediment cores, which were wrapped in GladWrap™ to prevent contamination of the instruments integration sphere. The DSR measurements were decomposed using a three-component R-mode factor model of the first-derivative transform of the percent reflectance spectra, which is analogous to a varimax-rotated, principle component analysis. The methodology employed with DSR data is more fully described in Ortiz [2011]. Empirical correlation documents that DSR factor 3 is closely related to down core variation of organic carbon concentration and bears a strong resemblance to Greenland oxygen isotope records [*Ortiz et al.*, 2004], a finding that was previously used to tie core PC08 to the GISP2 layer-counted calendar age model [*Marchitto et al.*, 2007].

2.4 Age-depth Modeling

Calendar age models for the Baja California cores PC10 and GC38 were constructed by tying them to the GISP2-based age model for PC08 [*Marchitto et al.*, 2007]. This was achieved primarily by mapping of planktic ^{14}C results from cores PC10 and GC38 onto those for PC08 [*Lindsay et al.*, 2015], based on the expectation that local gradients in $\Delta^{14}C$ of near surface waters remained negligible. This approach was supplemented by between-core correlation of sedimentary reflectance data only where ^{14}C results were unavailable due to low carrier abundance or showed significant scatter (see Supplemental Figs. S1 and S2 in Appendix C). Reflectance data were otherwise reserved for *post facto* evaluation of the ^{14}C-derived age models.

In previous work, PC08 ^{14}C results for the planktic foraminifera *Globigerinoides ruber*, *Globigerina bulloides* and *Globigerinoides sacculifer* revealed large changes in apparent

reservoir age during deglaciation, with *G. ruber* generally showing the most coherent (least noisy) trends over time [*Lindsay et al.*, 2015]. We thus use the PC08 *G. ruber* ^{14}C – calendar age relationship as a species-specific local reference curve in order to derive calendar age estimates for the other cores, free of assumptions regarding the magnitude and uncertainty of past reservoir ages that are otherwise required of conventional marine ^{14}C calibration algorithms. To create the local reference curve, the PC08 *G. ruber* record was interpolated between ^{14}C measurements using a Monte Carlo approach that allowed for greater uncertainty at points farther from measurements (see supplemental methods in Appendix C). *G. ruber* ^{14}C measurements from PC10 and GC38 were then mapped onto the reference curve using the standard statistical method recommended for use with INTCAL calibration curves [*Stuiver et al.*, 2005], resulting in probability density distributions (PDFs) of calendar age for each measurement.

The PCA Factor 3 of the Diffuse Spectral Reflectance (DSR) of Baja California cores is closely tied to organic carbon content, and its downcore variation most likely indicates changes in regional productivity during deglaciation [*Ortiz et al.*, 2004]. It is therefore reasonable to expect that changes in DSR Factor 3 should have occurred in all three cores more or less simultaneously, although the signal may be expected to decrease with depth below the Oxygen Minimum Zone. We chose DSR tie points between the two new cores and PC08, with estimated normally-distributed 1-σ age uncertainties of ±200 years. In core GC38, no DSR-based tie-points younger than ~32ka were assigned (see Supplemental Fig. S2 in Appendix C), permitting the use of DSR agreement during deglaciation as an independent check on the planktic ^{14}C-based match to the PC08 age model. In core PC10, two DSR tie points were used in the deglacial interval because of insufficient planktic abundance in the uppermost section, and ^{14}C age reversals in the lower section.

^{14}C- and DSR- derived PDFs are shown to depth for the deglacial sections of the target cores in Figure 3.4. ^{14}C-derived PDFs are broad in many cases due to the presence of age plateaus in the planktic ^{14}C record from PC08 (see Supplemental Figs. S1 and S2 in Appendix C). A population of age-depth models was created by randomly selecting ages from the individual PDFs using a Monte Carlo approach, but discarding any age model resulting in an age reversal or intervals of excessively high sedimentation rate. For the upper bounds of the sedimentation rate filter, we used 30 cm/ka for GC38 and 60 cm/ka for PC10. To account for the fact that age uncertainties will be larger with core distance from levels with either ^{14}C- or DSR-derived PDFs, we interpolated between these levels in both directions using a second Monte Carlo step that randomly sampled a population of sedimentation rates defined by the mean and 1σ standard deviation of all previously permitted realizations of the sedimentation rate in a particular core. In essence this assumes that the low frequency variability in sedimentation rate revealed by our age-depth modeling is a reasonable approximation of the potential high frequency variability between depths with explicit age control. The resultant set of age models are depicted by the black line with grey envelope (median age and 1-σ range) for each core in Figure 3.4.

In GC38, the raw ^{14}C data is relatively smooth throughout the deglacial period (see Supplemental Fig. S1 in Appendix C), suggesting that sedimentation was continuous over that interval, although the probability density distributions of age for *G. ruber* ^{14}C in GC38 indicate a period of rapid sedimentation around 14.5 ka. We omitted the middle two *G. ruber* ^{14}C dates in this segment from our calculations to reduce the computation time needed to accumulate a large number of realizations passing the sedimentation rate filter (see Fig. 3.4). Because of the relatively high sedimentation rate implied by the bracketing measurements, the ages of the

intervening depths are still well constrained.

In PC10, the section below about 4.5 mcd was previously found to contain a hiatus [*Van Geen et al.*, 2003], possibly because of winnowing at the core location during the period of low sea level prior to ~15 ka [*Dean et al.*, 2006]. Our ^{14}C measurements between 4.5 and 3.4 mcd are scattered and contain multiple age reversals (Supplemental Fig. S2 in Appendix C) and a very large negative B-P age (-1300 ^{14}C years at 3.41 mcd). We considered this evidence that sedimentation was disturbed up to at least 3.4 mcd, and excluded deeper results from all following figures. One ^{14}C-derived PDF at 3.06 mcd, and two from below 3.2 mcd were omitted from the Monte Carlo calculations to reduce computation time (Fig. 3.4). The two *G. ruber* PDFs

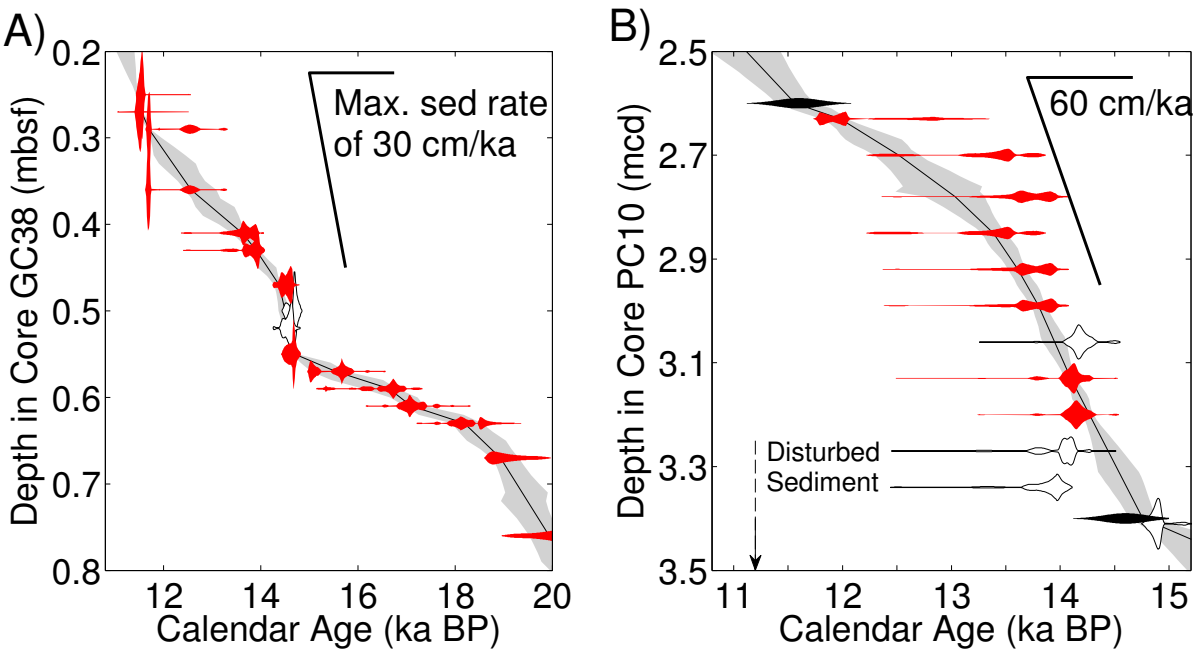

Figure 3.4: Age models for **A)** core GC38 and **B)** core PC10. Filled shapes show the probability density distributions of calendar age vs. depth in core from DSR tiepoints (filled black) and *G. ruber* ^{14}C (filled red) that were used to construct each age model. Distributions from *G. ruber* ^{14}C dates that were left out of the Monte-Carlo age model step are plotted as empty white shapes. The resulting age models following Monte-Carlo filtering and interpolation (see text for details) are shown by the solid black lines and grey 1-sigma uncertainty envelopes.

below 3.2 mcd cause an age reversal that hints that the sediment disturbance may extend up to about 3.2 mcd, but is not conclusive. Therefore we indicate potential sediment disturbance below 3.2 mcd in Figure 3.4 and Supplemental Figure S2 (see Appendix C), but retain the data from between 3.2 and 3.4 mcd in our results figures. The revised age model for PC10 places the start of undisturbed sedimentation in PC10 at ~14.3 – 14.6 ka (Fig. 3.4).

It is important to note that the primary aim of the age-depth modeling here is to create a common chronology that attempts to minimize between-core differences of estimated calendar age during the deglacial study interval, rather than to derive the most accurate possible estimate of absolute calendar age and age uncertainty. Thus, we do not attempt to propagate additional uncertainty or bias associated with the underlying PC08 and GISP2 age models. Any such shared biases would have only a very small influence on reconstructed vertical $\Delta^{14}C$ gradients between cores, since individual $\Delta^{14}C$ estimates assigned to similar calendar ages in different cores would move along age-decay trajectories together.

3. Results and Discussion

In Figure 3.5 we show estimated planktic and benthic $\Delta^{14}C$, DSR, sedimentation rates, and B-P age differences for all three Baja California cores on the common age model, along with an estimate of atmospheric $\Delta^{14}C$ from INTCAL13 [*Reimer et al.*, 2013]. Similar estimates of *G. ruber* $\Delta^{14}C$ for cores PC08 and GC38 confirm that the local ^{14}C age-based method of mapping the calendar age model from core PC08 into GC38 will deliver comparable $\Delta^{14}C$, as expected based on our *a priori* assumptions. The same is true of core PC10, but with somewhat larger discrepancies as a result of disturbed sediment older than about 14.3 ka BP and use of a DSR tie point at 11.6 ka BP.

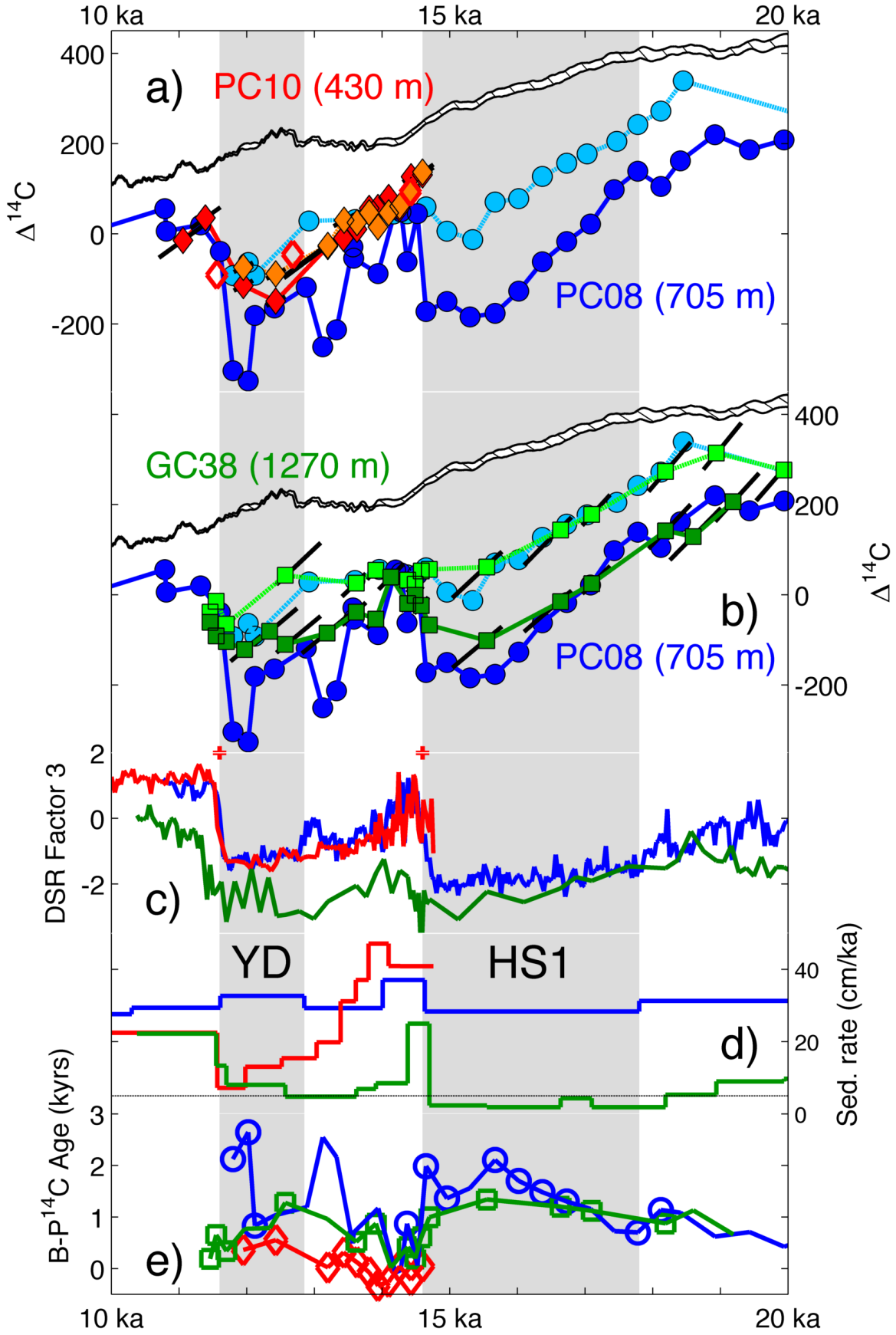
10 ka
15 ka
20 ka
a)
PC10 (430 m)
PC08 (705 m)
Δ14C
400
200
0
-200
GC38 (1270 m)
b)
PC08 (705 m)
DSR Factor 3
2
0
-2
c)
YD
HS1
d)
Sed. rate (cm/ka)
40
20
0
B-P14C Age (kyrs)
3
2
1
0
e)

Figure 3.5: Results from the Baja California margin plotted versus time. **a)** *Uvigerina* spp. (red filled diamonds), mixed benthic (open red diamonds; and *G. ruber* (orange filled diamonds) $\Delta^{14}C$ from core PC10 (432 m), compared to benthic (dark blue filled circles) and *G. ruber* (light blue filled circles) $\Delta^{14}C$ from core PC08 [705 m; *Lindsay et al.*, 2015; *Marchitto et al*., 2007] and INTCAL13 atmospheric $\Delta^{14}C$ [hatched field; *Reimer et al.*, 2013]. Solid black error lines connect the values from combined measurement and calendar age uncertainties. **b)** Benthic (dark green filled squares) and *G. ruber* (light green filled squares) $\Delta^{14}C$ from core GC38 (1270 m), compared to *G. ruber* (light blue filled circles) and benthic (dark blue filled circles) $\Delta^{14}C$ from core PC08 and INTCAL13 atmospheric $\Delta^{14}C$ (hatched field). Solid black error lines connect the values from combined measurement and calendar age uncertainties. **c)** PC10 (red line), GC38 (green line) and PC08 (blue line) DSR Factor 3. To aid visual comparison over this time period, GC38 DSR Factor 3 was shifted towards the other records by adding 4 normalized units. **d)** PC10 (red line), GC38 (green line) and PC08 (blue line) accumulation rates. The thin black line indicates the 5cm/ka level. Red plus signs mark the ages of two DSR-based tiepoints used in the PC10 age model. **e)** PC10 paired BP ages (red open diamonds and red line), all (green line) and paired only (open green squares) GC38 BP ages (green open squares), all (blue line) and paired only (open blue circles) PC08 BP ages. Gray vertical fields indicate the age ranges of Heinrich Stadial 1 (HS1) and the Younger Dryas (YD).

When placed on the common age model, the timing of changes in B-P ^{14}C age difference (Fig. 3.5e) are also similar between the three cores, suggesting that there are not large inter-core biases in the chronologies. In addition, changes in DSR Factor 3 during the deglacial study interval in GC38, which as noted earlier were not used for derivation of the age model after ~30 ka, are consistent with DSR changes seen in PC08 (Fig. 3.5c). The same is true for DSR variations in PC10 between assigned DSR tie-points at ~11.6 and 14.6 ka, providing additional confidence in the age alignment of all three cores.

3.1 Sedimentation Rate Variations

Variations of sedimentation rate in PC10 and GC38 (Figure 3.5d), while large, are consistent with the DSR changes measured in PC10 and GC38 (Figure 3.5c), which indicate higher productivity during the BA and lower productivity during YD and HS1 [*Ortiz et al.*, 2004, see also Section 2 and Fig. S3.3 in Appendix C]. The relatively constant sedimentation rate

history of PC08 is due to the fact that dry bulk density is observed to decrease in association with increasing organic carbon content, which would act to reduce apparent variations of sedimentation rate associated with primary production [*Ortiz et al.*, 2004]. The original PC08 age model nonetheless indicates a sedimentation rate during the early BA that is ~30% higher than the average rate for the core. The general pattern of sedimentation rate changes required by our age models is also consistent with mass accumulation rates of biogenic material in cores from much of the North Pacific, which indicate a large productivity spike during the BA [*Kohfeld and Chase*, 2011].

3.2 B-P Age Differences

Raw ^{14}C age differences between benthic foraminifera and those of co-deposited planktic foraminifera (or for interpolated planktic ages) show broadly similar time-dependent patterns for all cores, but are frequently largest in core PCO8 from 705 mwd (Fig. 5e). Given the use of a single planktic species for planktic ^{14}C measurements and our *a priori* assumption that spatial gradients of surface water $\Delta^{14}C$ across the study transect were negligible, differences of B-P age between cores are expected to reflect primarily differences of benthic foraminifera age, and thus gradients in ^{14}C age of bottom waters bathing the different sites.

The slightly negative and near-zero B-P ages that we observe in PC10 during the early BA (-300 - 50 ^{14}C yrs) may well be reliable, reflecting a combination of lower sea level and larger seasonal variation in near-surface $\Delta^{14}C$ during the BA than at present. For example, Lindsay *et al.* [2015] observed planktic interspecies $\Delta^{14}C$ differences of 60-100‰ (~400-700 ^{14}C yrs) during deglaciation that they attributed to large $\Delta^{14}C$ differences between the northern and southern source waters that seasonally affected the upper water column near core PC08. Lowest

values were recorded by *G. ruber,* reflecting the larger reservoir age (lower $\Delta^{14}C$) of upwelling southern-sourced waters during late summer and fall when this species is thought to be most abundant [*Lindsay et al.*, 2015]. Global eustatic sea levels that were then ~90 m lower than today [*Fleming et al.*, 1998] may also have caused benthic foraminifera in the shallow PC10 core location to experience seasonal $\Delta^{14}C$ changes comparable to those at the surface. However, in contrast to the planktic species, the benthic species are expected to calcify throughout the year. Thus negative B-P ages during the early BA may reflect the difference between the negative extreme (*G. ruber*) and mean value (benthics) of the seasonal cycle of $\Delta^{14}C$ near the surface.

3.3 $\Delta^{14}C$ Results

As suggested by the B-P ages, the $\Delta^{14}C$ results from core GC38 reveal that $\Delta^{14}C$ at 1270 m water depth was low relative to the atmosphere, but 100-200‰ higher than in PC08 during the anomalous depletion events of HS1, late BA and YD (Fig. 5b). Benthic $\Delta^{14}C$ in PC10 was likewise ~150‰ lower with respect to atmosphere during the YD than during the BA, but was consistently 50-200‰ higher than in PC08 during the late BA and YD (Fig. 5a). This suggests that the most ^{14}C-depleted waters near Baja California during transient $\Delta^{14}C$ anomalies occurred in the vicinity of PC08 (705 m), with a $\Delta^{14}C$ minimum somewhere between the depths of GC38 (1270 m) and PC10 (420 m).

3.4 Vertical $\Delta^{14}C$ Gradients

To visualize the $\Delta^{14}C$ depth gradient over time, we averaged the difference between estimated benthic foraminiferal $\Delta^{14}C$ for the available Baja Margin records and that of the coeval atmosphere [*Reimer et al.*, 2013] over the time periods YD, early BA (14.6-13.5 ka), HS1, and

the Last Glacial Maximum (LGM, here defined as 20-17.8 ka with an upper age limit based on the length of the GC38 benthic record). Time-averaged offsets from the atmosphere are expressed as $\Delta\Delta^{14}C$ and compared to the closest depth profiles of estimated "natural" $\Delta^{14}C$ from GLODAP [*Key*, 2004] in Figure 3.6. No adjustment was made to the profiles to account for changing water depths due to lower sea levels in the past.

Some degree of negative deviation from the modern profile (including the surface) may be expected as a result of both reduced atmospheric CO_2 concentration and elevated atmospheric ^{14}C activity relative to today. For example, given constant gas transfer velocity, the air-sea exchange of CO_2 (and the associated isotopic exchanges) will scale directly to the atmospheric CO_2 burden. Thus, lower CO_2 levels during the LGM and deglaciation should be expected to produce lower $\Delta\Delta^{14}C$ at the ocean surface (i.e. greater surface reservoir age [*Bard*, 1988]) and also at depth where signatures were influenced by surface conditions in outcrop regions elsewhere. Elevated atmospheric $\Delta^{14}C$ may also be expected to increase $\Delta\Delta^{14}C$ at depth for any given absolute ventilation age (time since surface equilibration) due to the exponential dependence of radioactive decay on initial ^{14}C activity. The small negative deviations from the modern profile that we observe for the LGM and the BA are likely due to a combination of these processes and would not seem to require significant changes in the regional circulation of the upper ocean.

The average gradients during HS1 and the YD had a notably different structure, with substantially lower $\Delta\Delta^{14}C$ at every depth and a conspicuous minimum at mid-depth (shallower than 1270 m modern water depth). During the YD, the addition of data from PC10 also allows us to constrain the $\Delta^{14}C$ minimum to deeper than 430 m modern water depth. The large negative deviation from the modern profile and the mid-depth $\Delta\Delta^{14}C$ minimum are together indicative of

significant changes in source water $\Delta^{14}C$ and, possibly, in the physical circulation.

Waters at depths of 500-1000 m near Baja California today are influenced predominately by EqPIW and NPIW, while unmodified NPDW lies beneath a transition zone at ~1000-1500 m

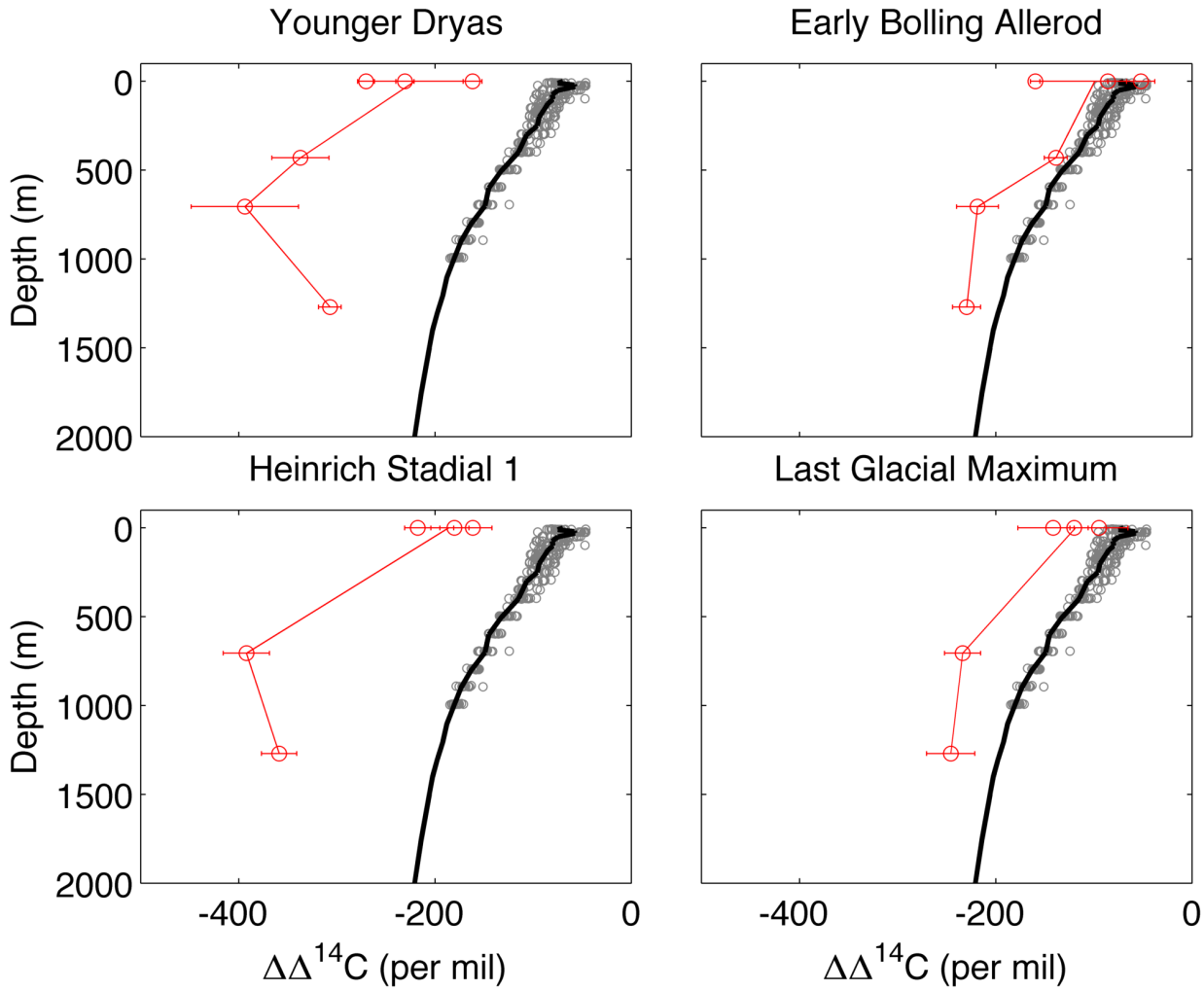

Figure 3.6: Average $\Delta\Delta^{14}C$ depth profiles from Baja California cores compared to modern observations. Depth profiles of reconstructed $\Delta\Delta^{14}C$ (red lines and open circles, calculated as core $\Delta^{14}C$ minus coeval INTCAL13 atmospheric $\Delta^{14}C$) were averaged over four time periods (YD: 12.85-11.6 ka, early BA: 14.6-13.5 ka, HS1: 17.8-14.6 ka, LGM: 20-17.8 ka). Averages are plotted at the surface for all three planktic species measured in PC08; the central surface value that each depth profile connects to is the average of the three planktic values from that time period. Horizontal error bars on the open red circles are the standard error of the mean. Estimated pre-industrial, pre-nuclear $\Delta\Delta^{14}C$ GLODAP bottle data[*Key*, 2004] from sites just south of Baja California (24-17° N) are plotted in each panel along with a depth profile from GLODAP gridded pre-industrial, pre-nuclear $\Delta\Delta^{14}C$ data (heavy black line;[*Key*, 2004] from the grid-cell 1° west of the site of GC38 (necessary because of the resolution of GLODAP bathymetry.)

(see section 1.1). As can be seen from the modern $\Delta^{14}C$ gradient (Figure 3.6), modern NPDW (water deeper than ~1500 m) has lower $\Delta^{14}C$ than modern intermediate water near Baja California. The profiles observed during HS1 and the YD suggest that cold periods near Baja California were associated with a reversed vertical $\Delta^{14}C$ gradient between upper deglacial NPDW and overlying intermediate waters, requiring that low $\Delta^{14}C$ waters arrived laterally, since they could not have been produced by upward mixing of deglacial NPDW with relatively high $\Delta^{14}C$ below.

We note that our reconstructed profiles and related conclusions are relatively robust to uncertainties in age modeling or differential bioturbation and dissolution, due to generally high sedimentation rates of the studied cores, averaging of signals over several kyr for each time interval, and the fact that any age biases shared amongst cores during particular intervals will have little affect on estimated gradients of $\Delta^{14}C$. A recent suggestion that the benthic $\Delta^{14}C$ anomalies in PC08 are artifacts caused by the GISP2-tuned age model of PC08 [*Davies-Walczak et al.*, 2014] is incompatible with the large B-P ages (which are independent of the age model) that we observe coincident with the benthic anomalies in PC08 [*Lindsay et al.*, 2015] and now GC38 (Fig. 5). This is illustrated by an alternative age model, based on PC08 planktic ^{14}C and an assumption of constant surface reservoir age, which fails to substantially influence the inferred magnitude and timing of the PC08 benthic $\Delta^{14}C$ anomalies [*Lindsay et al.*, 2015, online supplement]. Removing the sedimentation rate limits used in our age modeling would result in slightly different $\Delta^{14}C$ estimates for PC10 and GC38, guided by more perfect *G. ruber* agreement with PC08, but the time-averaged $\Delta^{14}C$ depth gradients would not change substantially.

3.5 Lateral Water Mass Mixing

Our reconstructions of the vertical $\Delta^{14}C$ gradient off of Baja California indicate that negative deglacial $\Delta^{14}C$ anomalies were largest during the HS1 and YD Northern Hemisphere cold periods, with $\Delta^{14}C$ minima occurring consistently at or near the depth of core PC08 (705 mwd). This suggests that the PC08 site was influenced by lateral advection of low ^{14}C waters and not directly by upward mixing of local deep waters. Today the site lies on density levels associated with NPIW to the north and EqPIW to the south, with NPIW characterized regionally by $\Delta^{14}C$ values that are ~30 ‰ lower than in EqPIW (Fig. 3.1).

To characterize the $\Delta^{14}C$ of these sources during deglaciation, we show on the lower axes of Figure 3.7 benthic $\Delta^{14}C$ results from Galapagos Rise core VM21-30 [*Stott et al.*, 2009] and SBB core ODP 893a [*Hendy et al.*, 2002; *Magana et al.*, 2010], along with Baja California core PC08 [*Marchitto et al.*, 2007; *Lindsay et al.*, 2015] and a $\Delta^{14}C$ reconstruction for northern NPIW based on a subset of results in Okazaki *et al.* [2010] for cores lying north of 35°N and above 1000 mwd. In the case of SBB core ODP 893a, ^{14}C results for samples containing the deep infaunal benthic taxon *Pyrgo* have been excluded as they are likely biased by old sources of organic carbon [*Magana et al.*, 2010]. To characterize SBB $\Delta\Delta^{14}C$ when local observations are not available, we added a 75‰ offset to the smoothing spline fit through the Okazaki et al. [2010] results. All $\Delta^{14}C$ results are given as the estimated offset from the coeval atmosphere (INTCAL13 [*Reimer et al.*, 2013], expressed as $\Delta\Delta^{14}C$. The available results would seem to require a N-S $\Delta^{14}C$ gradient during deglaciation opposite to the modern one, with relatively elevated $\Delta^{14}C$ in NPIW and substantially lower $\Delta^{14}C$ to the south in EqPIW or its deglacial analog. A similar conclusion could be reached in the absence of the VM21-30 record, since low ^{14}C waters reaching the location of PC08 could not have been sourced either from below or from

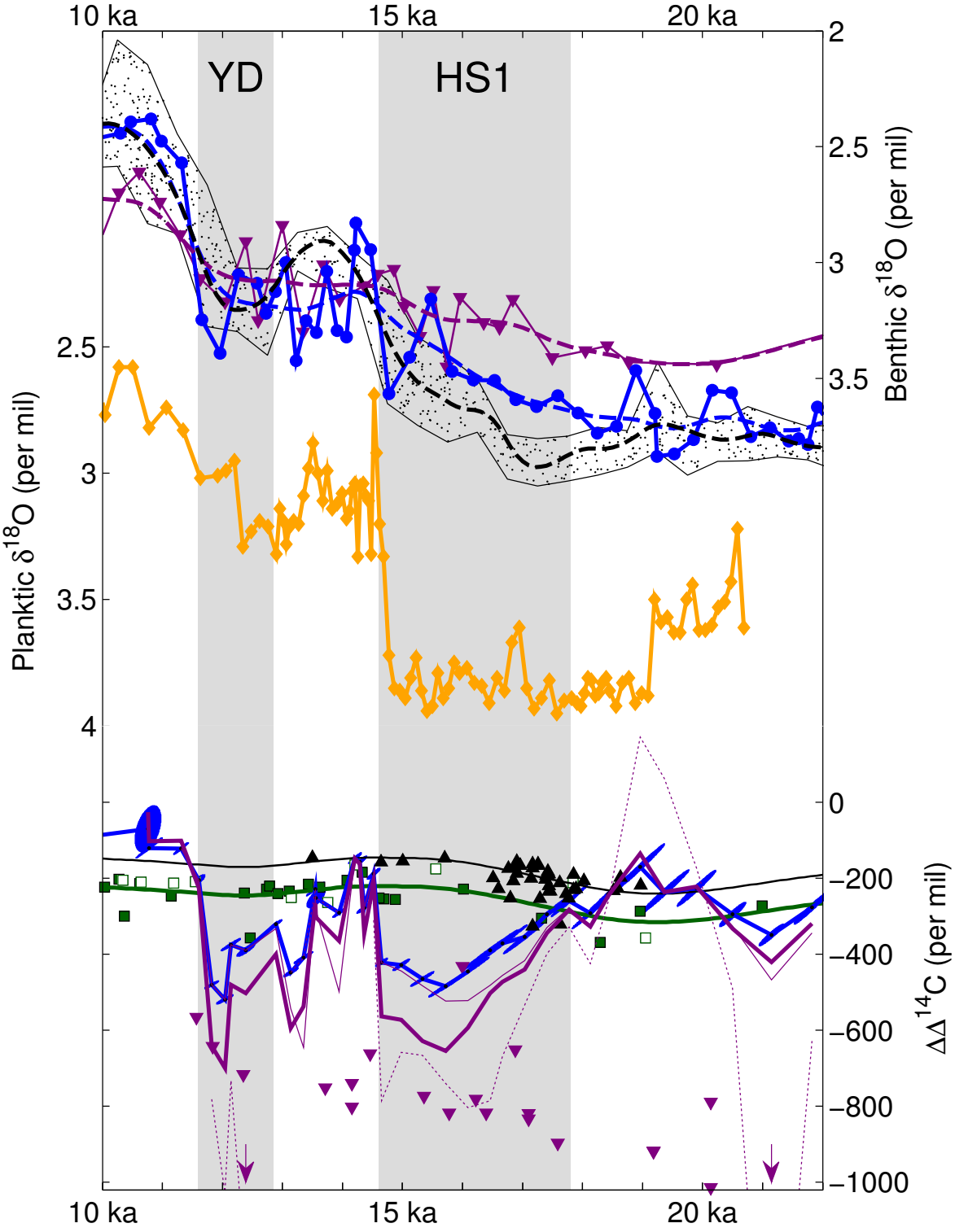
10 ka
15 ka
20 ka
YD
HS1
Planktic δ18O (per mil)
Benthic δ18O (per mil)
ΔΔ14C (per mil)
2
2.5
3
3.5
4
0
−200
−400
−600
−800
−1000

Figure 3.7: Comparison of regional $\delta^{18}O$ and $\Delta\Delta^{14}C$ records. **Top:** $\delta^{18}O$ data from Baja California core PC08 (blue filled circles and thin line, this study, bold dashed blue line is smoothing spline), Galapagos Rise core VM21-30 (purple inverted triangles and thin line; [*Koutavas et al.,* 2006], shown on the age model of Stott *et al.,* [2009]; bold dashed purple line is smoothing spline) and the 90 percentile range of 500-year windows of SBB cores ODP893A and MD2503 (black speckled envelope, [*Hendy & Kennett*, 2003, *Hill et al.,* 2006], bold dashed black line is smoothing spline). **Middle:** *N. pachyderma* sinistral $\delta^{18}O$ from core MD02-2489 (yellow diamonds, [*Gebhardt et al.*, 2008] on the updated age model of Rae *et al.* [2014]. **Bottom:** Benthic $\Delta\Delta^{14}C$ from PC08 (blue solid line and ellipses; [*Lindsay et al.*, 2015; *Marchitto et al*., 2007]), the Galapagos Rise (purple inverted triangles; [*Stott et al.*, 2009], all available *Pyrgo*-free SBB data (black triangles, [*Hendy et al.*, 2002; *Magana et al.*, 2010]), and a subset of the compilation of Okazaki *et al*. [2010] (north of 35°N and shallower than 1000 m from the NE Pacific (filled green squares) and NW Pacific (open green squares), with a smoothing spline to all data (solid green line)). Also shown is estimated Galapagos Rise $\Delta\Delta^{14}C$ based on PC08 and estimated SBB $\Delta\Delta^{14}C$ (black line, equals Okazaki spline fit plus 75‰), calculated using source water mixtures from modern T and S (bold purple line), unadjusted $\delta^{18}O$ gradients (thin dotted purple line), and adjusted $\delta^{18}O$ gradients (thin solid purple line). $\Delta\Delta^{14}C$ is calculated by subtracting coeval INTCAL13 $\Delta^{14}C$ from benthic $\Delta^{14}C$. PC08 $\Delta\Delta^{14}C$ error ellipses are 1 sigma and account for both marine and atmospheric uncertainties.

the north. Given the concern that the record in core V21-30 may have been biased to low values by local sources of geologic carbon [*Stott and Timmermann*, 2011], it is reasonable to ask how ^{14}C-depleted the deglacial EqPIW must have been in order to produce the observed Baja California anomalies after mixing with relatively well-ventilated deglacial NPIW. To address this question, we compliment our analysis with water mass mixing constraints based in part on measured benthic $\delta^{18}O$.

New $\delta^{18}O$ results obtained in *Uvigerina* spp. for core PC08 (for discussion of $\delta^{13}C$ data see Appendix C and Supplementary Figure S3.3) are shown on the upper axis of Figure 3.7, along with *Uvigerina* spp. $\delta^{18}O$ results for Galapagos Rise core VM21-30 [*Koutavas et al.*, 2006; age model from *Stott et al.*, 2009] and the infaunal benthic (mostly *Uvigerina* spp.) $\delta^{18}O$ record from Santa Barbara Basin cores ODP 893a [*Hendy and Kennett*, 2003] and MD2503 [*Hill et al.*, 2006]. Because the composite SBB benthic $\delta^{18}O$ record exhibits high variability, for clarity it is represented here by the 1-sigma range for results from successive 500-yr bins on the age model

of Hendy & Kennett [2003]. For purposes of evaluating instantaneous isotopic gradients between different water masses, all $\delta^{18}O$ records were also fitted with smoothing splines.

Because differences in modern annual average T and S for the core sites considered here are small and offsetting (Fig. 3.2), we expect only very small differences between $\delta^{18}O$ of calcite formed off Baja California and at sites influenced directly by NPIW and EqPIW (within ~0.2 ‰, see Appendix C, section 3). In contrast to the modern situation, a significant $\delta^{18}O$ difference is seen between similar benthic species in the Galapagos Rise and the SBB records during the LGM, which increases during the early HS1 and then collapses at the start of the BA, due primarily to changes in the SBB record. The large decrease in benthic $\delta^{18}O$ during the BA at SBB was originally attributed to increased northward penetration of relatively warm EqPIW [*Hendy & Kennett*, 2003]. We note, however, that a recent planktic *N. pachyderma* $\delta^{18}O$ record from the Gulf of Alaska [Fig. 3.7, middle axis; *Gebhardt et al.*, 2008; age model from *Rae et al.*, 2014] contains similar shifts, suggesting that deglacial $\delta^{18}O$ changes at SBB were largely a response to changes in North Pacific surface temperature imprinted on NPIW which bathes the site today. The shift to heavier $\delta^{18}O$ values near the start of HS1 in SBB, which we now attribute to changes in the northern end member, is not present in the PC08 record, suggesting that the proportion of southern-sourced waters at the Baja California site may have increased at that time. This inference is consistent with Nd isotope evidence from PC08 sediments [*Basak et al.*, 2010].

In order to project the expected $\Delta\Delta^{14}C$ of EqPIW in the vicinity of Galapagos Rise core V21-30, we calculate the difference between PC08 $\Delta\Delta^{14}C$ and the approximation of the SBB $\Delta\Delta^{14}C$ record, and apply a simple two end-member mixing model guided by estimates of deglacial source water mixtures at the location of PC08. Projected deglacial values of EqPIW $\Delta\Delta^{14}C$ are given on the lower axis of Figure 3.7 according to three different mixing estimates: 1)

an assumed constant 2/3 fraction of EpPIW at the location of PC08, as indicated by the modern hydrographic data (bold purple line), 2) the proportional difference between spline fits to the three $\delta^{18}O$ records, at times when the $\delta^{18}O$ gradient between the Galapagos Rise and SBB was larger than 0.05‰ (thin dotted purple line), and 3) the proportional $\delta^{18}O$ differences after subtracting 0.25‰ and 0.15‰, respectively, from the Baja and Galapagos Rise $\delta^{18}O$ spline fits in order to account for small density differences (Fig. 3.3) between the core locations today (thin solid line in Fig. 7, $\delta^{18}O$ adjustment details given in Appendix C Section 3).We corrected implausible mixture values to the nearest end member (i.e. if PC08 $\delta^{18}O$ did not lie between the coeval end member $\delta^{18}O$ values we used 100% of the nearest one).

The fixed source water mixing scenario produces the mid-range of $\Delta\Delta^{14}C$ estimates and would require EqPIW at the time of the largest PC08 $\Delta\Delta^{14}C$ anomaly during HS1 to be ~175‰ below measured values in PC08, but significantly above those based on measurements in VM21-30 [*Stott et al.*, 2009]. Scenario 2 tends to exaggerate the EqPIW $\Delta^{14}C$ required to explain the deviation of Baja California $\Delta^{14}C$ from North Pacific $\Delta^{14}C$, and generates several points that are impossibly low (imply negative ^{14}C concentrations, calendar age indicated by arrows along bottom axis) or implausibly high (points above 0‰ at ~19ka). These illustrate the need to adjust PC08 and VM21-30 $\delta^{18}O$ to account for small density differences between these core locations and SBB in the modern ocean. When these adjustments are made (mixing scenario 3), the projected EqPIW $\Delta\Delta^{14}C$ values are significantly higher, but even the extreme estimates from mixing scenario 2 frequently lie above values indicated by VM21-30 ^{14}C measurements. The extremely low $\Delta^{14}C$ values from VM21-30 at ~18-20 ka seem especially unlikely, given the lack of a measured $\Delta\Delta^{14}C$ gradient between Baja California and SBB at that time. The collapse of the regional $\delta^{18}O$-of-calcite gradient during the BA allows for the possibility that the source mixture

at Baja California changed substantially to one dominated by NPIW, isolating the site from any low-$\Delta^{14}C$ signal in equatorial waters. Alternatively, if the Baja California source water mixture remained comparable to the modern one, deglacial EqPIW $\Delta^{14}C$ must have shifted rapidly from relatively low to relatively high values, similar to our Baja Margin reconstruction.

Overall, this analysis suggests that reasonable water mass mixing scenarios do not require unreasonably low $\Delta^{14}C$ in EqPIW at the location of Galapagos Rise core VM21-30, and that either local geologic sources of ^{14}C-dead CO_2 [*Stott and Timmermann*, 2011] or age model bias may have influenced that record. If there was a local volcanic source, it is unlikely to have played a significant role in controlling deglacial ocean and atmosphere CO_2 and $\Delta^{14}C$ more broadly, due to simple mass balance and alkalinity constraints. For example, the quantity of ^{14}C-dead carbon that would have to be added to the upper ocean in order to reduce its $\Delta^{14}C$ signature by -200‰ is ~25% of the preexisting DIC pool. Adding that proportion of unbuffered DIC would increase the DIC:Alkalinity ratio, causing carbonate ion concentrations to drop by approximately 90% and carbonate preservation to decline dramatically. However, carbonate preservation in Baja Margin core PC08 improved during deglacial ^{14}C depletion events relative to surrounding intervals [*Ortiz et al.*, 2004; *Lindsay et al.*, 2015], suggesting that any plume of volcanic carbon was highly localized and did not reach the Baja Margin. Indeed, at least one new record from Galapagos Rise itself does not show the largest depletions evident in core V21-30 [*Bova and Herbert*, 2014]. Such highly localized releases would have little influence on the CO_2 and $\Delta^{14}C$ signatures of the upper ocean and atmosphere as a whole.

3.6 Deep Ocean Sources of ^{14}C-depleted DIC

There is growing evidence for widespread ^{14}C-depletion in the deep Pacific and Southern

Oceans during the LGM [*Sikes et al.*, 2000; *Skinner et al.*, 2010, 2014; *Burke and Robinson*, 2012; *de la Fuente et al.*, 2015; *Keigwin and Lehman*, 2015; *Tiedemann et al.*, 2015], and several cores in the 2.5-3.6 km depth range indicate $\Delta^{14}C$ as low or lower than our records from the Baja California Margin during HS1 [*de la Fuente et al.*, 2015; *Tiedemann et al.*, 2015]. Thus there appear to be deep ocean sources of DIC having $\Delta^{14}C$ signatures low enough to explain our observations, and the presence of still more depleted sources can not yet be ruled out. Whether the existing deep ocean $\Delta^{14}C$ reconstructions can be explained entirely by ingrowth and aging of DIC due to reduced ventilation during glacial times [*Broecker and Peng*, 1986; *Schmittner*, 2003; *Butzin et al.*, 2005; *Skinner et al.*, 2014] or require an additional and possibly widespread source of ^{14}C-dead, geologic carbon emanating from deep ocean ridges in response to hydro-isostatic changes [cf. *Lund and Asimow*, 2011] is not addressed by our analysis of the upper ocean records that are the focus of this work.

4. Conclusions

Our results and analysis indicate that mid-depth depletion events observed off of the Baja California Margin were proximally sourced from equatorial intermediate waters, and we speculate that these waters acquired their anomalous $\Delta^{14}C$ signature from distal sources in the deep Southern and/or Pacific Oceans [*Sikes et al.*, 2000; *Skinner et al.*, 2010, 2014; *Burke and Robinson*, 2012; *de la Fuente et al.*, 2015; *Keigwin and Lehman*, 2015; *Tiedemann et al.*, 2015]. Large B-P ages during HS1 and YD observed in new results from core GC38 presented here and previously in PC08 [*Lindsay et al.*, 2015] confirm that deglacial ^{14}C anomalies near Baja California reflect real changes in ocean chemistry and cannot be dismissed as artifacts of age model bias. The vertical structure of $\Delta^{14}C$ gradients revealed by our depth transect are similar to

the modern gradient during the LGM and early BA, but contain a pronounced mid-depth minimum during HS1, late BA and the YD, ruling out vertical mixing of NPDW as the source of anomalously aged carbon during regional mid-depth ^{14}C-depletion events during deglaciation. Inspection of the $\Delta^{14}C$ differences between intermediate-depth cores in the Eastern Equatorial and North Pacific further indicated that observed anomalies could not have been caused by southward penetration of NPIW, and must have been due instead to compositional changes in deglacial EqPIW. Although localized volcanic sources of ^{14}C-dead CO_2 may have influenced some $\Delta^{14}C$ reconstructions in the region [*Stott et al.*, 2009; *Stott and Timmermann*, 2011], significant differences amongst individual reconstructions suggest that the influence was not widespread and could not have been large enough to influence the chemistry of the upper ocean and atmosphere as a whole. This continues to leave the deep ocean as the most likely source of aged, ^{14}C-depleted DIC influencing the upper ocean during deglaciation. The routing of these waters remains uncertain, but our analysis suggests that it must include the mid-depths of the Equatorial Pacific, pointing to an ultimate source in the deep Southern and Pacific Oceans.

Chapter IV: Variable Southern Ocean sea-to-air fluxes of CO_2 tagged by deep ocean ^{14}C

Abstract:

The Southern Ocean (SO) sink for anthropogenic carbon has accounted for a large fraction of the cumulative global ocean carbon sink since the beginning of the industrial era. However, several studies suggest that ongoing global warming and/or regional changes in stratospheric ozone may alter the westerly winds that drive SO overturning, a climate-carbon cycle feedback that has been predicted to decrease the efficiency of the SO carbon sink by upwelling more carbon-rich, radiocarbon-depleted water from the deep ocean. Here we demonstrate the use of precise measurements of radiocarbon in carbon dioxide from Drake Passage air ($\Delta^{14}C$ of CO_2) to detect short-term fluctuations in the Southern Ocean gross sea-to-air carbon flux and their source. Drake Passage (DRP) boundary layer air has been sampled since 2006 at roughly 2-week intervals, resulting in a 6-year high-resolution $^{14}CO_2$ time-series. We compare detrended and deseasonalized concentration anomalies to several indices of atmospheric variability, at sampled and monthly resolution. CO_2 anomalies are correlated at both timescales with the Southern Annular Mode (SAM), an index of SO westerly wind strength, and $\Delta^{14}C$ anomalies are anti-correlated with both the CO_2 anomalies and the SAM. This is interpreted as evidence for enhanced outgassing of low-$\Delta^{14}C$ deep ocean carbon during positive SAM/stronger westerly wind conditions. Similar correlations are also observed with the Southern Oscillation Index (SOI), an index of atmospheric conditions associated with tropical sea surface temperature variability. This may be caused by a teleconnection that promotes greater upwelling in the Pacific sector of the SO during La Niña conditions. Deasonalized monthly CO_2 and $\Delta^{14}C$ rates-of-change from Drake Passage, and CO_2 rates from nearby Palmer Station, are also found to

correlate at lower significance with the SAM but not the SOI. Our findings are consistent with the sign of the mechanism suggested by recent modeling and other observational studies of the SO carbon sink [Butler *et al.*, 2007; Le Quéré *et al.*, 2007; Lovenduski *et al.*, 2008], and support the existence of a climate-carbon cycle feedback that may have also contributed to rising CO_2 concentrations during periods of global warming in the pre-industrial past.

1. Introduction

The global ocean has absorbed almost half of all CO_2 released by fossil fuel burning since 1800, making it the largest cumulative sink for anthropogenic carbon [*Sabine and Tanhua*, 2010; *Khatiwala et al.*, 2013]. Air-sea gas exchange and deep mixing processes in the Southern Ocean (SO) account for approximately 40% of the global ocean uptake [*Sabine et al.*, 2004]. If ocean circulation and climate were unchanging, the global ocean sink would be a simple function of the atmospheric carbon inventory, increasing predictably as CO_2 accumulated in the atmosphere [*Mikaloff Fletcher et al.*, 2006]. However, climate and circulation are not expected to remain constant, and some models have predicted that both ocean and land sinks will diminish as a result of climate change [*Friedlingstein et al.*, 2001, 2006]. Understanding controls on major carbon sinks such as the SO sink is important, because their collective behavior will help determine future global atmospheric CO_2 concentrations and thus strongly influence the total global radiative forcing for any given anthropogenic CO_2 emissions scenario [*Friedlingstein et al.*, 2006].

Any net flux of CO_2 gas between the atmosphere and the ocean is the sum of opposing gross fluxes. The net uptake or release is driven by the difference in partial pressure of CO_2 (pCO_2) between the ocean and the atmosphere, and scaled by the gas exchange velocity, which is

usually parameterized as a quadratic function of the wind speed [*Wanninkhof*, 1992; *Sweeney et al.*, 2007; *Naegler*, 2009]. Deep waters throughout the ocean naturally have high levels of dissolved inorganic carbon (DIC; Figure 4.1C) due to the rain of organic matter from the warm sunlit surface ocean that is subsequently respired at depth. Divergent wind-driven surface transport in the Southern Ocean supports the upwelling of large amounts of CO_2-rich deep water to the surface. Nevertheless, anthropogenic emissions have raised the pCO_2 of the atmosphere above even that of most upwelling waters. Thus locally high windspeeds result in a large net CO_2 flux into the surface of the SO [*Takahashi et al.*, 2009]. This excess anthropogenic carbon is subsequently sequestered from the atmosphere as surface waters sink beneath warmer water at the northern boundary of the Southern Ocean and move northward as mid-depth Sub-Antarctic Mode Water (SAMW) and Antarctic Intermediate Water [AAIW; *Sabine et al.*, 2004].

While the combined global ocean and land sinks appear to be growing along with the atmospheric carbon inventory [*Ballantyne et al.*, 2012], estimates of the SO carbon sink from observations of surface ocean pCO_2 and from atmospheric inversions suggest a weakening trend during the 1990s and early 2000s [*Le Quéré et al.*, 2007; *Metzl*, 2009; *Takahashi et al.*, 2009], followed by a recovery in more recent years [*Lenton et al.*, 2013; *Landschützer et al.*, 2015]. The large inter-annual to inter-decadal variability in the SO carbon sink is not well understood, but there are indications that it has occurred partly in response to a natural oscillation of atmospheric pressure and circulation called the Southern Annular Mode (SAM, also sometimes referred to as the Antarctic Oscillation or AAO) which in its positive index state is associated with stronger, poleward-shifted SO westerly winds [*Hall and Visbeck*, 2002]. Wind patterns associated with the SAM in its positive index state are thought to promote additional upwelling of carbon rich deep water, raising surface ocean pCO_2. All other things being equal, any decrease in the ocean-atm

pCO_2 difference will act to reduce the net uptake of atmospheric CO_2 [*Butler et al.*, 2007; *Le Quéré et al.*, 2007; *Lovenduski et al.*, 2008]. Ozone depletion and global warming in the latter half of the 20th century are thought to have contributed to a secular trend in the SAM towards the positive state [*Thompson et al.*, 2000; *Thompson and Solomon*, 2002; *Arblaster and Meehl*, 2006], raising the possibility of a dynamical feedback to future warming that may weaken the SO carbon sink and decrease the fraction of excess anthropogenic CO_2 absorbed by the oceans.

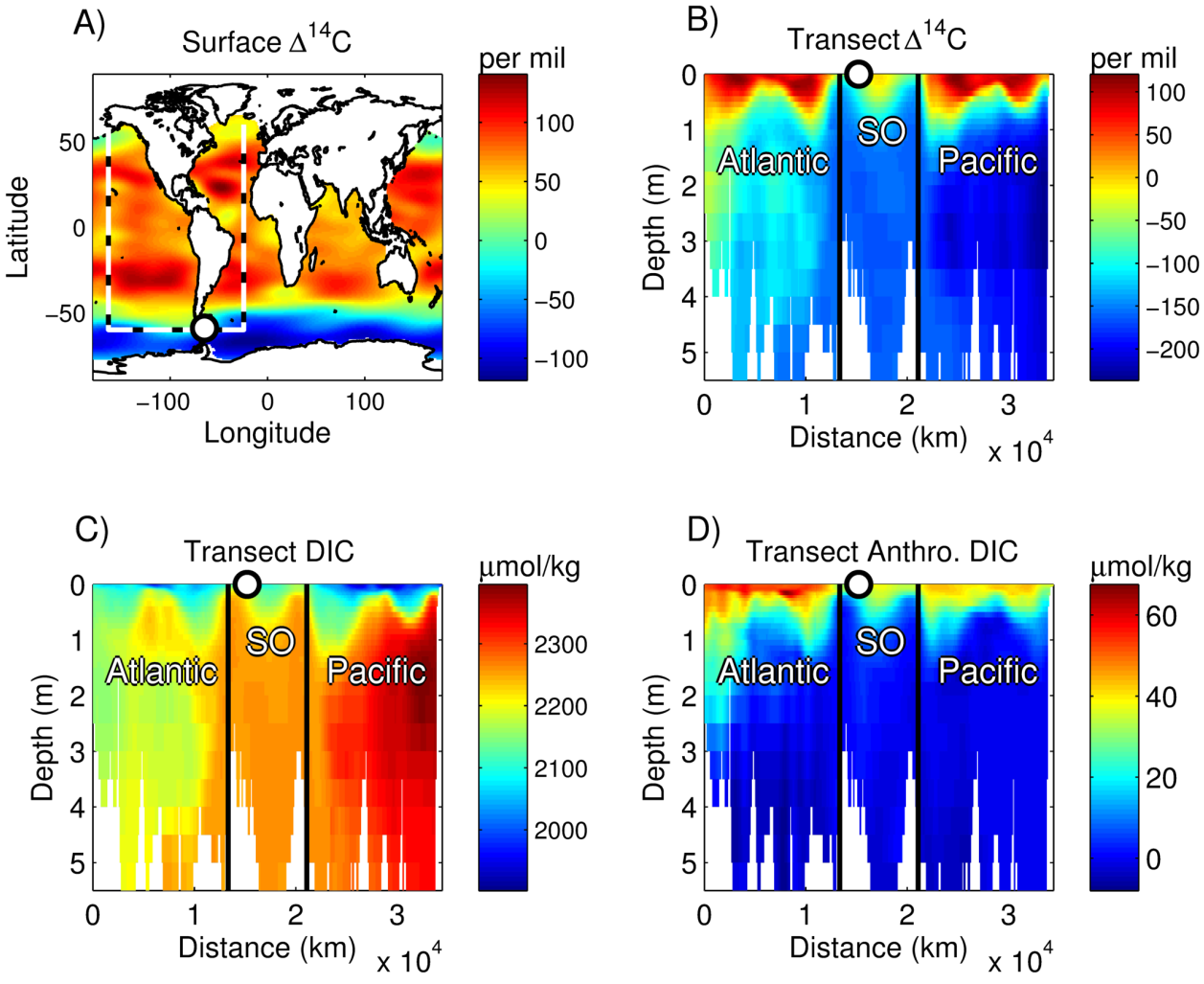

Figure 4.1: A) Surface ocean $\Delta^{14}C$ from the GLODAP dataset [*Key*, 2004] is plotted along with the path of the transect in the other panels (dashed black and white line). **B)** Transect of GLODAP ocean $\Delta^{14}C$. **C)** Transect of GLODAP dissolved inorganic carbon concentrations. **D)** Transect of GLODAP estimated anthropogenic DIC concentrations. The location of DRP sampling in the Southern Ocean (SO) is shown in all four panels as a black circle with white center

In this study we make use of ^{14}C measured in atmospheric CO_2 as a tracer for carbon escaping from the SO. Radioactive decay of ^{14}C causes $\Delta^{14}C$ (^{14}C:C ratio relative to a standard) in DIC in the ocean interior to decrease quantitatively with time since equilibration with the atmosphere (Figure 4.1B). Due to very long residence times in the subsurface, deep waters upwelling in the SO have unusually low $\Delta^{14}C$ (Figure 4.1A and 4.1B) that is subsequently carried into the atmosphere by the large sea-air gross CO2 flux driven by the strong westerly winds. The only other major sources of low-$\Delta^{14}C$ CO_2 to the atmosphere are ^{14}C-free emissions of CO_2 from combustion of fossil fuels, almost all of which occur in the Northern Hemisphere - too far away from the Southern Ocean to contribute meaningfully to short-term local and regional atmospheric $\Delta^{14}C$ variability (Figure 4.2A). Gross CO_2 fluxes from the terrestrial biosphere and the low-latitude ocean tend to have $\Delta^{14}C$ equal to or higher than the atmosphere, and are also located far from the SO (Figure 4.2B and 4.2C). Consequently, the large negative isoflux (the product of the gross mass flux of CO_2 into the atmosphere and the isotopic difference between the ocean surface and the atmosphere) from the SO is the dominant cause of the regional minimum in atmospheric $\Delta^{14}C$ at high southern latitudes (Figure 4.2D).

We present new measurements of ^{14}C and CO_2 in samples collected from the Drake Passage approximately every few weeks from year 2006 to 2014 (^{14}C not measured yet in samples after 2012) which we use in an attempt to better constrain the source of atmospheric CO_2 variability in the region on inter-annual to sub-seasonal timescales. We compare our results to the time series of the SAM in order to determine whether inferred fluctuations in the SO gross and net fluxes of CO_2 (from observed changes in $\Delta^{14}C$ and CO_2, respectively) are consistent with mechanisms proposed in earlier studies [e.g. *Le Quéré et al.*, 2007; *Lovenduski et al.*, 2008; *Conrad and Lovenduski*, 2015]. If anomalous windstress associated with positive index states of

the SAM brings excess deep ocean CO_2 to the Southern Ocean surface, we may expect anomalously elevated CO_2 and lower $\Delta^{14}C$ in the overlying air. Increases in wind speed alone (i.e., those not resulting in anomalous upwelling) will also lower observed $\Delta^{14}C$, but would decrease CO_2. We also attempt to evaluate the possible influence of other modes of atmospheric

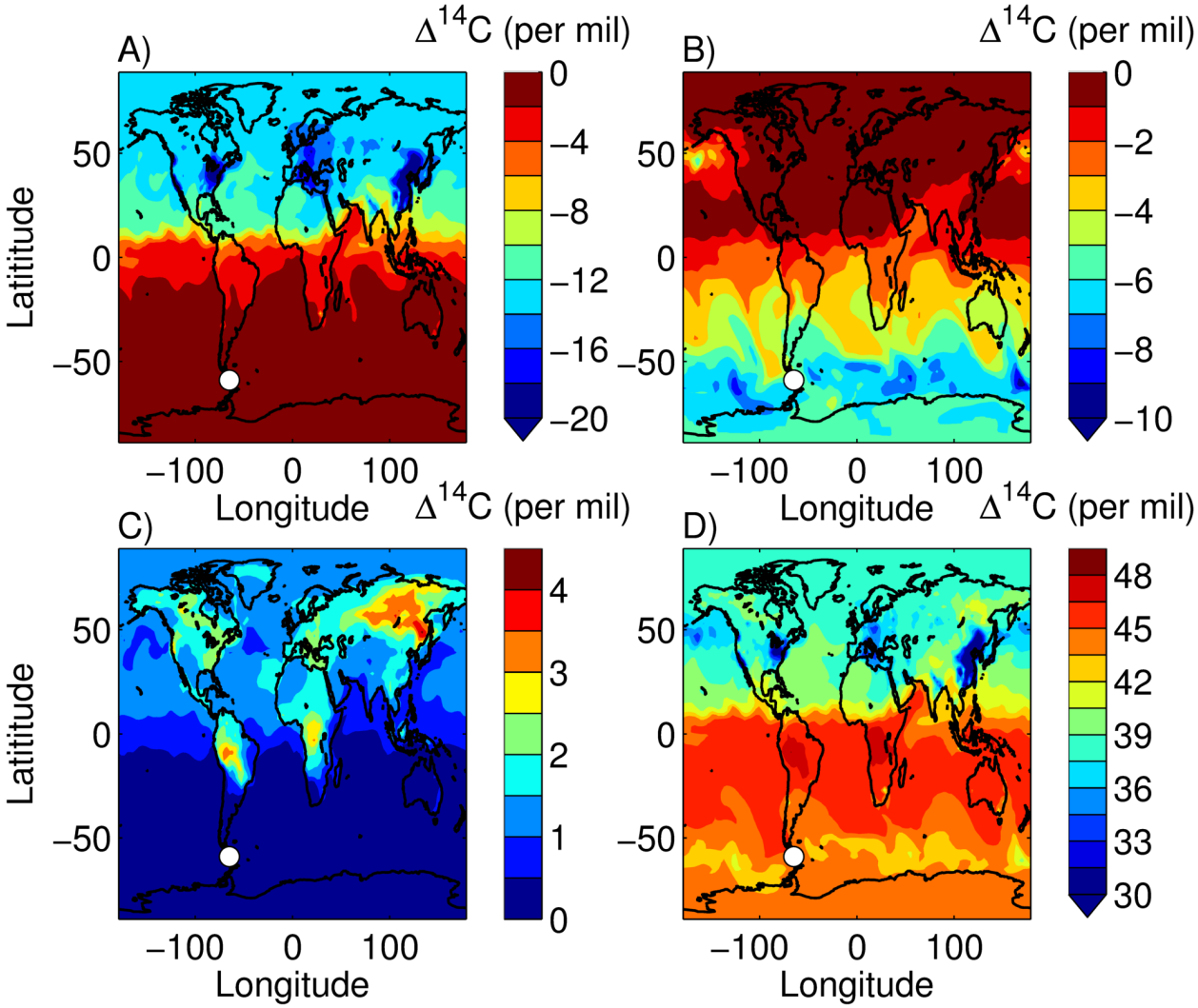

Figure 4.2: Maps of simulated atmospheric $\Delta^{14}C$ in the lower troposphere due to fossil CO_2 emissions (**A**, per mil relative to maximum value), ocean gas exchange (**B**, per mil relative to maximum value), terrestrial respiration (**C**, per mil relative to minimum value) and total carbon fluxes (**D**, per mil). The location of DRP is shown with a round white symbol. Saturation of the color scale is indicated by the triangle-shaped end of color scale bars. All data shown are estimates for July 15th, 2010 from the TM5 atmospheric transport model (Lehman *et al.*, in prep).

variability that either influence SAM or which may influence regional winds and our observations of $\Delta^{14}C$ and CO_2 via long distance teleconnections.

2. Data and Methods

Air samples were collected near the center of Drake Passage (site code DRP, 59° S, 64.69° W, 10 masl) on board the RV Gould as part of the National Oceanic and Atmospheric Administration Earth System Research Laboratory (NOAA/ESRL) Global Greenhouse Gas Reference Network [*Schnell et al.*, 2004]. Sampling in 2003, 2005 and 2006 was carried out along a latitudinal transect, before repeat sampling was initiated at the current coordinates in June of 2006. In this study we use only data from samples collected at the fixed location since June 2006. Samples have been collected approximately fortnightly (~20/year), but with frequent sampling gaps of 1-2 months length in the austral winter. $\Delta^{14}C$ of CO_2 has been measured in DRP flask samples through mid 2012. CO_2 samples were extracted from NOAA flasks and processed at the INSTAAR Radiocarbon Laboratory before ^{14}C measurement at the Keck Carbon Cycle Accelerator Mass Spectrometer facility at the University of California Irvine, following procedures outlined in Turnbull *et al*.[2007, 2010]. The measurements are expressed as $\Delta^{14}C$ [*Stuiver and Polach*, 1977] and have a long-term (1-sigma) repeatability of 1.8‰ [*Lehman et al.*, 2013]. CO_2 mole fractions were measured by NOAA, using standard procedures that result in a measurement precision of ±0.1 ppm [*Conway et al.*, 1994, data available at http://www.esrl.noaa.gov/gmd/dv/site/site.php?code=DRP]. Data quality flags from NOAA were used to omit measurements from the study that have suspected contamination or other problems, and we also used an objective definition of outliers to further reduce noise from potential sampling or measurement problems.

To calculate CO_2 and $\Delta^{14}C$ anomalies and exclude outliers, we used the curve fitting routine from NOAA ESRL/GMD of Thoning *et al* [1989] to fit and remove the long-term trends of CO_2 and $\Delta^{14}C$, including the seasonal cycle for CO_2 (see Figures 4.3 and 4.4, top axes). The fitted function for $\Delta^{14}C$ is a 5^{th}-order polynomial, while for CO_2 it is a 5^{th}-order polynomial plus three harmonic terms with frequencies of 1,2, and 3 cycles per year to represent the annual seasonal cycle. CO_2 and $\Delta^{14}C$ anomalies are defined as the residuals from the fitted functions (Figures 4.3 and 4.4, lower panels). CO_2 or $\Delta^{14}C$ data points that fell more than 3 standard deviations from the fit were omitted and the function was refit until no outliers remained. Nine DRP flask samples from the 2007-2008 season were filtered out by this method due to extremely high $\Delta^{14}C$ values, likely because of contamination by highly ^{14}C-enriched CO_2 from shipboard biological laboratories, leading to lower temporal resolution in the residuals from that part of the time-series (see Figure 4.4).

3. Results and Discussion

Both CO_2 concentrations (Figure 4.3) and $\Delta^{14}C$ (Figure 4.4) measured at DRP display long term secular trends. The long-term rise in CO_2 concentrations is a result of global CO_2 sources, dominated by emissions from fossil fuel burning that exceed global sinks. The long-term decrease in $\Delta^{14}C$ results from assimilation of excess bomb ^{14}C by the biosphere and ocean and dilution of atmospheric ^{14}C by global emissions of ^{14}C-free fossil CO_2. The latter now dominates the secular trend, as return fluxes of previously assimilated excess ^{14}C from the terrestrial biosphere (the so-called terrestrial biospheric disequilibrium isoflux, which is positive) and the ocean disequilibrium isoflux (which is negative) are approximately equal and offsetting [*Turnbull et al.*, 2009; *Levin et al.*, 2010]. Importantly with respect to our application, the

dominant contributions to each of these three global isoflux terms are widely separated in space, with the contribution of ^{14}C-free CO_2 from combustion of fossil fuel occurring primarily in the mid latitudes of the Northern Hemisphere, the most positive contributions to the terrestrial disequilibrium isoflux in the tropics, and the most negative contributions to the ocean disequilibrium isoflux over the SO (map Fig. 4.2A-C).

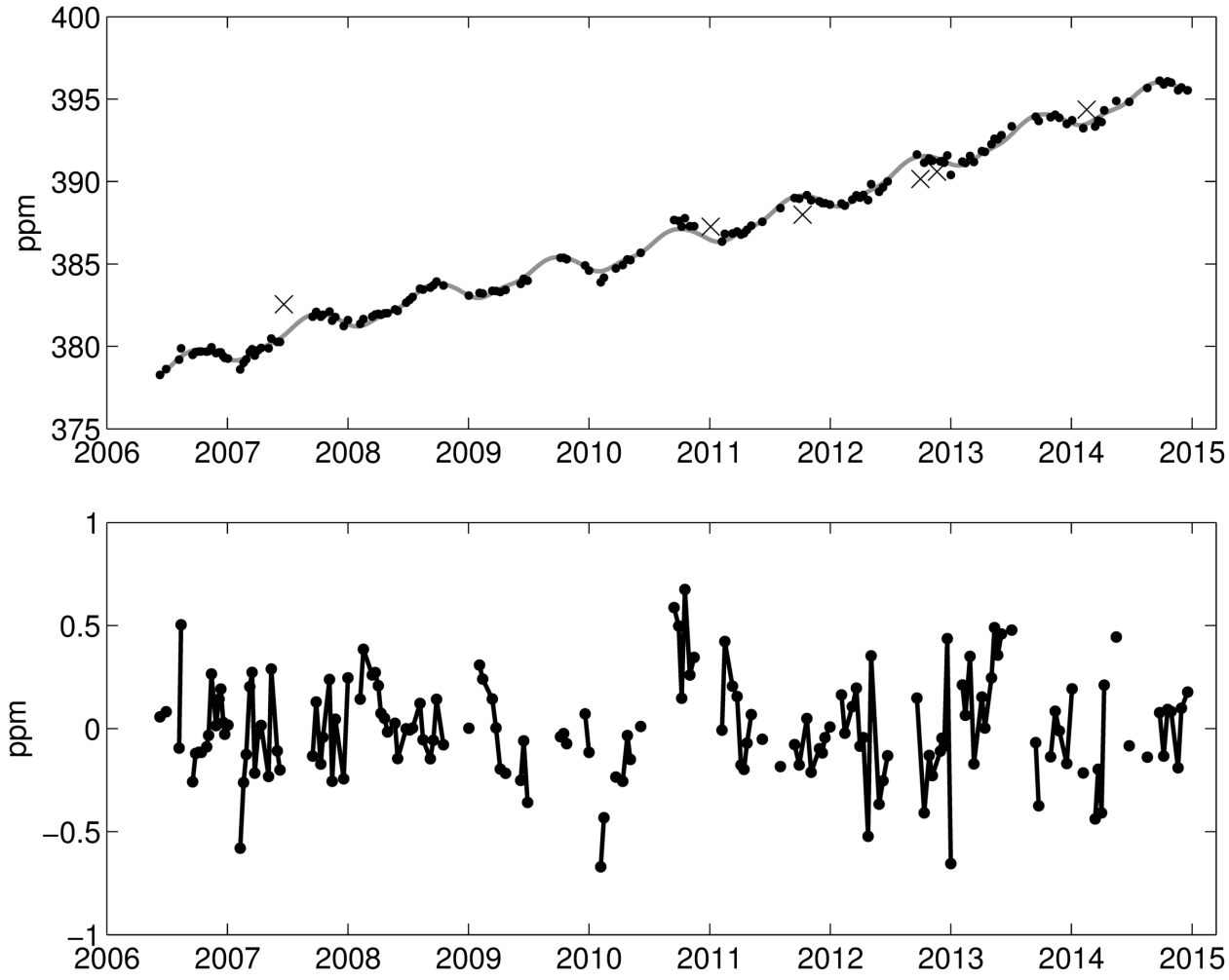

Figure 4.3: DRP CO_2 concentrations (round black symbols, top panel) and 5th-order polynomial plus harmonic fit (grey line). Data that was removed by the outlier filter is shown as black X symbols. Anomalous DRP CO_2 concentrations are defined as the residuals from the fit (black symbols, lower panel). A black line connects residuals separated by a gap of less than 1 month.

CO_2 and $\Delta^{14}C$ anomalies at DRP (Figures 4.3 and 4.4) represent short-term departures from long-term secular trends and also, for CO_2, from estimated seasonal variations caused by the transport of seasonal CO_2 signals from photosynthesis and respiration in the Southern Hemisphere. There is no significant seasonal component in the $\Delta^{14}C$ time series. In order to evaluate possible relationships between anomalous CO_2, $\Delta^{14}C$ and local modes of atmospheric variability we first compare measured anomalies at DRP and the SAM (Figure 4.5). There are several different indices of the Southern Annular Mode, which is the leading mode of Southern

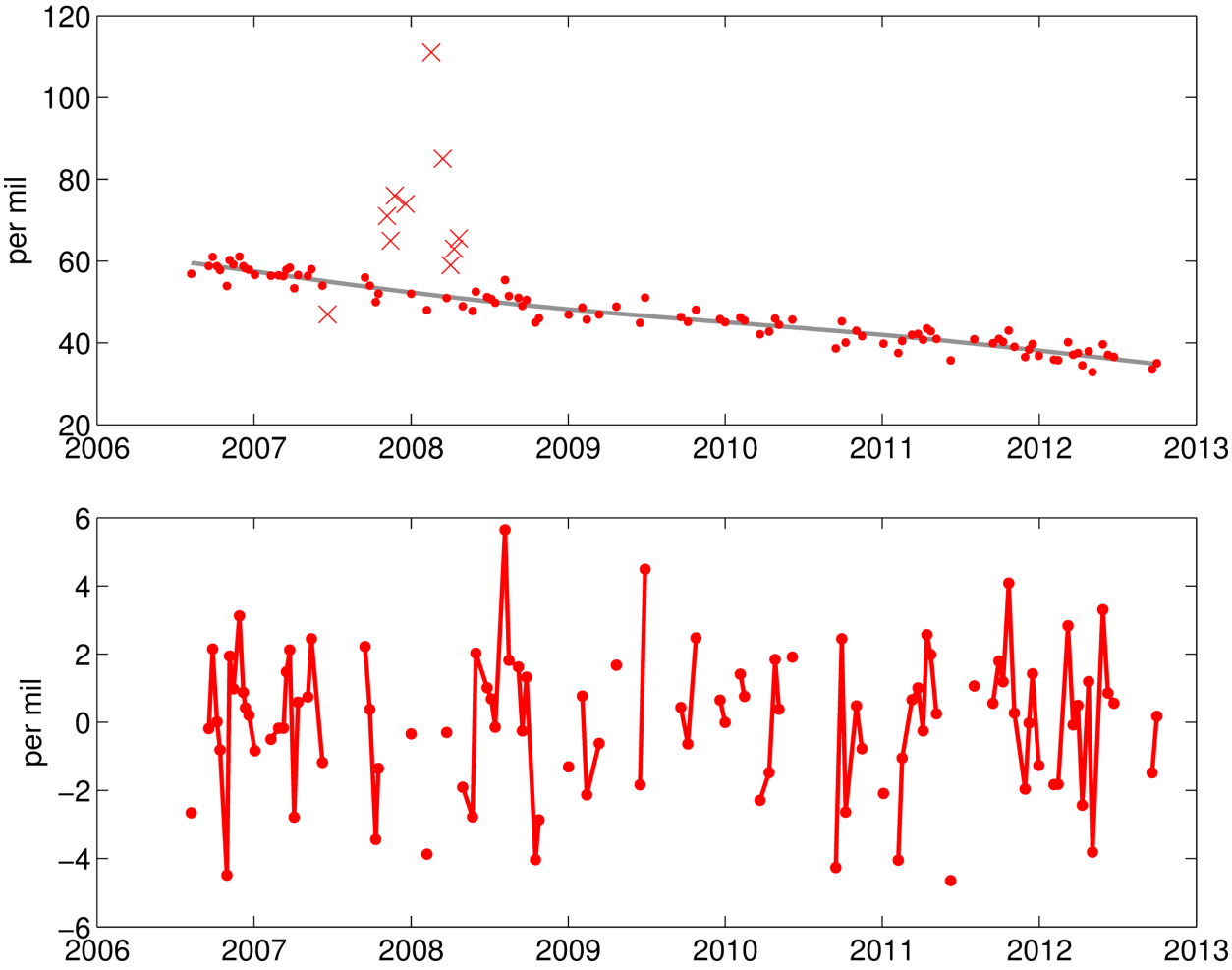

Figure 4.4: DRP $\Delta^{14}C$ (red filled circles, top panel) and 5th-order polynomial fit (grey line). Data that was removed by the outlier filter is shown as red X symbols. Anomalous $\Delta^{14}C$ is defined as the residuals from the fit (red solid line, lower panel). A red line connects residuals separated by a gap of less than 1 month.

Hemisphere atmospheric pressure and zonal wind variability [see *Ho et al.*, 2012 for a comparison]. Here we use the EOF-based "AAO" index from NCEP because it is available at daily resolution (source: ftp://ftp.cpc.ncep.noaa. gov/cwlinks). Significance of all correlations we report was assessed using the Monte Carlo approach described by Ebisuzaki [1997], which accounts for autocorrelation in each time-series.

High CO_2 and low $\Delta^{14}C$ anomalies both tend to occur when recent SAM values were high, although the negative correlation between CO_2 and $\Delta^{14}C$ anomalies is not highly significant ($R = -0.16$, $p = 0.12$). The SAM statistically resembles a red-noise process with a correlation time-scale of ~10 days and consequently most of the power in the SAM is at low frequencies (wavelength >20 days) [*Hartmann and Lo*, 1998]. The CO_2 and $\Delta^{14}C$ anomalies also appear to have a low-frequency component of variability, and it is this component that appears to covary with the SAM. (Gaps and uneven temporal sampling in our observation time-series prevent us

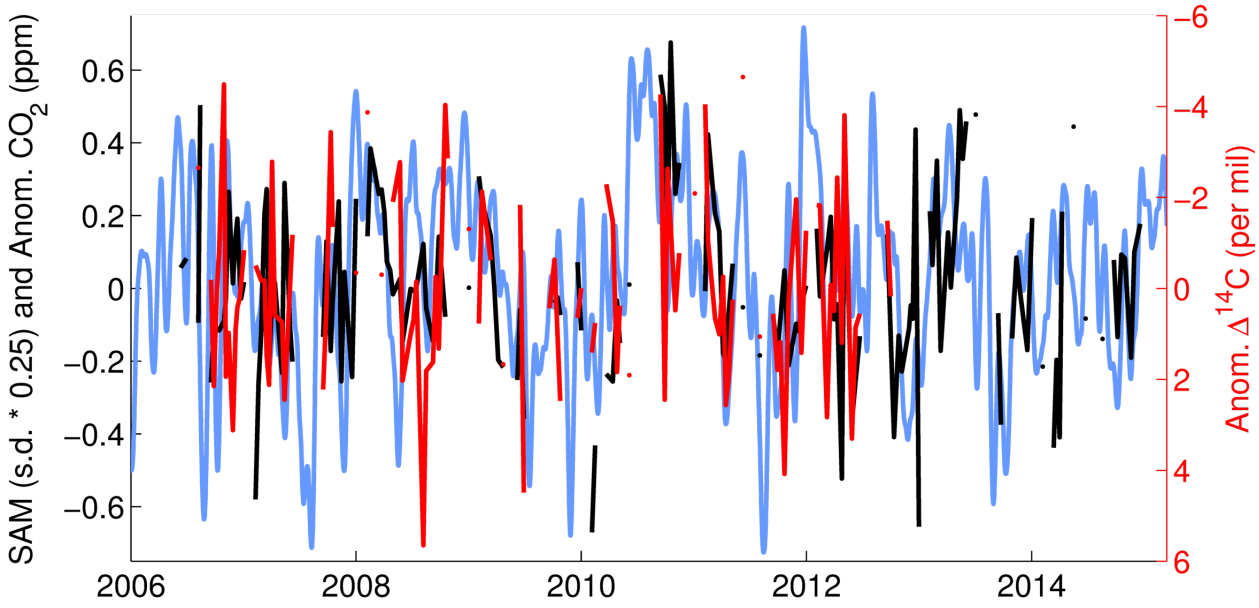

Figure 4.5: Anomalous DRP CO_2 concentrations (discontinuous black line, left axis) and preceding 30-day average SAM (blue line, scaled by 0.25 to fit on left axis) compared to anomalous DRP $\Delta^{14}C$ (discontinuous red line, right inverted Y axis).

from calculating coherence spectra with the SAM to confirm this impression.)

Lag correlations for both DRP time-series and daily SAM values are shown in Figure 4.6. At zero lag, CO_2 anomalies are significantly correlated with the SAM (R = 0.20, p = 0.02), while $\Delta^{14}C$ anomalies are anticorrelated with the SAM (R = -0.18, p = 0.08), but with lower significance than for CO2. The correlation between CO_2 anomalies at DRP and daily SAM values quickly drops for positive lags of a few days but then reaches a maximum at +29 days (i.e., sampling lags the SAM index, R=0.28, P<0.01). For $\Delta^{14}C$, peak negative correlation with

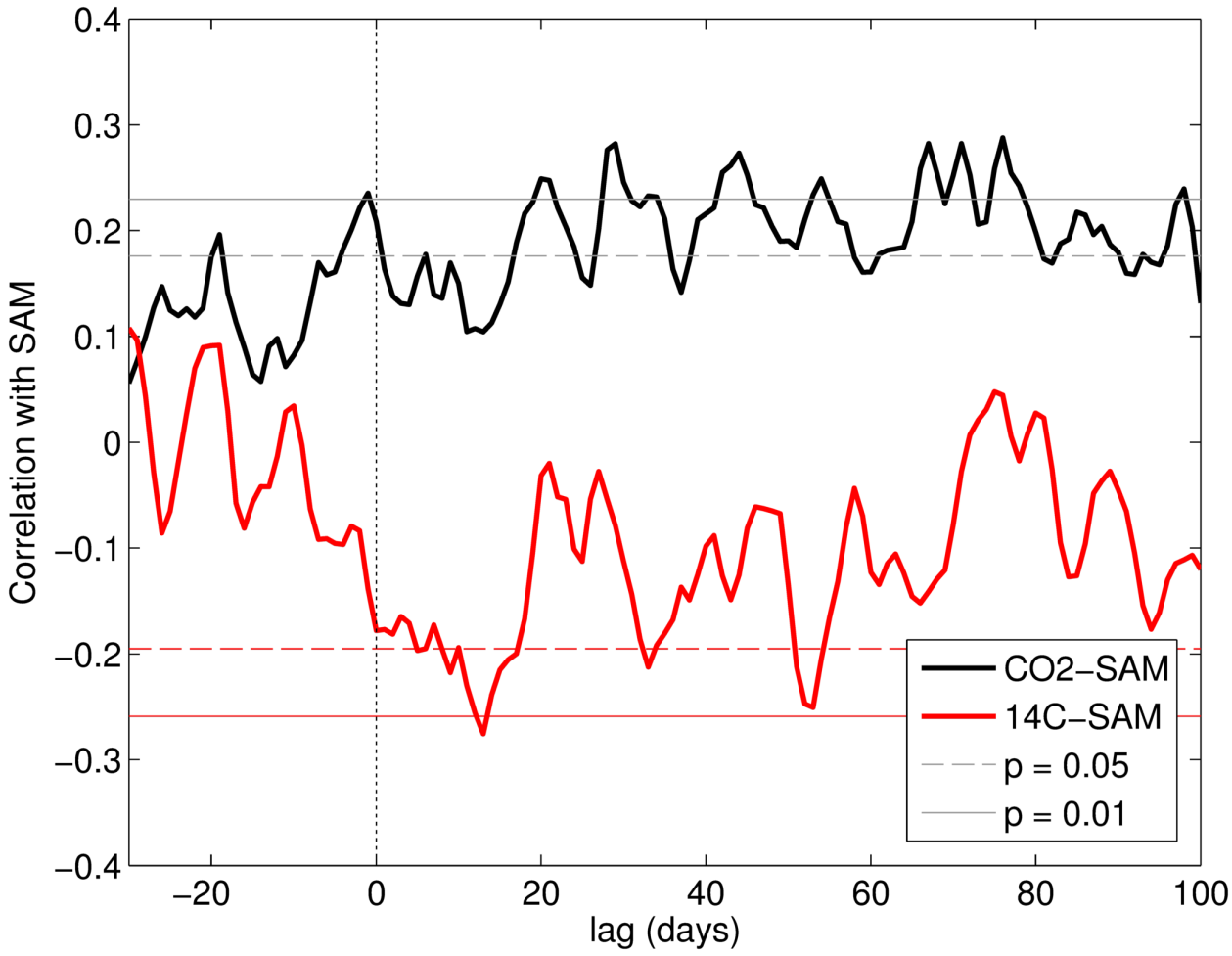

Figure 4.6: Pearson correlation coefficients (R) calculated between anomalous DRP CO_2 concentrations (black line) and $\Delta^{14}C$ (red line) and daily SAM values at multiple leads and lags (positive lag is SAM leading DRP observations). Grey dashed (p = 0.05) and solid (p = 0.01) lines show statistical significance.

SAM occurs at about +2 weeks (R = -0.28 at 13 days, $p < 0.01$). Note that the theoretical maximum correlation between time-series is limited by signal-to-noise constraints that, in our case, greatly reduce the potential maximum value of R. Here we define the signal:noise ratio as the ratio of the standard deviation of observed anomalies (which include measurement error) to the standard deviation of known random measurement error. For $\Delta^{14}C$, that ratio is 1.1-1.2 (i.e. 2.2‰:1.8‰), leading to maximum correlation |R| of 0.4-0.6 as determined by random Monte Carlo re-sampling of artificial observations (and their errors) for very long series (in this case, having an arbitrary 10,000 degrees of freedom, see Figure 4.7). For shorter series, correlations may be higher or lower than the theoretical limit. For the case of a series comparable in length to our observations at DRP (n = ~ 110), the two sigma envelope for |R| includes values ranging from 0.26-0.68. The absolute value of the largest correlation we observed between $\Delta^{14}C$ at DRP and the daily SAM index (R=-0.28) is less than the theoretical upper limit and just outside the associated 2-sigma envelope (at red bar in Figure 4.7). This suggests that a process related to the SAM may explain a large fraction of the observed $\Delta^{14}C$ variability at DRP.

Taken at face value, the observed correlations of CO_2 and $\Delta^{14}C$ anomalies at DRP with the SAM suggest an atmospheric response to concomitant lowering of surface ocean $\Delta^{14}C$ of DIC and increase of surface ocean pCO_2, leading to anomalous outgassing of low-$\Delta^{14}C$ carbon from the Southern Ocean surface during periods when the SAM index is elevated. The increased outgassing must exceed any counteracting wind-driven increase in the air-sea flux of atmospheric carbon into the ocean. The positive lags at which we observe the largest correlations of CO_2 and $\Delta^{14}C$ anomalies to the SAM may reflect the timescale required to build up chemical and isotopic anomalies within the near surface boundary layer. Given constraints from observed wind speeds, calculated lag times for the maximum correlations also imply a spatial length scale

over which the measured anomalies may be integrated. Winds at the latitude of DRP are large, with an average speed of ~10 m/s. Simple conflation with the 2 week timescale implied by lag correlations of $\Delta^{14}C$ and the SAM index suggests that air parcels intercepted at the DRP location have traveled at least ~10,000 km, or across the length of the entire Pacific Sector of the SO

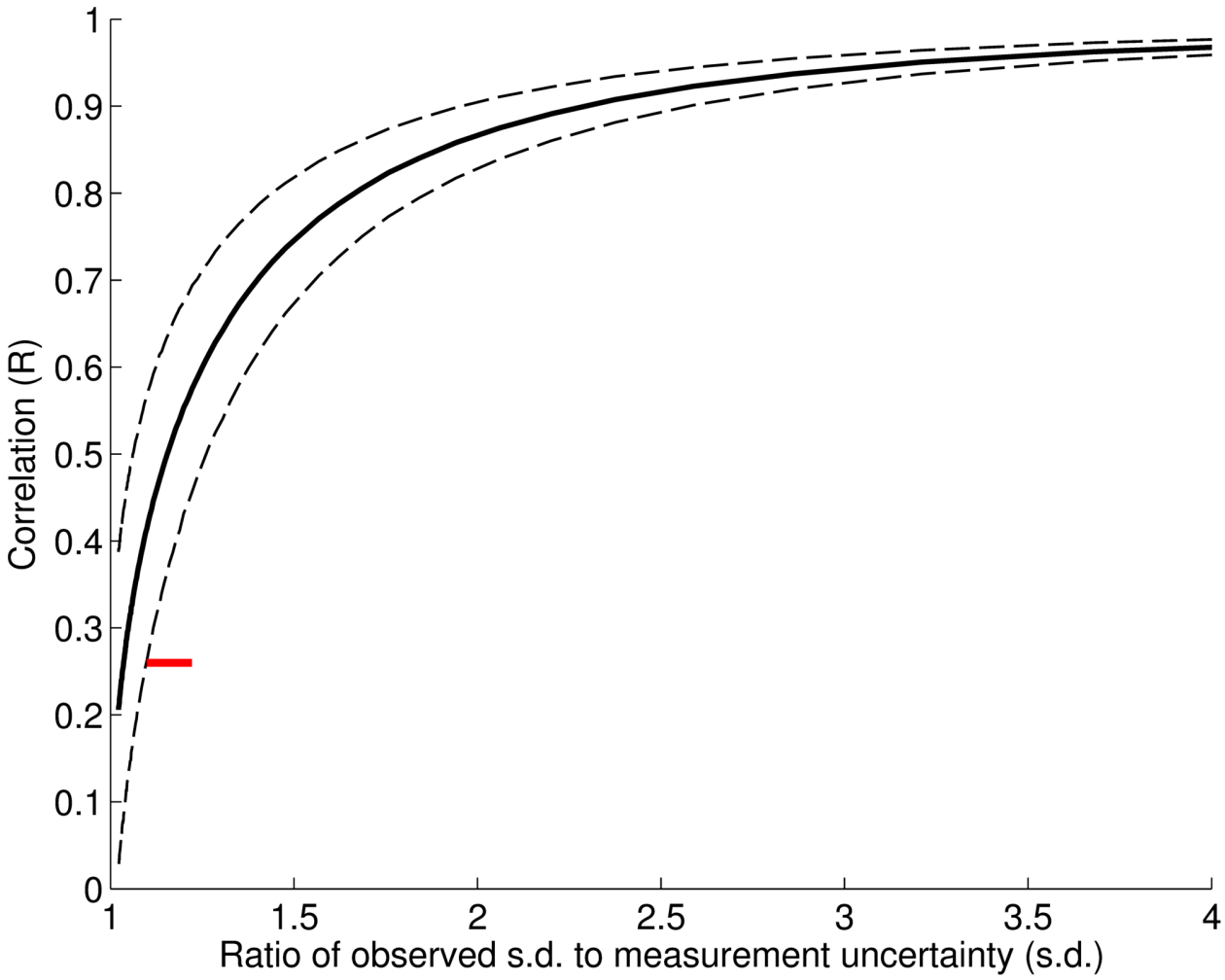

Figure 4.7: Monte Carlo simulated correlation values in the ideal case of very long time-series (solid black line) as a function of the signal to noise ratio, here defined as total variability (signal + noise) divided by measurement error (noise). The 2-sigma envelope of R values from time-series the length of the $\Delta^{14}C$ time-series from DRP is shown (dashed lines) along with the largest absolute R value calculated between $\Delta^{14}C$ anomalies at DRP and the daily SAM (0.26) plotted versus a signal:noise range of 1.1-1.2 (red bar, see text for explanation.)

during the development of the observed atmospheric anomalies. Thus, the $\Delta^{14}C$ signal recorded at DRP may reflect gross sea to air fluxes integrated over a large area of the SO surface, primarily in the Pacific Sector.

The CO_2 correlations, which peak first at 0 days lag and at 20-30 days, suggest either the predominant influence of fluxes within a few hundred km of Drake Passage or over much longer temporal and spatial scales. Considering that winds circuit the earth in ~30 days at this latitude, we assume that mixing must be strong enough to erase anomalies within that timeframe. We speculate that the continued high correlations between CO_2 anomalies at DRP and the SAM at large lags (i.e. those larger than ~ 2 wks) may be caused by the persistence of the SAM, which as we mentioned earlier has a strong low-frequency component. It is also possible that the chemical and isotopic inertia of the ocean mixed layer causes the ocean-atmosphere gross flux to retain a memory of upwelling intensity for several months [c.f. *Verdy et al.*, 2007]. The repeated peaks in the CO_2-SAM correlations at positive lag appear suggestive of a 10-20 day periodicity, but the SAM is not significantly periodic at that frequency [*Hartmann and Lo*, 1998] and the approximately 2-week long sampling interval at DRP is too infrequent to reliably record such a short-period oscillation in the observations, even if real.

The correlations we observe are of the same sense as expected for, and therefore consistent with, the upwelling mechanism suggested by earlier modeling studies [*Le Quéré et al.*, 2007; *Lovenduski et al.*, 2007, 2008]. They also are in agreement with observations of ΔpCO_2 within Drake Passage, which have been found to correlate with the SAM at annual resolution, likely because of anomalous upwelling during years when the SAM index is elevated [*Munro et al.*, 2015], as well as a previous study that found that atmospheric CO_2 concentration anomalies at Palmer Station on the Antarctic Peninsula tended to rise during months when the index SAM

was generally high [*Butler et al.*, 2007]. We conclude that greater upwelling due to strong westerly winds during intervals of high-SAM raises surface ocean pCO_2 in Drake Passage and the Southern Ocean upstream of Drake Passage, increasing the gross sea-air flux of CO_2 and decreasing the net carbon sink. The excess CO_2 offgassed to the atmosphere is, in the remote SO region, uniquely tagged by the low $\Delta^{14}C$ of the deep ocean.

3.1 Potential Influence of Tropical Teleconnections

We next evaluate the potential correlation of CO_2 and $\Delta^{14}C$ anomalies at DRP with other modes of atmospheric variability that could influence atmospheric transport, upwelling or other biogeochemical processes in the Southern Ocean. For example, tropical teleconnections associated with El Niño – Southern Oscillation (ENSO) and the Quasi-Biennial Oscillation (QBO) can influence Southern Ocean surface winds, potentially affecting upwelling and thereby our CO_2 and $\Delta^{14}C$ observations at DRP [*Genthon et al.*, 2003; *Labitzke*, 2004; *L'Heureux and Thompson*, 2006; *Ding et al.*, 2012]. Some of the atmospheric variability over the SO that is related to these indices is also captured in the SAM index, and can be thought of as tropical atmospheric conditions forcing or modulating the SAM. For instance, positive SAM conditions have been found to coincide with the cold phase of ENSO and vice versa. These influences are most pronounced during austral summer when ENSO can explain 25% of the variability of the SAM [*L'Heureux and Thompson*, 2006]. Significant correlations exist between tropical SSTs and the SAM in all seasons [*Ding et al.*, 2012], although the relationship between ENSO and the SAM did not remain stationary over the period 1980-2000 [*Fogt and Bromwich*, 2006]. A relationship has also been proposed between the QBO (a quasi-periodic reversal of zonal winds in the tropical stratosphere) and the SAM, via modulation of solar forcing [*Labitzke*, 2004].

There are also mechanisms by which ENSO and the QBO may affect SO carbon fluxes independent of the SAM. The 2nd leading mode of atmospheric pressure variability in the Southern Hemisphere (of which SAM is the 1st) is concentrated in the Pacific sector of the Southern Ocean and highly correlated with ENSO [*Genthon et al.*, 2003]. A recent modeling study found that changes in winds associated with cold ENSO (La Niña) conditions caused more deep ocean DIC to upwell in the Pacific Sector of the SO [*Conrad and Lovenduski*, 2015], suggesting a plausible source of CO_2 and $\Delta^{14}C$ variability at DRP independent of the SAM, but correlated with ENSO.

The state of the tropical atmosphere may also affect vertical atmospheric mixing, which could affect atmospheric observations at DRP. Both ENSO and the QBO, which are correlated during the 2005-2010 period, are thought to affect stratosphere-troposphere exchange [*Neu et al.*, 2014], which may influence the amount of stratospheric air mixed into the troposphere (cross tropopause exchange) at mid-latitudes. Because fossil emissions are concentrated at the surface, and natural ^{14}C production is concentrated in the upper atmosphere, stratospheric air tends to have lower CO_2 concentrations and higher $\Delta^{14}C$ than tropospheric air [*Nakamura et al.*, 1992].

To evaluate possible teleconnections influencing our observations at DRP, we show lag correlations between monthly average CO_2 and $\Delta^{14}C$ anomalies from DRP and monthly average time-series of the normalized Southern Oscillation Index (SOI), normalized Quasi-Biennial Oscillation (QBO; SOI and QBO data source: www.cpc.ncep.noaa.gov/data/indices) and the SAM (Figure 4.8). The Southern Oscillation Index is the atmospheric expression of ENSO, and thus should be most relevant to the teleconnection between ENSO and winds in the Pacific Sector of the SO. The reversal of winds that characterizes the QBO propagates slowly down through the stratosphere with a reversing timescale of ~18 months, and thus the phasing of the

QBO time-series depends on pressure height. We used a QBO product that represents zonal windspeeds at the 30 mb level in the equatorial stratosphere. We have calculated correlations out to -5 and +18 months lag to estimate the effect of choosing a different level at which to measure the QBO phenomenon. Because each index has different autocorrelation characteristics, the significance of correlations are slightly different for each combination of observed variable and index due to differences in effective degrees of freedom. Consequently, significant correlations

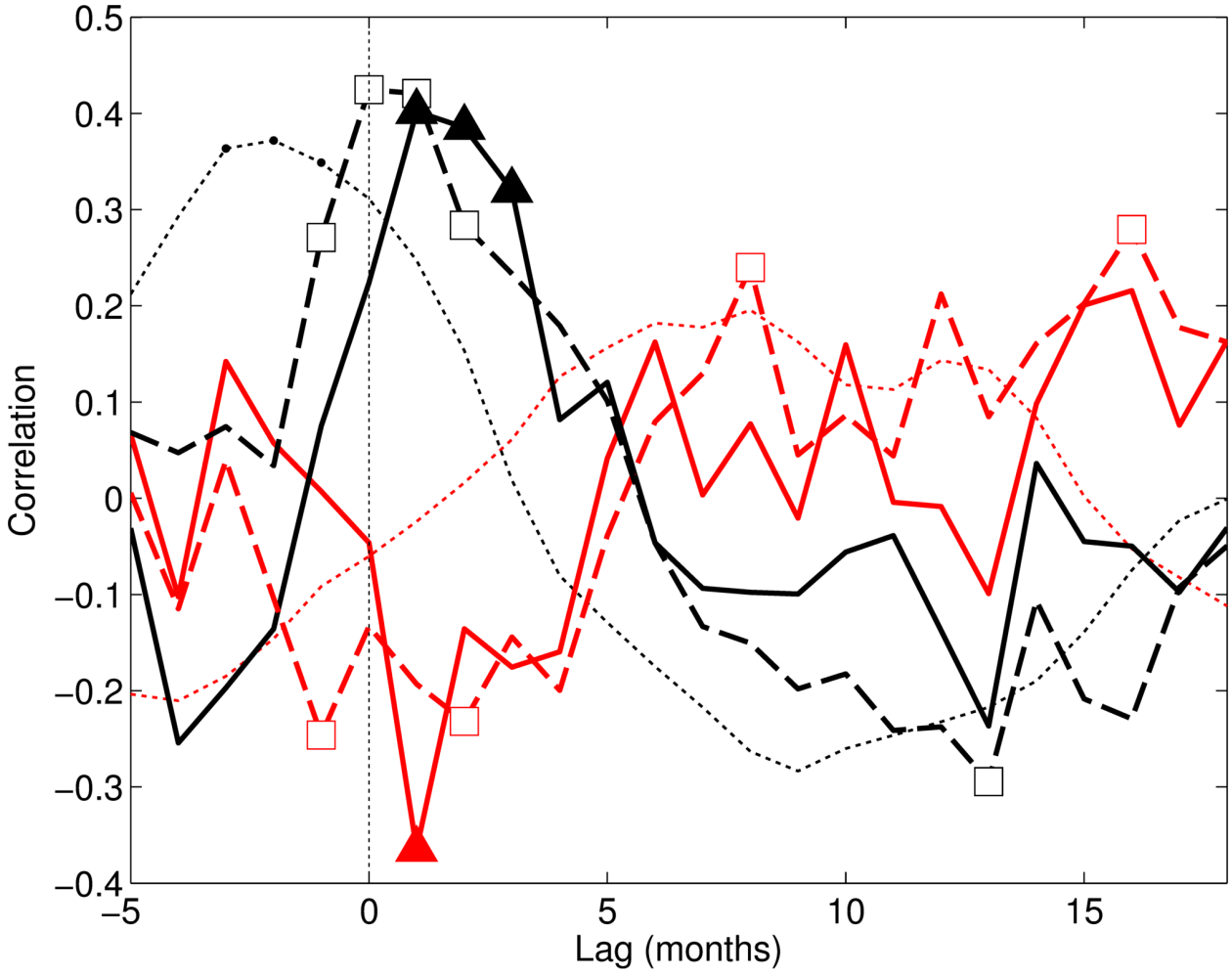

Figure 4.8: Pearson correlation coefficients (R) between monthly DRP CO_2 concentration anomalies (all black lines), monthly $\Delta^{14}C$ anomalies (all red lines), and the SAM (solid lines), the SOI (dashed lines) and the QBO (dotted lines) at several leads and lags. Positive lags indicate the index leading the observations from DRP. Statistically significant ($p < 0.05$) correlations to each index are indicated by filled triangles (SAM), empty squares (SOI) and bold dots (QBO).

($p < 0.05$) are represented in Figure 4.8 with discrete symbols instead of horizontal lines.

The negative correlation (not shown) between monthly average CO_2 and $\Delta^{14}C$ anomalies at DRP is larger than observed for individual samples ($R = -0.23$, $p = 0.09$). Peak correlation of monthly average observations of both CO_2 and $\Delta^{14}C$ at DRP and the SAM are greater than for daily values, but with similar significance due to the reduction in degrees of freedom. Correlations between monthly CO_2 anomalies and the SAM peak at 1 month lag (observations lag index), as do negative correlations with monthly $\Delta^{14}C$. Note that because the temporal resolution of the analysis is lower, peak correlations at 1-month lag for monthly averages cannot be meaningfully differentiated from the 13-day lag observed for maximum anti-correlation between $\Delta^{14}C$ anomalies and daily SAM values.

Monthly average CO_2 anomalies at DRP also are correlated with the SOI, peaking at lags of 0 and 1 month. Months with, or just following, La Niña-like atmospheric conditions are associated with higher CO_2 concentrations at DRP. This is opposite the sense of the relationship that has been observed between global CO_2 growth rates and La Niña events, which is primarily attributed to a terrestrial carbon cycle response that results in less respiration of terrestrial carbon when ENSO is in the cold phase [e.g. *Wang et al.*, 2013]. The SOI is also significantly anti-correlated with $\Delta^{14}C$ anomalies at DRP at lags of -1 and +2 months, opposite the relationship that would be expected if the locally observed excess CO_2 was sourced from the remote terrestrial biosphere, which is expected to produce a positive ^{14}C isoflux and therefore a high $\Delta^{14}C$ tag in CO_2 (Figure 2C). Rather, observed correlations between CO_2 and $\Delta^{14}C$ anomalies at DRP and the SOI suggest a mechanism that associates higher CO_2 concentrations with lower $\Delta^{14}C$, and for the SOI that is either increased upwelling in the Pacific sector of the SO or decreased troposphere-stratosphere mixing.

The QBO is significantly correlated with monthly CO_2 anomalies at DRP when the data leads the index by 1-3 months, and has no significant relationship to observed $\Delta^{14}C$ anomalies at any lag. This negative lag, which is small relative to the 18-month timescale of downward propagation, could indicate that the QBO at a slightly higher level in the stratosphere than 30 mb has a relationship to our observations, with the westerly phase correlated with higher CO_2 anomalies- as the QBO is expected to propagate from about the 20 mb level down to the 30 mb level over the course of ~3 months [*Baldwin et al.*, 2001]. However, the lack of significant correlation between the QBO and $\Delta^{14}C$ anomalies from DRP at any reasonable lag suggests that the QBO has not influenced CO_2 and $\Delta^{14}C$ anomalies at DRP directly. The observed correlation between CO_2 anomalies at DRP and the QBO may reflect linkages between the QBO and the SAM and the SOI, rather than a direct control via troposphere-stratosphere mixing.

These limited results suggest that, like the SAM, ENSO may influence Southern Ocean fluxes in the Pacific sector by enhancing outgassing of upwelled deep ocean carbon during La Niña conditions, consistent with recent modeling of Southern Ocean carbon dynamics[*Verdy et al.*, 2007; *Conrad and Lovenduski*, 2015]. A strong effect from troposphere-stratosphere mixing seems unlikely, as there is no clear correlation between $\Delta^{14}C$ anomalies at DRP and the QBO. We note that these correlations are sensitive to the type of function chosen to define the anomalies, as well as the numerical cutoff chosen to define outliers. In particular, the CO_2 anomalies, when fit with a quadratic function instead of a 5^{th}-order polynomial, retain more low-frequency variability. Using this alternate CO_2 fit, the anti-correlation between CO_2 and $\Delta^{14}C$ anomalies at DRP increases and becomes significant ($p < 0.05$), while correlations between CO_2 and the SAM decrease, remaining significant at fewer lags. Correlations to the SOI and the QBO do not change substantially. As an additional check on the robustness of our conclusions based

on correlation of anomalies, we next evaluate relationships based on the observed CO_2 and $\Delta^{14}C$ rates of change.

3.2 Rates of Change

Unlike concentration anomalies, the rates of change of CO_2 and $\Delta^{14}C$ are theoretically directly proportional to the instantaneous fluxes acting on the observations and associated air parcel. Butler *et al.* [2007] found that the rate of change of CO_2 at Palmer Station (PSA) on the Antarctic Peninsula near Drake Passage during the period 1980-2005 regresses significantly onto the SAM. Their method calculated anomalous rates of change, or "tendency," by dividing the change in average monthly CO_2 across three months by the elapsed time and subtracting the climatological average monthly rate to remove the average seasonal cycle. The trade-off inherent to this method is a loss of information due to the temporal averaging that is necessary to reduce noise, particularly in our case, where the necessary observations in neighboring months are not always available. We have repeated the original analysis of Butler *et al.* [2007] (see Butler *et al.* [2007] for details of the calculation methods) using the updated CO_2 record from PSA, which now extends from 1980 to 2015 (downloaded from http://www.esrl.noaa.gov/gmd/dv/data/?site=psa) , and also on the CO_2 and $\Delta^{14}C$ records from DRP. We excluded outliers from the observations from DRP in the same manner as before, but all other aspects of this analysis are independent of the function fits applied in our analysis of discrete anomalies above.

Regressions (zero lag) of CO_2 rate anomalies onto the SAM index from Butler et al. [2007] and our updated regressions of PSA and DRP CO_2 rates of change are shown in Table 4.1. The DRP climatology that is subtracted from monthly average rates to calculate rate

Station Name	Regression onto the SAM, cold season	Regression onto the SAM, warm season	Regression onto the SAM, all months
PSA as in Butler *et al.,* [2007]	**0.032**	0.017	**0.025**
PSA through 2014	**0.029**	0.020	**0.025**
DRP	0.031	0.012	0.019

Table 4.1: Regressions of CO_2 rates of change from Butler et al., 2007, compared to updated regressions from PSA and DRP calculated using the same method. Units are ppm/month per standard deviation of the SAM. Cold months are April-September and warm months are October-March. Significant regressions are in bold.

anomalies is questionable due to the short length of the time-series and its frequent gaps in austral winter, and the regression values between the DRP rates and the SAM are not statistically significant. We show them despite those caveats because they are consistent with the significant regressions at PSA, including the pattern of greater regression values in winter. The weaker regressions found for austral summer months are likely related to biological activity, which causes greater variability of SO surface DIC and alkalinity in warm months than during the light-limited austral winter [*Munro et al.*, 2015].

$\Delta^{14}C$ rate anomalies at DRP are anti-correlated with CO_2 rate anomalies at DRP with low significance ($R = -0.23$, $p = 0.15$). This is essentially the same relationship observed for monthly concentration anomalies using the previous method, but with lower significance because of a further reduction in degrees of freedom. CO_2 rate-of-change anomalies at PSA correlate most highly with the SAM ($R = 0.17$, $p < 0.001$) at zero months lag, while correlations between the shorter time-series of CO_2 rate anomalies from DRP and the SAM are not significant at any lag (lag correlations not shown).

CO_2 rate anomalies at PSA and CO_2 and $\Delta^{14}C$ rate anomalies at DRP are not significantly correlated with the SOI at zero lag. CO_2 anomalous rates at PSA are negatively correlated with the SOI with high significance ($p < 0.05$) at 3-5 months lag (higher growth rates following El

Niño conditions), consistent with a transported signal of the globally observed relationship between ENSO and the terrestrial biosphere's influence on global CO_2 growth rates [e.g. *Wang et al.*, 2013]. A similar significant ($p < 0.05$) anti-correlation between CO_2 rates and the SOI is observed at DRP at 2 months lag (lag correlations not shown). We do not observe any significant relationships between $\Delta^{14}C$ rate anomalies at DRP and the SOI. The evidence for a relationship between SO upwelling and the SOI, which was supported by correlations between CO_2 and $\Delta^{14}C$ concentration anomalies and the SOI at DRP, is not apparent in CO_2 and $\Delta^{14}C$ data from DRP when viewed as rate anomalies, or in CO_2 rate anomalies from PSA. It is possible that this is due to the different timescales emphasized by the different methods. For example, a local CO_2 response to SO upwelling during La Niña periods might, when averaged over the three months to calculate the rate of change, be swamped by the transported signal of the terrestrial CO_2 response, which is of the opposite sign but may lag ENSO by several months [*Wang et al.*, 2013].

The strongest and most consistent relationships that we observe in this second analysis are the correlations and regressions between CO_2 and $\Delta^{14}C$ rates of change and the SAM. These are consistent with the dominant mode of CO_2 variability near Drake Passage being caused by changes in the flux of low-$\Delta^{14}C$ carbon from the deep SO, as described previously. Butler *et al*. [2007] likewise concluded that the relationship they observed between CO_2 rates-of-change at PSA and the SAM was likely due to greater upwelling of deep ocean carbon during periods of high SAM, and our CO_2 and $\Delta^{14}C$ results from the DRP location are consistent with that attribution.

4. Conclusions

The anti-correlation between CO_2 and $\Delta^{14}C$ anomalies at DRP suggests that greater upwelling in the SO increases the sea-air gross carbon flux and lowers its $\Delta^{14}C$, temporarily reducing the net uptake of carbon and decreasing the $\Delta^{14}C$ of overlying air. The correlations we observe between our observations and the SAM are consistent with increased upwelling and decreased net carbon uptake caused by the stronger westerly winds during periods with higher SAM conditions, and are consistent with the sense of the relationship between the SAM and the SO carbon sink suggested by previous observational [*Butler et al.*, 2007] and modeling studies [*Le Quéré et al.*, 2007; *Lovenduski et al.*, 2007].

Correlations between monthly CO_2 and $\Delta^{14}C$ anomalies at DRP and the SOI appear consistent with a tropical teleconnection linking the ENSO state to upwelling upwind of the DRP location, leading to more ocean carbon outgassing at least in the Pacific Sector of the SO during La Niña periods. This conclusion is consistent with recent model results [*Conrad and Lovenduski*, 2015] but is not as clearly supported across the different tracers and locations that we examine here, possibly because of an opposing CO_2 signal that is transported from the terrestrial biosphere on the 3-month timescale of the rate anomalies.

These suggested links between SO upwelling, carbon exchange and dominant modes of atmospheric variability have the potential to improve our understanding and prediction of a major portion of the global ocean sink for anthropogenic carbon, by illuminating some causes of its short term variability. Knowledge of these mechanisms may help predict how the SO carbon sink will change in the future due to physical feedbacks from global warming. If these relationships are stationary, they may also help shed light on major changes in the global carbon cycle during late Pleistocene glacial-interglacial cycles, when the response of the SO to changes

in the westerly winds may have helped redistribute carbon from the deep ocean to the atmosphere during periods of global warming [e.g. *Toggweiler et al.*, 2006; *Anderson et al.*, 2009].

Chapter V: Radiocarbon evidence for the reemergence of mode waters with rising anthropogenic carbon concentrations

Abstract:

The quantity of radiocarbon (^{14}C) in the atmosphere was nearly doubled by nuclear weapons testing in the 1960s. Since then, the terrestrial biosphere and the ocean have absorbed most of the excess ^{14}C from the atmosphere, although atmospheric radiocarbon activity ($\Delta^{14}C$) continues to decline due to ongoing emissions of ^{14}C-free CO_2 from combustion of fossil fuels. The large transient decline in atmospheric $\Delta^{14}C$ combined with gas exchange at the surface and spatially variable time scales of ocean mixing have led to large $\Delta^{14}C$ gradients in the surface ocean between upwelling- and downwelling-dominated regions. These gradients continue to evolve over time. We examine the rate of change of surface ocean $\Delta^{14}C$ between CLIVAR (2000-2011) and WOCE era (1990s) or other slightly earlier (1980s) datasets and find spatial patterns that reveal mixing between ^{14}C-enriched mode waters, ^{14}C-depleted deep waters and surface waters that are well-equilibrated with the atmosphere. The $\Delta^{14}C$ of mode water reaching equatorial upwelling regions has increased between the WOCE and CLIVAR time periods, and the greater contribution of ^{14}C to the low-latitude surface ocean appears to have significantly offset the $\Delta^{14}C$ decline otherwise imparted by air-sea gas exchange with the atmosphere. Consequently, $\Delta^{14}C$ gradients between low-latitude upwelling regions and gyre centers have weakened proportionally more than between gyre centers and regions where pre-industrial water still upwells, such as the Southern Ocean. Properly accounting for the re-emergence of water with post-industrial characteristics is important to constrain ocean circulation models that seek to explain DIC, pH and other anthropogenically perturbed tracers in the surface ocean. Because of the history of $\Delta^{14}C$ in the atmosphere, ocean $\Delta^{14}C$ is a useful tracer for this purpose.

1. Introduction:

The ocean has absorbed almost half of the cumulative anthropogenic CO_2 emissions since 1800 [*Sabine and Tanhua*, 2010; *Khatiwala et al.*, 2013], but this excess carbon is stored in waters that will return to the surface after a wide range of residence times in the ocean interior. In the 1990s, 40% of anthropogenic carbon in the ocean was in mode and intermediate waters that are formed near the surface in the Southern Ocean, subducted below warmer waters to the north, and transported below the thermocline into the three other major ocean basins [*Sabine et al.*, 2004b]. CFC-based ventilation ages in the Pacific Ocean suggest that high-latitude mode waters reach the equatorial subsurface with an average transit time of several decades [*Fine et al.*, 2001], and model results suggest that subtropical and subpolar mode waters comprise a significant portion of the upwelling volume in the equatorial pacific [*Rodgers*, 2003]. Therefore, at least some of the anthropogenic carbon stored in mode waters will return to the surface near the equator. Re-emerging anthropogenic carbon could increase the rate of equatorial CO_2 outgassing, decreasing the net ocean carbon sink, as well as increasing the rate that pH is decreasing in equatorial surface waters. It is important that this process be observed and understood, so that it is accurately represented in coupled climate-carbon cycle models used to predict future ocean and atmosphere CO_2 inventories and ocean pH from current and predicted CO_2 emissions.

Partial pressures of CO_2 (pCO2) in Western Equatorial Pacific surface waters appear to have risen over the period 1990-2009 at a rate higher than can be explained by exchange with the atmosphere, suggesting that increasing amounts of carbon were transported to equatorial upwelling by subsurface currents [*Ishii et al.*, 2009]. The hypothesized mechanism of Ishii et al.

[2009] does not require changing transport, as steady-state general circulation patterns would result in the eventual reemergence of mode waters that, when last at the surface, were exposed to rising 20th century atmospheric CO_2 concentrations. Water that equilibrated with the atmosphere in the mid 20th century also carries evidence of the large signal from excess radiocarbon production from above-ground nuclear weapons testing, providing another way to look for evidence of re-emerging 20th century carbon.

Radiocarbon (^{14}C) is a rare radioactive isotope of carbon that is produced when high-energy particles collide with nitrogen in the atmosphere. Production occurs both naturally as a result of cosmic rays and anthropogenically as a byproduct of nuclear reactions used in power generation and weapons. Nuclear weapons testing in the 1950s and 1960s caused a transient spike in global ^{14}C production, nearly doubling the $\Delta^{14}C$ (^{14}C:^{12}C referenced to a standard and reported in units of per mil) of atmospheric CO_2 before atmospheric weapons testing was banned. ^{14}C decays with a half-life of 5700 years [*Godwin*, 1962; National Nuclear Data Center, Brookhaven National Laboratory, www.nndc.bnl.gov] and consequently almost all of the ^{14}C produced by weapons testing still exists. The pool of carbon dissolved in the deep ocean has $\Delta^{14}C$ below that of the atmosphere due to radioactive decay since equilibration with the atmosphere. Exchange with the shallow ocean and the biosphere, as well as dilution from the addition of ^{14}C-free CO_2 ($\Delta^{14}C$ = -1000 ‰) from fossil fuel burning, has caused atmospheric $\Delta^{14}C$ to decline since the 1960s [*Levin and Hesshaimer*, 2000]. Conversely, the flux of high-$\Delta^{14}C$ CO_2 into the ocean from air-sea gas exchange initially raised surface ocean $\Delta^{14}C$, producing a transient tracer in the ocean that has been used extensively to constrain carbon uptake and mixing (see Nydal [2000] for a review).

In this study we compare a global compilation of recent (post-2000) radiocarbon

observations from the surface ocean to the 1990s-era Global Ocean Data Analysis Project [GLODAP, *Key*, 2004] radiocarbon dataset (post-2000 observation locations and gridded GLODAP $\Delta^{14}C$ plotted in Figure 5.1), enabling us to look for evidence of the re-emergent anthropogenic carbon inferred by Ishii *et al.,* [2009] over roughly the same time period. The patterns of $\Delta^{14}C$ in dissolved inorganic carbon (DIC) seen at the ocean surface in the 1990s (see Figure 5.1) were caused primarily by spatially varying rates of upwelling, and help to illustrate where carbon is most likely to re-emerge from the ocean interior. The lowest $\Delta^{14}C$ was observed in the Southern Ocean, where a large proportion of the DIC pool is old, ^{14}C-depleted carbon that has been recently upwelled from the deep ocean. The highest $\Delta^{14}C$ was observed in the center of the subtropical gyres, where water collects that has been at or near the surface for years, exchanging CO_2 with the atmosphere and approaching isotopic equilibrium. Surface $\Delta^{14}C$ near the equator was intermediate between that of the Southern Ocean and gyre centers during the

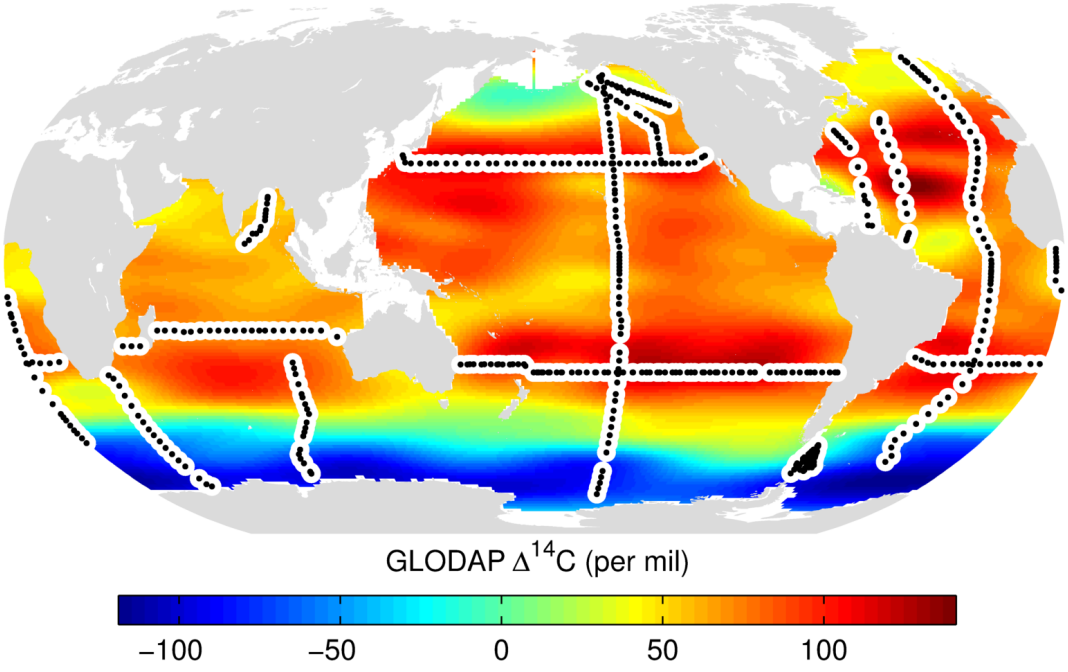

Figure 5.1: Locations of post-2000 surface $\Delta^{14}C$ observations used in this study (black dots), overlaying color contour of GLODAP surface $\Delta^{14}C$.

1990s. In the eastern equatorial Pacific Ocean, the weak minimum in surface $\Delta^{14}C$ is due to upwelling of Subantarctic Mode Water [SAMW, potential density ~26.8 σ_θ, *McCartney*, 1977, 1982], which carries poorly equilibrated DIC from the Southern Ocean surface with an average transit time of several decades [*Toggweiler and Dixon*, 1991; *Fine et al.*, 2001; *Rodgers*, 2003]

Excess bomb ^{14}C and DIC in the GLODAP dataset is defined as the increase above pre-industrial levels, and estimated using empirical methods [*Rubin and Key*, 2002; *Sabine et al.*, 2004b]. Within the density level of SAMW, both excess $\Delta^{14}C$ and DIC have very similar spatial patterns, revealing a snapshot of isopycnal mixing and advection in the process of transmitting the high ^{14}C and CO_2 concentrations of the recent atmosphere from high to low latitudes (Figure 5.2). It is clear from these correlated gradients that as SAMW transmits greater amounts of anthropogenic carbon to the low-latitude surface, the DIC it carries should also include a transient signal of increasing $\Delta^{14}C$.

Previous studies comparing $\Delta^{14}C$ from repeat occupations of a transect in the Pacific found that $\Delta^{14}C$ increased in low-latitude mid-depth waters denser than ~26.25 σ_θ between the 1990s and early 2000s, while it declined in the well-equilibrated shallow ocean due to more recent exchange with the atmosphere [*Jenkins et al.*, 2010; *Graven et al.*, 2012]. Thus, the positive rate of change of $\Delta^{14}C$ in SAMW as it upwells into the low-latitude ocean and brings higher anthropogenic concentrations of DIC should contrast with the declining $\Delta^{14}C$ in shallower water, unlike the trend of increasing DIC which is the same sign as in the atmosphere and shallow ocean. In addition to this advantage, $\Delta^{14}C$ is normalized using ^{13}C to correct for fractionation due to temperature variations or biological activity, both of which can impose trends on pCO_2 observations even when the flux of upwelling DIC is constant.

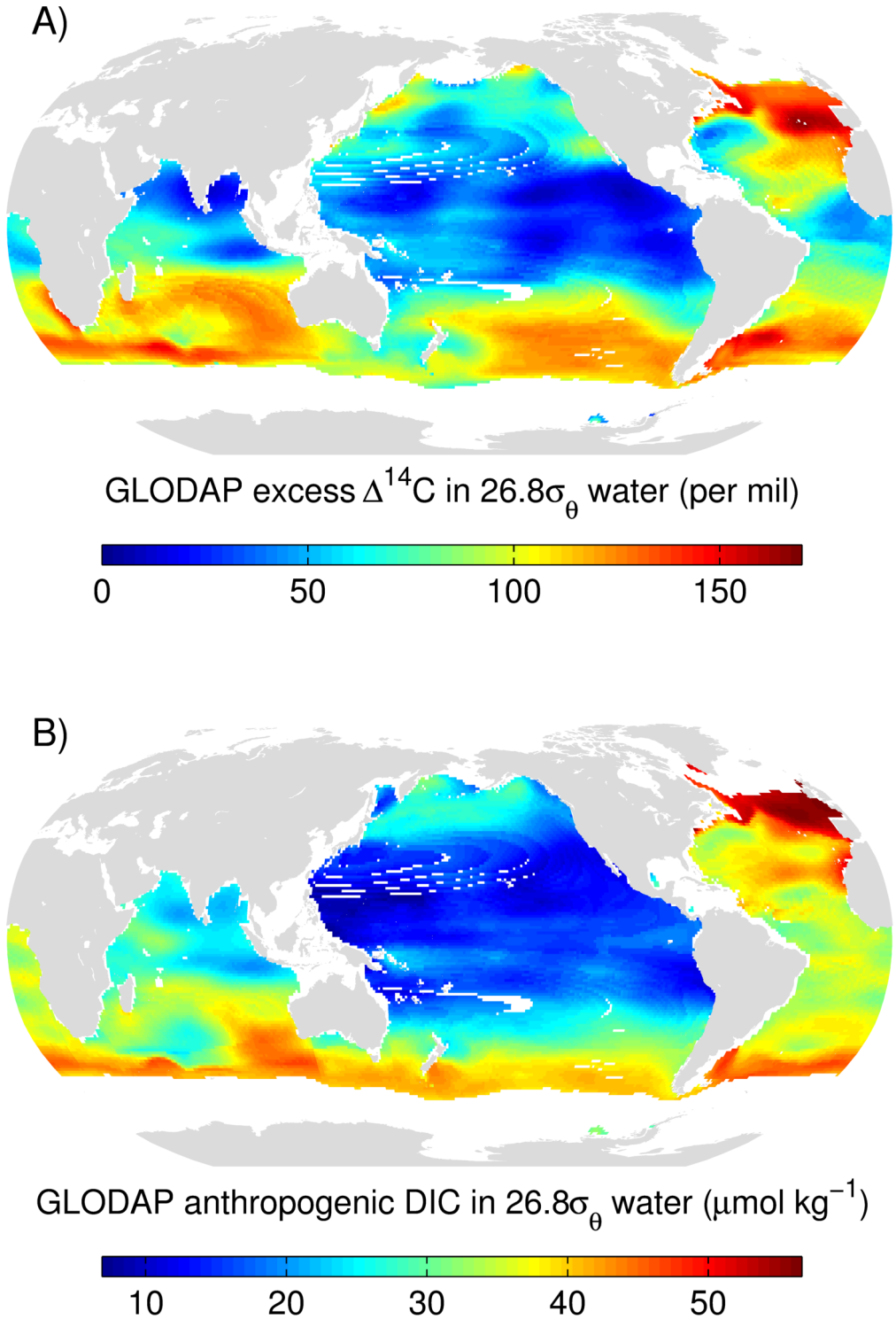

Figure 5.2: A) Color contour plots of excess $\Delta^{14}C$ and **B)** anthropogenic DIC from the GLODAP gridded dataset [*Key*, 2004] in waters with 26.8 ± 0.05 σ_θ. Density anomaly was estimated using the Gibbs Seawater Oceanographic Toolbox [*MacDougall and Barker*, 2011] and temperature and salinity from the World Ocean Atlas 2013 [WOA13; *Locarnini et al.*, 2013; *Zweng et al.*, 2013]. GLODAP data was linearly interpolated to match the WOA13 grid, binned by density anomaly, and then averaged at each horizontal location.

Observations and modeling of $\Delta^{14}C$ trends in the Equatorial Pacific suggest that the subsurface was already a source of excess ^{14}C to the surface by the mid 1970s, via shallow meridional cells that feed water into the equatorial subsurface from the gyre centers [*Quay et al.*, 1983; *Mahadevan*, 2001]. Thus anthropogenic carbon is likely already recycled on a sub-decadal timescale in these shallow cells. Here we ask the question whether rising $\Delta^{14}C$ in waters denser than ~26.25 σ_θ, i.e. in subtropical mode water and SAMW, has become detectible at the low-latitude surface since the 1990s. If so, that would be evidence that all densities of water that contribute to equatorial upwelling are now bringing re-emergent, excess anthropogenic carbon to the surface.

2. Data and Methods:

The GLODAP dataset contains observations of DIC concentrations and $\Delta^{14}C$ in the ocean, primarily from samples collected in the 1990s but with a small proportion sampled in the previous two decades [*Key*, 2004]. GLODAP $\Delta^{14}C$ is available both as an interpolated and gridded data set with a nominal date of 1995, and as individual measurements on bottle samples. Ocean $\Delta^{14}C$ was surveyed again in the early 2000s as part of the Climate Variability and Predictability (CLIVAR) repeat hydrography program [www.clivar.org]. We have compiled near-surface $\Delta^{14}C$ observations (<50 mwd or < 50 dbars if only pressure data was available) from CLIVAR and other post-2000 cruises from all available sources [*Fukasawa and Murata*, 2001; *Guilderson et al.*, 2006, 2012; *Dutta et al.*, 2010; *Kumamoto et al.*, 2011, E. Druffel, unpublished data; A. McNichol & R. Key, unpublished data]. Surface ocean $\Delta^{14}C$ from both GLODAP and from our post-2000 compilation varies from near or slightly above coeval atmospheric $\Delta^{14}C$ to several hundred per mil below it in the Southern Ocean (Figure 5.3).

We calculated rates of $\Delta^{14}C$ change for each post-2000 surface $\Delta^{14}C$ observation, in units of ‰ per year, by subtracting the geographically closest GLODAP gridded surface $\Delta^{14}C$ value from the post-2000 surface $\Delta^{14}C$ and dividing by the time elapsed since Jan 1, 1995. The use of the interpolated $\Delta^{14}C$ dataset enabled later measurements to be used even if they were not from precisely the same location as bottle data used in the earlier dataset. The inclusion of data from the 1980s and 1970s could bias parts of the GLODAP surface $\Delta^{14}C$ map to higher than true 1995 values (see Figure 5.3), which would result in a negative bias in our observed rates. Such a bias

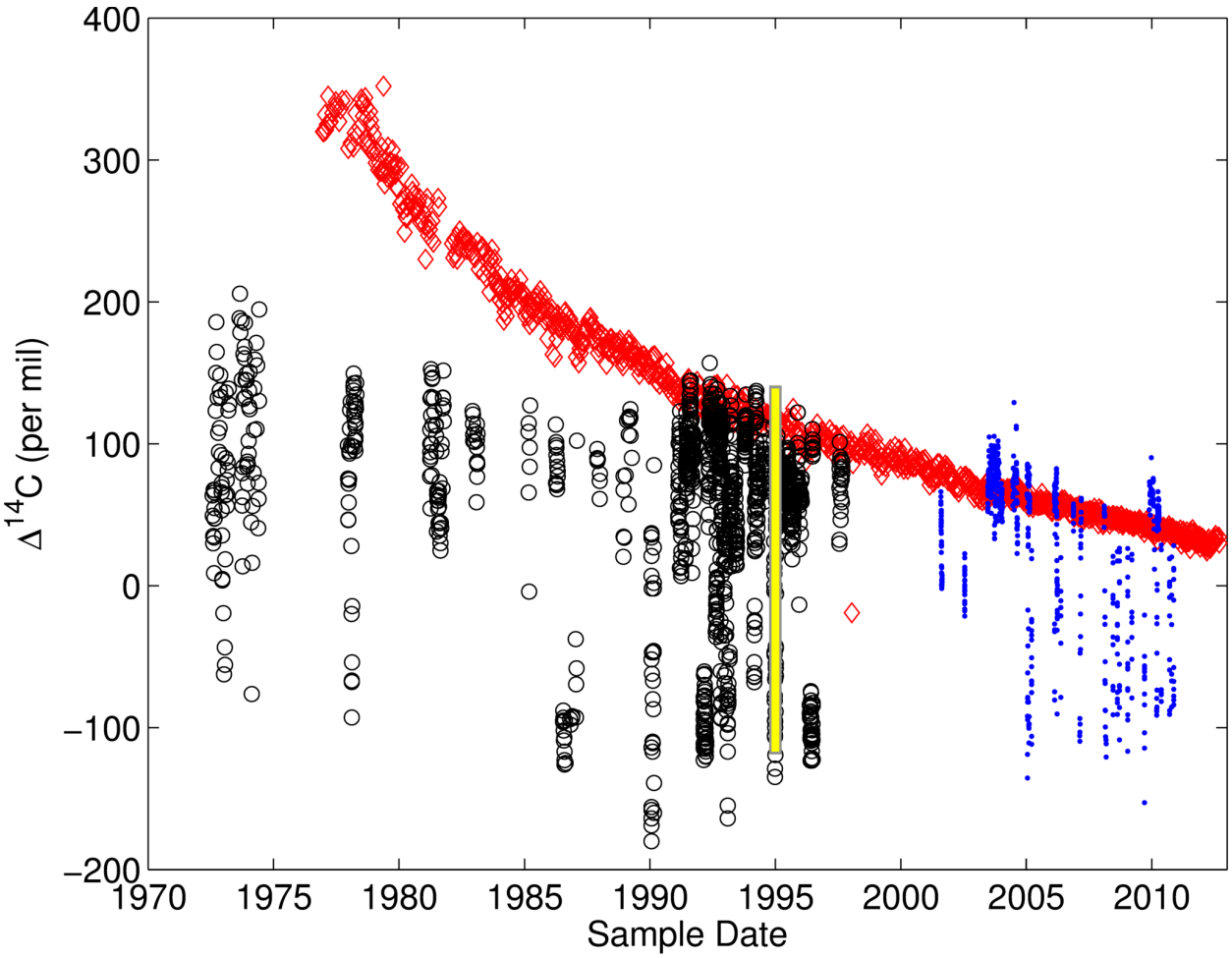

Figure 5.3: GLODAP surface ocean $\Delta^{14}C$ of DIC from bottle samples (open black circles) and the gridded dataset (yellow bar; [*Key*, 2004]), compiled surface ocean $\Delta^{14}C$ observations since 2000 (small blue symbols), and atmospheric $\Delta^{14}CO_2$ measurements from Schauinsland and Niwot Ridge (red diamonds, [*Levin and Kromer*, 1997; *Turnbull et al.*, 2007]), plotted versus sampling date.

would act to diminish any signal of rising $\Delta^{14}C$ in upwelling SAMW and thus our conclusions based on anomalously high rates of change in regions affected by these waters are conservative.

3. Results and Discussion:

Rates of $\Delta^{14}C$ change have similar meridional gradients in each ocean basin (Figure 5.4), likely due to similar patterns of upwelling and circulation. $\Delta^{14}C$ has declined most rapidly since the 1990s near the center of the subtropical gyres, at around 40° N and S. These lowest rates are less negative than the rate of change in the atmosphere for the period 1995-2013 (bottom dashed black line in Figure 5.4), except for those at the center of the North Pacific gyre that are roughly equal to the atmospheric rate. Near-zero rates are observed near the equator in all ocean basins, while strongly positive rates are observed at the most northern latitudes in the Atlantic Ocean. Rates in most of the Southern Ocean are negative, but less so than the atmospheric rate, with rates closer to zero at the most southerly latitudes. We define the northern boundary of the Southern Ocean here as the 20 ‰ $\Delta^{14}C$ isoline in the GLODAP gridded surface product, as it appears to trace the Subantarctic Front that separates the upwelling-dominated low $\Delta^{14}C$ waters of the Antarctic Circumpolar Current from the high $\Delta^{14}C$ waters that characterize the southern Subtropical gyres.

The difference between rates of $\Delta^{14}C$ change observed in the far northern North Pacific and North Atlantic oceans may be due to decadal changes in surface convection and mixing that occurred in recent decades, possibly combined with biases of sampling dates in the GLODAP dataset. Most of the GLODAP surface $\Delta^{14}C$ observations from the North and South Atlantic Ocean were sampled before 1990, while most of those from the North and South Pacific surface were sampled during the 1990s (Figure 5.5). Mixed layer depths in the subsequent 15 year period

(1990-2004) in the high-latitude North Atlantic (north of ~50° N) were significantly larger than in the 1970s and 1980s, and also grew slightly larger in the North Pacific [*Carton et al.*, 2008]. Deeper mixed layer depths after 2000 in the North Atlantic may have exhumed mode water with high excess $\Delta^{14}C$ stored previously when atmospheric $\Delta^{14}C$ was higher (see Figure 5.2),

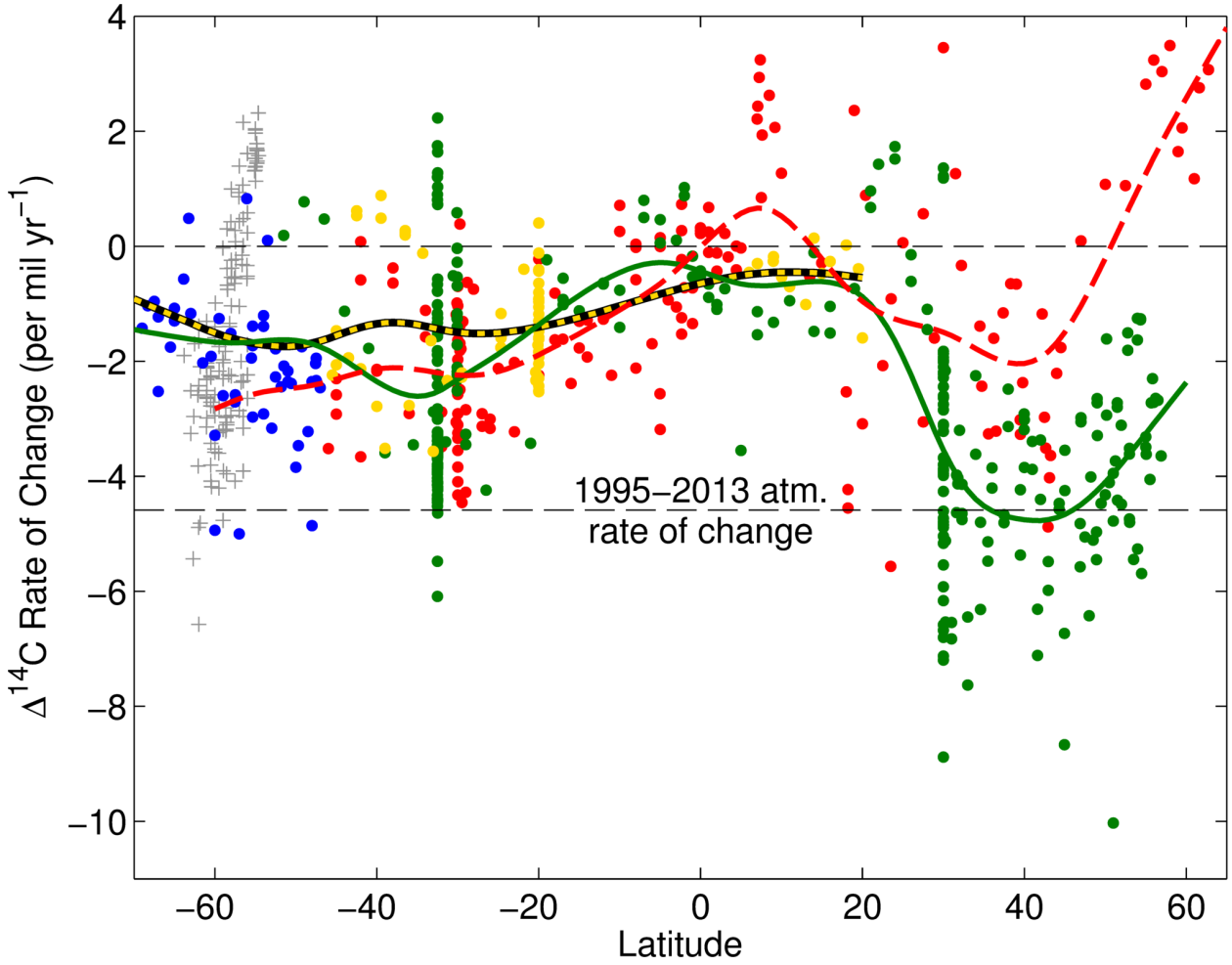

Figure 5.4: $\Delta^{14}C$ rates of change since the 1990s plotted versus latitude. Each rate is based on a single surface ocean $\Delta^{14}C$ observation and the corresponding $\Delta^{14}C$ from the GLODAP gridded dataset, from locations in Drake Passage (grey plus signs), elsewhere in the Southern Ocean (blue circles), the Pacific Ocean (green circles), the Indian Ocean (yellow circles) and the Atlantic Ocean (red circles). Smoothing spline fits are plotted for the Pacific (green solid line), Indian (yellow and black dashed line) and Atlantic (red solid line) ocean basins, including data at far southern latitudes but excluding Drake Passage data. Grey dashed lines indicate no change (0 ‰ per year) and the linear trend of atmospheric $\Delta^{14}C$ over the period 1995-2013 (-4.6‰ per year). The boundary between the Southern Ocean and the ocean basins to the north is defined as the 20‰ isoline in GLODAP surface $\Delta^{14}C$.

transiently elevating surface $\Delta^{14}C$ and leading to transiently positive rates of $\Delta^{14}C$ change in the North Atlantic. Increased mixed layer depths since the 1990s in the Pacific, which is more stratified and contains less excess ^{14}C in the shallow subsurface (Figure 5.2) may have exposed more pre-industrial water, transiently lowering $\Delta^{14}C$.

Surface $\Delta^{14}C$ in Drake Passage (grey pluses in Figure 5.4) has been sampled much more frequently than other locations in the Southern Ocean, which likely explains the larger range of observed rates of change. Drake Passage spans the Antarctic Circumpolar Current, where the juxtaposition of deep, aged water upwelling to the south and better-equilibrated subtropical water

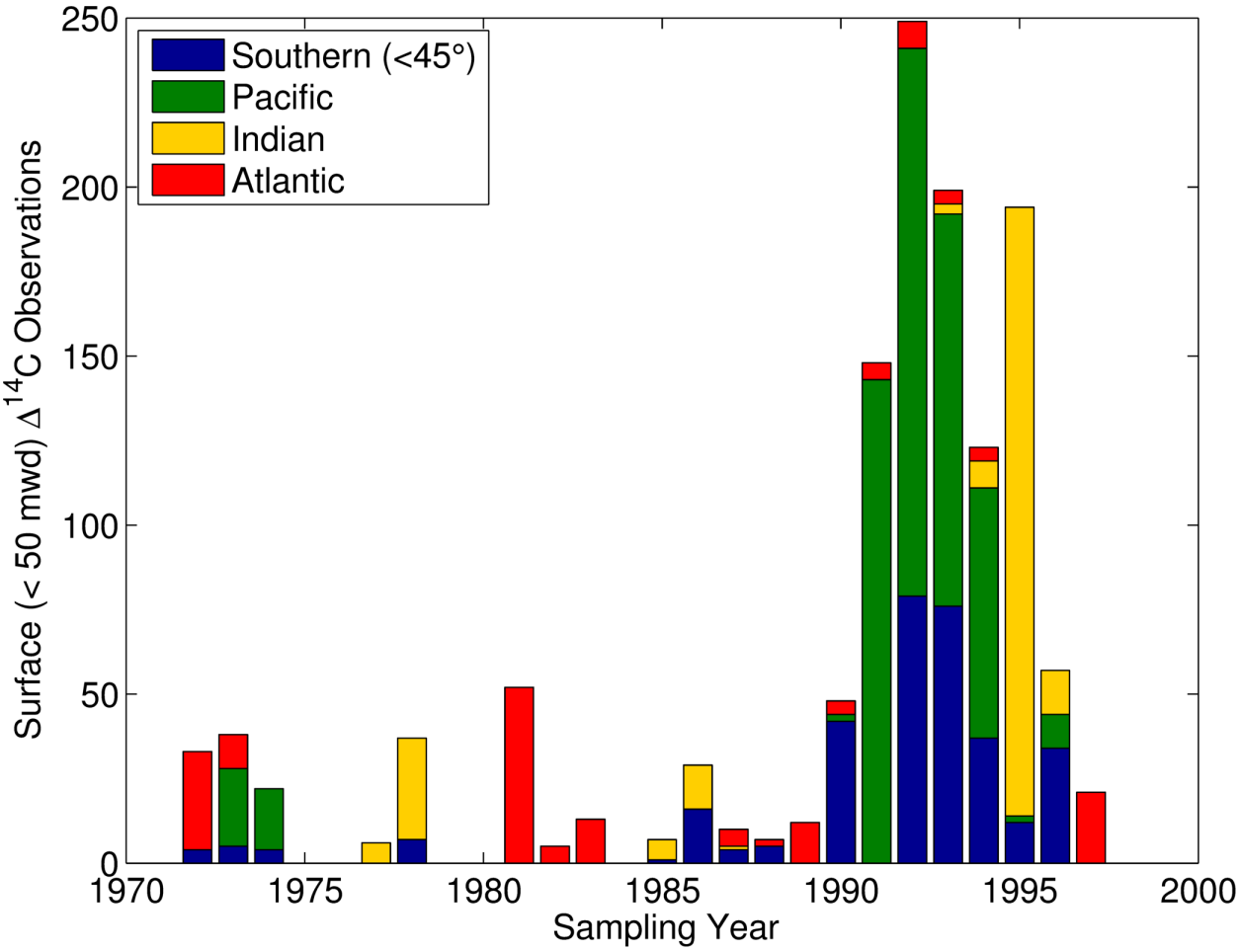

Figure 5.5: Histogram of surface ocean (< 50 mwd) $\Delta^{14}C$ observations from the Southern Ocean (< -45° latitude; dark blue bars), Pacific Ocean (green bars), Indian Ocean (yellow bars) and Atlantic Ocean (red bars) that were used to construct the GLODAP gridded $\Delta^{14}C$ dataset [*Key*, 2004], plotted by sampling year.

from the north causes a sharp gradient in surface $\Delta^{14}C$ (see Figure 5.1). Transport variability such as eddies operating across that steep gradient may have caused the large variability in rates observed by the frequent sampling. To avoid an artifact from this unequal sampling, the Drake Passages observations were not included in the data used to calculate the smoothing splines for the Pacific or Atlantic Oceans in Figure 5.4, but are discussed in our conclusions with respect to local mixing phenomena.

Regional sampling issues aside, the global pattern of rates in Figure 5.4 can be explained by DIC sourced from the deep and mid-depth ocean, with different isotopic trends, combining with atmospheric carbon taken up by the surface ocean. The excess ^{14}C produced during the 20th century has not yet reached the oldest waters that upwell in the Southern Ocean, and thus the $\Delta^{14}C$ of the densest upwelling deep waters in the Southern Ocean is unchanging ($\Delta^{14}C$ rate = 0 ‰ per year). Air-sea gas exchange while water remains at the surface introduces carbon from the atmosphere that is experiencing negative rates of $\Delta^{14}C$ change. By the time surface water accumulates at gyre centers, the DIC it contains is largely composed of carbon that was recently in the atmosphere, and thus the $\Delta^{14}C$ trends in gyre centers will tend to mirror the rate of change in the atmosphere. The near-zero and positive rates of $\Delta^{14}C$ change in surface waters near the equator in all ocean basins suggest that SAMW, or some other component of the upwelling water, has increasing $\Delta^{14}C$ that counteracts the atmospheric trend. As argued in the introduction, this is consistent with anthropogenic carbon resurfacing from SAMW.

The extent of mixing between upwelling water and well-equilibrated surface water can be visualized by plotting the calculated rates versus the 1990s $\Delta^{14}C$ for their location (Figure 5.6). The 1990s $\Delta^{14}C$ essentially reflects the combination of carbon sourced from the atmosphere and the ocean interior and what the $\Delta^{14}C$ was in those carbon sources at the time. Given quasi-steady

state circulation, we expect the $\Delta^{14}C$ rate of change since the 1990s to likewise reflect the fractional combination of carbon from the same water masses and what the rate of $\Delta^{14}C$ change was for each carbon source, and therefore the post-2000 rates vs. the 1990s $\Delta^{14}C$ should plot roughly linearly where carbon from only two water sources is combined.

When viewed in this way, rates of $\Delta^{14}C$ change in the Southern Ocean (excluding Drake Passage) describe a mixing line between an unchanging deep ocean and the atmospheric rate.

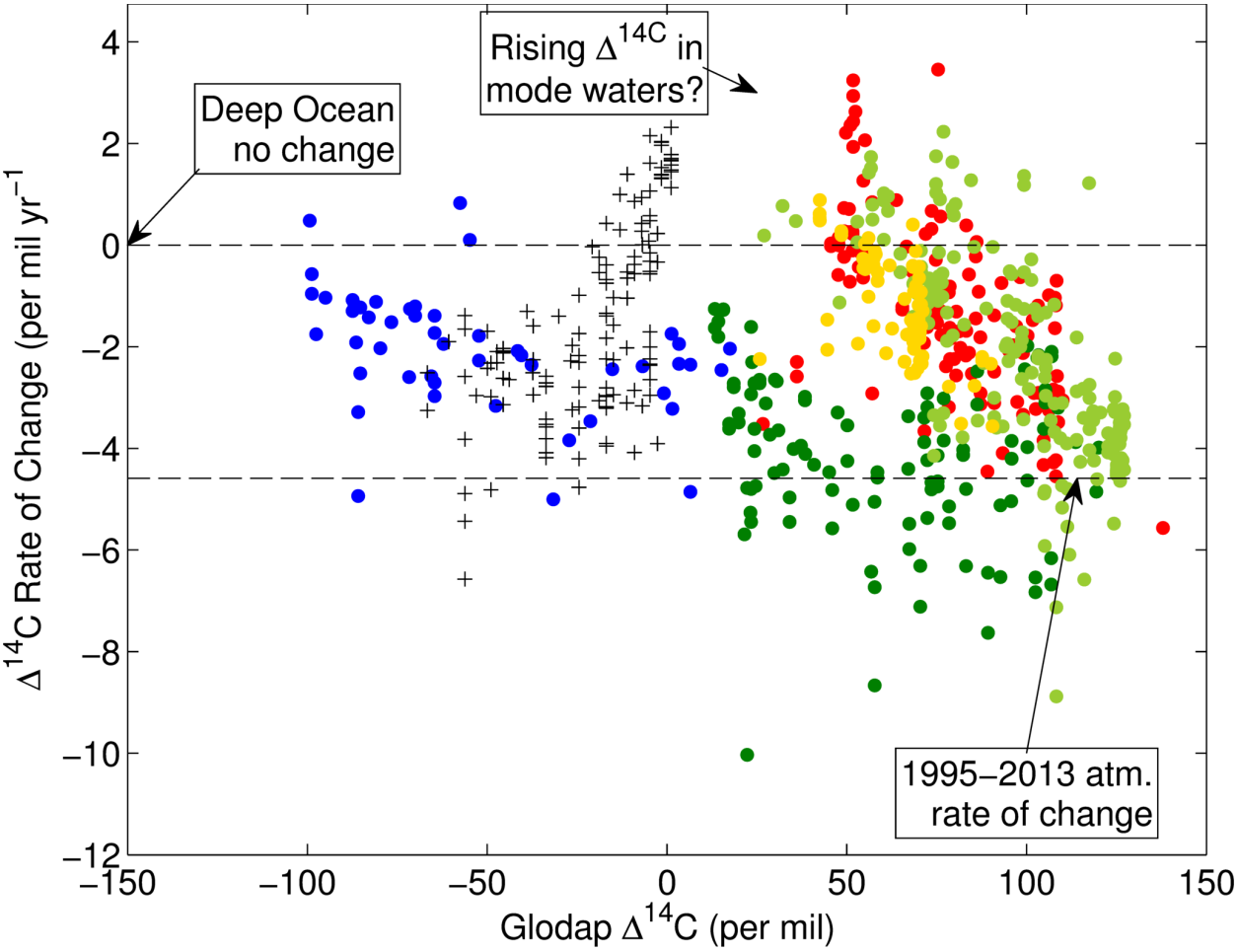

Figure 5.6: $\Delta^{14}C$ rates of change since the 1990s plotted versus GLODAP $\Delta^{14}C$. Colors and symbols are the same as in Figures 4, except that rates from the low latitude and southern subtropical Pacific Ocean (south of 30° N and north of the Southern Ocean) are plotted as light green circles to differentiate them from the far North Pacific rates. Rough estimated rates of change and 1990s $\Delta^{14}C$ of end-member values for the apparent mixing lines within the data are labeled with arrows.

The estimated rates and 1990s $\Delta^{14}C$ of these carbon sources are shown by points corresponding to 0 ‰ per year and -150 ‰ for the deep ocean and -4.6 ‰ per year and 114 ‰ for the atmosphere. Results from the North Pacific north of 30° N (dark green filled circles in Figure 5.6) also appear to fall on this mixing line. This may be caused by upwelling of water in the North Pacific subpolar gyre that had a $\Delta^{14}C$ rate of change of about -2 ‰/year and 1990s $\Delta^{14}C$ of ~0 ‰. Alternatively, it could have been caused by deep water with similar characteristics to Southern Ocean deep water (0 ‰ per year, -150 ‰ 1990s $\Delta^{14}C$) that upwelled in both locations, but combined with a much greater proportion of recently equilibrated water in the North Pacific than in the Southern Ocean. As described previously, the observed rates in the far North Pacific were possibly affected by changes in winter mixed layer depth, and thus may not reliably reflect the rate of change of $\Delta^{14}C$ in any single water mass. The focus of this study is instead on the low-latitude results.

Rates of $\Delta^{14}C$ change in the low-latitude and southern hemisphere subtropical surface ocean in all three ocean basins (Atlantic data from >30° N is omitted from Figure 5.6) appear to lay along a different mixing line between atmospheric carbon and a carbon source with rising $\Delta^{14}C$ and 1990s $\Delta^{14}C$ below 50 ‰. This is consistent with the previously observed rising $\Delta^{14}C$ in waters denser than 26.25 σ_θ [*Jenkins et al.*, 2010; *Graven et al.*, 2012] emerging in the densest upwelling water at the equator. Given the high correlation between excess $\Delta^{14}C$ and anthropogenic DIC in the density layer of SAMW, increasing concentrations of anthropogenic DIC must also now be entrained in SAMW and welling up in equatorial regions, leading to a regionally anomalous increase in pCO_2. We conclude that $\Delta^{14}C$ observations made since the 1990s are consistent with Ishii et al.'s [2009] pCO_2 observations, and imply that all densities of upwelling water at the equator now carry rising concentrations of anthropogenic carbon.

The steep $\Delta^{14}C$ gradient between the Southern Ocean and the Southern subtropical gyres appears to separate regimes during the 1990s-2000s with contrasting rates of $\Delta^{14}C$ change, indicated by the switch from negative to positive rates of $\Delta^{14}C$ change at about 20 ‰ 1990s $\Delta^{14}C$. In this view, the large variability in rates calculated from the frequent observations at Drake Passage appears to be due to mixing between re-emergent mode water and a point on the atmosphere-deep ocean mixing line, perhaps as a result of eddy transport across the Subantarctic front.

The results from the low latitude Atlantic, Pacific and Indian oceans all appear to lie along a similar mixing line that requires SAMW with $\Delta^{14}C$ that increased ~3‰ per year and had a 1990s $\Delta^{14}C$ of ~30‰, consistent with the characteristics of SAMW observed by Jenkins et al. (2010) at about 20° S in the South Pacific. No extrapolation of the low-latitude mixing lines towards lower 1990s values could reach a reasonable pre-industrial $\Delta^{14}C$ value for the subsurface ocean (-50‰ or lower) while staying below a rate of 0 ‰ per year, and thus it is very unlikely that this end-member could represent a mode water with preindustrial characteristics. These consistent results across ocean basins also make it unlikely that high $\Delta^{14}C$ rates near the equator are an artifact of, for example, reduced upwelling in the Easter Equatorial Pacific due to sampling an El Niño year, or a shift to upwelling less-dense and better-equilibrated mode water, as this change in dynamics would have had to occur nearly simultaneously and cause a nearly identical bias in all three oceans. More ^{14}C observations from the ongoing GO-SHIP repeat hydrography effort (www.go-ship.org), particularly from undersampled equatorial regions such as the eastern equatorial Pacific, could help better characterize the densest equatorial upwelling water, but the window of time to observe the transient pattern exploited in this study is limited by the short decadal-scale duration of the bomb carbon pulse in mode waters. SAMW closer to the

formation region in the Southern Ocean already appears to have decreasing $\Delta^{14}C$ over this same time period [*Jenkins et al.*, 2010].

In the future, surface ocean $\Delta^{14}C$ trends will continue to be a function of the rate of $\Delta^{14}C$ change in the atmosphere, combined with the $\Delta^{14}C$ trends in upwelling waters, but as the transient spatial gradients seen in the GLODAP dataset continue to evolve the current contrast between trends at the surface and in mode waters will be erased. Continued emissions of fossil CO_2 have already begun to reverse the $\Delta^{14}C$ gradient between the atmosphere and the best-equilibrated parts of the surface ocean (see Figure 5.2) and over time the reversing $\Delta^{14}C$ gradient between the ocean and atmosphere will propagate to the spatial $\Delta^{14}C$ gradients in the ocean interior. The surface $\Delta^{14}C$ rates that we show in this study are gradually eroding $\Delta^{14}C$ gradients in the surface ocean, reducing high $\Delta^{14}C$ in gyre centers and increasing or holding $\Delta^{14}C$ close to steady in upwelling locations. Given "business as usual" fossil CO_2 emissions, the simulated average $\Delta^{14}C$ gradient between the surface and the mid-depth ocean in a general circulation model reverses by 2060 [*Graven*, 2015], which would also reverse the effect of upwelling on surface ocean $\Delta^{14}C$ and result in low $\Delta^{14}C$ at gyre centers and higher $\Delta^{14}C$ at the equator. How ocean general circulation models reproduce recent observed changes in ocean $\Delta^{14}C$ is highly correlated with the size of the ocean carbon sinks they simulate [*Graven et al.*, 2012], and therefore an ongoing effort such as GO-SHIP to generate frequent and well-spaced ^{14}C observations in the ocean is important for developing confidence in model predictions of future carbon absorption and sequestration by the ocean. Accurate knowledge of surface ocean $\Delta^{14}C$ is also important for constraining the ocean ^{14}C disequilibrium isoflux and closing the atmospheric ^{14}C budget. In Appendix F we describe a method that uses the observed relationships from this chapter to adjust GLODAP surface ocean $\Delta^{14}C$ for changes since the 1995 nominal date, for the

purpose of calculating the ocean ^{14}C disequilibrium isoflux.

4. Conclusions:

We demonstrate that in the 1990s, gradients of excess (anthropogenic) $\Delta^{14}C$ and DIC in the potential density layer of SAMW were remarkably similar, enabling $\Delta^{14}C$ to serve as a tracer for high anthropogenic DIC concentrations in mode waters like SAMW. The contrast since the 1990s between declining $\Delta^{14}C$ in the surface ocean and transient increasing $\Delta^{14}C$ in low-latitude mode waters that was demonstrated previously by others [*Jenkins et al.*, 2010; *Graven et al.*, 2012] makes re-emergent carbon from mode waters more easily detectible in surface waters. We find that $\Delta^{14}C$ trends since the 1990s in the low-latitudes and equatorial regions of all three ocean basins are consistent with increased reemergence of anthropogenic DIC in equatorial upwelling areas in all three ocean basins, as Ishii *et al.*, [2009] inferred in the western equatorial Pacific. Post-industrial, post-nuclear carbon has been recycled in shallow overturning cells near the equator since the 1970s, but our results show that now even the densest water that upwells near the equator last equilibrated with the atmosphere after the 1960s, and thus is bringing and will continue to bring increasing concentrations of anthropogenic carbon.

The spatial $\Delta^{14}C$ gradients in the ocean that this analysis exploits are transient, and their continuing evolution will depend on both ocean circulation, which could change in response to climate change, and the trajectory of future fossil CO_2 emissions that will dilute ^{14}C in the atmosphere. As long as strong $\Delta^{14}C$ gradients remain in the ocean, continued observation of ^{14}C will be useful to trace the movement of marine carbon, and as a test for ocean circulation models. Over a half-century since it began, the dispersal and mixing of bomb radiocarbon in the ocean continues to be of use for constraining ocean carbon cycle dynamics

Chapter VI: Summary

This dissertation increases our knowledge of carbon dynamics in the present-day and deglacial ocean. I have used radiocarbon as a tracer to track carbon within the coupled ocean-atmosphere portion of the global carbon cycle, with the aim of understanding how it reacts to both natural variation and anthropogenic alteration of the global climate and carbon systems.

In Chapter II, I presented time-series of reconstructed surface ocean $\Delta^{14}C$ from near Baja California, generated using the tests of three species of planktic foraminifera preserved in an ocean sediment core. The records revealed periods during the last deglaciation when surface ocean $\Delta^{14}C$ near Baja California was very low relative to the coeval atmosphere. The timing of these surface anomalies, during the Heinrich Stadial 1 (HS1) and Younger Dryas (YD) periods, coincided with previously discovered low-$\Delta^{14}C$ anomalies in intermediate waters in the same location and in the Arabian Sea, as well as CO_2 increases and $\Delta^{14}C$ decreases in the deglacial atmosphere. Additionally, inter-species $\Delta^{14}C$ differences suggested that planktic foraminifera with a seasonal habitat that exposed them more to shallow subsurface waters sourced from the eastern equatorial Pacific had recorded a stronger low-$\Delta^{14}C$ anomaly, while species more sensitive to North Pacific surface water showed higher $\Delta^{14}C$. These findings suggested that anomalously old carbon had reached the low-latitude Pacific surface, likely from the same source that caused the intermediate depth anomalies, and had taken a route to the Baja California surface ocean that passed through the eastern equatorial Pacific subsurface.

In Chapter III, I presented radiocarbon measurements on foraminifera from two additional sediment cores from the Baja California region, one deeper and one shallower than the previously studied core, to construct a regional depth transect. The combined dataset of measurements from the region enabled the reconstruction of the deglacial $\Delta^{14}C$ depth gradient

from the surface down to almost 1,300 m modern water depth. The water column at all observed depths was found to be ^{14}C-depleted during HS1 and the YD, and a mid-depth $\Delta^{14}C$ minimum was observed during HS1 and the YD. I interpreted this pattern as further evidence that anomalously old carbon had arrived laterally in deglacial intermediate waters during those periods. Comparison to previously-published $\Delta^{14}C$ and $\delta^{18}O$ records from locations to the north and south in the intermediate-depth eastern Pacific illustrated that $\Delta^{14}C$ in the deglacial intermediate North Pacific was too high to have caused the anomalies near Baja California, and suggested that intermediate water in the Eastern Equatorial Pacific had $\Delta^{14}C$ that was moderately lower than the Baja California mid-depth record during HS1 and the YD.

The results presented in Chapters II and III seem to rule out scenarios that call for aged carbon in deglacial North Pacific intermediate water, and are best explained by carbon that arrived at Baja California within intermediate and shallow subsurface waters proximally sourced from the south. The anomalies likely reflect times when very low-$\Delta^{14}C$ water from the glacial deep ocean, as has been recently reconstructed in the South and Equatorial Pacific and the Southern Ocean below 2.5-3 km, was entrained by upwelling in the Southern Ocean, injecting pulses of low-$\Delta^{14}C$ water into the shallow Southern Ocean that then propagated into parts of the mid-depth ocean and caused the observed atmospheric changes. Together with the results from the Arabian Sea, these conclusions support hypotheses that call for changes in Southern Ocean sea ice and upwelling to explain glacial-interglacial CO_2 variations.

Several aspects of this scenario remain uncertain. For instance, given that no significant low-$\Delta^{14}C$ anomalies have been observed at intermediate depths in the Southern Hemisphere, questions remain about the route that these pulses could have taken from the Southern Ocean surface through the South Pacific during deglaciation. Another question concerns the source of

the carbon that caused the intermediate-depth anomalies observed during the YD, by which time available reconstructions no longer show an anomalously old deep ocean. Additional $\Delta^{14}C$ reconstructions with independent calendar age constraints, particularly in under-sampled regions such as the Western Equatorial Pacific and the Indian and Pacific sectors of the Southern Ocean, may help resolve these mysteries. A coordinated effort to generate regional marine radiocarbon calibration curves in these oceans might also help provide consistent chronological constraints, aiding the comparison of new and existing $\Delta^{14}C$ reconstructions, as well as improving the reliability of radiocarbon-based age models that provide calendar age scales for many marine paleoclimate reconstructions.

In Chapter IV, I presented a new time-series of $^{14}CO_2$ measurements from air sampled over Drake Passage (DRP) during the period 2006-2012. At sub-monthly and monthly timescales, I found that low $\Delta^{14}C$ anomalies are associated with higher CO_2 concentrations, and that low $\Delta^{14}C$, high-CO_2 conditions are significantly correlated at short lags with the positive (windier) phase of the SAM, as well as the positive (warm; La Niña) phase of the Southern Oscillation Index (SOI). To investigate the robustness of these results, I checked for similar relationships using rate anomalies, a method previously used by Butler et al. [2007] on the longer CO_2 record from Palmer Station, Antarctica (PSA). I found that the CO_2 rate regressed onto the SAM similarly at both DRP and PSA, although only the PSA record was long enough for the regressions to be significant. The relationship between CO_2 anomalies and the SOI was not apparent at either location using the alternate method, perhaps because of an opposing terrestrial CO_2 response that overprints the ocean response in rate anomaly data that has been averaged over time-periods longer than a month.

In the remote Southern Ocean region, the low-$\Delta^{14}C$ signature effectively tags the ocean as

the source of the high-CO_2 anomalies. The $\Delta^{14}C$-CO_2 relationship is the opposite of what would be expected from a simple increase in windspeed-dependent gas exchange and requires an associated upwelling response that brings more carbon-rich water to the surface and raises surface ocean pCO_2. Our data are therefore consistent with an upwelling response to atmospheric forcing that, all other variables held constant, causes more deep ocean carbon to escape to the atmosphere during high-SAM (and perhaps also La Niña) conditions and leads to temporary reductions in the local net carbon sink. If, as predicted, global warming causes a permanent shift towards higher-SAM conditions, this could result in a relatively weakened Southern Ocean net carbon sink in the coming decades. In the past, this positive wind-driven feedback could have interacted synergistically with retreating sea ice and reduced salinity stratification in the Southern Ocean during deglacial warming to re-establish exchange between the coupled upper ocean-atmosphere reservoirs and a mass of low-$\Delta^{14}C$ water that had been sequestered in the glacial deep ocean.

Future work to increase the confidence of these results could focus on integrating the available atmospheric $\Delta^{14}C$ data with seawater observations, particularly estimates of pCO_2 variability in the Southern Ocean. Additional precise atmospheric $^{14}CO_2$ measurements from other monitoring locations in the Southern Ocean region could also help investigate these relationships, perhaps by leveraging archived CO_2 samples to lengthen existing $\Delta^{14}C$ timeseries (e.g. the very short PSA $\Delta^{14}C$ record published by Graven *et al.*, [2007]). Any method that used some form of archived carbon to reconstruct Southern Ocean atmospheric $\Delta^{14}C$ since 1970 would have the benefit of both a better signal:noise ratio (due to greater ocean-atmosphere isotopic disequilibrium) and a shorter wait time to generate a long time series, compared to a sampling campaign initiated today and continued into the future.

In Chapter V, I used published datasets of ocean $\Delta^{14}C$ observations to estimate the rates of surface ocean $\Delta^{14}C$ change since the 1990s. Spatial and mixing patterns within these results reveal that the rising $\Delta^{14}C$ of mode waters since the 1990s, caused by the continuing spread of bomb ^{14}C into the ocean interior, is detectible at the surface near the equator in all three major ocean basins. From that observation I inferred that anthropogenic (post-nuclear) carbon previously absorbed by the ocean at high latitudes is now returning to the low-latitude surface in thermocline and mode waters, which until now were not implicated in the recycling of anthropogenic carbon. This is consistent with a recent study that found that rates of pCO_2 rise in the equatorial Pacific are higher than can be explained by exchange with the atmosphere, implying an increasing supply of carbon via the subsurface. I noted that this does not necessarily imply any acceleration in the transport of mode water from the Southern Ocean to low latitudes, as it would occur eventually in a steady state ocean through the convolution of CO_2 and $\Delta^{14}C$ histories of the atmosphere with the ventilation age distribution of upwelling waters. These observations, bolstered by more ^{14}C measurements from repeat hydrographic efforts, could serve as a useful test of ocean circulation models that are used to predict the assimilation of anthropogenic carbon by the ocean.

References

Ahagon, N. (2003), Mid-depth circulation in the northwest Pacific during the last deglaciation: Evidence from foraminiferal radiocarbon ages, *Geophys. Res. Lett.*, *30*(21), 2097, doi:10.1029/2003GL018287.

Allen, K. a., E. L. Sikes, B. Hönisch, A. C. Elmore, T. P. Guilderson, Y. Rosenthal, and R. F. Anderson (2015), Southwest Pacific deep water carbonate chemistry linked to high southern latitude climate and atmospheric CO2 during the Last Glacial Termination, *Quat. Sci. Rev.*, *122*, 180–191, doi:10.1016/j.quascirev.2015.05.007.

Anderson, B. E., S. Ali, L. I. Bradtmiller, S. H. H. Nielsen, M. Q. Fleisher, and L. H. Burckle (2009), Wind-Driven Upwelling in the Southern Ocean and the Deglacial Rise in Atmospheric CO2, *Science (80-.).*, *323*(March), 1443–1448.

Anon (n.d.), National Nuclear Data Center, Available from: www.nndc.bnl.gov

Antonov, J. I., D. Seidov, T. P. Boyer, R. A. Locarnini, A. V. Mishonov, H. E. Garcia, O. K. Baranova, M. M. Zweng, and D. R. Johnson (2010), *WORLD OCEAN ATLAS 2009 Volume 2 : Salinity*, NOAA Atlas., edited by S. Levitus, U.S. Gov. Printing Office, Washing D.C.

Arblaster, J. M., and G. a. Meehl (2006), Contributions of External Forcings to Southern Annular Mode Trends, *J. Clim.*, *19*(12), 2896–2905, doi:10.1175/JCLI3774.1.

Bakun, A., and C. S. Nelson (1977), CLIMATOLOGY OF UPWELLING RELATED PROCESSES OFF BAJA CALIFORNIA, in *California Cooperative Ocean Fisheries Investigation Reports*, edited by B. Izadore, H. W. Frey, J. Radovich, and J. L. Reid, pp. 107–127, STATE OF CALIFORNIA DEPARTMENT OF FISH AND GAME MARINE RESEARCH COMMITTEE.

Baldwin, M. P. et al. (2001), The quasi-biennial oscillation, *Rev. Geophys.*, *39*(2), 179–229, doi:10.1029/1999RG000073.

Ballantyne, a P., C. B. Alden, J. B. Miller, P. P. Tans, and J. W. C. White (2012), Increase in observed net carbon dioxide uptake by land and oceans during the past 50 years., *Nature*, *488*(7409), 70–2, doi:10.1038/nature11299.

Bard, E. (1988), C ages measured in planktonic foraminifera: Paleoceanographic implications, *Paleoceanography*, *3*(6), 635, doi:10.1029/PA003i006p00635.

Bard, E., M. Arnold, J. Duprat, J. Moyes, and J. Duplessy (1987), Reconstruction of the last deglaciation: deconvolved records of d18O profiles, micropaleontological variations and

accelerator mass spectrometric 14C dating, *Clim. Dyn.*, *1*, 101–112.

Barker, S., W. Broecker, E. Clark, and I. Hajdas (2007), Radiocarbon age offsets of foraminifera resulting from differential dissolution and fragmentation within the sedimentary bioturbated zone, *Paleoceanography*, *22*(2), 1–11, doi:10.1029/2006PA001354.

Basak, C., E. E. Martin, K. Horikawa, and T. M. Marchitto (2010), Southern Ocean source of 14C-depleted carbon in the North Pacific Ocean during the last deglaciation, *Nat. Geosci.*, *3*(11), 770–773, doi:10.1038/ngeo987.

Berger, R., R. E. Taylor, and W. F. Libby (1966), Radiocarbon content of marine shells from the california and mexican west coast., *Science*, *153*(3738), 864–6, doi:10.1126/science.153.3738.864.

Bostock, H. C., B. N. Opdyke, and M. J. M. Williams (2010), Characterising the intermediate depth waters of the Pacific Ocean using δ13C and other geochemical tracers, *Deep Sea Res. Part I Oceanogr. Res. Pap.*, *57*(7), 847–859, doi:10.1016/j.dsr.2010.04.005.

Bova, S., and T. Herbert (2014), In pursuit of the mystery reservoir: marine radiocarbon evidence from the eastern tropical Pacific for a deglacial CO_2 source, *AGU 2014 Fall Meet. Abstr. # PP13D-05*.

Broecker (1982), Glacial to interglacial changes in oceanic chemstry, *Prog Occeanogr*, *11*, 151–197.

Broecker, W., and S. Barker (2007), A 190‰ drop in atmosphere's Δ14C during the "Mystery Interval" (17.5 to 14.5 kyr), *Earth Planet. Sci. Lett.*, *256*(1-2), 90–99, doi:10.1016/j.epsl.2007.01.015.

Broecker, W., E. Clark, S. Barker, I. Hajdas, G. Bonani, and E. Moreno (2007), Radiocarbon age of late glacial deep water from the equatorial Pacific, *Paleoceanography*, *22*(2), PA2206, doi:10.1029/2006PA001359.

Broecker, W. S., and T.-H. Peng (1986), Glacial To Interglacial Changes in the Operation of the Global Carbon Cycle, *Radiocarbon*, *28*(2), 309–327.

Bryan, S. P., T. M. Marchitto, and S. J. Lehman (2010), The release of 14C-depleted carbon from the deep ocean during the last deglaciation: Evidence from the Arabian Sea, *Earth Planet. Sci. Lett.*, *298*(1-2), 244–254, doi:10.1016/j.epsl.2010.08.025.

Burke, A., and L. F. Robinson (2012), The Southern Ocean's role in carbon exchange during the last deglaciation., *Science*, *335*(6068), 557–61, doi:10.1126/science.1208163.

Butler, A. H., D. W. J. Thompson, and K. R. Gurney (2007), Observed relationships between the Southern Annular Mode and atmospheric carbon dioxide, *Global Biogeochem. Cycles*, *21*(4), GB4014, doi:10.1029/2006GB002796.

Butzin, M., M. Prange, and G. Lohmann (2005), Radiocarbon simulations for the glacial ocean: The effects of wind stress, Southern Ocean sea ice and Heinrich events, *Earth Planet. Sci. Lett.*, *235*(1-2), 45–61, doi:10.1016/j.epsl.2005.03.003.

Carriquiry, J. D., A. Sanchez, and G. Leduc (2015), Southern Ocean influence on the Eastern Tropical North Pacific's intermediate depth circulation during the last glacial maximum, *Paleoceanography*, n/a–n/a, doi:10.1002/2014PA002766.

Carton, J. a., S. a. Grodsky, and H. Liu (2008), Variability of the oceanic mixed layer, 1960-2004, *J. Clim.*, *21*(5), 1029–1047, doi:10.1175/2007JCLI1798.1.

Cléroux, C., P. deMenocal, and T. Guilderson (2011), Deglacial radiocarbon history of tropical Atlantic thermocline waters: Absence of CO2 reservoir purging signal, *Quat. Sci. Rev.*, *30*(15-16), 1875–1882, doi:10.1016/j.quascirev.2011.04.015.

Connolly, T. P., B. M. Hickey, I. Shulman, and R. E. Thomson (2014), Coastal Trapped Waves, Alongshore Pressure Gradients, and the California Undercurrent*, *J. Phys. Oceanogr.*, *44*(1), 319–342, doi:10.1175/JPO-D-13-095.1.

Conrad, C. J., and N. S. Lovenduski (2015), Climate Driven Variability in the Southern Ocean Carbonate System, *J. Clim.*, (Dic), 150406095007000, doi:10.1175/JCLI-D-14-00481.1.

Conway, T. J., P. P. Tans, L. S. Waterman, and K. W. Thoning (1994), Evidence for interannual variability of the carbon-cycle from the National Oceanic and Atmospheric Administration/ Climate Monitoring and Diagnostics Laboratory global air-sampling network., *J. Geophys. Res. D*, *99*(94), 22831–22855.

Cravatte, S., W. S. Kessler, and F. Marin (2012), Intermediate Zonal Jets in the Tropical Pacific Ocean Observed by Argo Floats*, *J. Phys. Oceanogr.*, *42*(9), 1475–1485, doi:10.1175/JPO-D-11-0206.1.

Davies-Walczak, M., a. C. Mix, J. S. Stoner, J. R. Southon, M. Cheseby, and C. Xuan (2014), Late Glacial to Holocene radiocarbon constraints on North Pacific Intermediate Water ventilation and deglacial atmospheric CO2 sources, *Earth Planet. Sci. Lett.*, *397*, 57–66, doi:10.1016/j.epsl.2014.04.004.

Dean, W. E., Y. Zheng, J. D. Ortiz, and A. van Geen (2006), Sediment Cd and Mo accumulation

in the oxygen-minimum zone off western Baja California linked to global climate over the past 52 kyr, *Paleoceanography*, *21*(4), n/a–n/a, doi:10.1029/2005PA001239.

Ding, Q., E. J. Steig, D. S. Battisti, and J. M. Wallace (2012), Influence of the tropics on the southern annular mode, *J. Clim.*, *25*(18), 6330–6348, doi:10.1175/JCLI-D-11-00523.1.

Duplessy, J., M. Arnold, E. Bard, A. Juillet-Leclerc, N. Kallel, and L. Labeyrie (1989), AMS 14C study of transient events and of the ventilation rate of the pacific intermediate water during the last deglaciation, *Radiocarbon*, *31*(3), 493–502.

Durazo, R. (2009), Climate and upper ocean variability off Baja California, Mexico: 1997–2008, *Prog. Oceanogr.*, *83*(1-4), 361–368, doi:10.1016/j.pocean.2009.07.043.

Dutta, K., G. V. R. Prasad, D. K. Ray, and S. Raghav (2010), Decadal changes in radiocarbon in the surface Bay of Bengal: Three decades after GEOSECS and one decade after WOCE, *Radiocarbon*, *52*(2-3), 1191–1196.

Ebisuzaki, W. (1997), A Method to Estimate the Statistical Significance of a Correlation When the Data Are Serially Correlated, *J. Clim.*, *10*, 2147–2153.

Fiedler, P. C., and L. D. Talley (2006), Hydrography of the eastern tropical Pacific: A review, *Prog. Oceanogr.*, *69*(2-4), 143–180, doi:10.1016/j.pocean.2006.03.008.

Fine, R. a., K. a. Maillet, K. F. Sullivan, and D. Willey (2001), Circulation and ventilation flux of the Pacific Ocean, *J. Geophys. Res.*, *106*(C10), 22159, doi:10.1029/1999JC000184.

Firing, E., S. E. Wijffels, and P. Hacker (1998), Equatorial subthermocline currents across the Pacific, *J. Geophys. Res.*, *103*(C10), 21413, doi:10.1029/98JC01944.

Fleming, K., P. Johnston, D. Zwartz, Y. Yokoyama, K. Lambeck, and J. Chappell (1998), Refining the eustatic sea-level curve since the Last Glacial Maximum using far- and intermediate-field sites, *Earth Planet. Sci. Lett.*, *163*(1-4), 327–342, doi:10.1016/S0012-821X(98)00198-8.

Fogt, R. L., and D. H. Bromwich (2006), Decadal variability of the ENSO teleconnection to the high-latitude south pacific governed by coupling with the Southern Annular mode, *J. Clim.*, *19*(6), 979–997, doi:10.1175/JCLI3671.1.

Francois, R. et al. (1997), Contribution of Southern Ocean surface-water stratification to low atmospheric CO2 concentrations during the last glacial period, *Nature*, *389*(6654), 929–935, doi:10.1038/40073.

Friedlingstein, P., L. Bopp, P. Ciais, J. Dufresne, L. Fairhead, P. Monfray, and J. Orr (2001),

Positive feedback between future climate change and the carbon cycle, *Geophys. Res. Lett.*, *28*(8), 1543–1546.

Friedlingstein, P. et al. (2006), Climate – Carbon Cycle Feedback Analysis : Results from the C4MIP Model Intercomparison, *J. Clim.*, *19*, 3337–3353.

Fukasawa, M., and A. Murata (2001), Carbon-related measurements during CLIVAR Repeat Section P17N_2001, , doi:10.3334/CDIAC/otg.CLIVAR_P17N_2001.

Galbraith, E. D., S. L. Jaccard, T. F. Pedersen, D. M. Sigman, G. H. Haug, M. Cook, J. R. Southon, and R. Francois (2007), Carbon dioxide release from the North Pacific abyss during the last deglaciation., *Nature*, *449*(7164), 890–3, doi:10.1038/nature06227.

Gebhardt, H., M. Sarnthein, P. M. Grootes, T. Kiefer, H. Kuehn, F. Schmieder, and U. Röhl (2008), Paleonutrient and productivity records from the subarctic North Pacific for Pleistocene glacial terminations I to V, *Paleoceanography*, *23*(4), 1–21, doi:10.1029/2007PA001513.

van Geen, A., Y. Zheng, J. M. Bernhard, K. G. Cannariato, J. Carriquiry, W. E. Dean, B. W. Eakins, J. D. Ortiz, and J. Pike (2003), On the preservation of laminated sediments along the western margin of North America, *Paleoceanography*, *18*(4), doi:10.1029/2003PA000911.

Genthon, C., G. Krinner, and M. Sacchettini (2003), Interannual Antarctic tropospheric circulation and precipitation variability, *Clim. Dyn.*, *21*(3-4), 289–307, doi:10.1007/s00382-003-0329-1.

Godwin, H. (1962), Half-life of Radiocarbon, *Nature*, *195*(4845), 984.

Graven, H. D. (2015), Impact of fossil fuel emissions on atmospheric radiocarbon and various applications of radiocarbon over this century, *Proc. Natl. Acad. Sci.*, *112*(31), 201504467, doi:10.1073/pnas.1504467112.

Graven, H. D., N. Gruber, R. Key, S. Khatiwala, and X. Giraud (2012), Changing controls on oceanic radiocarbon: New insights on shallow-to-deep ocean exchange and anthropogenic CO 2 uptake, *J. Geophys. Res.*, *117*(C10), C10005, doi:10.1029/2012JC008074.

Guilderson, T. P., E. B. Roark, P. D. Quay, S. R. Flood, and C. Moy (2006), Seawater radiocarbon evolution in the gulf of alaska: 2002 observations, , *48*(1), 1–15.

Guilderson, T. P., C. Sweeney, P. D. Quay, T. Newberger, and J. Stutsman (2012), Drake Passage Radiocarbon (Δ14C) of Dissolved Inorganic Carbon (DIC): Measurements from

R/V Laurence M. Gould Transects., , doi:10.3334/CDIAC/OTG.DRAKE_C14.

Hain, M. P., D. M. Sigman, and G. H. Haug (2011), Shortcomings of the isolated abyssal reservoir model for deglacial radiocarbon changes in the mid-depth Indo-Pacific Ocean, *Geophys. Res. Lett.*, *38*(4), L04604, doi:10.1029/2010GL046158.

Hall, A., and M. Visbeck (2002), Synchronous Variability in the Southern Hemisphere Atmosphere , Sea Ice , and Ocean Resulting from the Annular Mode, *J. Clim.*, *15*, 3043–3057.

Hartmann, D. L., and F. Lo (1998), Wave-Driven Zonal Flow Vacillation in the Southern Hemisphere, *J. Atmos. Sci.*, *55*, 1303–1315, doi:10.1175/1520-0469(1998)055<1303:WDZFVI>2.0.CO;2.

Hendy, I. L., and J. P. Kennett (2003), Tropical forcing of North Pacific intermediate water distribution during Late Quaternary rapid climate change?, *Quat. Sci. Rev.*, *22*(5-7), 673–689, doi:10.1016/S0277-3791(02)00186-5.

Hendy, I. L., J. P. Kennett, E. B. Roark, and B. L. Ingram (2002), Apparent synchroneity of submillennial scale climate events between Greenland and Santa Barbara Basin , California from 30 – 10 ka, *Quat. Sci. Rev.*, *21*, 1167–1184.

Hickey, B. M. (1979), The California Current System--hypotheses and facts, *Prog. Oceanogr.*, *8*(October 1978), 191–279.

Hickey, B. M. (1998), Coastal Oceanography of Western North America from the Tip of Baja California to Vancouver Island, in *The Sea*, edited by A. R. Robinson and K. H. Brink, pp. 345–393, John Wiley & Sons., Inc., New York.

Hill, T. M., J. P. Kennett, D. K. Pak, R. J. Behl, C. Robert, and L. Beaufort (2006), Pre-Bolling warming in Santa Barbara Basin, California: surface and intermediate water records of early deglacial warmth, *Quat. Sci. Rev.*, *25*, 2835–2845, doi:10.1016/j.quascirev.2006.03.012.

Ho, M., a. S. Kiem, and D. C. Verdon-Kidd (2012), The Southern Annular Mode: A comparison of indices, *Hydrol. Earth Syst. Sci.*, *16*(3), 967–982, doi:10.5194/hess-16-967-2012.

Hughen, K., S. Lehman, J. Southon, J. Overpeck, O. Marchal, C. Herring, and J. Turnbull (2004), 14C activity and global carbon cycle changes over the past 50,000 years., *Science*, *303*(5655), 202–7, doi:10.1126/science.1090300.

IPCC (2013), Working Group 1 Contribution to the Fifth Assessment Report of the Intergovernmental Panel on Climate Change, in *Climate Change 2013 The Physical Science*

Basis, edited by T. F. Stocker et al., Cambridge University Press, New York, NY.

Ishii, M. et al. (2009), Spatial variability and decadal trend of the oceanic CO2 in the western equatorial Pacific warm/fresh water, *Deep Sea Res. Part II Top. Stud. Oceanogr.*, *56*(8-10), 591–606, doi:10.1016/j.dsr2.2009.01.002.

Ito, T. (2004), What controls the uptake of transient tracers in the Southern Ocean?, *Global Biogeochem. Cycles*, *18*(2), GB2021, doi:10.1029/2003GB002103.

Jenkins, W. J., K. L. Elder, A. P. Mcnichol, and K. Von Reden (2010), The passage of the bomb carbon pulse into the Pacific Ocean, *Radiocarbon*, *52*(2), 1182–1190.

Keigwin, L. D., and S. J. Lehman (2015), Radiocarbon evidence for a possible abyssal front near 3.1 km in the glacial equatorial Pacific Ocean, *Earth Planet. Sci. Lett.*, *425*, 93–104, doi:10.1016/j.epsl.2015.05.025.

Kessler, W. S. (2006), The circulation of the eastern tropical Pacific: A review, *Prog. Oceanogr.*, *69*(2-4), 181–217, doi:10.1016/j.pocean.2006.03.009.

Key, R. M. (2004), A global ocean carbon climatology: Results from Global Data Analysis Project (GLODAP), *Global Biogeochem. Cycles*, *18*(4), 1–23, doi:10.1029/2004GB002247.

Khatiwala, S. et al. (2013), Global ocean storage of anthropogenic carbon, *Biogeosciences*, *10*(4), 2169–2191, doi:10.5194/bg-10-2169-2013.

Knox, F., and M. B. Mcelroy (1984), Changes in Atmospheric CO2: Influence of the Marine Biota at High Latitude, *J. Geophys. Res.*, *89*(D3), 4629–4637.

Kohfeld, K. E., and Z. Chase (2011), Controls on deglacial changes in biogenic fluxes in the North Pacific Ocean, *Quat. Sci. Rev.*, *30*(23-24), 3350–3363, doi:10.1016/j.quascirev.2011.08.007.

Koutavas, A., P. B. deMenocal, G. C. Olive, and J. Lynch-Stieglitz (2006), Mid-Holocene El Niño–Southern Oscillation (ENSO) attenuation revealed by individual foraminifera in eastern tropical Pacific sediments, *Geology*, *34*(12), 993, doi:10.1130/G22810A.1.

Kumamoto, Y., A. Murata, S. Watanabe, and M. Fukasawa (2011), Temporal and spatial variations in bomb-produced radiocarbon along BEAGLE2003 lines—Revisits of WHP P06, A10, and I03/I04 in the Southern Hemisphere Oceans, *Prog. Oceanogr.*, *89*(1-4), 49–60, doi:10.1016/j.pocean.2010.12.007.

L'Heureux, M. L., and D. W. J. Thompson (2006), Observed Relationships between the El Niño – Southern Oscillation and the Extratropical Zonal-Mean Circulation, *J. Atmos. Ocean.*

Technol., *19*(2002), 276–288.

de la Fuente, M., L. Skinner, E. Calvo, C. Pelejero, and I. Cacho (2015), Increased reservoir ages and poorly ventilated deep waters inferred in the glacial Eastern Equatorial Pacific, *Nat. Commun.*, *6*(May), 7420, doi:10.1038/ncomms8420.

Labitzke, K. (2004), On the signal of the 11-year sunspot cycle in the stratosphere and its modulation by the quasi-biennial oscillation, *J. Atmos. Solar-Terrestrial Phys.*, *66*(13-14 SPEC. ISS.), 1151–1157, doi:10.1016/j.jastp.2004.05.011.

Landschützer, P., N. Gruber, F. A. Haumann, C. Rödenbeck, D. C. E. Bakker, S. Van Heuven, M. Hoppema, N. Metzl, C. Sweeney, and T. Takahashi (2015), The reinvigoration of the Southern Ocean carbon sink, *Science (80-.).*, *349*(6253), 1221–1224.

Lehman, S. J. et al. (2013), Allocation of Terrestrial Carbon Sources using 14CO2: Methods, Measurement, and Modeling, *Radiocarbon*, *55*(2), 1484–1495.

Lenton, A. et al. (2013), Sea-air CO2 fluxes in the Southern Ocean for the period 1990-2009, *Biogeosciences Discuss.*, *10*(1), 285–333, doi:10.5194/bgd-10-285-2013.

Levin, I., and V. Hesshaimer (2000), RADIOCARBON – A UNIQUE TRACER OF GLOBAL CARBON CYCLE DYNAMICS, *Radiocarbon*, *42*(1), 69–80.

Levin, I., and B. Kromer (1997), Twenty years of atmospheric 14co2 observations at schauinsland station, germany, *Radiocarbon*, *39*(2), 205–218.

Levin, I., B. Kromer, H. Schoch-fischer, M. Bruns, M. Munnich, D. Berdau, J. C. Vogelt, and K. O. Munnich (1985), 25 Years of Tropospheric 14C Observations in Central Europe, *Radiocarbon*, *27*(1), 1–19.

Levin, I., T. Naegler, B. Kromer, M. Diehl, R. J. Francey, A. J. Gomez-Pelaez, L. P. Steele, D. Wagenbach, R. Weller, and D. E. Worthy (2010), Observations and modelling of the global distribution and long-term trend of atmospheric 14 CO 2, *Tellus B*, *62*(1), 26–46, doi:10.1111/j.1600-0889.2009.00446.x.

Lindsay, C. M., S. J. Lehman, T. M. Marchitto, and J. D. Ortiz (2015), The surface expression of radiocarbon anomalies near Baja California during deglaciation, *Earth Planet. Sci. Lett.*, *422*, 67–74, doi:10.1016/j.epsl.2015.04.012.

Locarnini, R. A. et al. (2013), WORLD OCEAN ATLAS 2013 Volume 1 : Temperature, in *NOAA Atlas NESDIS 74*, vol. 1, edited by S. Levitus and A. Mishonov.

Lovenduski, N. S., N. Gruber, S. C. Doney, and I. D. Lima (2007), Enhanced CO 2 outgassing in

the Southern Ocean from a positive phase of the Southern Annular Mode, *Global Biogeochem. Cycles*, *21*(2), GB2026, doi:10.1029/2006GB002900.

Lovenduski, N. S., N. Gruber, and S. C. Doney (2008), Toward a mechanistic understanding of the decadal trends in the Southern Ocean carbon sink, *Global Biogeochem. Cycles*, *22*(3), 1–9, doi:10.1029/2007GB003139.

Lund, D. C., and P. D. Asimow (2011), Does sea level influence mid-ocean ridge magmatism on Milankovitch timescales?, *Geochemistry, Geophys. Geosystems*, *12*(12), 1–26, doi:10.1029/2011GC003693.

Lynn, R. J., and J. J. Simpson (1987), The California Current System : The Seasonal Variability of its Physical Characteristics, *J. Geophys. Res.*, *92*(7), 12947–12966.

MacDougall, T. J., and P. M. Barker (2011), *Getting started with TEOS-10 and the Gibbs Seawater (GSW) Oceanographic Toolbox*, WG127 ed., SCOR/IAPSO.

Magana, A. L., J. R. Southon, J. P. Kennett, E. B. Roark, M. Sarnthein, and L. D. Stott (2010), Resolving the cause of large differences between deglacial benthic foraminifera radiocarbon measurements in Santa Barbara Basin, *Paleoceanography*, *115*(4), PA4102, doi:10.1029/2010PA002011.

Mahadevan, a. (2001), An analysis of bomb radiocarbon trends in the Pacific, *Mar. Chem.*, *73*(3-4), 273–290, doi:10.1016/S0304-4203(00)00113-4.

Marchitto, T. M., S. J. Lehman, J. D. Ortiz, J. Flückiger, and A. van Geen (2007), Marine radiocarbon evidence for the mechanism of deglacial atmospheric CO2 rise., *Science*, *316*(5830), 1456–9, doi:10.1126/science.1138679.

Martin, J. H. (1990), Glacial-Interglacial CO2 change: The Iron Hypothesis, *Paleoceanography*, *5*(1), 1–13.

Martínez-Botí, M. A., G. Marino, G. L. Foster, P. Ziveri, M. J. Henehan, J. W. B. Rae, P. G. Mortyn, and D. Vance (2015), Boron isotope evidence for oceanic carbon dioxide leakage during the last deglaciation, *Nature*, *518*, 219–222, doi:10.1038/nature14155.

Martínez-Garcia, A., A. Rosell-Melé, S. L. Jaccard, W. Geibert, D. M. Sigman, and G. H. Haug (2011), Southern Ocean dust-climate coupling over the past four million years., *Nature*, *476*(7360), 312–5, doi:10.1038/nature10310.

McCartney, M. S. (1977), Subantarctic Mode Water, in *A Voyage of Discovery: George Deacon 70th Anniversary Volume*, edited by M. V. Angel, pp. 103–119, Pergamon Press, Oxford.

McCartney, M. S. (1982), The subtropical recirculation of mode waters, *J. Mar. Res.*, *40*(Supplement), 427–464.

Metzl, N. (2009), Decadal increase of oceanic carbon dioxide in Southern Indian Ocean surface waters (1991–2007), *Deep Sea Res. Part II Top. Stud. Oceanogr.*, *56*(8-10), 607–619, doi:10.1016/j.dsr2.2008.12.007.

Mikaloff Fletcher, S. E. et al. (2006), Inverse estimates of anthropogenic CO 2 uptake, transport, and storage by the ocean, *Global Biogeochem. Cycles*, *20*(2), 1–16, doi:10.1029/2005GB002530.

Monnin, E., a Indermühle, a Dällenbach, J. Flückiger, B. Stauffer, T. F. Stocker, D. Raynaud, and J. M. Barnola (2001), Atmospheric CO2 concentrations over the last glacial termination., *Science*, *291*(5501), 112–4, doi:10.1126/science.291.5501.112.

Mortyn, P. G., J. C. Herguera, and M. a. Martínez-Botí (2011), Instrumental validation of Globigerinoides ruber Mg/Ca as a proxy for NE Pacific summer SST, *Geophys. Res. Lett.*, *38*(16), n/a–n/a, doi:10.1029/2011GL047803.

Munro, D. R., N. S. Lovenduski, T. Takahashi, B. B. Stephens, T. Newberger, and C. Sweeney (2015), Recent evidence for a strengthening CO_2 sink in the Southern Ocean from carbonate system measurements in the Drake Passage (2002-2015), *Geophys. Res. Lett.*, n/a–n/a, doi:10.1002/2015GL065194.

Naegler, T. (2009), Reconciliation of excess 14 C-constrained global CO 2 piston velocity estimates, *Tellus B*, *61*(2), 372–384, doi:10.1111/j.1600-0889.2008.00408.x.

Nakamura, T., T. Nakazawa, N. Nakai, H. Kitagawa, H. Honda, T. Itoh, T. Machida, and E. Matsumoto (1992), Measurement of 14C concentrations of stratospheric CO2 by accelerator mass spectrometry, *Radiocarbon*, *34*(3), 745–752.

Neu, J. L., T. Flury, G. L. Manney, M. L. Santee, N. J. Livesey, and J. Worden (2014), Tropospheric ozone variations governed by changes in stratospheric circulation, *Nat. Geosci.*, *7*(5), 340–344, doi:10.1038/NGEO2138.

Nydal, R. (2000), Radiocarbon in the Ocean, *Radiocarbon*, *42*(1), 81–98.

Okazaki, Y., a Timmermann, L. Menviel, N. Harada, a Abe-Ouchi, M. O. Chikamoto, a Mouchet, and H. Asahi (2010), Deepwater formation in the North Pacific during the Last Glacial Termination., *Science*, *329*(5988), 200–4, doi:10.1126/science.1190612.

Ortiz, J. D. (2011), Application of Visible/near Infrared derivative spectroscopy to Arctic

paleoceanography, *IOP Conf. Ser. Earth Environ. Sci.*, *14*, 012011, doi:10.1088/1755-1315/14/1/012011.

Ortiz, J. D., A. C. Mix, and R. W. Collier (1995), Environmental control of living symbiotic and asymbiotic, , *10*(6), 987–1009.

Ortiz, J. D., S. B. O'Connell, J. DelViscio, W. Dean, J. D. Carriquiry, T. Marchitto, Y. Zheng, and a. van Geen (2004), Enhanced marine productivity off western North America during warm climate intervals of the past 52 k.y., *Geology*, *32*(6), 521, doi:10.1130/G20234.1.

Ostlund, G., H. Craig, W. S. Broecker, and D. Spencer (Eds.) (1987), *GEOSECS Atlantic, Pacific and Indian Ocean Expeditions, Shorebased Data and Graphics*, Vol. 7., U.S. Government Printing Office, Washington D.C.

Petit, J. R. et al. (1999), Climate and atmospheric history of the past 420 , 000 years from the Vostok ice core , Antarctica,

De Pol-Holz, R., L. Keigwin, J. Southon, D. Hebbeln, and M. Mohtadi (2010), No signature of abyssal carbon in intermediate waters off Chile during deglaciation, *Nat. Geosci.*, *3*(3), 192–195, doi:10.1038/ngeo745.

Quay, P. D., M. Stuiver, and W. S. Broecker (1983), Upwelling rates for the equatorial Pacific Ocean derived from the bomb 14C distribution, *J. Mar. Res.*, *41*, 769–792.

Le Quéré, C. et al. (2007), Saturation of the southern ocean CO2 sink due to recent climate change., *Science*, *316*(5832), 1735–8, doi:10.1126/science.1136188.

Rae, J. W. B., M. Sarnthein, G. L. Foster, A. Ridgewell, P. M. Grootes, and T. Elliott (2014), Deep water formation in the North Pacific and deglacial CO2 rise, *Paleoceanography*, *29*, 1–23, doi:10.1002/2013PA002570.Received.

Rafter, T. A., and G. J. Fergusson (1957), Atom bomb effect - recent increase of carbon-14 content of the atmosphere and biosphere, *Science (80-.).*, *126*(3273), 557–558, doi:10.1126/science.126.3273.557.

Rasmussen, S. O. et al. (2014), A stratigraphic framework for abrupt climatic changes during the Last Glacial period based on three synchronized Greenland ice-core records: refining and extending the INTIMATE event stratigraphy, *Quat. Sci. Rev.*, *106*, 14–28, doi:10.1016/j.quascirev.2014.09.007.

Reimer, P. J. et al. (2004), INTCAL04 TERRESTRIAL RADIOCARBON AGE CALIBRATION, 0-26 CAL KYR BP, *Radiocarbon*, *46*(3), 0–26.

Reimer, P. J., E. Bard, A. Bayliss, J. W. Beck, P. G. Blackwell, C. Bronk, R. Caitlin, E. B. Hai, and R. L. Edwards (2013), INTCAL13 and MARINE13 radiocarbon age calibration curves 0 – 50,000 years cal bp, *Radiocarbon*, *55*(4).

Revelle, R., and H. E. Suess (1957), Carbon Dioxide Exchange Between Atmosphere and Ocean and the Question of an Increase of Atmospheric CO2 during the Past Decades, *Tellus*, *9*(1), 18–27, doi:10.1111/j.2153-3490.1957.tb01849.x.

Rodgers, K. B. (2003), Extratropical sources of Equatorial Pacific upwelling in an OGCM, *Geophys. Res. Lett.*, *30*(2), 1084, doi:10.1029/2002GL016003.

Rose, K. a, E. L. Sikes, T. P. Guilderson, P. Shane, T. M. Hill, R. Zahn, and H. J. Spero (2010), Upper-ocean-to-atmosphere radiocarbon offsets imply fast deglacial carbon dioxide release., *Nature*, *466*(7310), 1093–7, doi:10.1038/nature09288.

Rowe, G. D., E. Firing, and G. C. Johnson (2000), Pacific Equatorial Subsurface Countercurrent Velocity, Transport, and Potential Vorticity, *J. Phys. Oceanogr.*, *30*, 1172–1187.

Rubin, S. I., and R. M. Key (2002), Separating natural and bomb-produced radiocarbon in the ocean: The potential alkalinity method, *Global Biogeochem. Cycles*, *16*(4), 52–1–52–19, doi:10.1029/2001GB001432.

Sabine, C. L., and T. Tanhua (2010), Estimation of Anthropogenic CO_2 Inventories in the Ocean, *Ann. Rev. Mar. Sci.*, *2*(1), 175–198, doi:10.1146/annurev-marine-120308-080947.

Sabine, C. L. et al. (2004a), SOM for The oceanic sink for anthropogenic CO2., *Science*, *305*(5682), 367–71, doi:10.1126/science.1097403.

Sabine, C. L. et al. (2004b), The oceanic sink for anthropogenic CO2., *Science*, *305*(5682), 367–71, doi:10.1126/science.1097403.

Sarmiento, J. L., and J. R. Toggweiler (1984), A new model for the role of the oceans in determining atmospheric Pco2, *Nature*, *308*.

Sarnthein, M., P. M. Grootes, J. P. Kennett, and M.-J. Nadeau (2007), 14C Reservoir Ages Show Deglacial Changes in Ocean Currents and Carbon Cycle, in *Ocean Circulation: Mechanisms and Impacts*, edited by A. Schmittner, J. C. H. Chiang, and S. R. Hemming, pp. 175–196, American Geophysical Union.

Sautter, L. R., and C. Sancetta (1992), Seasonal associations of phytoplankton and planktic foraminifera in an upwelling region and their contribution to the seafloor, , *18*, 263–278.

Schmittner, A. (2003), Southern Ocean sea ice and radiocarbon ages of glacial bottom waters,

Earth Planet. Sci. Lett., *213*, 53–62, doi:10.1016/S0012-821X(03)00291-7.

Schnell, R. C., A.-M. Buggle, and R. M. Rosson (2004), Climate monitoring and diagnostics laboratory summary report no. 27 2002-2003,

Seierstad, I. K. et al. (2014), Consistently dated records from the Greenland GRIP, GISP2 and NGRIP ice cores for the past 104 ka reveal regional millennial-scale δ18O gradients with possible Heinrich event imprint, *Quat. Sci. Rev.*, *106*, 29–46, doi:10.1016/j.quascirev.2014.10.032.

Siani, G., E. Michel, R. De Pol-Holz, T. Devries, F. Lamy, M. Carel, G. Isguder, F. Dewilde, and A. Lourantou (2013), Carbon isotope records reveal precise timing of enhanced Southern Ocean upwelling during the last deglaciation., *Nat. Commun.*, *4*(May), 2758, doi:10.1038/ncomms3758.

Siegenthaler, U., and T. Wenk (1984), Rapid atmospheric CO2 variations and ocean circulation, *Nature*, *308*.

Sigman, D. M., and E. A. Boyle (2000), Glacial/interglacial variations in in atmospheric carbon dioxide, *Nature*, *407*(October), 859–869.

Sigman, D. M., M. P. Hain, and G. H. Haug (2010), The polar ocean and glacial cycles in atmospheric CO(2) concentration., *Nature*, *466*(7302), 47–55, doi:10.1038/nature09149.

Sikes, E. L., C. R. Samson, T. P. Guilderson, and W. R. Howard (2000), Old radiocarbon ages in the southwest Pacific Ocean during the last glacial period and deglaciation, *Nature*, *405*, 555–559.

Skinner, L., I. N. McCave, L. Carter, S. Fallon, A. Scrivner, and F. Primeau (2014), Reduced ventilation and enhanced magnitude of the deep Pacific carbon pool during the last glacial period, *Earth Planet. Sci. Lett.*, *411*, 1–21, doi:10.1016/j.epsl.2014.11.024.

Skinner, L. C., S. Fallon, C. Waelbroeck, E. Michel, and S. Barker (2010), Ventilation of the deep Southern Ocean and deglacial CO2 rise., *Science (80-.).*, *328*(5982), 1147–51, doi:10.1126/science.1183627.

Sortor, R. N., and D. C. Lund (2011), No evidence for a deglacial intermediate water Δ14C anomaly in the SW Atlantic, *Earth Planet. Sci. Lett.*, *310*(1-2), 65–72, doi:10.1016/j.epsl.2011.07.017.

Spero, H. J., and D. W. Lea (2002), The cause of carbon isotope minimum events on glacial terminations., *Science*, *296*(5567), 522–5, doi:10.1126/science.1069401.

Spero, H. J., K. M. Mielke, E. M. Kalve, D. W. Lea, and D. K. Pak (2003), Multispecies approach to reconstructing eastern equatorial Pacific thermocline hydrography during the past 360 kyr, *Paleoceanography*, *18*(1), n/a–n/a, doi:10.1029/2002PA000814.

Stephens, B. B., and R. F. Keeling (2000), The influence of Antarctic sea ice on glacial-interglacial CO2 variations, *Nature*, *404*, 171–174.

Stern, J. V., and L. E. Lisiecki (2013), North Atlantic circulation and reservoir age changes over the past 41,000 years, *Geophys. Res. Lett.*, *40*(14), 3693–3697, doi:10.1002/grl.50679.

Stott, L., and A. Timmermann (2011), Hypothesized Link Between Glacial/Interglacial Atmospheric CO2 Cycles and Storage/Release of CO2-Rich Fluids From Deep-Sea Sediments, in *Abrupt Climate Change: Mechanisms, Patterns, and Impacts*, edited by H. Rashid, L. Polyak, and E. Mosley-Thompson, pp. 123–138, American Geophysical Union, Washing D.C.

Stott, L., J. Southon, A. Timmermann, and A. Koutavas (2009), Radiocarbon age anomaly at intermediate water depth in the Pacific Ocean during the last deglaciation, *Paleoceanography*, *24*(2), PA2223, doi:10.1029/2008PA001690.

Stuiver, M., and H. Polach (1977), Reporting of 14C Data, *Radiocarbon*, *19*(3), 355–363.

Stuiver, M., P. J. Reimer, and R. W. Reimer (2005), CALIB 5.0. [www Program and Documentation], Available from: http://calib.qub.ac.uk/calib/manual/chapter1.html

Svensson, a. et al. (2008), A 60 000 year Greenland stratigraphic ice core chronology, *Clim. Past*, *4*(1), 47–57, doi:10.5194/cp-4-47-2008.

Sweeney, C., E. Gloor, A. R. Jacobson, R. M. Key, G. McKinley, J. L. Sarmiento, and R. Wanninkhof (2007), Constraining global air-sea gas exchange for CO 2 with recent bomb 14 C measurements, *Global Biogeochem. Cycles*, *21*(2), GB2015, doi:10.1029/2006GB002784.

Takahashi, T. et al. (2009), Climatological mean and decadal change in surface ocean pCO2, and net sea–air CO2 flux over the global oceans, *Deep Sea Res. Part II Top. Stud. Oceanogr.*, *56*(8-10), 554–577, doi:10.1016/j.dsr2.2008.12.009.

Talley, L. D. (1993), Distribution and Formation of North Pacific Intermediate Water, *J. Phys. Oceanogr.*, *23*, 517–537.

Thompson, D. W. J., and S. Solomon (2002), Interpretation of recent Southern Hemisphere climate change., *Science*, *296*(5569), 895–9, doi:10.1126/science.1069270.

Thompson, D. W. J., J. M. Wallace, and G. C. Hegerl (2000), Annular Modes in the Extratropical Circulation . Part II : Trends *, *J. Clim.*, *13*(689), 1018–1036.

Thoning, K. W., P. P. Tans, and W. D. Komhyr (1989), Atmospheric carbon dioxide at Mauna Loa Observatory: 2. Analysis of the NOAA GMCC data, 1974–1985, *J. Geophys. Res.*, *94*(D6), 8549, doi:10.1029/JD094iD06p08549.

Thornalley, D. J. R., I. N. McCave, and H. Elderfield (2011), Tephra in deglacial ocean sediments south of Iceland: Stratigraphy, geochemistry and oceanic reservoir ages, *J. Quat. Sci.*, *26*(2), 190–198, doi:10.1002/jqs.1442.

Tiedemann, R., T. A. Ronge, F. Lamy, P. Köhler, M. Frische, R. De Pol-holz, K. Pahnke, B. V Alloway, L. Wacker, and J. Southon (2015), New Constraints on the Glacial Extent of the Pacific Carbon Pool and its Deglacial Outgassing, , *233*(408), 229–233.

Toggweiler, J. R. (1999), Variation of atmospheric CO2 by ventilation of the ocean ' s deepest water, *Paleoceanography*, *14*(5), 571–588.

Toggweiler, J. R., and K. Dixon (1991), The Peru Upwelling and the Ventilation of the South Pacific, , *96*(Cll).

Toggweiler, J. R., J. L. Russell, and S. R. Carson (2006), Midlatitude westerlies, atmospheric CO 2 , and climate change during the ice ages, *Paleoceanography*, *21*(2), 1–15, doi:10.1029/2005PA001154.

Tsuchiya, M. (1991), Flow path of the Antarctic Intermediate Water in the western equatorial South Pacific Ocean, *Deep Sea Res. Part A. Oceanogr. Res. Pap.*, *38*(1965), S273–S279, doi:10.1016/S0198-0149(12)80013-6.

Turnbull, J., P. Rayner, J. Miller, T. Naegler, P. Ciais, and A. Cozic (2009), On the use of 14 CO 2 as a tracer for fossil fuel CO 2 : Quantifying uncertainties using an atmospheric transport model, *J. Geophys. Res.*, *114*(D22), D22302, doi:10.1029/2009JD012308.

Turnbull, J. C., S. J. Lehman, J. B. Miller, R. J. Sparks, J. R. Southon, and P. P. Tans (2007), A new high precision 14 CO 2 time series for North American continental air, *J. Geophys. Res.*, *112*(D11), D11310, doi:10.1029/2006JD008184.

Turnbull, J. C., S. J. Lehman, S. Morgan, and C. Wolak (2010), A NEW AUTOMATED EXTRACTION SYSTEM FOR 14C MEASUREMENT FOR ATMOSPHERIC CO2, *Radiocarbon*, *52*(2), 1261–1269.

Verdy, A., S. Dutkiewicz, M. J. Follows, J. Marshall, and A. Czaja (2007), Carbon dioxide and

oxygen fluxes in the Southern Ocean: Mechanisms of interannual variability, *Global Biogeochem. Cycles*, *21*(2), GB2020, doi:10.1029/2006GB002916.

Voelker, A. H. L., M. Sarnthein, P. M. Grootes, H. Erlenkeuser, C. Laj, A. Mazaud, M.-J. Nadeau, and M. Schleicher (1998), Correlation of Marine 14C Ages from the Nordic Seas with the GISP2 Isotope Record: Implications for 14C Calibration Beyond 25 ka BP, *Radiocarbon*, *40*(1), 517–534.

Waelbroeck, C., J. C. Duplessy, E. Michel, L. Labeyrie, D. Paillard, and J. Duprat (2001), The timing of the last deglaciation in North Atlantic climate records., *Nature*, *412*(6848), 724–7, doi:10.1038/35089060.

Wang, W., P. Ciais, R. R. Nemani, J. G. Canadell, S. Piao, S. Sitch, M. A. White, H. Hashimoto, C. Milesi, and R. B. Myneni (2013), Variations in atmospheric CO2 growth rates coupled with tropical temperature, *Proc. Natl. Acad. Sci.*, *110*(32), 13061–13066, doi:10.1073/pnas.1219683110.

Wanninkhof, R. (1992), Relationship Between Wind Speed and Gas Exchange Over the Ocean, *J. Geophys. Res.*, *97*(92), 7373–7382.

You, Y. (2003), The pathway and circulation of North Pacific Intermediate Water, *Geophys. Monogr. Ser.*, *30*(24), 24–27, doi:10.1029/2003GL018561.

Zweng, M. M. et al. (2013), WORLD OCEAN ATLAS 2013 Volume 2 : Salinity, in *NOAA Atlas NESDIS 74*, vol. 2, edited by S. Levitus and A. Mishonov, p. 39.

Appendix A

Auxiliary Material for Chapter II

1.1 Alternative ^{14}C Age Model

In the main paper we present decay-corrected radiocarbon initial activity ($\Delta^{14}C$) from core MV99/GC31/PC08 calculated using a calendar age model that matches sediment reflectance to the layer-counted GISP2 $\delta^{18}O$ record [*Marchitto et al*. 2007, hereafter M07]. A recent study in the Gulf of Alaska found that tuning downcore planktic $\delta^{18}O$ to NGRIP $\delta^{18}O$ on the GICC05 age scale results in deglacial benthic $\Delta^{14}C$ anomalies of similar magnitude and timing as the Baja California benthic anomalies [*Davies-Walczak et al.*, 2014]. The same study suggested that the Baja California anomalies might be an artifact of the age model method, as there are only modest benthic anomalies evident in the Gulf of Alaska core when using a planktic ^{14}C-based age model that assumes constant sea surface reservoir age. Here we demonstrate that an alternative age model based on our new planktic ^{14}C results from PC08 and a constant reservoir age is unrealistic and would only slightly change the magnitude of the benthic anomalies.

1.2 Alternative Age Model Methods

PC08 ^{14}C measurements from the planktic foraminifera *G. bulloides* and *G. sacculifer* were calibrated to the IntCal13 marine calibration curve [*Reimer et al.*, 2013] using a constant reservoir correction based on the closest available estimate of the local pre-industrial surface reservoir effect ($\Delta R = 329 \pm 45$ ^{14}C years; mollusk shell collected at Cabo San Lucas; Berger, Taylor, and Libby, 1966; http://calib.qub.ac.uk/marine/). The ^{14}C offsets in PC08 between *G. sacculifer, G. bulloides* and *G. ruber* cannot be reconciled with the assumption of constant reservoir age for all three. For the age model we therefore only used the *G. bulloides* and *G. sacculifer* samples, which do not differ systematically and tend to be better equilibrated

(younger) than *G. ruber*, likely because of a different seasonal growth habitat (see main text). We also omitted the measurement that caused the single *G. sacculifer* $\Delta^{14}C$ outlier (see main text). The calibrated dates are plotted versus core depth in Figure S1. The calendar age – depth relationship was interpolated using the most flexible smoothing spline that would not cause age reversals. To avoid nonsensical distortion of the spline in the uppermost section we included two M07 tiepoints from the early Holocene (where planktic foraminiferal abundances are insufficient for ^{14}C measurement).

1.3 Alternative Age Model Results

The alternative age model requires two sharp spikes in sedimentation rate (Figure S2), one to ~70 cm/ka at the start of Heinrich Stadial 1 (HS1) and one to ~400 cm/ka during the Bølling-Allerød (BA). This contrasts with the nearly constant sedimentation rates that result from the M07 age model. PC08 reflectance data (DSR Factor 3) on the M07 age model aligns well with GISP2 $\delta^{18}O$ on the new GICC05 age scale [*Rasmussen et al.*, 2014; *Seierstad et al.*, 2014], but on the alternative PC08 age model the sharp transitions in sediment reflectance during sudden Northern Hemisphere warming appear to lead Greenland climate, especially for the Younger Dryas (YD) (Figure S3). In the case of the Gulf of Alaska core, there are reasons to expect planktic $\delta^{18}O$ to begin changing before the BA (e.g. global ice volume decrease), and the authors presented ample evidence that sedimentation rate changes were related to proximity to land ice [*Davies-Walczak et al.*, 2014]. We have no reason to expect sediment reflectance changes in PC08 to lead Greenland transitions, and find no other evidence to support the large spikes in sedimentation required by the alternative age model. For these reasons we conclude that the assumption of constant surface reservoir age is likely a bad one near Baja California during the

last deglaciation, and thus recommend that this alternative age model not be used. In any case, PC08 $\Delta^{14}C$ calculated using the alternative age model also has large benthic $\Delta^{14}C$ anomalies (Figure S4). The alternative age model shifts the timing of the most recent benthic anomaly 1,000 years older, but only increases the lowest $\Delta^{14}C$ value by ~70‰ compared to the same measurement on the M07 age model, minimally affecting the depletion of ~500‰ relative to the coeval atmosphere recorded by those measurements on the M07 age model. PC08 benthic $\Delta^{14}C$ from ~25 to 14 ka on the alternative age model is also slightly (~50‰ or less) increased compared to M07 values and moved older by up to 700 years, but the general structure of the record is unchanged.

1.4 Carbonate Preservation in PC08

The alternative hypothesis of Stott and Timmerman [2011] proposes the large-scale release of ^{14}C-dead volcanic CO_2 into intermediate waters during deglaciation, possibly accompanied by fluids high in dissolved alkalinity. They present low-resolution *G. ruber* Li/Ca data that suggests this additional CO_2 was not fully buffered, leading to widespread lower carbonate ion concentrations. In PC08, benthic abundances (a proxy for export productivity) and planktic fragmentation (a proxy for dissolution) are correlated during MIS 3 [*Ortiz et al.*, 2004], likely because of low CO_3^{2-} concentrations in sediment pore-water during more productive periods. The increase in benthic abundances during stadials is dominated by low-oxygen infaunal taxa such as *Bolivina* and *Brizalina*; changes in *Uvigerina* abundances across climate boundaries are relatively minimal. While the resolution of the abundance and fragmentation data is lower during the deglaciation, the same relationship appears to hold (Figure S5). We do not see evidence during HS1 and the YD of the poorer preservation that would be caused by the large addition of

dissolved CO_2 hypothesized by Stott and Timmerman (2011); rather, fragmentation is lower during these intervals than during the BA and the Holocene.

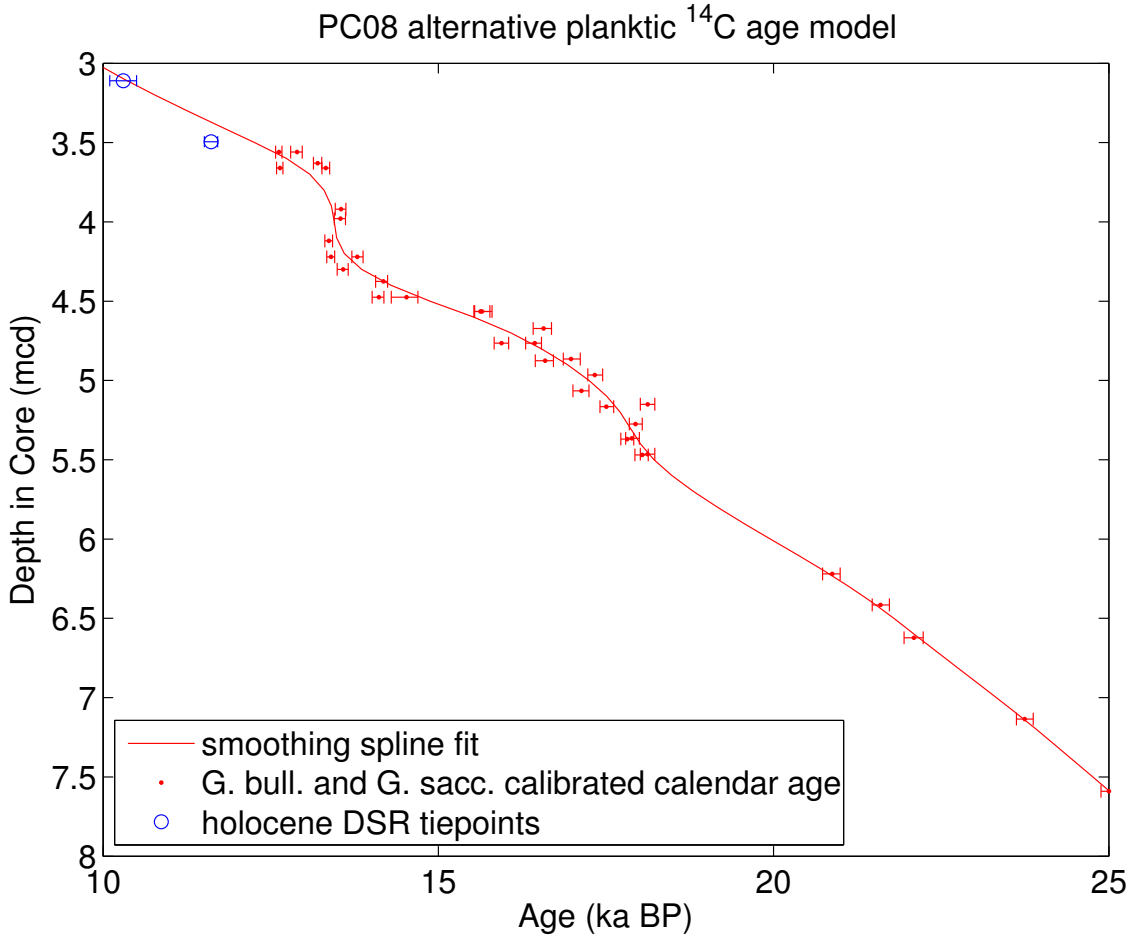

Figure S1: Depth in core is plotted versus calendar age for the alternative PC08 age model. The smoothing spline was fit to *G. bulloides* and *G. sacculfer* ^{14}C ages calibrated with a constant pre-industrial modern reservoir age correction. Tie-point ages from the M07 age model are used higher in the core to prevent nonsensical distortion of the spline. Horizontal error bars represent 1-sigma calendar age error.

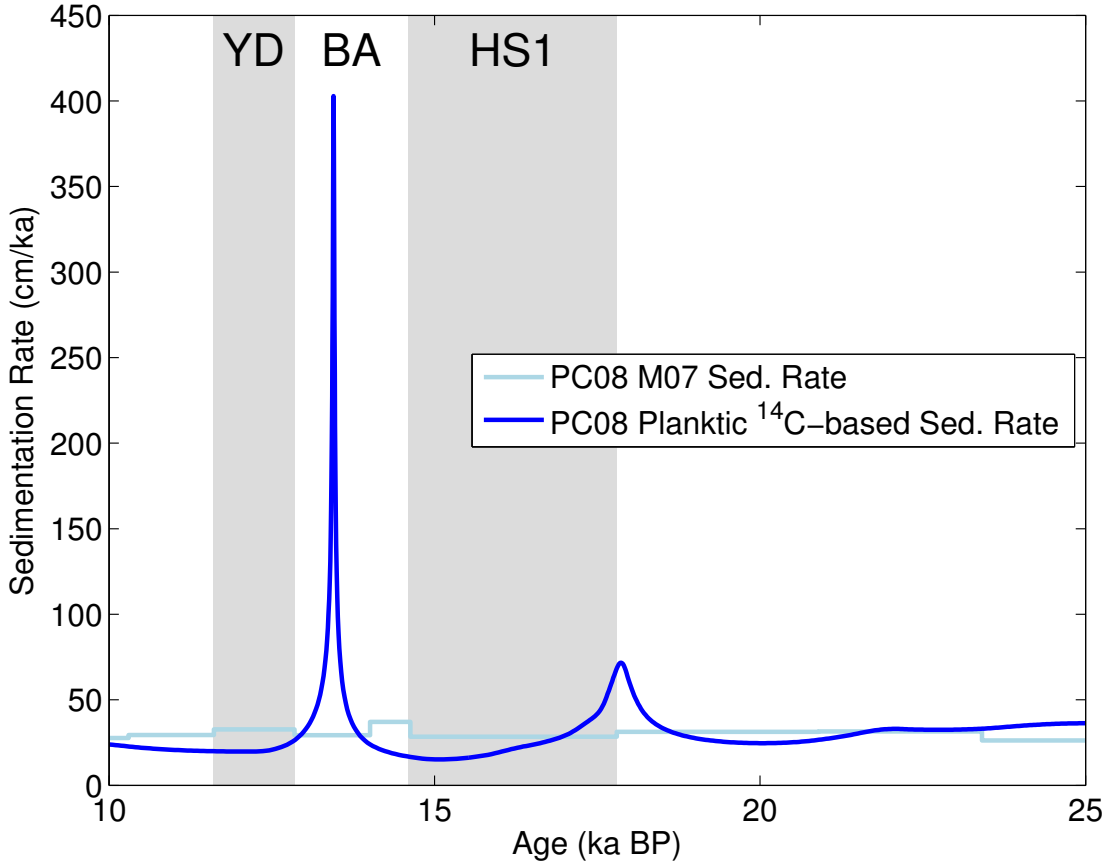

Figure S2: Comparison of the deglacial sedimentation rates from the M07 age model [*Marchitto et al.*, 2007] and the alternative planktic ^{14}C-based age model with constant reservoir age. Grey fields indicate the Heinrich 1 (HS1) and Younger Dryas (YD) stadials bracketing the Bølling-Allerød period (BA).

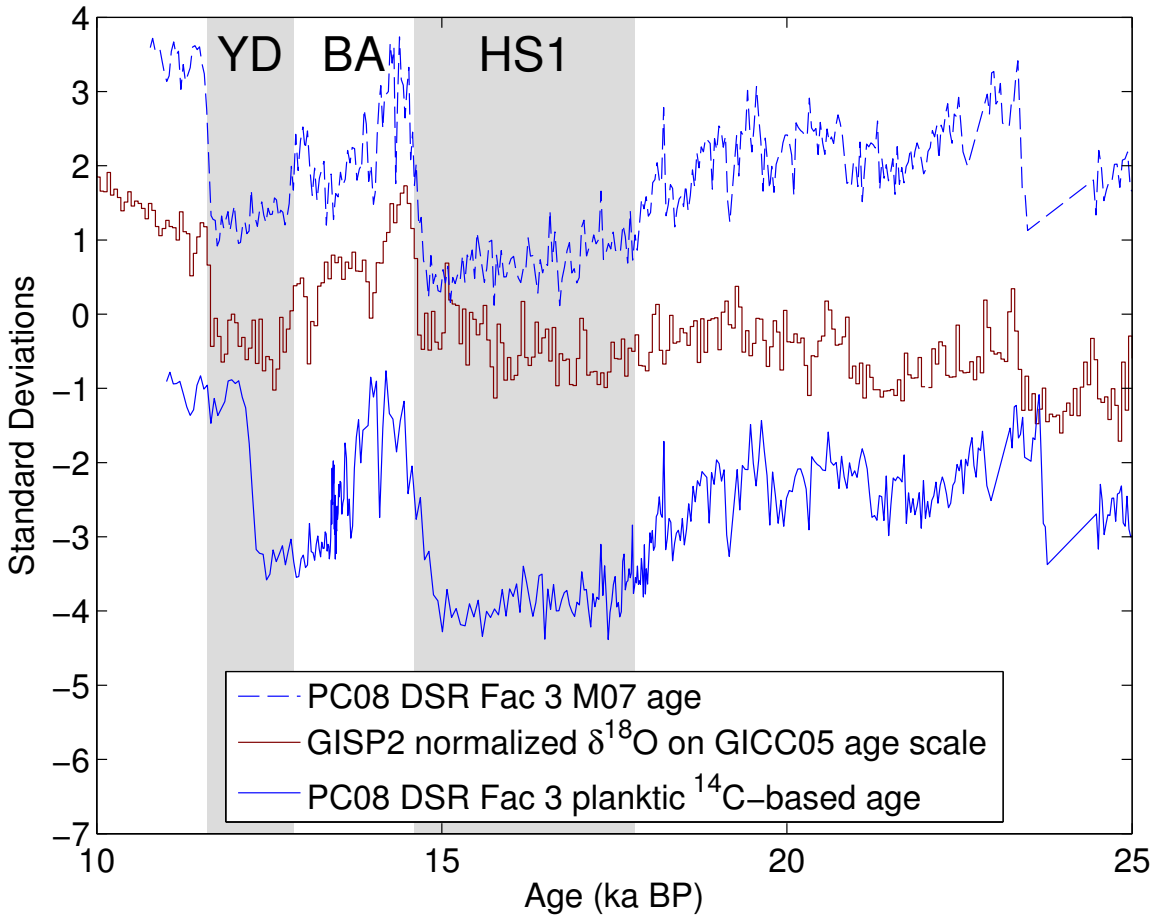

Figure S3: Diffuse Spectral Reflectance (DSR) Factor 3 from PC08 [*Ortiz et al.*, 2004] on both the M07 and alternative age models, compared to normalized GISP2 $\delta^{18}O$ on the GICC05 age scale. The two DSR records are shifted respectively up and down by constant amounts to aid comparison of the timing. Grey fields indicate the Heinrich 1 (HS1) and Younger Dryas (YD) stadials bracketing the Bølling-Allerød period (BA).

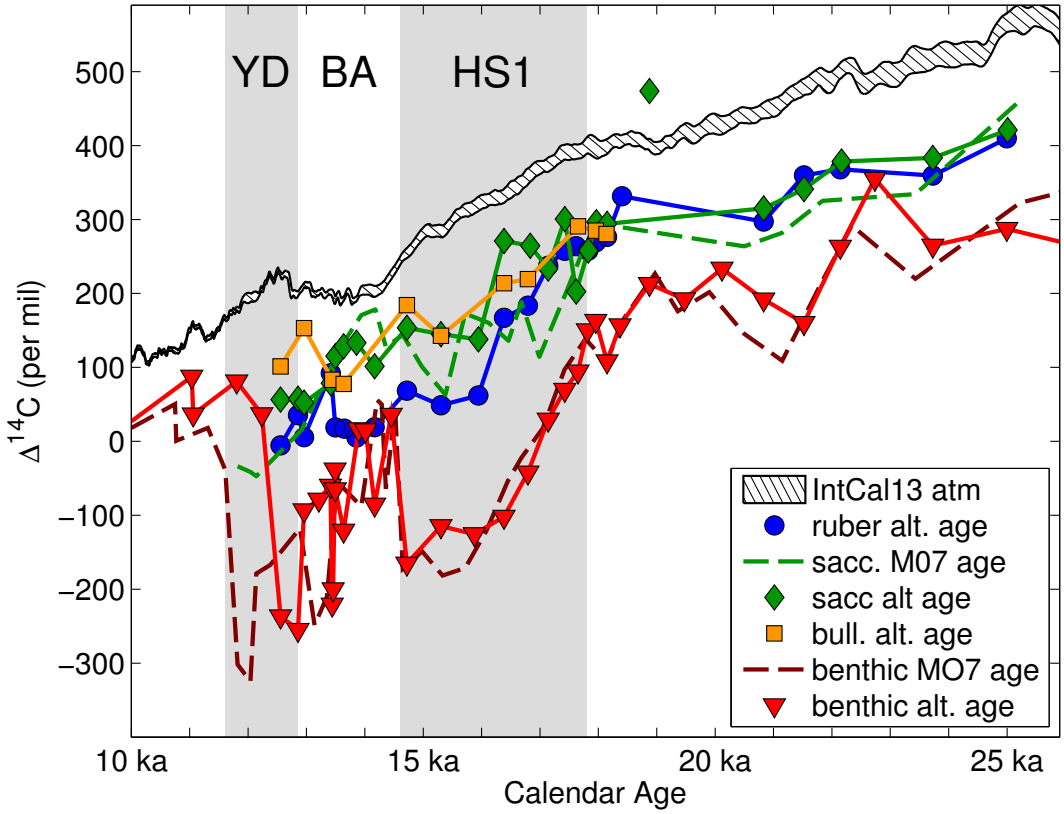

Figure S4: Comparison of PC08 planktic and benthic $\Delta^{14}C$ on the alternative age model with benthic and *G. sacculifer* $\Delta^{14}C$ on the M07 age model, and with IntCal13 atmospheric $\Delta^{14}C$ [*Reimer et al.*, 2013]. Grey fields indicate the Heinrich 1 (HS1) and Younger Dryas (YD) stadials bracketing the Bølling-Allerød period (BA).

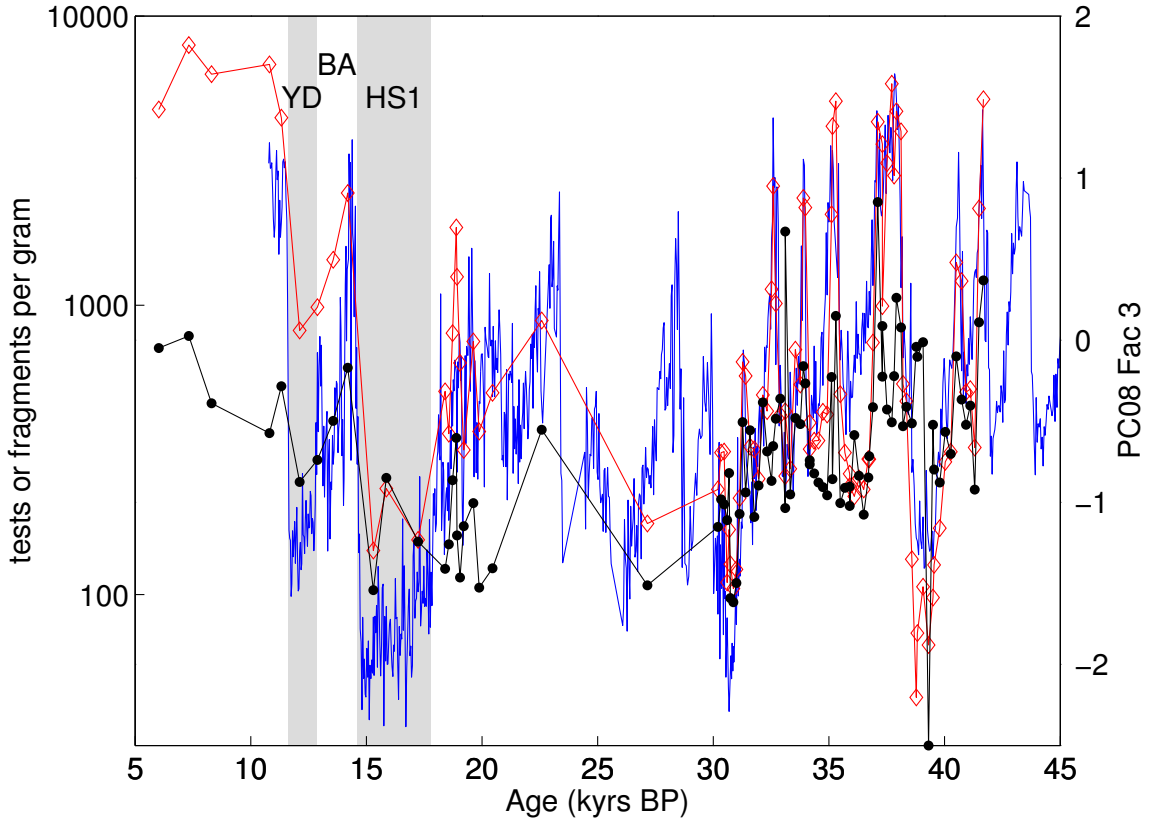

Figure S5: PC08 benthic abundance (red diamonds), planktic fragmentation counts (black filled circles), and DSR Factor 3 (blue line) [*Ortiz et al.*, 2004], plotted on the M07 age model. Grey fields indicate the Heinrich 1 (HS1) and Younger Dryas (YD) stadials bracketing the Bølling-Allerød period (BA).

Appendix A References

Berger, R., Taylor, R. E., & Libby, W. F. (1966). Radiocarbon content of marine shells from the california and mexican west coast. *Science (New York, N.Y.)*, *153*(3738), 864–6. doi:10.1126/science.153.3738.864

Davies-Walczak, M., Mix, a. C., Stoner, J. S., Southon, J. R., Cheseby, M., & Xuan, C. (2014). Late Glacial to Holocene radiocarbon constraints on North Pacific Intermediate Water ventilation and deglacial atmospheric CO2 sources. *Earth and Planetary Science Letters*, *397*, 57–66. doi:10.1016/j.epsl.2014.04.004

Marchitto, T. M., Lehman, S. J., Ortiz, J. D., Flückiger, J., & van Geen, A. (2007). Marine radiocarbon evidence for the mechanism of deglacial atmospheric CO2 rise. *Science (New York, N.Y.)*, *316*(5830), 1456–9. doi:10.1126/science.1138679

Ortiz, J. D., O'Connell, S. B., DelViscio, J., Dean, W., Carriquiry, J. D., Marchitto, T., … van Geen, a. (2004). Enhanced marine productivity off western North America during warm climate intervals of the past 52 k.y. *Geology*, *32*(6), 521. doi:10.1130/G20234.1

Rasmussen, S. O., Bigler, M., Blockley, S. P., Blunier, T., Buchardt, S. L., Clausen, H. B., … Winstrup, M. (2014). A stratigraphic framework for abrupt climatic changes during the Last Glacial period based on three synchronized Greenland ice-core records: refining and extending the INTIMATE event stratigraphy. *Quaternary Science Reviews*, *106*, 14–28. doi:10.1016/j.quascirev.2014.09.007

Reimer, P. J., Bard, E., Bayliss, A., Beck, J. W., Blackwell, P. G., Bronk, C., … Edwards, R. L. (2013). INTCAL13 and MARINE13 radiocarbon age calibration curves 0 – 50,000 years cal bp. *Radiocarbon*, *55*(4).

Seierstad, I. K., Abbott, P. M., Bigler, M., Blunier, T., Bourne, A. J., Brook, E., … Vinther, B. M. (2014). Consistently dated records from the Greenland GRIP, GISP2 and NGRIP ice cores for the past 104 ka reveal regional millennial-scale δ18O gradients with possible Heinrich event imprint. *Quaternary Science Reviews*, *106*, 29–46. doi:10.1016/j.quascirev.2014.10.032

Stott, L., & Timmermann, A. (2011). Hypothesized Link Between Glacial/Interglacial Atmospheric CO2 Cycles and Storage/Release of CO2-Rich Fluids From Deep-Sea Sediments. In H. Rashid, L. Polyak, & E. Mosley-Thompson (Eds.), *Abrupt Climate Change: Mechanisms, Patterns, and Impacts* (Geophysica., pp. 123–138). Washington D.C.: American Geophysical Union.

Appendix B

^{14}C Data used in Chapter II
Core: MV99-MC19/GC31/PC08 (Van Geen et al., 2003)
Latitude: 23.47° Longitude: -111.6 Depth: 705 m

Composite Depth (m)	Sample Type	Taxa	Source	CURL/OS Number	^{14}C Age (years)	^{14}C Age Unc. (1σ)	Calendar Age (years BP)	Cal. Age Unc. (1σ)	$\Delta^{14}C$ (‰)
0.1	benthic	mixed benthics	van Geen *et al.* 2003	OS-33198	1720	30	330	126	-160
0.25	benthic	mixed benthics	van Geen *et al.* 2003	OS-33199	2050	35	840	218	-142
0.27	benthic	mixed benthics	van Geen *et al.* 2003	OS-33201	2050	30	910	232	-135
0.4	benthic	mixed benthics	van Geen *et al.* 2003	OS-33200	2320	35	1350	327	-118
0.475	benthic	mixed benthics	van Geen *et al.* 2003	OS-25612	2230	35	1600	383	-81
0.755	benthic	*Bolivina* spp.	van Geen *et al.* 2003	OS-22946	3030	40	2550	597	-66
0.95	benthic	mixed benthics	van Geen *et al.* 2003	OS-33202	3690	45	3210	747	-69
1.255	benthic	*Bolivina* spp.	van Geen *et al.* 2003	OS-22947	3840	50	4240	983	35
1.48	benthic	mixed benthics	van Geen *et al.* 2003	OS-33203	5130	60	4650	869	-73
1.755	benthic	*Bolivina* spp.	van Geen *et al.* 2003	OS-22948	5810	40	5580	672	-47
2.255	benthic	*Bolivina* spp.	van Geen *et al.* 2003	OS-22949	7190	50	7270	366	-16
2.755	benthic	*Bolivina* spp.	van Geen *et al.* 2003	OS-22955	8980	60	9050	355	-23
3.255	benthic	*Bolivina* spp.	van Geen *et al.* 2003	OS-23513	10050	410	10750	230	50
3.26	benthic	mixed benthics	Marchitto et al., 2007	CURL-8750	10460	30	10770	226	1
3.41	benthic	mixed benthics	Marchitto *et al*., 2007	CURL-8752	10845	30	11310	123	18
3.495	benthic	mixed benthics	van Geen *et al.* 2003	OS-25611	11600	70	11610	99	-39
3.56	benthic	*Uvigerina* spp.	This study	CURL-14079	14370	35	11820	110	-302
3.63	benthic	*Uvigerina* spp.	This study	CURL-12828	14855	45	12040	141	-325
3.66	benthic	mixed benthics	Marchitto et al., 2007	CURL-8751	13380	35	12140	158	-179
3.755	benthic	*Bolivina* spp.	van Geen *et al.* 2003	OS-22956	13500	70	12390	149	-166
3.91	benthic	mixed benthics	Marchitto et al., 2007	CURL-8444	13530	30	12880	102	-119
3.98	benthic	*Uvigerina* spp.	This study	CURL-12827	15065	45	13130	124	-250
4.04	benthic	*Uvigerina* spp.	This study	CURL-12822	14870	45	13350	160	-210
4.11	benthic	mixed benthics	Marchitto *et al*., 2007	CURL-8445	13420	25	13540	154	-32
4.115	benthic	*Bolivina* spp.	van Geen *et al.* 2003	OS-22957	13650	150	13560	150	-57
4.22	benthic	*Uvigerina* spp.	Marchitto *et al*., 2007	CURL-8746	14285	35	13940	103	-88
4.31	benthic	mixed benthics	Marchitto et al., 2007	CURL-8446	13370	30	14210	111	56
4.34	benthic	*Uvigerina* spp.	This study	CURL-12826	13495	35	14290	121	50
4.375	benthic	*Uvigerina* spp.	Marchitto et al., 2007	CURL-8721	14485	35	14360	119	-64
4.43	benthic	*Uvigerina* spp.	This study	CURL-12823	13760	40	14520	104	44
4.475	benthic	*Uvigerina* spp.	Marchitto et al., 2007	CURL-8726	15755	40	14650	100	-172
4.565	benthic	*Uvigerina* spp.	Marchitto *et al*., 2007	CURL-8720	15850	40	14980	128	-149

4.66	benthic	mixed benthics	Marchitto et al., 2007	CURL-8447	16505	40	15330	189	-182
4.765	benthic	*Uvigerina* spp.	Marchitto *et al*., 2007	CURL-8724	16785	45	15710	268	-172
4.865	benthic	*Uvigerina* spp.	Marchitto et al., 2007	CURL-8729	16665	40	16080	348	-121
4.965	benthic	*Uvigerina* spp.	Marchitto *et al*., 2007	CURL-8744	16425	45	16450	430	-53
5.065	benthic	*Uvigerina* spp.	Marchitto et al., 2007	CURL-8742	16390	40	16680	390	-22
5.165	benthic	*Uvigerina* spp.	Marchitto *et al*., 2007	CURL-8743	16425	50	17050	341	18
5.265	benthic	*Uvigerina* spp.	Marchitto et al., 2007	CURL-8749	16185	45	17420	308	97
5.365	benthic	*Uvigerina* spp.	Marchitto *et al*., 2007	CURL-8748	16235	40	17780	296	138
5.47	benthic	*Uvigerina* spp.	Marchitto et al., 2007	CURL-8745	16810	40	18140	306	107
5.56	benthic	mixed benthics	Marchitto *et al*., 2007	CURL-8448	16680	40	18440	332	167
5.72	benthic	*Uvigerina* spp.	This study	CURL-12804	16790	60	18970	407	227
5.88	benthic	*Uvigerina* spp.	This study	CURL-12803	17510	60	19360	420	176
6.04	benthic	*Uvigerina* spp.	This study	CURL-12825	17860	60	19890	313	200
6.22	benthic	*Uvigerina* spp.	This study	CURL-12809	18830	70	20500	221	145
6.415	benthic	*Uvigerina* spp.	Marchitto et al., 2007	CURL-8728	19720	60	21150	208	109
6.615	benthic	*Uvigerina* spp.	Marchitto *et al*., 2007	CURL-8722	19640	60	21820	298	215
6.808	benthic	mixed benthics	van Geen *et al.* 2003	OS-33204	19650	80	22340	280	292
7.135	benthic	*Uvigerina* spp.	Marchitto *et al*., 2007	CURL-8727	21170	70	23430	101	220
7.585	benthic	*Uvigerina* spp.	Marchitto et al., 2007	CURL-8725	22260	70	25230	441	324
8.56	benthic	mixed benthics	van Geen *et al.* 2003	OS-33205	25500	170	29020	141	399
9.01	benthic	mixed benthics	Marchitto et al., 2007	CURL-8449	27200	130	30700	195	388
9.71	benthic	mixed benthics	Marchitto *et al*., 2007	CURL-8450	29230	160	33120	119	444
10.06	benthic	*Uvigerina* spp.	Marchitto et al., 2007	CURL-7188	30830	170	34570	167	410
10.21	benthic	*Uvigerina* spp.	Marchitto *et al*., 2007	CURL-7189	30460	190	35100	130	575
10.21	benthic	*Bolivina* spp.	Marchitto et al., 2007	CURL-7192	31370	180	35100	130	406
10.41	benthic	mixed benthics	van Geen *et al.* 2003	OS-33206	31200	280	35920	147	586
10.41	benthic	*Uvigerina* spp.	Marchitto et al., 2007	CURL-7187	31750	190	35920	147	481
10.91	benthic	*Bolivina* spp.	Marchitto *et al*., 2007	CURL-7193	34400	260	37900	122	353
3.56	planktic	*G. ruber*	This study	CURL-14070	12245	40	11820	112	-90
3.63	planktic	*G. ruber*	This study	CURL-12806	12210	30	12040	142	-62
3.66	planktic	*G. ruber*	This study	CURL-12204	12550	35	12140	158	-90
3.92	planktic	*G. ruber*	This study	CURL-12233	12330	30	12920	102	28
4.12	planktic	*G. ruber*	This study	CURL-12208	12965	35	13580	141	29
4.225	planktic	*G. ruber*	This study	CURL-12229	13125	30	13960	101	56
4.3	planktic	*G. ruber*	This study	CURL-12207	13425	30	14180	108	45
4.375	planktic	*G. ruber*	This study	CURL-12221	13615	35	14360	119	43
4.475	planktic	*G. ruber*	This study	CURL-9831	13770	40	14650	101	60
4.565	planktic	*G. ruber*	This study	CURL-9834	14490	35	14980	129	8
4.6725	planktic	*G. ruber*	This study	CURL-12231	15010	40	15370	200	-9
4.765	planktic	*G. ruber*	This study	CURL-9913	14680	40	15710	271	76
4.865	planktic	*G. ruber*	This study	CURL-9841	14965	40	16080	351	86
4.965	planktic	*G. ruber*	This study	CURL-9925	14945	40	16450	434	138
5.065	planktic	*G. ruber*	This study	CURL-9848	15090	35	16680	395	149

5.15	planktic	*G. ruber*	This study	CURL-12222	15240	35	16990	352	171
5.275	planktic	*G. ruber*	This study	CURL-12225	15480	35	17450	309	202
5.365	planktic	*G. ruber*	This study	CURL-9905	15535	35	17780	298	242
5.47	planktic	*G. ruber*	This study	CURL-9851	15675	45	18130	307	273
5.5725	planktic	*G. ruber*	This study	CURL-12226	15585	35	18480	335	343
6.22	planktic	*G. ruber*	This study	CURL-12832	18150	70	20500	222	246
6.415	planktic	*G. ruber*	This study	CURL-9839	18445	50	21150	212	300
6.615	planktic	*G. ruber*	This study	CURL-9853	19000	50	21810	297	314
7.135	planktic	*G. ruber*	This study	CURL-9832	20590	60	23430	100	311
7.585	planktic	*G. ruber*	This study	CURL-9840	21530	70	25220	430	448
3.56	planktic	*G. sacculifer*	This study	CURL-14063	11760	30	11820	164	-34
3.63	planktic	*G. sacculifer*	This study	CURL-12812	12040	30	12040	103	-42
3.66	planktic	*G. sacculifer*	This study	CURL-12227	12185	25	12140	142	-47
3.92	planktic	*G. sacculifer*	This study	CURL-12211	12430	25	12920	102	16
4.12	planktic	*G. sacculifer*	This study	CURL-12223	12240	25	13580	108	126
4.22	planktic	*G. sacculifer*	This study	CURL-9849	12280	25	13940	118	171
4.3	planktic	*G. sacculifer*	This study	CURL-12214	12460	25	14180	100	178
4.375	planktic	*G. sacculifer*	This study	CURL-9838	12990	25	14360	130	127
4.475	planktic	*G. sacculifer*	This study	CURL-9854	13155	35	14650	202	144
4.565	planktic	*G. sacculifer*	This study	CURL-9919	13785	25	14980	276	101
4.6725	planktic	*G. sacculifer*	This study	CURL-12220	14455	35	15380	367	63
4.765	planktic	*G. sacculifer*	This study	CURL-9856	13995	40	15720	443	173
4.875	planktic	*G. sacculifer*	This study	CURL-12212	14470	30	16120	401	160
4.965	planktic	*G. sacculifer*	This study	CURL-12228	14970	35	16460	356	136
5.065	planktic	*G. sacculifer*	This study	CURL-9926	14820	40	16680	311	189
5.15	planktic	*G. sacculifer*	This study	CURL-12205	15640	50	16990	300	114
5.275	planktic	*G. sacculifer*	This study	CURL-12209	15480	50	17450	309	202
5.37	planktic	*G. sacculifer*	This study	CURL-12224	15370	35	17800	406	271
5.47	planktic	*G. sacculifer*	This study	CURL-9835	15565	50	18140	225	293
5.72	planktic	*G. sacculifer*	This study	CURL-12811	15225	45	18970	211	491
6.22	planktic	*G. sacculifer*	This study	CURL-12831	18040	70	20500	298	264
6.415	planktic	*G. sacculifer*	This study	CURL-9911	18555	50	21150	100	282
6.6225	planktic	*G. sacculifer*	This study	CURL-12206	18960	80	21840	447	325
7.135	planktic	*G. sacculifer*	This study	CURL-9908	20450	60	23430	100	334
7.59	planktic	*G. sacculifer*	This study	CURL-12213	21480	70	25250	140	463
3.56	planktic	*G. bulloides*	This study	CURL-16659	11425	35	11820	112	8
3.66	planktic	*G. bulloides*	This study	CURL-15503	11450	30	12140	156	44
3.98	planktic	*G. bulloides*	This study	CURL-15505	12420	35	13140	122	44
4.22	planktic	*G. bulloides*	This study	CURL-15490	12650	35	13940	102	118
4.475	planktic	*G. bulloides*	This study	CURL-15506	12945	40	14650	101	174
4.565	planktic	*G. bulloides*	This study	CURL-16670	13800	40	14980	129	99
4.765	planktic	*G. bulloides*	This study	CURL-15486	14365	40	15720	270	120
4.865	planktic	*G. bulloides*	This study	CURL-15499	14725	45	16080	350	119

5.165	planktic	*G. bulloides*	This study	CURL-15482	15100	45	17040	351	199
5.365	planktic	*G. bulloides*	This study	CURL-15504	15435	50	17780	304	258
5.465	planktic	*G. bulloides*	This study	CURL-15502	15640	50	18120	313	277

Appendix C

Auxiliary Material for Chapter III

1. Age Modeling Supplementary Methods

As described in section 2.4, calendar age models for cores PC10 and GC38 were constructed primarily by mapping ^{14}C *G. ruber* measurements onto the *G. ruber* ^{14}C record of PC08, supplemented where necessary by tie points based on the sediment reflectance (Figures S1 and S2). The PC08 *G. ruber* reference curve (light-blue shaded fields in Figures S1 and S2) was constructed by interpolating the PC08 *G. ruber* ^{14}C age vs. the previously-published GISP2-tied calendar age model (Marchitto et al. 2007) using a Monte-Carlo approach. Similar to our method of interpolating age models (see section 2.4), the low-frequency variability in the rate of change (^{14}C years / calendar year) within PC08 was used as an approximation of the high-frequency variability, which when input to the Monte Carlo algorithm allowed us to estimate the larger uncertainty of the reference curve between control points. Because there is no planktic material available in the early Holocene section of PC08, three benthic measurements were included in the interpolation. This effectively assigned a minimum age to the youngest G. ruber dates that mapped onto the youngest part of the reference curve, ensuring that the age models for PC10 and GC38 would not result in *G. ruber* surface $\Delta^{14}C$ values implausibly lower than coeval PC08 (705m water depth) benthic $\Delta^{14}C$.

2. PC08 benthic $\delta^{13}C$

The $\delta^{13}C$ of intermediate waters was at a minimum during the last deglaciation in the eastern equatorial Pacific (Carriquiry *et al.*, 2015; Mix *et al.* 1991). The $\delta^{13}C$ of *Uvigerina perigrina* from core MV99/GC31/PC08 reaches its lowest values between 20 and 10ka, but the deglacial

minimum is punctuated by heavier values during Heinrich Stadial 1 (HS1) and the Younger Dryas (YD; see Figure S3, left axis). This is likely due to changes in porewater concentrations of respired (low-$\delta^{13}C$) carbon varying the isotopic offset between porewaters and bottom water in response to changes in local export productivity. We compare $\delta^{13}C$ from cores PC08 and GC31 to Factor 3 of the diffuse spectral reflectance (DSR), which is correlated with organic carbon content of the core sediments and local export productivity (Ortiz et al. 2004) The comparison suggests that lower productivity, and thus a smaller porewater offset, during HS1 and the YD may have caused the infaunal *U. perigrina* to record heavier $\delta^{13}C$ during those periods, overprinting the regional deglacial $\delta^{13}C$ minimum.

3. The Modern $\delta^{18}O$ of Calcite Gradient between SBB and Galapagos Rise

In the modern ocean, the $\delta^{18}O$ of seawater in the tropical Pacific regresses onto salinity with a slope of 0.27 ‰/psu (LeGrande and Schmidt 2006). Multiplying by the salinity difference between SBB and Galapagos Rise core VM21-30 core locations (~0.3 psu, Fig. 2 in the main text) suggests that SBB seawater $\delta^{18}O$ should be ~0.1 ‰ lower than at Galapagos Rise. The temperature effect on the $\delta^{18}O$ of calcite would oppose the seawater $\delta^{18}O$ gradient, because intermediate water at the equator is generally warmer than at SBB. Multiplying the temperature difference between SBB and Galapagos Rise core locations (1.2°C, Fig. 2 in the main text) by a typical temperature calibration of 0.25 ‰/°C (Bemis, Spero, and Lea 1998) adds 0.3 ‰, with the result that modern Galapagos Rise $\delta^{18}O$ of calcite should be ~0.2‰ lighter than at SBB, a small offset relative to the scatter in downcore $\delta^{18}O$ data (Fig. 7 in the main text). Galapagos Rise core VM21-30 and Baja California core PC08 are at slightly deeper, colder density levels than the SBB sill depth (Fig. 3 in the main text), by approximately 0.6 and 1 °C respectively. Using the

same temperature calibration, we therefore subtracted 0.15 and 0.25‰ from the VM21-30 and PC08 $\delta^{18}O$ splines before calculating the mixing ratios for Scenario 3 described in section 3.6 in the main text.

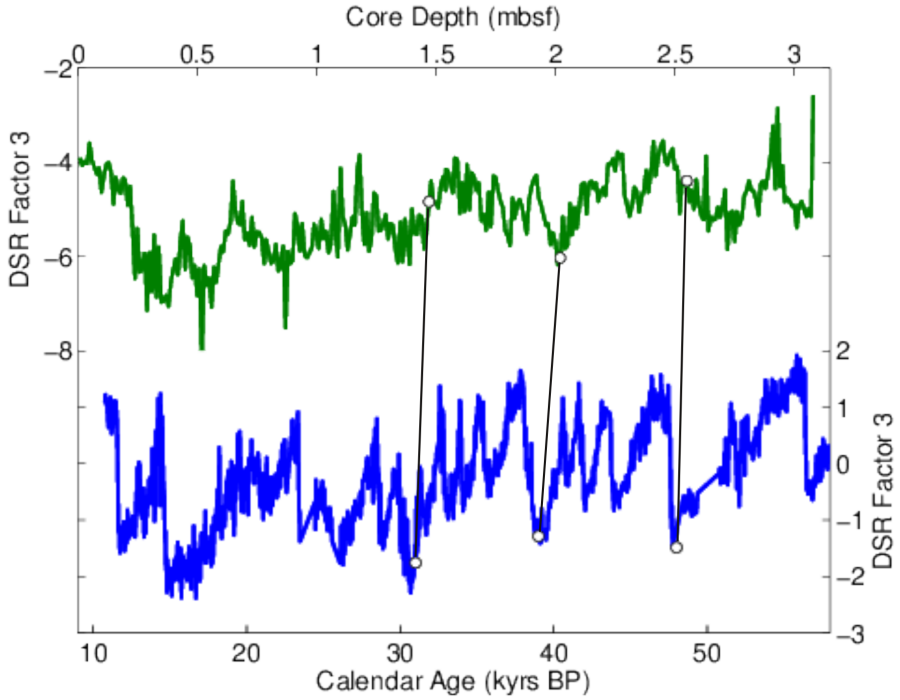

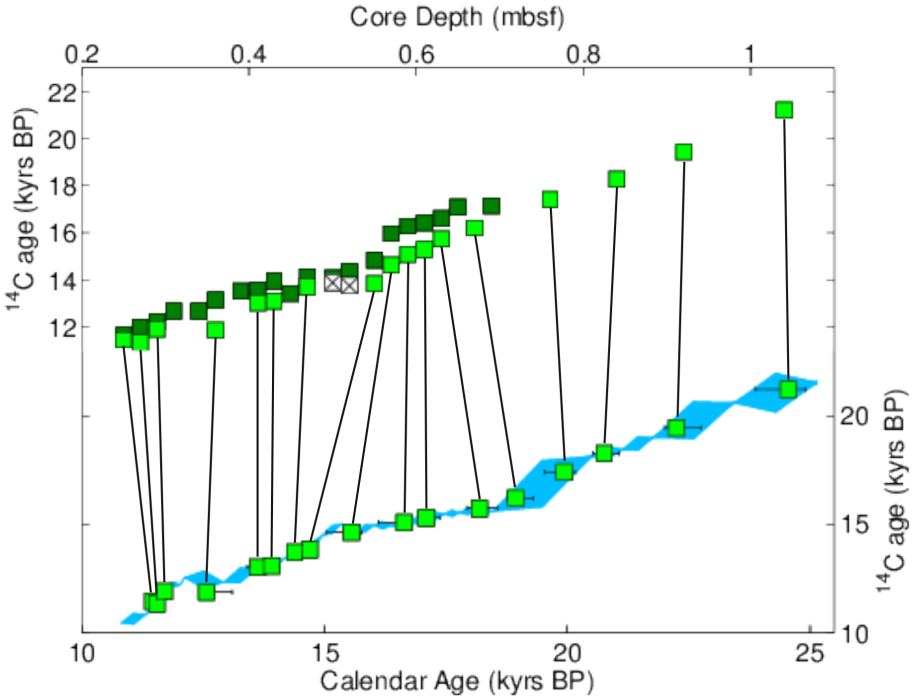

Figure S1: A) DSR Factor 3 tiepoints used to place GC38 (green, vs. depth in core on top axis) onto the age model of core PC08 (blue, vs. calendar age on the bottom axis). B) Deglacial GC38 *Uvigerina* (dark green squares) and *G. ruber* (light green squares and white squares with Xs) ^{14}C measurements vs. depth in core (top axes). Tiepoints to the PC08 *G. ruber* ^{14}C reference curve (light blue shape vs. calendar age on the lower axis) represent the results of our Monte Carlo age modeling. The *G. ruber* ^{14}C measurements that were used in the age model are plotted again (light green squares on the lower axis) with the resulting horizontal calendar age error bars. The white squares with Xs are *G. ruber* measurements not used in the age modeling. Note that the scale of the x-axis in B) is zoomed compared to A).

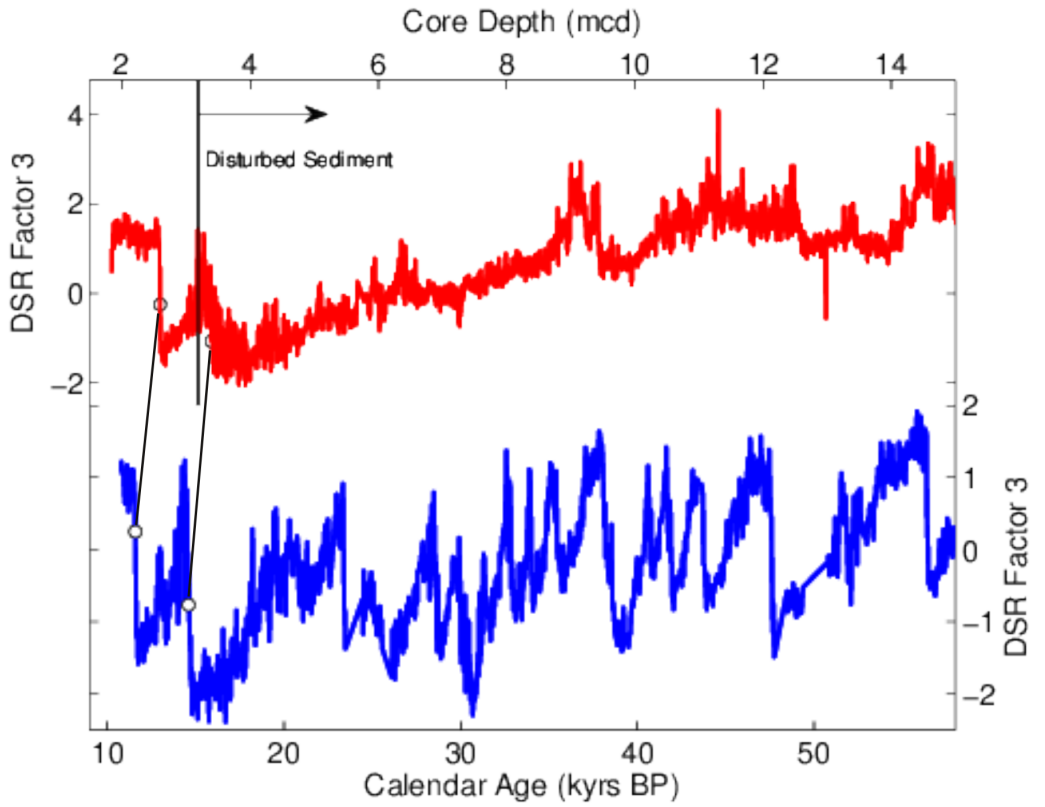
Core Depth (mcd)
2
4
6
8
10
12
14
DSR Factor 3
Disturbed Sediment
4
2
0
−2
2
1
0
−1
−2
DSR Factor 3
10
20
30
40
50
Calendar Age (kyrs BP)

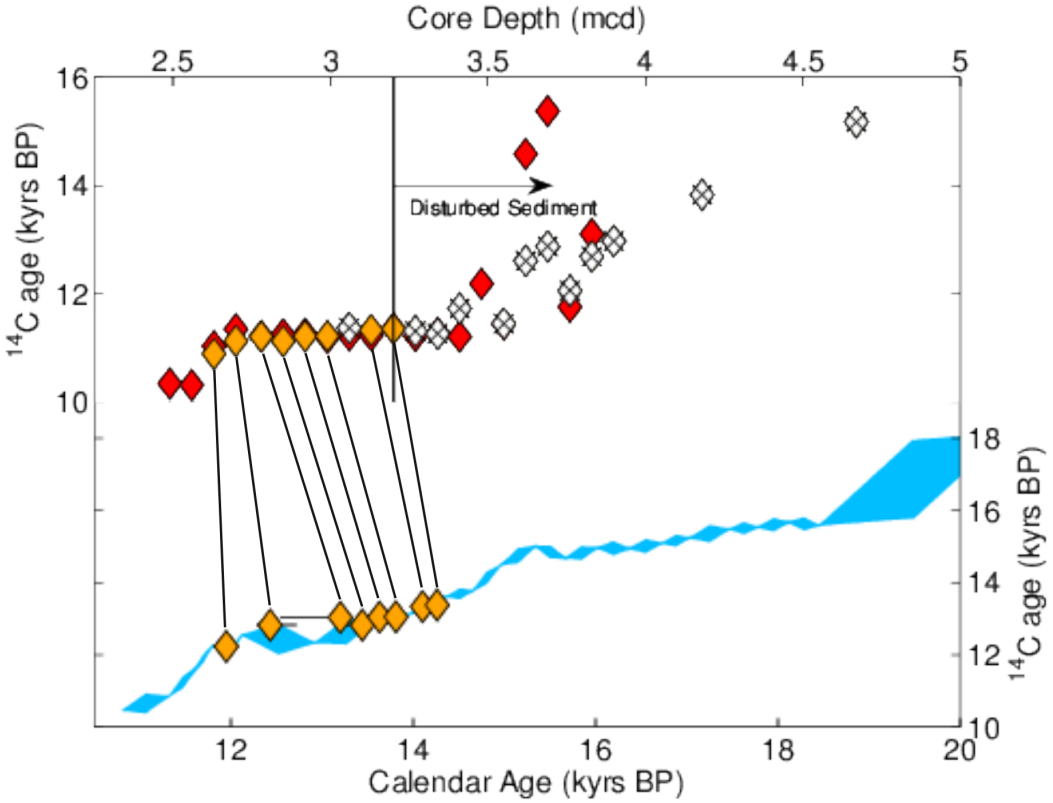
Core Depth (mcd)
2.5
3
3.5
4
4.5
5
16
14
12
10
^{14}C age (kyrs BP)
Disturbed Sediment
18
16
14
12
10
^{14}C age (kyrs BP)
12
14
16
18
20
Calendar Age (kyrs BP)

Figure S2: A) DSR Factor 3 tiepoints used to place PC10 (red, vs. composite depth on top axis) onto the age model of core PC08 (blue, vs. calendar age on the bottom axis). B) PC10 *Uvigerina* (red diamonds) and *G. ruber* (orange diamonds and white diamonds with Xs) ^{14}C measurements vs. composite depth (top axes). Tiepoints to the PC08 *G. ruber* ^{14}C reference curve (light blue shape vs. calendar age on the lower axis) represent the results of our Monte Carlo age modeling. The *G. ruber* ^{14}C measurements that were used in the age model are plotted again (orange diamonds on the lower axis) with the resulting horizontal calendar age error bars. The white diamonds are *G. ruber* measurements not used in the age modeling. Note that the scale of the X axis in B) is zoomed compared to A).

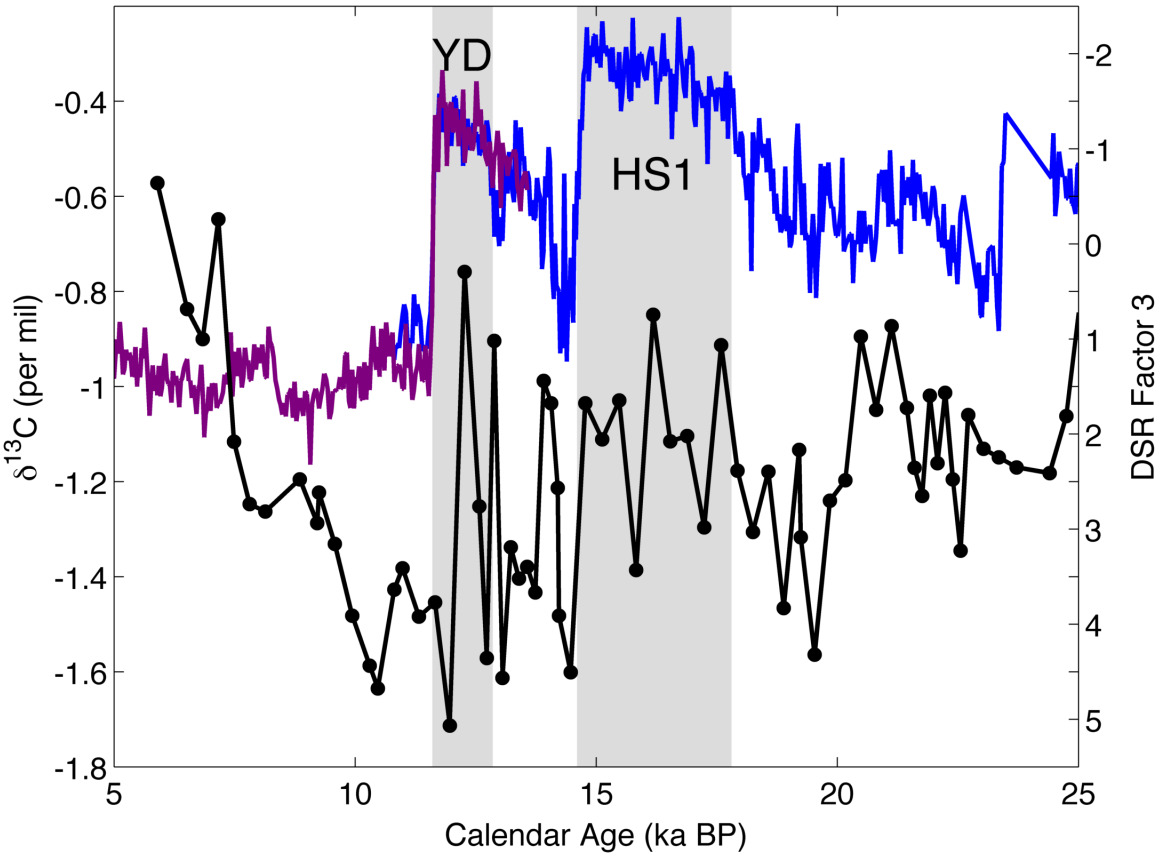

Figure S3: PC08 and GC31 DSR Factor 3 (blue and purple lines, right reversed axis) compared to PC08 and GC31 δ^{13}C measured in *Uvigerina* spp. Gray fields indicate Heirich Stadial 1 (HS1) and the Younger Dryas (YD). High DSR values are associated with higher organic carbon content in the cores and were likely caused by greater local export productivity.

Appendix D

New data presented in Chapter III

1. DSR tiepoints and ^{14}C data from Baja California core MV99-MC17/GC32/PC10

DSR-based Tiepoints to Marchitto *et al.*'s (2007) PC08 age model		
Composite depth in PC10 (m)	M07 Calendar Age	Estimated 1σ Cal. Age Uncertainty
2.6	11600	200
3.4	14600	200

Composite Depth (m)	Sample Type	Taxa	Source	CURL Number	^{14}C Age (years)	^{14}C Age Unc. (1σ)	M07 Calendar Age (yrs BP)	Cal. Age Low Unc. (1σ)	Cal. Age Upper Unc. (1σ)	$\Delta^{14}C$ (‰)
2.598	benthic	mixed	van Geen et al., 2003	n/a	12000	70	11560	-179	170	-91
2.735	benthic	mixed	van Geen et al., 2003	n/a	12700	80	12680	-206	358	-46
3.265	benthic	mixed	van Geen et al., 2003	n/a	13300	75	14420	-112	134	93
2.49	benthic	*Uvigerina spp.*	this study	CURL-14675	10865	30	11060	-357	345	-15
2.56	benthic	*Uvigerina spp.*	this study	CURL-14682	10790	30	11390	-219	205	35
2.63	benthic	*Uvigerina spp.*	this study	CURL-14677	12590	35	11950	-140	90	-115
2.7	benthic	*Uvigerina spp.*	this study	CURL-14678	13375	40	12430	-140	280	-149
2.78	benthic	*Uvigerina spp.*	this study	CURL-14685	13055	35	13200	-650	120	-28
2.85	benthic	*Uvigerina spp.*	this study	CURL-14661	13130	35	13430	-155	75	-10
2.92	benthic	*Uvigerina spp.*	this study	CURL-14684	13165	35	13630	-110	60	10
2.99	benthic	*Uvigerina spp.*	this study	CURL-14671	12980	35	13810	-80	60	56
3.06	benthic	*Uvigerina spp.*	this study	CURL-14666	13090	35	13940	-104	115	58
3.13	benthic	*Uvigerina spp.*	this study	CURL-14672	13080	35	14100	-60	40	80
3.2	benthic	*Uvigerina spp.*	this study	CURL-14676	13420	35	14260	-60	50	56
3.27	benthic	*Uvigerina spp.*	this study	CURL-14663	13065	35	14430	-122	139	126
3.34	benthic	*Uvigerina spp.*	this study	CURL-14683	13200	35	14600	-157	176	131
3.41	benthic	*Uvigerina spp.*	this study	CURL-15081	13030	60	14860	-134	164	*
3.48	benthic	*Uvigerina spp.*	this study	CURL-14662	15475	50	15640	-561	609	*
3.55	benthic	*Uvigerina spp.*	this study	CURL-14657	13585	35	16430	-1023	1099	*
3.62	benthic	*Uvigerina spp.*	this study	CURL-14679	21460	90	17230	-1513	1625	*
3.69	benthic	*Uvigerina spp.*	this study	CURL-15092	23440	130	17920	-1798	1694	*
3.76	benthic	*Uvigerina spp.*	this study	CURL-15091	14405	45	18710	-1283	1197	*

3.83	benthic	*Uvigerina spp.*	this study	CURL-15086	17770	60	19480	-764	726	*
2.63	planktic	*G. ruber*	this study	CURL-15096	12230	45	11950	-140	90	-74
2.7	planktic	*G. ruber*	this study	CURL-15095	12825	45	12430	-140	280	-89
2.78	planktic	*G. ruber*	this study	CURL-15082	13035	50	13200	-650	120	-26
2.85	planktic	*G. ruber*	this study	CURL-15084	12820	50	13440	-155	75	30
2.92	planktic	*G. ruber*	this study	CURL-14659	13045	35	13630	-110	60	25
2.99	planktic	*G. ruber*	this study	CURL-14686	13055	35	13810	-80	60	46
3.06	planktic	*G. ruber*	this study	CURL-15090	13425	45	13940	-104	115	15
3.13	planktic	*G. ruber*	this study	CURL-15080	13335	50	14100	-60	40	47
3.2	planktic	*G. ruber*	this study	CURL-15083	13380	60	14260	-60	50	61
3.27	planktic	*G. ruber*	this study	CURL-14665	13285	35	14430	-122	139	96
3.34	planktic	*G. ruber*	this study	CURL-14674	13155	35	14600	-157	176	137
3.41	planktic	*G. ruber*	this study	CURL-14673	14330	40	14860	-134	164	*
3.55	planktic	*G. ruber*	this study	CURL-14660	13625	40	16430	-1023	1099	*
3.62	planktic	*G. ruber*	this study	CURL-15087	16530	70	17230	-1513	1625	*
3.69	planktic	*G. ruber*	this study	CURL-15097	17200	70	17920	-1798	1694	*
3.76	planktic	*G. ruber*	this study	CURL-15088	15160	60	18710	-1283	1197	*
3.83	planktic	*G. ruber*	this study	CURL-15099	16720	70	19480	-764	726	*
3.9	planktic	*G. ruber*	this study	CURL-14664	17440	60	20250	-290	306	*
4.18	planktic	*G. ruber*	this study	CURL-14658	19580	80	22300	-818	782	*
4.67	planktic	*G. ruber*	this study	CURL-14500	22940	190	25680	-1420	1646	*

*no $\Delta^{14}C$ was calculated for samples from below the sediment disturbance starting at ~3.4 mcd

2. DSR tiepoints and ^{14}C data from Baja California core Core: MV99-GC38

DSR-based Tiepoints to Marchitto *et al.*'s (2007) PC08 age model		
Depth in GC38 (m)	M07 Calendar Age	Estimated 1σ Cal. Age Uncertainty
1.47	31000	200
2.02	39000	200
2.55	48000	200

Core Depth (mbsf)	Sample Type	Taxa	Source	CURL Number	^{14}C Age (years)	^{14}C Age Unc. (1σ)	M07 Calendar Age (yrs BP)	Cal. Age Low Unc. (1σ)	Cal. Age Upper Unc. (1σ)	$\Delta^{14}C$ (‰)
0.25	planktic	*G. ruber*	this study	CURL-15098	11450	35	11460	-30	20	-38
0.27	planktic	*G. ruber*	this study	CURL-15089	11340	35	11550	-30	20	-14
0.29	planktic	*G. ruber*	this study	CURL-15093	11910	35	11700	-30	30	-65

0.36	planktic	*G. ruber*	this study	CURL-13424	11875	30	12570	-130	522	43
0.41	planktic	*G. ruber*	this study	CURL-13429	13030	30	13620	-210	140	26
0.43	planktic	*G. ruber*	this study	CURL-13422	13090	30	13910	-130	60	54
0.47	planktic	*G. ruber*	this study	CURL-12810	13715	40	14380	-100	50	33
0.5	planktic	*G. ruber*	this study	CURL-13421	13895	30	14490	-117	116	23
0.52	planktic	*G. ruber*	this study	CURL-14077	13755	30	14580	-104	106	53
0.55	planktic	*G. ruber*	this study	CURL-13409	13845	30	14700	-40	60	56
0.57	planktic	*G. ruber*	this study	CURL-14073	14630	40	15550	-510	220	62
0.59	planktic	*G. ruber*	this study	CURL-14074	15090	40	16640	-540	160	144
0.61	planktic	*G. ruber*	this study	CURL-13427	15300	30	17100	-140	270	178
0.63	planktic	*G. ruber*	this study	CURL-13423	15735	40	18190	-250	370	273
0.67	planktic	*G. ruber*	this study	CURL-13430	16210	40	18940	-190	370	314
0.76	planktic	*G. ruber*	this study	CURL-13410	17415	40	19940	-410	222	276
0.84	planktic	*G. ruber*	this study	CURL-13428	18270	50	20760	-230	300	267
0.92	planktic	*G. ruber*	this study	CURL-13418	19440	50	22250	-240	510	312
1.04	planktic	*G. ruber*	this study	CURL-13408	21210	60	24550	-670	360	390
1.48	planktic	*G. ruber*	this study	CURL-12807	26360	190	31150	-227	224	627
0.25	benthic	*Uvigerina spp.*	this study	CURL-13071	11635	35	11460	-30	20	-60
0.27	benthic	*Uvigerina spp.*	this study	CURL-13084	11985	35	11550	-30	20	-90
0.29	benthic	*Uvigerina spp.*	this study	CURL-13059	12250	35	11700	-30	30	-104
0.31	benthic	*Uvigerina spp.*	this study	CURL-13060	12665	40	11970	-207	243	-121
0.34	benthic	*Uvigerina spp.*	this study	CURL-13077	12670	40	12340	-238	405	-81
0.36	benthic	*Uvigerina spp.*	this study	CURL-13082	13150	40	12570	-130	522	-110
0.39	benthic	*Uvigerina spp.*	this study	CURL-13056	13525	40	13190	-373	355	-84
0.41	benthic	*Uvigerina spp.*	this study	CURL-13069	13545	40	13620	-210	140	-38
0.43	benthic	*Uvigerina spp.*	this study	CURL-13072	13955	45	13910	-130	60	-53
0.45	benthic	*Uvigerina spp.*	this study	CURL-13075	13420	40	14130	-179	185	39
0.47	benthic	*Uvigerina spp.*	this study	CURL-13063	14125	45	14380	-100	50	-19
0.5	benthic	*Uvigerina spp.*	this study	CURL-13064	14090	45	14490	-117	116	-1
0.52	benthic	*Uvigerina spp.*	this study	CURL-13062	14360	45	14580	-104	106	-24
0.55	benthic	*Uvigerina spp.*	this study	CURL-13076	14835	50	14700	-40	60	-66
0.57	benthic	*Uvigerina spp.*	this study	CURL-13079	15970	60	15550	-510	220	-102
0.59	benthic	*Uvigerina spp.*	this study	CURL-13416	16290	40	16640	-540	160	-15
0.61	benthic	*Uvigerina spp.*	this study	CURL-13417	16420	40	17100	-140	270	25
0.63	benthic	*Uvigerina spp.*	this study	CURL-13425	16610	40	18190	-250	370	142
0.65	benthic	*Uvigerina spp.*	this study	CURL-13419	17100	40	18600	-346	410	129
0.69	benthic	*Uvigerina spp.*	this study	CURL-13426	17135	40	19190	-265	381	207

2. Uvigerina spp. $\delta^{18}O$ data from PC08 Baja California core MV99-MC19/GC31/PC08
Generated by Jose Carriquiry at the Universidad Autonoma de Baja California, Instituto de Investigaciones Oceanologicas

Composite Depth (m)	M07 Calendar Age (yrs BP)	$\delta^{18}O$ (‰)
1.82	5897	2.04
2.01	6514	2.6
2.11	6838	2.27
2.21	7162	2.324
2.31	7487	2.275
2.41	7811	2.189
2.51	8135	2.546
2.71	8852	2.444
2.81	9214	2.428
2.82	9250	2.429
2.91	9576	2.479
3.01	9938	2.463
3.11	10300	2.441
3.16	10470	2.392
3.26	10810	2.379
3.31	10981	2.476
3.41	11321	2.57
3.51	11656	3.246
3.61	11962	3.392
3.71	12268	3.053
3.81	12574	3.089
3.86	12728	3.219
3.91	12884	3.125
3.96	13055	2.999
4.01	13225	3.423
4.06	13396	3.251
4.11	13566	3.302
4.16	13737	3.037
4.21	13908	3.293
4.26	14064	3.322
4.31	14199	2.947
4.32	14226	2.83
4.41	14468	2.944
4.51	14771	3.566
4.61	15123	3.409
4.71	15475	3.158
4.81	15828	3.47
4.91	16180	3.507
5.01	16532	3.509
5.11	16884	3.591
5.21	17236	3.621
5.31	17589	3.574
5.41	17928	3.649
5.51	18247	3.736
5.61	18567	3.707
5.71	18887	3.466
5.81	19206	3.652
5.82	19238	3.836
5.91	19526	3.826
6.01	19845	3.765
6.11	20165	3.552
6.21	20485	3.562
6.31	20804	3.751
6.41	21122	3.712
6.51	21440	3.77
6.56	21599	3.76
6.61	21758	3.785
6.66	21917	3.623
6.71	22076	3.683
6.76	22234	3.702
6.81	22393	3.512
6.86	22552	3.666
6.91	22711	3.749
7.01	23029	3.588
7.11	23346	3.692
7.21	23715	3.746
7.39	24402	3.683
7.48	24746	3.581
7.58	25127	3.528
7.68	25509	3.643
7.78	25891	3.624
7.88	26272	3.681
7.93	26463	3.66
7.98	26654	3.615

8.03	26845	3.626
8.08	27035	3.73
8.13	27226	3.578
8.18	27417	3.759
8.23	27608	3.602
8.28	27799	3.601
8.33	27989	3.656
8.38	28180	3.536
8.43	28371	3.614
8.48	28562	3.437
8.53	28829	3.52
8.58	29114	3.507
8.63	29400	3.576
8.68	29686	3.415
8.73	29971	3.46
8.77	30093	3.558
8.86	30333	3.447
8.91	30467	3.488
8.96	30600	3.605
9.01	30733	3.549
9.11	31000	3.451
9.16	31133	3.576
9.21	31267	3.627
9.26	31400	3.473
9.31	31586	3.345
9.36	31772	3.503
9.41	31958	3.489
9.46	32144	3.542
9.51	32329	3.439
9.56	32515	3.43
9.61	32701	3.531
9.66	32893	3.45
9.71	33110	3.489
9.76	33327	3.408
9.81	33544	3.393
9.86	33761	3.397
9.91	33978	3.406
9.96	34169	3.43
10.06	34546	3.42
10.11	34734	3.363
10.16	34923	3.427
10.21	35111	3.517
10.26	35299	3.58

10.27	35337	3.361
10.36	35693	3.578
10.46	36097	3.669
10.56	36501	3.544
10.66	36906	3.446
10.71	37108	3.558
10.76	37310	3.633
10.81	37513	3.51
10.86	37715	3.673
10.91	37917	3.194
10.96	38119	3.368
11.06	38585	3.588
11.16	39065	3.45
11.21	39306	3.534
11.26	39546	3.502
11.31	39787	3.622
11.36	40027	3.611
11.41	40267	3.525
11.46	40508	3.629
11.51	40738	3.507
11.56	40925	3.502
11.61	41113	3.539
11.66	41300	3.458
11.71	41488	3.554
11.76	41675	3.554
11.77	41713	3.489
11.81	41863	3.462
11.86	42054	3.558
11.96	42440	3.527
12.01	42632	3.713
12.06	42825	3.614
12.11	43018	3.583
12.16	43210	3.52
12.21	43403	3.318
12.26	43596	3.265
12.31	43793	3.164
12.36	44005	3.433
12.41	44218	3.169
12.46	44431	3.295
12.51	44643	3.375
12.56	44856	2.885
12.61	45069	3.176
12.66	45281	3.27

12.71	45494	3.256
12.76	45707	3.114
12.81	45920	3.229
12.86	46132	3.21
12.91	46345	3.126
12.96	46558	3.253
13.01	46770	3.33
13.06	46983	3.254
13.11	47196	2.921
13.21	47621	3.234
13.26	47834	3.187
13.4	48430	3.324
13.49	48812	3.268
13.59	49238	3.064
13.69	49663	3.227
13.79	50089	3.242
13.89	50514	3.28
13.99	50940	3.278
14.09	51365	3.285
14.19	51790	3.276
14.29	52216	3.196
14.35	52471	3.462
14.44	52854	3.239
14.54	53279	3.254
14.64	53705	3.245
14.74	54130	3.154
14.84	54556	3.216
14.94	54981	3.201
15.04	55406	3.217
15.14	55832	3.198
15.24	56257	3.345
15.34	56683	3.288
15.44	57108	3.277
15.54	57533	3.242
15.64	57959	3.159

Appendix E

Post-2000 surface ocean $\Delta^{14}C$ observations compiled for Chapter V

Section ID	Decimal Date	Latitude	Longitude	Δ14C	NODC Expocode	Data source
n/a	2005.202740	-54.641	-64.973	24.8	n/a	Ellen Druffel, unpublished
n/a	2005.202740	-55.001	-64.959	19.1	n/a	Ellen Druffel, unpublished
n/a	2005.205479	-56.001	-64.665	-31.7	n/a	Ellen Druffel, unpublished
n/a	2005.205479	-56.5	-64.504	-34.9	n/a	Ellen Druffel, unpublished
n/a	2005.205479	-57.002	-64.344	-38.2	n/a	Ellen Druffel, unpublished
n/a	2005.205479	-57.516	-64.185	-50.7	n/a	Ellen Druffel, unpublished
n/a	2005.205479	-58	-64.026	-25.5	n/a	Ellen Druffel, unpublished
n/a	2005.205479	-58.492	-63.865	-23.8	n/a	Ellen Druffel, unpublished
n/a	2005.205479	-59	-63.688	-57	n/a	Ellen Druffel, unpublished
n/a	2005.208219	-59.515	-63.519	-67.4	n/a	Ellen Druffel, unpublished
n/a	2005.208219	-60.001	-63.347	-69.6	n/a	Ellen Druffel, unpublished
n/a	2005.208219	-60.497	-63.168	-75.3	n/a	Ellen Druffel, unpublished
n/a	2005.208219	-61.004	-62.992	-67.2	n/a	Ellen Druffel, unpublished
n/a	2005.208219	-62.028	-62.616	-106.1	n/a	Ellen Druffel, unpublished
n/a	2005.208219	-62.7	-62.2	-111.7	n/a	Ellen Druffel, unpublished
n/a	2002.534247	47.5	-128.04	19.6	n/a	Guilderson *et al.*, 2006
n/a	2002.534247	48	-129.56	8.3	n/a	Guilderson *et al.*, 2006
n/a	2002.534247	48.51	-131.09	13.1	n/a	Guilderson *et al.*, 2006
n/a	2002.534247	49.01	-132.62	22.6	n/a	Guilderson *et al.*, 2006
n/a	2002.534247	49.5	-134.14	11.4	n/a	Guilderson *et al.*, 2006
n/a	2002.534247	50.02	-135.74	8.3	n/a	Guilderson *et al.*, 2006
n/a	2002.534247	50.5	-137.27	7.5	n/a	Guilderson *et al.*, 2006
n/a	2002.534247	51	-138.96	7.5	n/a	Guilderson *et al.*, 2006
n/a	2002.534247	51.5	-140.47	-1.1	n/a	Guilderson *et al.*, 2006
n/a	2002.534247	52	-142.11	-4	n/a	Guilderson *et al.*, 2006
n/a	2002.534247	53	-145.41	-11.1	n/a	Guilderson *et al.*, 2006
n/a	2002.534247	53.5	-146.98	-17.7	n/a	Guilderson *et al.*, 2006
n/a	2002.534247	54.01	-148.6	-16.5	n/a	Guilderson *et al.*, 2006
n/a	2002.534247	54.5	-150.32	-21.4	n/a	Guilderson *et al.*, 2006
n/a	2002.534247	55.07	-152.85	-3	n/a	Guilderson *et al.*, 2006
n/a	2002.534247	55.52	-152.71	-6.3	n/a	Guilderson *et al.*, 2006
n/a	2002.534247	56	-152.55	3.8	n/a	Guilderson *et al.*, 2006
n/a	2002.534247	56.5	-152.38	10.3	n/a	Guilderson *et al.*, 2006
n/a	2002.536986	56.9	-151.86	3.5	n/a	Guilderson *et al.*, 2006
n/a	2002.536986	53.02	-146.52	-12.8	n/a	Guilderson *et al.*, 2006
n/a	2002.536986	51.98	-144.5	4	n/a	Guilderson *et al.*, 2006

n/a	2002.536986	51.24	-143.11	0.5	n/a	Guilderson *et al.*, 2006
n/a	2006.145205	-56.78	-64.37	-31	n/a	Guilderson *et al.*, 2012
n/a	2006.145205	-56.78	-64.37	-27	n/a	Guilderson *et al.*, 2012
n/a	2006.150685	-58.2	-63.98	-32.4	n/a	Guilderson *et al.*, 2012
n/a	2006.150685	-58.2	-63.89	-31.8	n/a	Guilderson *et al.*, 2012
n/a	2006.156164	-61.04	-62.94	-80.5	n/a	Guilderson *et al.*, 2012
n/a	2006.156164	-61.04	-62.94	-74.7	n/a	Guilderson *et al.*, 2012
n/a	2006.339726	-56.03	-64.63	-10.6	n/a	Guilderson *et al.*, 2012
n/a	2006.339726	-56.5	-64.5	19.8	n/a	Guilderson *et al.*, 2012
n/a	2006.339726	-57.6	-64.15	-15.4	n/a	Guilderson *et al.*, 2012
n/a	2006.339726	-58	-64	-40.6	n/a	Guilderson *et al.*, 2012
n/a	2006.339726	-58.5	-63.85	-21.3	n/a	Guilderson *et al.*, 2012
n/a	2006.339726	-59	-63.7	-78.7	n/a	Guilderson *et al.*, 2012
n/a	2006.364384	-57.51	-65.45	-3.9	n/a	Guilderson *et al.*, 2012
n/a	2008.480874	-54.83	-64.97	20.6	n/a	Guilderson *et al.*, 2012
n/a	2008.480874	-55.11	-64.93	16.1	n/a	Guilderson *et al.*, 2012
n/a	2008.483607	-56.04	-64.65	-12.3	n/a	Guilderson *et al.*, 2012
n/a	2008.483607	-56.63	-64.46	-6.8	n/a	Guilderson *et al.*, 2012
n/a	2008.483607	-56.63	-64.46	-9	n/a	Guilderson *et al.*, 2012
n/a	2008.483607	-58.05	-64.01	-36.1	n/a	Guilderson *et al.*, 2012
n/a	2008.483607	-58.71	-63.78	-41.5	n/a	Guilderson *et al.*, 2012
n/a	2008.486339	-60.18	-63.28	-71.1	n/a	Guilderson *et al.*, 2012
n/a	2008.486339	-60.54	-63.16	-71	n/a	Guilderson *et al.*, 2012
n/a	2008.486339	-61.05	-62.97	-73.6	n/a	Guilderson *et al.*, 2012
n/a	2008.486339	-62.11	-62.59	-91	n/a	Guilderson *et al.*, 2012
n/a	2008.595628	-62	-62.63	-75.1	n/a	Guilderson *et al.*, 2012
n/a	2008.595628	-61	-63	-79.9	n/a	Guilderson *et al.*, 2012
n/a	2008.598361	-60.43	-63.18	-90.6	n/a	Guilderson *et al.*, 2012
n/a	2008.598361	-60	-63.35	-82.4	n/a	Guilderson *et al.*, 2012
n/a	2008.598361	-59.48	-63.53	-48.2	n/a	Guilderson *et al.*, 2012
n/a	2008.598361	-59.97	-63.7	-37.9	n/a	Guilderson *et al.*, 2012
n/a	2008.598361	-58.46	-63.87	-27.1	n/a	Guilderson *et al.*, 2012
n/a	2008.598361	-57.42	-64.2	-12.1	n/a	Guilderson *et al.*, 2012
n/a	2008.598361	-56.5	-64.5	-36.6	n/a	Guilderson *et al.*, 2012
n/a	2008.601093	-57.93	-64.03	-14.2	n/a	Guilderson *et al.*, 2012
n/a	2008.601093	-56	-64.67	-28	n/a	Guilderson *et al.*, 2012
n/a	2008.601093	-55	-64.97	17.4	n/a	Guilderson *et al.*, 2012
n/a	2008.601093	-54.8	-64.97	24	n/a	Guilderson *et al.*, 2012
n/a	2008.704918	-54.8	-64.97	23.9	n/a	Guilderson *et al.*, 2012
n/a	2008.704918	-55.02	-64.78	26.4	n/a	Guilderson *et al.*, 2012
n/a	2008.70765	-56	-64.63	17.4	n/a	Guilderson *et al.*, 2012

n/a	2008.70765	-56.5	-64.48	1.9	n/a	Guilderson *et al.*, 2012
n/a	2008.70765	-57.05	-64.32	2.8	n/a	Guilderson *et al.*, 2012
n/a	2008.70765	-58.03	-64.01	-55.3	n/a	Guilderson *et al.*, 2012
n/a	2008.70765	-58.57	-63.82	-71.1	n/a	Guilderson *et al.*, 2012
n/a	2008.70765	-58.98	-63.68	-70.4	n/a	Guilderson *et al.*, 2012
n/a	2008.70765	-59.53	-63.5	-73.8	n/a	Guilderson *et al.*, 2012
n/a	2008.710383	-60.53	-63.15	-85.8	n/a	Guilderson *et al.*, 2012
n/a	2008.710383	-62.07	-62.58	-108.6	n/a	Guilderson *et al.*, 2012
n/a	2009	-54.83	-64.97	26.2	n/a	Guilderson *et al.*, 2012
n/a	2009	-56.05	-65.48	-7.3	n/a	Guilderson *et al.*, 2012
n/a	2009	-56.52	-65.7	-57.5	n/a	Guilderson *et al.*, 2012
n/a	2009	-55	-64.97	19.9	n/a	Guilderson *et al.*, 2012
n/a	2009	-57.02	-65.97	6.1	n/a	Guilderson *et al.*, 2012
n/a	2009.00274	-57.48	-66.2	-4	n/a	Guilderson *et al.*, 2012
n/a	2009.00274	-58.53	-66.75	-54.8	n/a	Guilderson *et al.*, 2012
n/a	2009.00274	-58.98	-66.98	-39.6	n/a	Guilderson *et al.*, 2012
n/a	2009.00274	-60.5	-67.82	-58.8	n/a	Guilderson *et al.*, 2012
n/a	2009.00274	-61	-67.67	-72.6	n/a	Guilderson *et al.*, 2012
n/a	2009.00274	-62.53	-66.77	-73.7	n/a	Guilderson *et al.*, 2012
n/a	2009.005479	-62.62	-64.18	-94.6	n/a	Guilderson *et al.*, 2012
n/a	2009.005479	-61.83	-60	-116.6	n/a	Guilderson *et al.*, 2012
n/a	2009.005479	-61	-60	-90.9	n/a	Guilderson *et al.*, 2012
n/a	2009.19726	-60	-61.7	-79.1	n/a	Guilderson *et al.*, 2012
n/a	2009.19726	-58	-62.75	-22.3	n/a	Guilderson *et al.*, 2012
n/a	2009.2	-57.5	-63.98	-18.6	n/a	Guilderson *et al.*, 2012
n/a	2009.2	-57	-63.28	-25.9	n/a	Guilderson *et al.*, 2012
n/a	2009.2	-56.5	-63.57	-51.8	n/a	Guilderson *et al.*, 2012
n/a	2009.2	-55	-64.67	18.2	n/a	Guilderson *et al.*, 2012
n/a	2009.2	-56	-64.82	-36.5	n/a	Guilderson *et al.*, 2012
n/a	2009.2	-54.8	-64.77	22.2	n/a	Guilderson *et al.*, 2012
n/a	2009.715068	-57.56	-63.96	-20.6	n/a	Guilderson *et al.*, 2012
n/a	2009.717808	-58.67	-63.7	-58.2	n/a	Guilderson *et al.*, 2012
n/a	2009.717808	-58.67	-63.7	-60.4	n/a	Guilderson *et al.*, 2012
n/a	2009.717808	-58.33	-63.8	-49.8	n/a	Guilderson *et al.*, 2012
n/a	2009.717808	-58.67	-63.7	-64.1	n/a	Guilderson *et al.*, 2012
n/a	2009.717808	-58.67	-63.7	-60.7	n/a	Guilderson *et al.*, 2012
n/a	2009.717808	-59	-63.6	-58.4	n/a	Guilderson *et al.*, 2012
n/a	2009.720548	-59.5	-63.43	-65.6	n/a	Guilderson *et al.*, 2012
n/a	2009.720548	-59.5	-63.43	-56.4	n/a	Guilderson *et al.*, 2012
n/a	2009.723288	-60.5	-63.09	-84	n/a	Guilderson *et al.*, 2012
n/a	2009.723288	-61	-62.92	-76.4	n/a	Guilderson *et al.*, 2012

n/a	2009.726027	-62	-62.58	-152.9	n/a	Guilderson *et al.*, 2012
n/a	2009.726027	-63	-62.24	-114.5	n/a	Guilderson *et al.*, 2012
n/a	2009.726027	-63	-62.24	-103.6	n/a	Guilderson *et al.*, 2012
n/a	2010.339726	-54.62	-64.95	25.4	n/a	Guilderson *et al.*, 2012
n/a	2010.339726	-55	-64.95	28.7	n/a	Guilderson *et al.*, 2012
n/a	2010.345205	-60.02	-63.33	-73.3	n/a	Guilderson *et al.*, 2012
n/a	2010.345205	-60.52	-63.17	-75.3	n/a	Guilderson *et al.*, 2012
n/a	2010.345205	-61	-62.98	-76.8	n/a	Guilderson *et al.*, 2012
n/a	2010.345205	-62	-62.62	-81.6	n/a	Guilderson *et al.*, 2012
n/a	2010.70137	-54.97	-64.97	18.9	n/a	Guilderson *et al.*, 2012
n/a	2010.70137	-55.03	-64.97	19.2	n/a	Guilderson *et al.*, 2012
n/a	2010.70411	-56	-65.15	1	n/a	Guilderson *et al.*, 2012
n/a	2010.70411	-57	-65.35	-0.3	n/a	Guilderson *et al.*, 2012
n/a	2010.70411	-58	-65.55	2.6	n/a	Guilderson *et al.*, 2012
n/a	2010.70411	-58.51	-65.65	-8.3	n/a	Guilderson *et al.*, 2012
n/a	2010.70411	-59.02	-65.76	-21.3	n/a	Guilderson *et al.*, 2012
n/a	2010.706849	-60.02	-65.96	-52.1	n/a	Guilderson *et al.*, 2012
n/a	2010.706849	-61.01	-66.17	-59.4	n/a	Guilderson *et al.*, 2012
n/a	2010.706849	-62.01	-66.4	-88	n/a	Guilderson *et al.*, 2012
n/a	2010.709589	-63.83	-66.82	-90.6	n/a	Guilderson *et al.*, 2012
n/a	2010.761644	-55	-64.96	20.2	n/a	Guilderson *et al.*, 2012
n/a	2010.764384	-56.5	-63.88	-6.7	n/a	Guilderson *et al.*, 2012
n/a	2010.764384	-58	-62.77	-27.4	n/a	Guilderson *et al.*, 2012
n/a	2010.764384	-58.52	-62.38	-67.2	n/a	Guilderson *et al.*, 2012
n/a	2010.764384	-60	-61.21	-62.3	n/a	Guilderson *et al.*, 2012
n/a	2010.767123	-61	-60.4	-85.6	n/a	Guilderson *et al.*, 2012
n/a	2010.832877	-54.85	-64.96	28.2	n/a	Guilderson *et al.*, 2012
n/a	2010.835616	-56	-64.45	4.5	n/a	Guilderson *et al.*, 2012
n/a	2010.835616	-56.56	-64.17	12.2	n/a	Guilderson *et al.*, 2012
n/a	2010.835616	-57.01	-63.93	11.1	n/a	Guilderson *et al.*, 2012
n/a	2010.835616	-58.03	-63.38	-10.1	n/a	Guilderson *et al.*, 2012
n/a	2010.835616	-58.62	-63.06	-67.4	n/a	Guilderson *et al.*, 2012
n/a	2010.835616	-59.02	-62.79	-57.7	n/a	Guilderson *et al.*, 2012
n/a	2010.835616	-59.51	-62.56	-77.8	n/a	Guilderson *et al.*, 2012
n/a	2010.838356	-60.54	-61.96	-73	n/a	Guilderson *et al.*, 2012
n/a	2010.838356	-61	-61.69	-84	n/a	Guilderson *et al.*, 2012
n/a	2010.838356	-61.83	-61.18	-80.5	n/a	Guilderson *et al.*, 2012
n/a	2006.865753	20	88.2	38.5	n/a	Dutta *et al.*, 2010
n/a	2006.865753	19.5	88.22	52.8	n/a	Dutta *et al.*, 2010
n/a	2006.868493	18	88.21	55.3	n/a	Dutta *et al.*, 2010
n/a	2006.868493	16.01	88.21	51.4	n/a	Dutta *et al.*, 2010

n/a	2006.871233	15	88.21	49.5	n/a	Dutta *et al.*, 2010
n/a	2006.871233	14	88.21	57.7	n/a	Dutta *et al.*, 2010
n/a	2006.873973	13.01	88.21	44	n/a	Dutta *et al.*, 2010
n/a	2006.876712	10.99	86.99	50.2	n/a	Dutta *et al.*, 2010
n/a	2006.876712	10.01	86.84	52.2	n/a	Dutta *et al.*, 2010
n/a	2006.879452	9	85.54	55.9	n/a	Dutta *et al.*, 2010
n/a	2006.879452	8.99	84.36	54.4	n/a	Dutta *et al.*, 2010
n/a	2006.882192	7.01	83.21	52.7	n/a	Dutta *et al.*, 2010
n/a	2006.882192	6	81.82	49.2	n/a	Dutta *et al.*, 2010
A10	2003.852055	-28.0475	-46.1267	86.4	49NZ20031106	Kumamoto *et al.*, 2011
A10	2003.854795	-28.8338	-43.5873	92.6	49NZ20031106	Kumamoto *et al.*, 2011
A10	2003.857534	-29.6075	-41.1617	84.5	49NZ20031106	Kumamoto *et al.*, 2011
A10	2003.860274	-30.0997	-39.0252	92.2	49NZ20031106	Kumamoto *et al.*, 2011
A10	2003.860274	-30.0997	-39.0252	92.6	49NZ20031106	Kumamoto *et al.*, 2011
A10	2003.863014	-29.997	-35.4885	77.4	49NZ20031106	Kumamoto *et al.*, 2011
A10	2003.868493	-30.0065	-32.0048	93.4	49NZ20031106	Kumamoto *et al.*, 2011
A10	2003.868493	-30.0065	-32.0048	98.7	49NZ20031106	Kumamoto *et al.*, 2011
A10	2003.873973	-30.0003	-28.9917	85.6	49NZ20031106	Kumamoto *et al.*, 2011
A10	2003.876712	-30.0023	-26.7182	102.1	49NZ20031106	Kumamoto *et al.*, 2011
A10	2003.876712	-30.2172	-25.0462	81	49NZ20031106	Kumamoto *et al.*, 2011
A10	2003.876712	-30.2172	-25.0462	97.6	49NZ20031106	Kumamoto *et al.*, 2011
A10	2003.879452	-30.0007	-22.4827	75.8	49NZ20031106	Kumamoto *et al.*, 2011
A10	2003.882192	-30.1078	-19.001	97.4	49NZ20031106	Kumamoto *et al.*, 2011
A10	2003.884932	-30.001	-16.339	70.6	49NZ20031106	Kumamoto *et al.*, 2011
A10	2003.884932	-30.001	-16.339	66.3	49NZ20031106	Kumamoto *et al.*, 2011
A10	2003.887671	-29.9968	-13.6645	76.2	49NZ20031106	Kumamoto *et al.*, 2011
A10	2003.890411	-30.001	-11.0028	88.6	49NZ20031106	Kumamoto *et al.*, 2011
A10	2003.893151	-29.9917	-8.9953	80.1	49NZ20031106	Kumamoto *et al.*, 2011
A10	2003.893151	-29.9917	-8.9953	69.3	49NZ20031106	Kumamoto *et al.*, 2011
A10	2003.89589	-29.9967	-4.8217	78.6	49NZ20031106	Kumamoto *et al.*, 2011
A10	2003.90137	-30.0048	-1.4903	56.9	49NZ20031106	Kumamoto *et al.*, 2011
A10	2003.90411	-29.7263	1.1318	78.7	49NZ20031106	Kumamoto *et al.*, 2011
A10	2003.90411	-29.7263	1.1318	68.8	49NZ20031106	Kumamoto *et al.*, 2011
A10	2003.906849	-29.4677	3.3075	49.4	49NZ20031106	Kumamoto *et al.*, 2011
A10	2003.909589	-29.7405	5.9503	71	49NZ20031106	Kumamoto *et al.*, 2011
A10	2003.912329	-29.7347	9.2952	68.2	49NZ20031106	Kumamoto *et al.*, 2011
A10	2003.912329	-29.7347	9.2952	86.7	49NZ20031106	Kumamoto *et al.*, 2011
A10	2003.915068	-29.3698	12.7902	68.8	49NZ20031106	Kumamoto *et al.*, 2011
A13.5	2010.19726	-54.0007	0.0002	-91.2	33RO20100308	A. McNichol & R. Key, unpublished data
A13.5	2010.19726	-54.0007	0.0002	-88.4	33RO20100308	A. McNichol & R. Key, unpublished data

A13.5	2010.2	-52.5102	0.2515	-79.4	33RO20100308	A. McNichol & R. Key, unpublished data
A13.5	2010.2	-52.5102	0.2515	-86.8	33RO20100308	A. McNichol & R. Key, unpublished data
A13.5	2010.20274	-51	0.416	-73.5	33RO20100308	A. McNichol & R. Key, unpublished data
A13.5	2010.20274	-50	0.5545	-85.6	33RO20100308	A. McNichol & R. Key, unpublished data
A13.5	2010.205479	-48.5007	0.7618	-47.5	33RO20100308	A. McNichol & R. Key, unpublished data
A13.5	2010.208219	-47	0.97	-22.3	33RO20100308	A. McNichol & R. Key, unpublished data
A13.5	2010.208219	-46	1.1085	-26.8	33RO20100308	A. McNichol & R. Key, unpublished data
A13.5	2010.210959	-45	1.247	1.1	33RO20100308	A. McNichol & R. Key, unpublished data
A13.5	2010.210959	-45	1.247	-3.2	33RO20100308	A. McNichol & R. Key, unpublished data
A13.5	2010.213699	-41.9993	1.1497	48.8	33RO20100308	A. McNichol & R. Key, unpublished data
A13.5	2010.213699	-41.9993	1.1497	38.7	33RO20100308	A. McNichol & R. Key, unpublished data
A13.5	2010.219178	-37.9998	0.9838	48.8	33RO20100308	A. McNichol & R. Key, unpublished data
A13.5	2010.219178	-37.9998	0.9838	44.8	33RO20100308	A. McNichol & R. Key, unpublished data
A13.5	2010.224658	-34	1.2187	54.6	33RO20100308	A. McNichol & R. Key, unpublished data
A13.5	2010.224658	-34	1.2187	47.6	33RO20100308	A. McNichol & R. Key, unpublished data
A13.5	2010.230137	-29.9998	1.833	53.3	33RO20100308	A. McNichol & R. Key, unpublished data
A13.5	2010.230137	-29.9998	1.833	43.7	33RO20100308	A. McNichol & R. Key, unpublished data
A13.5	2010.235616	-26.9998	1.66	39.5	33RO20100308	A. McNichol & R. Key, unpublished data
A13.5	2010.235616	-26.9998	1.66	42.8	33RO20100308	A. McNichol & R. Key, unpublished data
A13.5	2010.238356	-24.9998	1.5498	50.9	33RO20100308	A. McNichol & R. Key, unpublished data
A13.5	2010.241096	-23	1.4432	50.8	33RO20100308	A. McNichol & R. Key, unpublished data
A13.5	2010.243836	-19.9998	1.2595	50.6	33RO20100308	A. McNichol & R. Key, unpublished data
A13.5	2010.243836	-19.9998	1.2595	44.5	33RO20100308	A. McNichol & R. Key, unpublished data
A13.5	2010.249315	-18	1.1748	66.2	33RO20100308	A. McNichol & R. Key, unpublished data
A13.5	2010.249315	-18	1.1748	53.8	33RO20100308	A. McNichol & R. Key, unpublished data
A13.5	2010.252055	-16	1.0017	41.2	33RO20100308	A. McNichol & R. Key, unpublished data
A13.5	2010.257534	-15	1	56.4	33RO20100308	A. McNichol & R. Key, unpublished data

A13.5	2010.257534	-15	1	49.3	33RO20100308	A. McNichol & R. Key, unpublished data
A13.5	2010.260274	-12	0.8662	46.9	33RO20100308	A. McNichol & R. Key, unpublished data
A13.5	2010.260274	-12	0.8662	46.1	33RO20100308	A. McNichol & R. Key, unpublished data
A13.5	2010.265753	-9.9998	0.7782	61.5	33RO20100308	A. McNichol & R. Key, unpublished data
A13.5	2010.265753	-9.9998	0.7782	54.6	33RO20100308	A. McNichol & R. Key, unpublished data
A13.5	2010.268493	-7.9997	-0.7167	46.1	33RO20100308	A. McNichol & R. Key, unpublished data
A13.5	2010.268493	-7.9997	-0.7167	45.3	33RO20100308	A. McNichol & R. Key, unpublished data
A13.5	2010.271233	-4.9997	-3.0003	50	33RO20100308	A. McNichol & R. Key, unpublished data
A13.5	2010.271233	-4.9997	-3.0003	47.7	33RO20100308	A. McNichol & R. Key, unpublished data
A13.5	2010.276712	-2.3333	-3.0007	45.7	33RO20100308	A. McNichol & R. Key, unpublished data
A13.5	2010.276712	-2.3333	-3.0007	60.4	33RO20100308	A. McNichol & R. Key, unpublished data
A13.5	2010.276712	-2.3333	-3.0007	53.4	33RO20100308	A. McNichol & R. Key, unpublished data
A13.5	2010.279452	-0.9992	-3.001	39.8	33RO20100308	A. McNichol & R. Key, unpublished data
A13.5	2010.279452	0.0008	-3.001	55.7	33RO20100308	A. McNichol & R. Key, unpublished data
A13.5	2010.279452	0.0008	-3.001	55	33RO20100308	A. McNichol & R. Key, unpublished data
A13.5	2010.282192	0.9997	-3.0003	55.4	33RO20100308	A. McNichol & R. Key, unpublished data
A13.5	2010.282192	0.9997	-3.0003	50	33RO20100308	A. McNichol & R. Key, unpublished data
A13.5	2010.284932	2.002	-3.001	51.5	33RO20100308	A. McNichol & R. Key, unpublished data
A13.5	2010.284932	2.002	-3.001	46.7	33RO20100308	A. McNichol & R. Key, unpublished data
A13.5	2010.287671	3.4032	-3.0005	51.4	33RO20100308	A. McNichol & R. Key, unpublished data
A13.5	2010.290411	4.432	-3	55.4	33RO20100308	A. McNichol & R. Key, unpublished data
A13.5	2010.290411	4.432	-3	49.1	33RO20100308	A. McNichol & R. Key, unpublished data
A16N	2003.465753	62.7485	-20.0003	70.3	33RO200306_01	A. McNichol, unpublished data
A16N	2003.468493	61.613	-20	65.6	33RO200306_01	A. McNichol, unpublished data
A16N	2003.468493	61.0007	-20.0018	52.2	33RO200306_01	A. McNichol, unpublished data
A16N	2003.471233	59.5	-19.9973	58	33RO200306_01	A. McNichol, unpublished data
A16N	2003.471233	58.9985	-19.9993	54	33RO200306_01	A. McNichol, unpublished data
A16N	2003.471233	58.0013	-19.9978	69.6	33RO200306_01	A. McNichol, unpublished data
A16N	2003.473973	56.9997	-19.9995	65	33RO200306_01	A. McNichol, unpublished data
A16N	2003.473973	56.0017	-19.999	66.7	33RO200306_01	A. McNichol, unpublished data

A16N	2003.476712	55.0025	-19.9997	63.3	33RO200306_01	A. McNichol, unpublished data
A16N	2003.479452	52.4995	-20.0002	55.1	33RO200306_01	A. McNichol, unpublished data
A16N	2003.482192	49.9995	-20.0012	74.7	33RO200306_01	A. McNichol, unpublished data
A16N	2003.487671	47.0002	-19.998	80.5	33RO200306_01	A. McNichol, unpublished data
A16N	2003.493151	44.5	-20	78.5	33RO200306_01	A. McNichol, unpublished data
A16N	2003.493151	43.9987	-20.0005	77.7	33RO200306_01	A. McNichol, unpublished data
A16N	2003.49589	42.4987	-19.9987	73.2	33RO200306_01	A. McNichol, unpublished data
A16N	2003.50137	39.4995	-20.0005	79	33RO200306_01	A. McNichol, unpublished data
A16N	2003.506849	36.4998	-20.0017	81.9	33RO200306_01	A. McNichol, unpublished data
A16N	2003.509589	34.4998	-20.8435	91.1	33RO200306_01	A. McNichol, unpublished data
A16N	2003.515068	31.5003	-22.5323	95.2	33RO200306_01	A. McNichol, unpublished data
A16N	2003.517808	29.9988	-23.3745	104.8	33RO200306_01	A. McNichol, unpublished data
A16N	2003.542466	27.4998	-24.7812	80.9	33RO200306_02	A. McNichol, unpublished data
A16N	2003.547945	25.0007	-26.1842	86.6	33RO200306_02	A. McNichol, unpublished data
A16N	2003.550685	22.5003	-27.5938	77.3	33RO200306_02	A. McNichol, unpublished data
A16N	2003.556164	20.0007	-29.0003	71	33RO200306_02	A. McNichol, unpublished data
A16N	2003.558904	17.9995	-28.9988	63.1	33RO200306_02	A. McNichol, unpublished data
A16N	2003.567123	13.4998	-28.9997	63.8	33RO200306_02	A. McNichol, unpublished data
A16N	2003.572603	9.9992	-28.4992	65.5	33RO200306_02	A. McNichol, unpublished data
A16N	2003.578082	7.5008	-27.2505	64.3	33RO200306_02	A. McNichol, unpublished data
A16N	2003.580822	4.9997	-26	66.4	33RO200306_02	A. McNichol, unpublished data
A16N	2003.586301	3.007	-24.9955	73.8	33RO200306_02	A. McNichol, unpublished data
A16N	2003.589041	1.0097	-24.9958	79.4	33RO200306_02	A. McNichol, unpublished data
A16N	2003.591781	-0.0003	-25.0002	76.3	33RO200306_02	A. McNichol, unpublished data
A16N	2003.591781	-0.9998	-25.0008	62	33RO200306_02	A. McNichol, unpublished data
A16N	2003.594521	-2	-25.0003	68.9	33RO200306_02	A. McNichol, unpublished data
A16N	2003.59726	-2.9987	-25.0022	66	33RO200306_02	A. McNichol, unpublished data
A16N	2003.6	-4	-25.0002	70.4	33RO200306_02	A. McNichol, unpublished data
A16N	2003.6	-4.9993	-25.0113	51	33RO200306_02	A. McNichol, unpublished data
A16N	2003.60274	-6.004	-24.9995	66.6	33RO200306_02	A. McNichol, unpublished data
A16S	2005.043836	-60.0137	-30.8955	-118.9	33RO200501	A. McNichol, unpublished data
A16S	2005.043836	-60.0137	-30.8955	-135.5	33RO200501	A. McNichol, unpublished data
A16S	2005.046575	-58.0268	-30.9155	-91.9	33RO200501	A. McNichol, unpublished data
A16S	2005.052055	-55.3327	-34.5317	-82	33RO200501	A. McNichol, unpublished data
A16S	2005.052055	-55.3327	-34.5317	-78.6	33RO200501	A. McNichol, unpublished data
A16S	2005.052055	-55.3327	-34.5317	-94.5	33RO200501	A. McNichol, unpublished data
A16S	2005.054795	-52.9965	-35.848	-79.4	33RO200501	A. McNichol, unpublished data
A16S	2005.057534	-51.0018	-34.6157	-61.4	33RO200501	A. McNichol, unpublished data
A16S	2005.063014	-48.0027	-32.7517	-42.4	33RO200501	A. McNichol, unpublished data
A16S	2005.063014	-48.0027	-32.7517	-17.2	33RO200501	A. McNichol, unpublished data
A16S	2005.068493	-44.9968	-30.9002	27.7	33RO200501	A. McNichol, unpublished data

A16S	2005.073973	-42.0007	-29.0333	34.7	33RO200501	A. McNichol, unpublished data
A16S	2005.076712	-40.0013	-27.8032	61.5	33RO200501	A. McNichol, unpublished data
A16S	2005.076712	-40.0013	-27.8032	61.2	33RO200501	A. McNichol, unpublished data
A16S	2005.084932	-36.0002	-25.3002	74	33RO200501	A. McNichol, unpublished data
A16S	2005.090411	-31.9987	-24.9988	73.6	33RO200501	A. McNichol, unpublished data
A16S	2005.090411	-31.9987	-24.9988	79.7	33RO200501	A. McNichol, unpublished data
A16S	2005.09589	-29.0005	-25.0023	64.3	33RO200501	A. McNichol, unpublished data
A16S	2005.09589	-29.0005	-25.0023	78.8	33RO200501	A. McNichol, unpublished data
A16S	2005.10137	-26.0003	-24.9993	76	33RO200501	A. McNichol, unpublished data
A16S	2005.10137	-26.0003	-24.9993	74.4	33RO200501	A. McNichol, unpublished data
A16S	2005.106849	-23	-25.0002	70	33RO200501	A. McNichol, unpublished data
A16S	2005.109589	-20.0015	-24.9992	83.6	33RO200501	A. McNichol, unpublished data
A16S	2005.109589	-20.0015	-24.9992	71.3	33RO200501	A. McNichol, unpublished data
A16S	2005.115068	-17.0012	-25.0017	56	33RO200501	A. McNichol, unpublished data
A16S	2005.120548	-14.0007	-25.0005	52	33RO200501	A. McNichol, unpublished data
A16S	2005.120548	-14.0007	-25.0005	58.5	33RO200501	A. McNichol, unpublished data
A16S	2005.126027	-11.0007	-25.0005	57.1	33RO200501	A. McNichol, unpublished data
A16S	2005.131507	-8	-25.0003	62.5	33RO200501	A. McNichol, unpublished data
A16S	2005.131507	-8	-25.0003	78.1	33RO200501	A. McNichol, unpublished data
A16S	2005.134247	-5.0012	-25.0013	54.4	33RO200501	A. McNichol, unpublished data
A16S	2005.139726	-2.3335	-25.0002	59.6	33RO200501	A. McNichol, unpublished data
A16S	2005.139726	-2.3335	-25.0002	62.5	33RO200501	A. McNichol, unpublished data
A20	2003.734247	43.2487	-50.6173	36.8	316N200309	A. McNichol & R. Key, unpublished data
A20	2003.734247	43.1023	-50.7482	33.4	316N200309	A. McNichol & R. Key, unpublished data
A20	2003.734247	42.9313	-50.889	33.1	316N200309	A. McNichol & R. Key, unpublished data
A20	2003.734247	42.6357	-51.1203	42.8	316N200309	A. McNichol & R. Key, unpublished data
A20	2003.734247	42.2073	-51.49	63.2	316N200309	A. McNichol & R. Key, unpublished data
A20	2003.739726	39.4778	-51.8	72.6	316N200309	A. McNichol & R. Key, unpublished data
A20	2003.747945	35.568	-52.3617	76.5	316N200309	A. McNichol & R. Key, unpublished data
A20	2003.750685	32.22	-52.3557	86.2	316N200309	A. McNichol & R. Key, unpublished data
A20	2003.756164	27.5148	-52.329	83.3	316N200309	A. McNichol & R. Key, unpublished data
A20	2003.767123	23.4993	-52.375	89.1	316N200309	A. McNichol & R. Key, unpublished data
A20	2003.775342	18.1993	-52.3352	71	316N200309	A. McNichol & R. Key, unpublished data
A20	2003.775342	18.1993	-52.3352	68.2	316N200309	A. McNichol & R. Key, unpublished data
A20	2003.778082	14.9587	-52.331	72.2	316N200309	A. McNichol & R. Key, unpublished data

A20	2003.786301	9.198	-52.4545	73.2	316N200309	A. McNichol & R. Key, unpublished data
A20	2003.789041	8.4965	-52.8148	75.5	316N200309	A. McNichol & R. Key, unpublished data
A20	2003.791781	7.6103	-53.2485	68.8	316N200309	A. McNichol & R. Key, unpublished data
A20	2003.791781	7.376	-53.3552	80.3	316N200309	A. McNichol & R. Key, unpublished data
A20	2003.791781	7.2452	-53.4202	77.6	316N200309	A. McNichol & R. Key, unpublished data
A20	2003.794521	7.0637	-53.5103	73.2	316N200309	A. McNichol & R. Key, unpublished data
A20	2003.794521	6.9803	-53.5715	69.2	316N200309	A. McNichol & R. Key, unpublished data
A22	2003.810959	11.3358	-64.7563	74.7	316N200310	A. McNichol & R. Key, unpublished data
A22	2003.813699	11.5057	-65.9985	77.6	316N200310	A. McNichol & R. Key, unpublished data
A22	2003.816438	14.3608	-65.994	66.8	316N200310	A. McNichol & R. Key, unpublished data
A22	2003.824658	17.9667	-65.1393	72.9	316N200310	A. McNichol & R. Key, unpublished data
A22	2003.827397	18.9795	-66.0062	71.9	316N200310	A. McNichol & R. Key, unpublished data
A22	2003.830137	20.3742	-66.0127	71.6	316N200310	A. McNichol & R. Key, unpublished data
A22	2003.835616	23.5372	-65.9972	78.6	316N200310	A. McNichol & R. Key, unpublished data
A22	2003.841096	28.8968	-65.9972	83	316N200310	A. McNichol & R. Key, unpublished data
A22	2003.852055	34.7412	-66.597	79.6	316N200310	A. McNichol & R. Key, unpublished data
A22	2003.854795	36.2127	-67.4748	79.8	316N200310	A. McNichol & R. Key, unpublished data
A22	2003.857534	37.3805	-68.1838	75.9	316N200310	A. McNichol & R. Key, unpublished data
A22	2003.860274	38.3295	-68.8737	71.7	316N200310	A. McNichol & R. Key, unpublished data
A22	2003.863014	39.0137	-69.3235	60.9	316N200310	A. McNichol & R. Key, unpublished data
A22	2003.863014	39.7938	-69.8497	45.7	316N200310	A. McNichol & R. Key, unpublished data
I04	2003.950685	-24.6733	36.9912	51	49NZ20031209	Kumamoto *et al.*, 2011
I04	2003.953425	-24.6612	39.9962	54.6	49NZ20031209	Kumamoto *et al.*, 2011
I04	2003.956164	-24.665	42.9973	56.4	49NZ20031209	Kumamoto *et al.*, 2011
I04	2003.956164	-24.665	42.9973	60.2	49NZ20031209	Kumamoto *et al.*, 2011
I03	2003.969863	-19.9965	50.0602	59.4	49NZ20031209	Kumamoto *et al.*, 2011
I03	2003.969863	-19.9965	50.0602	56.9	49NZ20031209	Kumamoto *et al.*, 2011
I03	2003.972603	-19.9853	52.7773	62.3	49NZ20031209	Kumamoto *et al.*, 2011
I03	2003.975342	-19.999	56.0922	59.5	49NZ20031209	Kumamoto *et al.*, 2011
I03	2003.980822	-20.38	59.2275	51.4	49NZ20031209	Kumamoto *et al.*, 2011

I03	2003.989041	-20.368	61.6312	49.9	49NZ20031209	Kumamoto *et al.*, 2011
I03	2003.991781	-20.0892	64.9342	49.9	49NZ20031209	Kumamoto *et al.*, 2011
I03	2003.991781	-20.0892	64.9342	54.9	49NZ20031209	Kumamoto *et al.*, 2011
I03	2003.994521	-19.9978	68.2133	54.7	49NZ20031209	Kumamoto *et al.*, 2011
I03	2003.994521	-19.9978	68.2133	62	49NZ20031209	Kumamoto *et al.*, 2011
I03	2004	-19.997	71.2558	50.3	49NZ20031209	Kumamoto *et al.*, 2011
I03	2004	-19.997	71.2558	60.5	49NZ20031209	Kumamoto *et al.*, 2011
I03	2004.002732	-20.0003	74.1672	54.7	49NZ20031209	Kumamoto *et al.*, 2011
I03	2004.005464	-19.9872	76.9078	64.7	49NZ20031209	Kumamoto *et al.*, 2011
I03	2004.005464	-19.9872	76.9078	72	49NZ20031209	Kumamoto *et al.*, 2011
I03	2004.010929	-19.9958	79.9975	51.4	49NZ20031209	Kumamoto *et al.*, 2011
I03	2004.010929	-19.9958	79.9975	64.6	49NZ20031209	Kumamoto *et al.*, 2011
I03	2004.013661	-19.996	82.7363	51.5	49NZ20031209	Kumamoto *et al.*, 2011
I03	2004.013661	-19.996	82.7363	46.2	49NZ20031209	Kumamoto *et al.*, 2011
I03	2004.016393	-19.99	85.3043	52.9	49NZ20031209	Kumamoto *et al.*, 2011
I03	2004.016393	-19.99	85.3043	56.1	49NZ20031209	Kumamoto *et al.*, 2011
I03	2004.021858	-19.9997	87.3332	47.8	49NZ20031209	Kumamoto *et al.*, 2011
I03	2004.021858	-19.9997	87.3332	56.7	49NZ20031209	Kumamoto *et al.*, 2011
I03	2004.02459	-19.992	90.2878	61.4	49NZ20031209	Kumamoto *et al.*, 2011
I03	2004.02459	-19.992	90.2878	66.3	49NZ20031209	Kumamoto *et al.*, 2011
I03	2004.027322	-19.9912	93.5328	53.7	49NZ20031209	Kumamoto *et al.*, 2011
I03	2004.032787	-19.991	96.9533	64.3	49NZ20031209	Kumamoto *et al.*, 2011
I03	2004.035519	-19.9902	100.4658	68.1	49NZ20031209	Kumamoto *et al.*, 2011
I03	2004.040984	-19.992	103.1287	45	49NZ20031209	Kumamoto *et al.*, 2011
I03	2004.040984	-19.992	103.1287	54.5	49NZ20031209	Kumamoto *et al.*, 2011
I03	2004.043716	-19.9962	106.6247	45.3	49NZ20031209	Kumamoto *et al.*, 2011
I03	2004.043716	-19.9962	106.6247	56.5	49NZ20031209	Kumamoto *et al.*, 2011
I03	2004.051913	-21.8248	111.9018	58.3	49NZ20031209	Kumamoto *et al.*, 2011
I8S	2007.128767	-63.8807	81.9622	-105.7	33RR20070204	A. McNichol & R. Key, unpublished data
I8S	2007.131507	-63.2593	82.0115	-93.5	33RR20070204	A. McNichol & R. Key, unpublished data
I8S	2007.134247	-60.4802	82.0018	-109.7	33RR20070204	A. McNichol & R. Key, unpublished data
I8S	2007.136986	-58.9985	81.9997	-103.2	33RR20070204	A. McNichol & R. Key, unpublished data
I8S	2007.139726	-57.5127	82.5232	-97.5	33RR20070204	A. McNichol & R. Key, unpublished data
I8S	2007.142466	-56.0578	84.262	-47.5	33RR20070204	A. McNichol & R. Key, unpublished data
I8S	2007.156164	-51.8205	88.7805	-44.9	33RR20070204	A. McNichol & R. Key, unpublished data
I8S	2007.158904	-50.5703	90.0307	-35.8	33RR20070204	A. McNichol & R. Key, unpublished data
I8S	2007.161644	-49.282	91.2197	-20	33RR20070204	A. McNichol & R. Key, unpublished data

I8S	2007.164384	-47.5633	92.7303	-7.3	33RR20070204	A. McNichol & R. Key, unpublished data
I8S	2007.169863	-44.9915	94.9972	19.5	33RR20070204	A. McNichol & R. Key, unpublished data
I8S	2007.169863	-44.9915	94.9972	26.7	33RR20070204	A. McNichol & R. Key, unpublished data
I8S	2007.169863	-43.5088	95.0047	29.5	33RR20070204	A. McNichol & R. Key, unpublished data
I8S	2007.172603	-42.0083	95.007	35	33RR20070204	A. McNichol & R. Key, unpublished data
I8S	2007.178082	-39.997	94.9953	44.5	33RR20070204	A. McNichol & R. Key, unpublished data
I8S	2007.178082	-38.9895	94.9878	39	33RR20070204	A. McNichol & R. Key, unpublished data
I8S	2007.183562	-36.0177	95.0083	51.8	33RR20070204	A. McNichol & R. Key, unpublished data
I8S	2007.189041	-33.0183	94.9742	47.1	33RR20070204	A. McNichol & R. Key, unpublished data
I8S	2007.191781	-31.3003	95.0023	61.6	33RR20070204	A. McNichol & R. Key, unpublished data
I8S	2007.191781	-29.5145	95.0055	60.8	33RR20070204	A. McNichol & R. Key, unpublished data
I8S	2007.191781	-29.5145	95.0055	59.9	33RR20070204	A. McNichol & R. Key, unpublished data
P02	2004.459016	32.4133	133.2912	73.6	318M200406	A. McNichol & R. Key, unpublished data
P02	2004.459016	32.4133	133.2912	73	318M200406	A. McNichol & R. Key, unpublished data
P02	2004.461749	31.6288	133.7515	56.4	318M200406	A. McNichol & R. Key, unpublished data
P02	2004.461749	31.6288	133.7515	62.6	318M200406	A. McNichol & R. Key, unpublished data
P02	2004.47541	30.24	134.4903	82.8	318M200406	A. McNichol & R. Key, unpublished data
P02	2004.469945	30	136.6072	69.8	318M200406	A. McNichol & R. Key, unpublished data
P02	2004.478142	29.993	139.9285	65	318M200406	A. McNichol & R. Key, unpublished data
P02	2004.483607	30	143.1773	82.9	318M200406	A. McNichol & R. Key, unpublished data
P02	2004.489071	29.9998	145.4867	74.5	318M200406	A. McNichol & R. Key, unpublished data
P02	2004.494536	29.9953	149.269	91.4	318M200406	A. McNichol & R. Key, unpublished data
P02	2004.497268	30.0003	152.4038	73.3	318M200406	A. McNichol & R. Key, unpublished data
P02	2004.505464	29.9985	156.8488	75.8	318M200406	A. McNichol & R. Key, unpublished data
P02	2004.508197	30.0023	159.8485	82.2	318M200406	A. McNichol & R. Key, unpublished data
P02	2004.513661	29.9987	164.155	129	318M200406	A. McNichol & R. Key, unpublished data
P02	2004.519126	29.9973	166.7387	53.4	318M200406	A. McNichol & R. Key, unpublished data

P02	2004.52459	30.0072	170.6937	76.7	318M200406	A. McNichol & R. Key, unpublished data
P02	2004.527322	29.9912	173.315	73.2	318M200406	A. McNichol & R. Key, unpublished data
P02	2004.532787	29.9948	177.1025	58.3	318M200406	A. McNichol & R. Key, unpublished data
P02	2004.532787	29.9948	177.1025	67.2	318M200406	A. McNichol & R. Key, unpublished data
P02	2004.535519	30.0035	179.547	75.7	318M200406	A. McNichol & R. Key, unpublished data
P02	2004.535519	30.0035	179.547	78.1	318M200406	A. McNichol & R. Key, unpublished data
P02	2004.540984	29.9992	-176.7557	73.5	318M200406	A. McNichol & R. Key, unpublished data
P02	2004.540984	29.9992	-176.7557	80.8	318M200406	A. McNichol & R. Key, unpublished data
P02	2004.546448	30.0002	-172.9833	81.3	318M200406	A. McNichol & R. Key, unpublished data
P02	2004.54918	29.9947	-170.3683	76.1	318M200406	A. McNichol & R. Key, unpublished data
P02	2004.551913	30.0028	-167.7482	76.2	318M200406	A. McNichol & R. Key, unpublished data
P02	2004.584699	29.9972	-163.846	75	318M200406	A. McNichol & R. Key, unpublished data
P02	2004.587432	29.9992	-161.0833	75.7	318M200406	A. McNichol & R. Key, unpublished data
P02	2004.587432	29.9992	-161.0833	73.1	318M200406	A. McNichol & R. Key, unpublished data
P02	2004.598361	30.0007	-158.3148	81.7	318M200406	A. McNichol & R. Key, unpublished data
P02	2004.603825	29.992	-155.5228	112.4	318M200406	A. McNichol & R. Key, unpublished data
P02	2004.603825	29.992	-155.5228	110.7	318M200406	A. McNichol & R. Key, unpublished data
P02	2004.606557	30.0015	-152.653	86.8	318M200406	A. McNichol & R. Key, unpublished data
P02	2004.606557	30.0015	-152.653	85.9	318M200406	A. McNichol & R. Key, unpublished data
P02	2004.612022	29.9993	-149.6555	80.1	318M200406	A. McNichol & R. Key, unpublished data
P02	2004.614754	29.9985	-146.6477	72.4	318M200406	A. McNichol & R. Key, unpublished data
P02	2004.614754	29.9985	-146.6477	77.8	318M200406	A. McNichol & R. Key, unpublished data
P02	2004.617486	29.9993	-143.644	60.2	318M200406	A. McNichol & R. Key, unpublished data
P02	2004.617486	29.9993	-143.644	80	318M200406	A. McNichol & R. Key, unpublished data
P02	2004.620219	29.9987	-140.6408	73.6	318M200406	A. McNichol & R. Key, unpublished data
P02	2004.625683	29.9958	-137.6392	65.2	318M200406	A. McNichol & R. Key, unpublished data
P02	2004.625683	29.9958	-137.6392	58	318M200406	A. McNichol & R. Key, unpublished data

P02	2004.628415	30	-133.5835	44.3	318M200406	A. McNichol & R. Key, unpublished data
P02	2004.628415	30	-133.5835	40.5	318M200406	A. McNichol & R. Key, unpublished data
P02	2004.631148	29.9997	-131.2753	22.7	318M200406	A. McNichol & R. Key, unpublished data
P02	2004.631148	29.9997	-131.2753	39.6	318M200406	A. McNichol & R. Key, unpublished data
P02	2004.636612	29.9997	-128.9627	48	318M200406	A. McNichol & R. Key, unpublished data
P02	2004.636612	29.9997	-128.9627	58.4	318M200406	A. McNichol & R. Key, unpublished data
P02	2004.639344	30.0008	-125.4938	47.1	318M200406	A. McNichol & R. Key, unpublished data
P02	2004.642077	30.2598	-123.2685	29.7	318M200406	A. McNichol & R. Key, unpublished data
P02	2004.642077	30.2598	-123.2685	43.3	318M200406	A. McNichol & R. Key, unpublished data
P02	2004.647541	31.7778	-120.2493	42.5	318M200406	A. McNichol & R. Key, unpublished data
P02	2004.647541	31.7778	-120.2493	43.5	318M200406	A. McNichol & R. Key, unpublished data
P02	2004.650273	32.309	-119.1495	29.4	318M200406	A. McNichol & R. Key, unpublished data
P02	2004.650273	32.309	-119.1495	35.3	318M200406	A. McNichol & R. Key, unpublished data
P02	2004.650273	32.309	-119.1495	30.4	318M200406	A. McNichol & R. Key, unpublished data
P06E	2003.70137	-32.497	-141.4943	91.5	49NZ20030909	Kumamoto *et al.*, 2011
P06E	2003.70411	-32.5085	-138.6703	93.1	49NZ20030909	Kumamoto *et al.*, 2011
P06E	2003.706849	-32.4938	-136.0055	94.8	49NZ20030909	Kumamoto *et al.*, 2011
P06E	2003.706849	-32.4938	-136.0055	89.8	49NZ20030909	Kumamoto *et al.*, 2011
P06E	2003.709589	-32.4963	-133.3373	85.6	49NZ20030909	Kumamoto *et al.*, 2011
P06E	2003.709589	-32.4963	-133.3373	94.1	49NZ20030909	Kumamoto *et al.*, 2011
P06E	2003.712329	-32.4943	-130.6598	96.8	49NZ20030909	Kumamoto *et al.*, 2011
P06E	2003.715068	-32.4943	-127.9973	105.2	49NZ20030909	Kumamoto *et al.*, 2011
P06E	2003.715068	-32.4943	-127.9973	91.2	49NZ20030909	Kumamoto *et al.*, 2011
P06E	2003.720548	-32.5055	-125.3337	90.5	49NZ20030909	Kumamoto *et al.*, 2011
P06E	2003.720548	-32.5055	-125.3337	76.5	49NZ20030909	Kumamoto *et al.*, 2011
P06E	2003.720548	-32.4867	-122.6605	88.2	49NZ20030909	Kumamoto *et al.*, 2011
P06E	2003.723288	-32.4928	-119.9957	88.3	49NZ20030909	Kumamoto *et al.*, 2011
P06E	2003.726027	-32.4907	-117.3175	95.9	49NZ20030909	Kumamoto *et al.*, 2011
P06E	2003.726027	-32.4907	-117.3175	98.5	49NZ20030909	Kumamoto *et al.*, 2011
P06E	2003.728767	-32.4978	-114.6645	86.9	49NZ20030909	Kumamoto *et al.*, 2011
P06E	2003.731507	-32.4978	-112.0022	95.4	49NZ20030909	Kumamoto *et al.*, 2011
P06E	2003.731507	-32.4978	-112.0022	94.6	49NZ20030909	Kumamoto *et al.*, 2011
P06E	2003.734247	-32.4958	-109.3403	98.5	49NZ20030909	Kumamoto *et al.*, 2011
P06E	2003.734247	-32.4958	-109.3403	89.7	49NZ20030909	Kumamoto *et al.*, 2011

P06E	2003.736986	-32.4975	-106.671	88.5	49NZ20030909	Kumamoto *et al.*, 2011
P06E	2003.736986	-32.4975	-106.671	97.8	49NZ20030909	Kumamoto *et al.*, 2011
P06E	2003.739726	-32.4988	-103.0043	88.5	49NZ20030909	Kumamoto *et al.*, 2011
P06E	2003.742466	-32.5117	-101.321	93.9	49NZ20030909	Kumamoto *et al.*, 2011
P06E	2003.750685	-32.5	-95.9957	91.7	49NZ20030909	Kumamoto *et al.*, 2011
P06E	2003.750685	-32.5073	-93.3315	85.8	49NZ20030909	Kumamoto *et al.*, 2011
P06E	2003.753425	-32.5072	-90.6687	58.6	49NZ20030909	Kumamoto *et al.*, 2011
P06E	2003.756164	-32.501	-87.9952	84.2	49NZ20030909	Kumamoto *et al.*, 2011
P06E	2003.756164	-32.501	-87.9952	93.7	49NZ20030909	Kumamoto *et al.*, 2011
P06E	2003.758904	-32.4997	-85.339	75.8	49NZ20030909	Kumamoto *et al.*, 2011
P06E	2003.761644	-32.5045	-82.6672	62.1	49NZ20030909	Kumamoto *et al.*, 2011
P06E	2003.767123	-32.5077	-79.9932	56.1	49NZ20030909	Kumamoto *et al.*, 2011
P06E	2003.769863	-32.4975	-77.3213	49	49NZ20030909	Kumamoto *et al.*, 2011
P06E	2003.772603	-32.5	-74.6643	47.9	49NZ20030909	Kumamoto *et al.*, 2011
P06E	2003.775342	-32.4942	-72.7105	44.9	49NZ20030909	Kumamoto *et al.*, 2011
P06W	2003.589041	-30.0943	154.1532	84.8	49NZ20030803	Kumamoto *et al.*, 2011
P06W	2003.591781	-30.0843	156.5247	85.1	49NZ20030803	Kumamoto *et al.*, 2011
P06W	2003.594521	-30.0765	158.6932	90.3	49NZ20030803	Kumamoto *et al.*, 2011
P06W	2003.59726	-30.0852	161.4985	86.9	49NZ20030803	Kumamoto *et al.*, 2011
P06W	2003.6	-30.0813	164.834	98.9	49NZ20030803	Kumamoto *et al.*, 2011
P06W	2003.6	-30.0813	164.834	95.4	49NZ20030803	Kumamoto *et al.*, 2011
P06W	2003.605479	-30.0873	167.0042	91.2	49NZ20030803	Kumamoto *et al.*, 2011
P06W	2003.608219	-30.087	169.005	84	49NZ20030803	Kumamoto *et al.*, 2011
P06W	2003.610959	-30.0957	171.516	91.4	49NZ20030803	Kumamoto *et al.*, 2011
P06W	2003.613699	-30.072	174.5113	94.7	49NZ20030803	Kumamoto *et al.*, 2011
P06W	2003.613699	-30.072	174.5113	88.5	49NZ20030803	Kumamoto *et al.*, 2011
P06W	2003.616438	-30.5747	177.0052	90.9	49NZ20030803	Kumamoto *et al.*, 2011
P06W	2003.619178	-32.5092	179.9227	87.2	49NZ20030803	Kumamoto *et al.*, 2011
P06W	2003.627397	-32.4958	-177.2585	96.1	49NZ20030803	Kumamoto *et al.*, 2011
P06W	2003.632877	-32.493	-174.3327	83.8	49NZ20030803	Kumamoto *et al.*, 2011
P06W	2003.635616	-32.503	-171.9133	85.2	49NZ20030803	Kumamoto *et al.*, 2011
P06W	2003.635616	-32.503	-171.9133	89.9	49NZ20030803	Kumamoto *et al.*, 2011
	2003.638356	-32.5143	-169.9978	83.7	49NZ20030803	Kumamoto *et al.*, 2011

P06W						
P06W	2003.643836	-32.4867	-166.4982	85.6	49NZ20030803	Kumamoto *et al.*, 2011
P06W	2003.643836	-32.4867	-166.4982	93.5	49NZ20030803	Kumamoto *et al.*, 2011
P06W	2003.649315	-32.4947	-163.8272	95.6	49NZ20030803	Kumamoto *et al.*, 2011
P06W	2003.652055	-32.4975	-161.152	78	49NZ20030803	Kumamoto *et al.*, 2011
P06W	2003.654795	-32.495	-158.1533	82.7	49NZ20030803	Kumamoto *et al.*, 2011
P06W	2003.654795	-32.495	-158.1533	90.9	49NZ20030803	Kumamoto *et al.*, 2011
P06W	2003.657534	-32.5082	-154.841	85.9	49NZ20030803	Kumamoto *et al.*, 2011
P06W	2003.663014	-32.5058	-150.504	98.2	49NZ20030803	Kumamoto *et al.*, 2011
P06W	2003.665753	-32.5127	-148.1517	82.5	49NZ20030803	Kumamoto *et al.*, 2011
P06W	2003.665753	-32.5127	-148.1517	91.4	49NZ20030803	Kumamoto *et al.*, 2011
P06W	2003.668493	-32.5167	-144.8305	90.6	49NZ20030803	Kumamoto *et al.*, 2011
P06W	2003.668493	-32.5167	-144.8305	87.3	49NZ20030803	Kumamoto *et al.*, 2011
P16N	2006.120548	-17.0002	-149.9995	70.4	325020060213	A. McNichol, unpublished data
P16N	2006.120548	-17.0002	-149.9995	65.3	325020060213	A. McNichol, unpublished data
P16N	2006.123288	-15	-150.8	59.6	325020060213	A. McNichol, unpublished data
P16N	2006.126027	-12.0003	-151.0008	64.5	325020060213	A. McNichol, unpublished data
P16N	2006.126027	-12.0003	-151.0008	64.3	325020060213	A. McNichol, unpublished data
P16N	2006.128767	-10	-151	52.8	325020060213	A. McNichol, unpublished data
P16N	2006.128767	-10	-151	60	325020060213	A. McNichol, unpublished data
P16N	2006.131507	-7.0002	-151.0007	66	325020060213	A. McNichol, unpublished data
P16N	2006.131507	-7.0002	-151.0007	62.7	325020060213	A. McNichol, unpublished data
P16N	2006.134247	-5	-151	58.1	325020060213	A. McNichol, unpublished data
P16N	2006.134247	-5	-151	53.6	325020060213	A. McNichol, unpublished data
P16N	2006.136986	-2.9997	-151.0005	61.5	325020060213	A. McNichol, unpublished data
P16N	2006.136986	-2	-151	71.7	325020060213	A. McNichol, unpublished data
P16N	2006.136986	-2	-151	70.1	325020060213	A. McNichol, unpublished data
P16N	2006.139726	-1	-151	59	325020060213	A. McNichol, unpublished data
P16N	2006.139726	-1	-151	63	325020060213	A. McNichol, unpublished data
P16N	2006.139726	0	-150.9998	65.9	325020060213	A. McNichol, unpublished data
P16N	2006.139726	0	-150.9998	64.9	325020060213	A. McNichol, unpublished data
P16N	2006.142466	1	-151	63	325020060213	A. McNichol, unpublished data
P16N	2006.142466	1	-151	65.6	325020060213	A. McNichol, unpublished data
P16N	2006.142466	2	-151	63.1	325020060213	A. McNichol, unpublished data
P16N	2006.142466	2	-151	64	325020060213	A. McNichol, unpublished data

P16N	2006.145205	3	-151	68.2	325020060213	A. McNichol, unpublished data
P16N	2006.147945	5	-151	36.3	325020060213	A. McNichol, unpublished data
P16N	2006.150685	7.0005	-151.3288	60	325020060213	A. McNichol, unpublished data
P16N	2006.150685	7.0005	-151.3288	55.5	325020060213	A. McNichol, unpublished data
P16N	2006.150685	9	-151.66	57	325020060213	A. McNichol, unpublished data
P16N	2006.153425	11.0003	-152.0007	58.9	325020060213	A. McNichol, unpublished data
P16N	2006.156164	14	-152	69.4	325020060213	A. McNichol, unpublished data
P16N	2006.156164	14	-152	54.1	325020060213	A. McNichol, unpublished data
P16N	2006.158904	16	-152	55.2	325020060213	A. McNichol, unpublished data
P16N	2006.158904	16	-152	60.4	325020060213	A. McNichol, unpublished data
P16N	2006.164384	19	-152.0003	60.4	325020060213	A. McNichol, unpublished data
P16N	2006.164384	21	-152	69	325020060213	A. McNichol, unpublished data
P16N	2006.164384	21	-152	72.2	325020060213	A. McNichol, unpublished data
P16N	2006.191781	22.0003	-152.0003	72.1	325020060213	A. McNichol, unpublished data
P16N	2006.194521	24	-152.0002	73.7	325020060213	A. McNichol, unpublished data
P16N	2006.194521	24	-152.0002	76.1	325020060213	A. McNichol, unpublished data
P16N	2006.19726	26.0002	-152.0003	74	325020060213	A. McNichol, unpublished data
P16N	2006.19726	26.0002	-152.0003	68.8	325020060213	A. McNichol, unpublished data
P16N	2006.2	28.0002	-152.0002	78.5	325020060213	A. McNichol, unpublished data
P16N	2006.2	28.0002	-152.0002	82.4	325020060213	A. McNichol, unpublished data
P16N	2006.20274	30	-152	72.7	325020060213	A. McNichol, unpublished data
P16N	2006.20274	30	-152	81.7	325020060213	A. McNichol, unpublished data
P16N	2006.205479	31.9998	-152.0003	72.9	325020060213	A. McNichol, unpublished data
P16N	2006.208219	33.9997	-152.0005	64.3	325020060213	A. McNichol, unpublished data
P16N	2006.208219	33.9997	-152.0005	79.6	325020060213	A. McNichol, unpublished data
P16N	2006.208219	36	-152.0002	48.7	325020060213	A. McNichol, unpublished data
P16N	2006.208219	36	-152.0002	52.6	325020060213	A. McNichol, unpublished data
P16N	2006.210959	37.9997	-152.0005	58.4	325020060213	A. McNichol, unpublished data
P16N	2006.210959	37.9997	-152.0005	51.1	325020060213	A. McNichol, unpublished data
P16N	2006.213699	40	-152	33.8	325020060213	A. McNichol, unpublished data
P16N	2006.213699	40	-152	43.1	325020060213	A. McNichol, unpublished data
P16N	2006.216438	41.9997	-151.9987	17.7	325020060213	A. McNichol, unpublished data
P16N	2006.216438	41.9997	-151.9987	29.3	325020060213	A. McNichol, unpublished data
P16N	2006.221918	44.9998	-151.9997	2.5	325020060213	A. McNichol, unpublished data
P16N	2006.221918	44.9998	-151.9997	10.4	325020060213	A. McNichol, unpublished data
P16N	2006.224658	47	-152.0002	4.9	325020060213	A. McNichol, unpublished data
P16N	2006.224658	47	-152.0002	4.1	325020060213	A. McNichol, unpublished data
P16N	2006.227397	49.0002	-151.9993	-4	325020060213	A. McNichol, unpublished data
P16N	2006.227397	49.0002	-151.9993	-4.8	325020060213	A. McNichol, unpublished data
P16N	2006.230137	50.9998	-151.9998	-90.4	325020060213	A. McNichol, unpublished data
P16N	2006.230137	50.9998	-151.9998	-31.4	325020060213	A. McNichol, unpublished data

P16N	2006.232877	53	-152	-23.3	325020060213	A. McNichol, unpublished data
P16N	2006.232877	53	-152	-22.2	325020060213	A. McNichol, unpublished data
P16N	2006.235616	55	-152.6597	-17.3	325020060213	A. McNichol, unpublished data
P16N	2006.235616	55	-152.6597	-19.3	325020060213	A. McNichol, unpublished data
P16N	2006.238356	55.67	-152.95	-6.3	325020060213	A. McNichol, unpublished data
P16N	2006.238356	55.8502	-153.0302	-2.2	325020060213	A. McNichol, unpublished data
P16N	2006.241096	56.2198	-153.1897	0.3	325020060213	A. McNichol, unpublished data
P16S	2005.027397	-16.9995	-150.0003	63.8	33RR200501	A. McNichol & R. Key, unpublished data
P16S	2005.030137	-18.9997	-150.0002	77.4	33RR200501	A. McNichol & R. Key, unpublished data
P16S	2005.032877	-21.0002	-149.9997	64.7	33RR200501	A. McNichol & R. Key, unpublished data
P16S	2005.041096	-26.4998	-150.0005	76.2	33RR200501	A. McNichol & R. Key, unpublished data
P16S	2005.043836	-29	-150.0003	83.9	33RR200501	A. McNichol & R. Key, unpublished data
P16S	2005.043836	-29	-150.0003	85.7	33RR200501	A. McNichol & R. Key, unpublished data
P16S	2005.046575	-31.5	-150	81.7	33RR200501	A. McNichol & R. Key, unpublished data
P16S	2005.049315	-32.9988	-150.0008	85	33RR200501	A. McNichol & R. Key, unpublished data
P16S	2005.054795	-35.5	-149.9992	72	33RR200501	A. McNichol & R. Key, unpublished data
P16S	2005.060274	-38.9997	-150	55.5	33RR200501	A. McNichol & R. Key, unpublished data
P16S	2005.063014	-40.9995	-150	61.6	33RR200501	A. McNichol & R. Key, unpublished data
P16S	2005.068493	-44.0003	-150	36.6	33RR200501	A. McNichol & R. Key, unpublished data
P16S	2005.071233	-46.4998	-150.0002	40.6	33RR200501	A. McNichol & R. Key, unpublished data
P16S	2005.076712	-48.9995	-149.9968	39.9	33RR200501	A. McNichol & R. Key, unpublished data
P16S	2005.082192	-51.5	-150.0005	28.9	33RR200501	A. McNichol & R. Key, unpublished data
P16S	2005.084932	-54.0018	-150.0002	-30.3	33RR200501	A. McNichol & R. Key, unpublished data
P16S	2005.090411	-56.9993	-149.9998	-82.1	33RR200501	A. McNichol & R. Key, unpublished data
P16S	2005.09863	-63.0002	-149.9995	-98.7	33RR200501	A. McNichol & R. Key, unpublished data
P16S	2005.10137	-64.9995	-150	-98.3	33RR200501	A. McNichol & R. Key, unpublished data
P16S	2005.10137	-64.9995	-150	-100.5	33RR200501	A. McNichol & R. Key, unpublished data
P16S	2005.10411	-67.0007	-149.908	-110.8	33RR200501	A. McNichol & R. Key, unpublished data
P16S	2005.10411	-67.0007	-149.908	-97.7	33RR200501	A. McNichol & R. Key, unpublished data
P16S	2005.109589	-69.0008	-149.9938	-97.3	33RR200501	A. McNichol & R. Key,

						unpublished data
P16S	2005.112329	-70.9995	-150.0025	-92.2	33RR200501	A. McNichol & R. Key, unpublished data
P17C	2001.594521	30.0002	-134.9947	66.2	49NZ200107_1	Fukasawa & Murata, 2001
P17C	2001.594521	30.0002	-134.9947	62.8	49NZ200107_1	Fukasawa & Murata, 2001
P17C	2001.59726	31.0107	-135.0015	59.3	49NZ200107_1	Fukasawa & Murata, 2001
P17C	2001.59726	31.0107	-135.0015	57.4	49NZ200107_1	Fukasawa & Murata, 2001
P17C	2001.6	33.0028	-135.0028	38.9	49NZ200107_1	Fukasawa & Murata, 2001
P17C	2001.6	33.0028	-135.0028	46.7	49NZ200107_1	Fukasawa & Murata, 2001
P17N	2001.6	34.5877	-135.0042	51.5	49NZ200107_1	Fukasawa & Murata, 2001
P17N	2001.6	34.5877	-135.0042	41.5	49NZ200107_1	Fukasawa & Murata, 2001
P17N	2001.60274	35.5038	-135.0095	42.3	49NZ200107_1	Fukasawa & Murata, 2001
P17N	2001.60274	35.5038	-135.0095	44.5	49NZ200107_1	Fukasawa & Murata, 2001
P17N	2001.605479	37.5013	-135.0022	42.7	49NZ200107_1	Fukasawa & Murata, 2001
P17N	2001.605479	37.5013	-135.0022	41.8	49NZ200107_1	Fukasawa & Murata, 2001
P17N	2001.608219	39.5035	-135.0112	44.4	49NZ200107_1	Fukasawa & Murata, 2001
P17N	2001.608219	39.5035	-135.0112	36.9	49NZ200107_1	Fukasawa & Murata, 2001
P17N	2001.610959	39.9702	-135.01	51.3	49NZ200107_1	Fukasawa & Murata, 2001
P17N	2001.610959	39.9702	-135.01	53.1	49NZ200107_1	Fukasawa & Murata, 2001
P17N	2001.610959	40.9908	-134.9867	49.1	49NZ200107_1	Fukasawa & Murata, 2001
P17N	2001.610959	40.9908	-134.9867	45.9	49NZ200107_1	Fukasawa & Murata, 2001
P17N	2001.613699	41.6415	-135.9917	28.7	49NZ200107_1	Fukasawa & Murata, 2001
P17N	2001.613699	41.6415	-135.9917	23.4	49NZ200107_1	Fukasawa & Murata, 2001
P17N	2001.616438	42.9657	-138.0527	31.1	49NZ200107_1	Fukasawa & Murata, 2001
P17N	2001.616438	42.9657	-138.0527	27.8	49NZ200107_1	Fukasawa & Murata, 2001
P17N	2001.619178	44.2937	-140.149	28.2	49NZ200107_1	Fukasawa & Murata, 2001
P17N	2001.619178	44.2937	-140.149	28.9	49NZ200107_1	Fukasawa & Murata, 2001
P17N	2001.619178	44.9488	-141.2313	13.2	49NZ200107_1	Fukasawa & Murata, 2001
P17N	2001.619178	44.9488	-141.2313	0.4	49NZ200107_1	Fukasawa & Murata, 2001
P17N	2001.624658	46.8985	-144.4443	14	49NZ200107_1	Fukasawa & Murata, 2001
P17N	2001.624658	46.8985	-144.4443	9	49NZ200107_1	Fukasawa & Murata, 2001
P17N	2001.627397	48.208	-146.6845	8.6	49NZ200107_1	Fukasawa & Murata, 2001
P17N	2001.627397	48.9135	-147.907	1.2	49NZ200107_1	Fukasawa & Murata, 2001
P17N	2001.627397	48.9135	-147.907	-2	49NZ200107_1	Fukasawa & Murata, 2001
P17N	2001.630137	50.1707	-150.1373	12.7	49NZ200107_1	Fukasawa & Murata, 2001
P17N	2001.630137	50.1707	-150.1373	3.9	49NZ200107_1	Fukasawa & Murata, 2001
P17N	2001.638356	51.4732	-152.5498	0.5	49NZ200107_1	Fukasawa & Murata, 2001
P17N	2001.638356	51.4732	-152.5498	0	49NZ200107_1	Fukasawa & Murata, 2001
P17N	2001.641096	52.7878	-155.0162	4.3	49NZ200107_1	Fukasawa & Murata, 2001

P17N	2001.641096	52.7878	-155.0162	2.3	49NZ200107_1	Fukasawa & Murata, 2001
P17N	2001.643836	53.9747	-157.3708	2.5	49NZ200107_1	Fukasawa & Murata, 2001
P17N	2001.643836	53.9747	-157.3708	5	49NZ200107_1	Fukasawa & Murata, 2001
P17N	2001.646575	54.3738	-158.1048	7.3	49NZ200107_1	Fukasawa & Murata, 2001
P17N	2001.646575	54.3738	-158.1048	7.2	49NZ200107_1	Fukasawa & Murata, 2001
P06W	2009.90411	-30.0799	157.4001	53.5	318M20091121	A. McNichol & R. Key, unpublished data
P06W	2009.912329	-30.08	162.5	73.1	318M20091121	A. McNichol & R. Key, unpublished data
P06W	2009.917808	-30.0804	167.5001	70.7	318M20091121	A. McNichol & R. Key, unpublished data
P06W	2009.928767	-30.08	172.5	63.9	318M20091121	A. McNichol & R. Key, unpublished data
P06W	2009.934247	-30.08	176.5001	65.3	318M20091121	A. McNichol & R. Key, unpublished data
P06W	2009.942466	-32.4998	-178.9104	49.7	318M20091121	A. McNichol & R. Key, unpublished data
P06W	2009.942466	-32.5001	-178.28	58	318M20091121	A. McNichol & R. Key, unpublished data
P06W	2009.947945	-32.4999	-176.7497	66.1	318M20091121	A. McNichol & R. Key, unpublished data
P06W	2009.950685	-32.5	-174.8403	59.7	318M20091121	A. McNichol & R. Key, unpublished data
P06W	2009.961644	-32.5	-170.2499	63.5	318M20091121	A. McNichol & R. Key, unpublished data
P06W	2009.969863	-32.5002	-164.2449	59.2	318M20091121	A. McNichol & R. Key, unpublished data
P06W	2009.978082	-32.5	-157.86	68.3	318M20091121	A. McNichol & R. Key, unpublished data
P06W	2009.983562	-32.5001	-153.5434	90.2	318M20091121	A. McNichol & R. Key, unpublished data
P06W	2009.989041	-32.4999	-149.3	73.4	318M20091121	A. McNichol & R. Key, unpublished data
P06E	2010.024658	-32.4998	-144.6565	63.2	318M20100105	A. McNichol & R. Key, unpublished data
P06E	2010.030137	-32.5009	-139.9162	67	318M20100105	A. McNichol & R. Key, unpublished data
P06E	2010.038356	-32.5001	-135.1784	72.9	318M20100105	A. McNichol & R. Key, unpublished data
P06E	2010.043836	-32.5001	-129.4501	58.8	318M20100105	A. McNichol & R. Key, unpublished data
P06E	2010.043836	-32.5001	-129.4501	60	318M20100105	A. McNichol & R. Key, unpublished data
P06E	2010.049315	-32.5	-124.08	64.8	318M20100105	A. McNichol & R. Key, unpublished data
P06E	2010.049315	-32.5	-124.08	64.8	318M20100105	A. McNichol & R. Key, unpublished data
P06E	2010.054795	-32.4995	-119.3686	75.6	318M20100105	A. McNichol & R. Key, unpublished data
P06E	2010.057534	-32.4995	-115.3408	58	318M20100105	A. McNichol & R. Key, unpublished data
P06E	2010.057534	-32.4995	-115.3408	57	318M20100105	A. McNichol & R. Key, unpublished data

P06E	2010.068493	-32.4993	-105.928	73.9	318M20100105	A. McNichol & R. Key, unpublished data
P06E	2010.082192	-32.5001	-91.6701	56.1	318M20100105	A. McNichol & R. Key, unpublished data
P06E	2010.087671	-32.5	-87.8799	60.6	318M20100105	A. McNichol & R. Key, unpublished data
P06E	2010.093151	-32.5	-81.5501	39.9	318M20100105	A. McNichol & R. Key, unpublished data
P06E	2010.093151	-32.5	-81.5501	45.6	318M20100105	A. McNichol & R. Key, unpublished data
P06E	2010.10411	-32.4999	-72.6828	11.6	318M20100105	A. McNichol & R. Key, unpublished data
P06E	2010.106849	-32.5015	-71.9229	25.4	318M20100105	A. McNichol & R. Key, unpublished data
I06S	2008.098361	-33.321	28.1253	41.1	33RR20080204	A. McNichol & R. Key, unpublished data
I06S	2008.106557	-34.3248	29.2871	56.2	33RR20080204	A. McNichol & R. Key, unpublished data
I06S	2008.112022	-36.5004	30.0024	51.1	33RR20080204	A. McNichol & R. Key, unpublished data
I06S	2008.112022	-36.5004	30.0024	52.1	33RR20080204	A. McNichol & R. Key, unpublished data
I06S	2008.112022	-36.5004	30.0024	51.7	33RR20080204	A. McNichol & R. Key, unpublished data
I06S	2008.117486	-39.4933	30.0098	48.9	33RR20080204	A. McNichol & R. Key, unpublished data
I06S	2008.117486	-39.4933	30.0098	54.1	33RR20080204	A. McNichol & R. Key, unpublished data
I06S	2008.122951	-42.4977	30.0118	50.5	33RR20080204	A. McNichol & R. Key, unpublished data
I06S	2008.122951	-42.4977	30.0118	49.4	33RR20080204	A. McNichol & R. Key, unpublished data
I06S	2008.128415	-45.499	29.9984	-3.6	33RR20080204	A. McNichol & R. Key, unpublished data
I06S	2008.131148	-47.5013	29.9984	-27.3	33RR20080204	A. McNichol & R. Key, unpublished data
I06S	2008.131148	-47.5013	29.9984	-22.2	33RR20080204	A. McNichol & R. Key, unpublished data
I06S	2008.13388	-49.7	29.9994	-66.8	33RR20080204	A. McNichol & R. Key, unpublished data
I06S	2008.139344	-51.4918	29.9934	-68.9	33RR20080204	A. McNichol & R. Key, unpublished data
I06S	2008.142077	-53.4984	29.9988	-53.5	33RR20080204	A. McNichol & R. Key, unpublished data
I06S	2008.144809	-55.5062	29.9943	-87.7	33RR20080204	A. McNichol & R. Key, unpublished data
I06S	2008.147541	-57.4982	30.0001	-99.5	33RR20080204	A. McNichol & R. Key, unpublished data
I06S	2008.153005	-59.4996	29.9987	-88	33RR20080204	A. McNichol & R. Key, unpublished data
I06S	2008.155738	-61.5	30	-106.4	33RR20080204	A. McNichol & R. Key, unpublished data
I06S	2008.177596	-68.2939	31.1577	-108.6	33RR20080204	A. McNichol & R. Key, unpublished data

I06S	2008.180328	-67.4987	29.9998	-111.4	33RR20080204	A. McNichol & R. Key, unpublished data
I06S	2008.18306	-65.5	30.0001	-120.7	33RR20080204	A. McNichol & R. Key, unpublished data

Appendix F

An empirical method to estimate changes in surface ocean $\Delta^{14}C$ since 1995

The surface ocean ^{14}C disequilibrium isoflux due to sea-air CO_2 exchange is a significant term in the global atmospheric $^{14}CO_2$ budget, and therefore efforts to model the $\Delta^{14}C$ of atmospheric CO_2 on a global scale [e.g. *Turnbull et al.*, 2009; *Miller et al.*, 2012] require constraining the changing ^{14}C disequilibrium between the atmosphere and the surface ocean. Because atmospheric CO_2 is well mixed, atmospheric $\Delta^{14}C$ is reasonably well constrained by time-series from a few locations, but surface ocean $\Delta^{14}C$ gradients are large relative to the atmosphere-ocean disequilibrium and change over time (see Chapter V). Measurements since 2000 are spatially and temporally sparse, and consequently atmospheric $\Delta^{14}C$ modeling efforts that continue past the 1990s have previously either assumed that the air-sea $\Delta^{14}C$ disequilibrium remained constant or relied on ad-hoc tuning of the ocean isoflux to balance the atmospheric ^{14}C budget.

Here we describe a purely empirical method to estimate changes in surface ocean $\Delta^{14}C$ since the 1995 nominal date of the GLODAP dataset [*Key*, 2004]. Our method uses the relationships between 1990s $\Delta^{14}C$ and the rate of $\Delta^{14}C$ change observed in sparse locations since then to modify the interpolated GLODAP surface ocean $\Delta^{14}C$ product, adjusting it by the estimated linear rate of $\Delta^{14}C$ change in each location. The resulting time-dependent fields of estimated surface ocean $\Delta^{14}C$, combined with estimates of atmospheric $\Delta^{14}C$ and the ocean-atm gross CO_2 flux, can be used to calculate the magnitude and distribution of the ocean ^{14}C isoflux term in model simulations of recent atmospheric $^{14}CO_2$.

As demonstrated in Chapter V, rates of surface ocean $\Delta^{14}C$ change, when plotted versus gridded GLODAP surface ocean $\Delta^{14}C$ from the corresponding locations, appear to delineate

mixing lines between atmospheric CO_2 and DIC in waters upwelling from the deep and mid-depth ocean. Specifically, rates of $\Delta^{14}C$ change in the Southern Ocean and the high-latitude North Pacific appear to lie on a mixing line between rates of change for deep, pre-industrial ocean DIC and for atmospheric CO_2, while the low-latitude oceans and the high-latitude North Atlantic appear to lie on a mixing line between atmospheric CO_2 and mode water DIC with rising $\Delta^{14}C$. We calculated best-fit lines for these two populations (Fig. S1). Results for Drake Passage, which appear to sample highly variable $\Delta^{14}C$ due to steep $\Delta^{14}C$ gradients at the northern edge of the Southern Ocean (see Chapter V), were omitted from both fits.

Using these two linear relationships, an interpolated map of estimated $\Delta^{14}C$ rates of change (Fig. S2) was generated based on the GLODAP gridded surface ocean $\Delta^{14}C$ field. The northern border of the Southern Ocean, which in Chapter 5 was defined as the 20 ‰ isoline in the GLODAP surface ocean $\Delta^{14}C$ map, is clearly visible as the dividing line between negative rates of $\Delta^{14}C$ change in the Southern Ocean and positive rates of change along the southern edge of the subtropical gyres.

We used the latitude 32° N west of 149.5° W, and 29° N east of 149.5°W, as the boundary between the low-latitude and high-latitude North Pacific. This was chosen because dividing the Pacific rates straight across 30°N, as was done in Chapter V, does not appear to cleanly separate them between the two mixing lines (see dark green symbols in Fig. 5.6 in the main text). The North Pacific boundary separates the more negative rates of $\Delta^{14}C$ change north of the center of the subtropical gyre from the less-negative rates of $\Delta^{14}C$ change in the gyres to the south (see Fig. S2). The sharp boundaries in the North Pacific and Southern Ocean are presumably smoother in the real ocean, but we consider them acceptable first approximations of the true spatial pattern.

To estimate surface ocean $\Delta^{14}C$ on a given date, the rates shown in Figure S2 can be multiplied by the elapsed time since the nominal GLODAP date of Jan. 1, 1995, and the resulting cumulative $\Delta^{14}C$ changes added to the GLODAP surface $\Delta^{14}C$ map. Surface ocean $\Delta^{14}C$ estimates produced this way are a better match to the observations than estimates produced by assuming a constant offset between GLODAP and atmospheric $\Delta^{14}C$, i.e. assuming that surface ocean $\Delta^{14}C$ since the 1990s decreased uniformly at the same rate as the atmosphere (Fig. S3). As there is theoretically no constraint requiring $\Delta^{14}C$ changes in the surface ocean to be constant over time, this approach or similar methods should not be used to extrapolate significantly beyond the limit of available data. The compilation of post-2000 surface ocean $\Delta^{14}C$ observations presented in Chapter V is therefore projected only to the end of 2010.

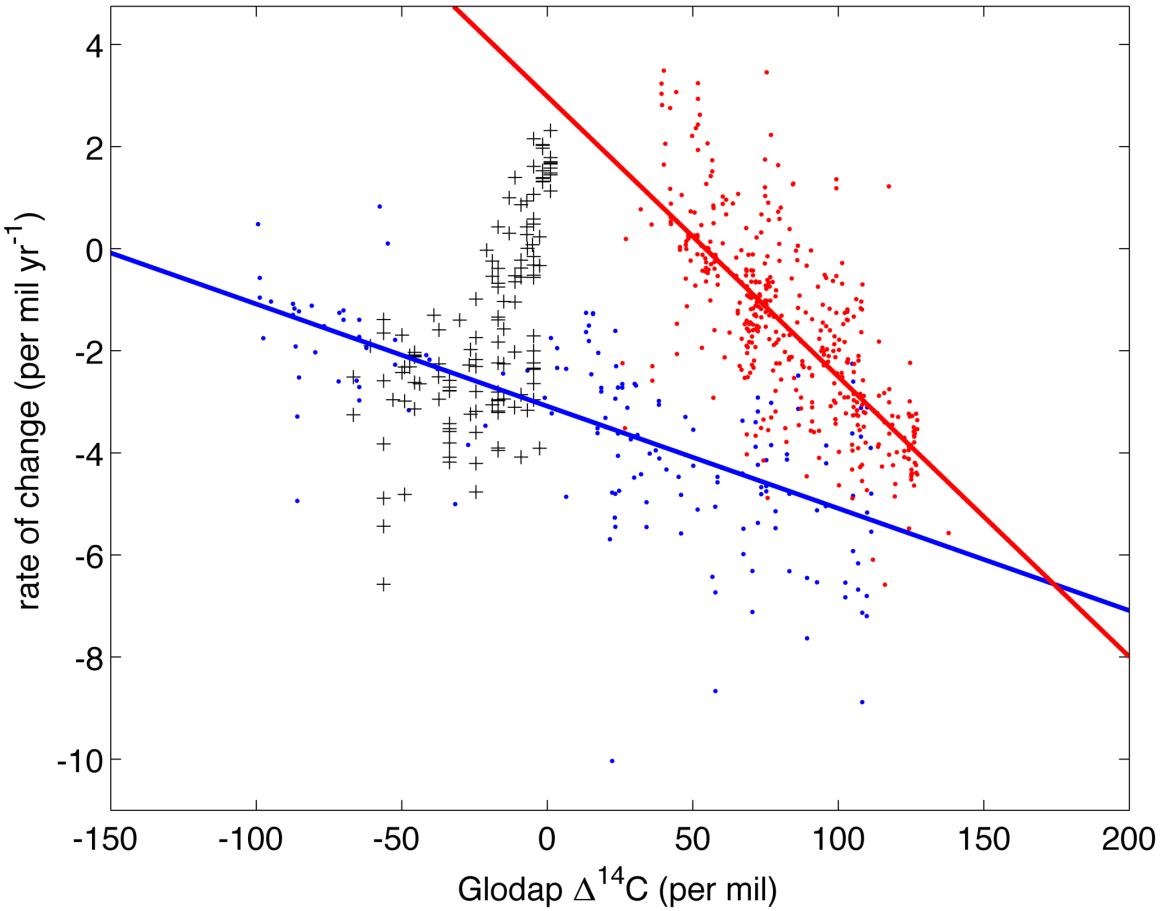

Figure S1: Best-fit lines to Southern Ocean and high-latitude (> ~30° N, see text) North Pacific (blue symbols) and low-latitude and North Atlantic (red symbols) rates of $\Delta^{14}C$ change versus GLODAP $\Delta^{14}C$, omitting all Drake Passage observations (black plus symbols). Southern Ocean & N. Pacific fit: (blue line): slope = -0.02 yr^{-1}, intercept = -3.085 ‰ yr^{-1}. Low-latitude and N. Atlantic fit (red line): slope = -0.055 yr^{-1}, intercept = 2.98 ‰ yr^{-1}.

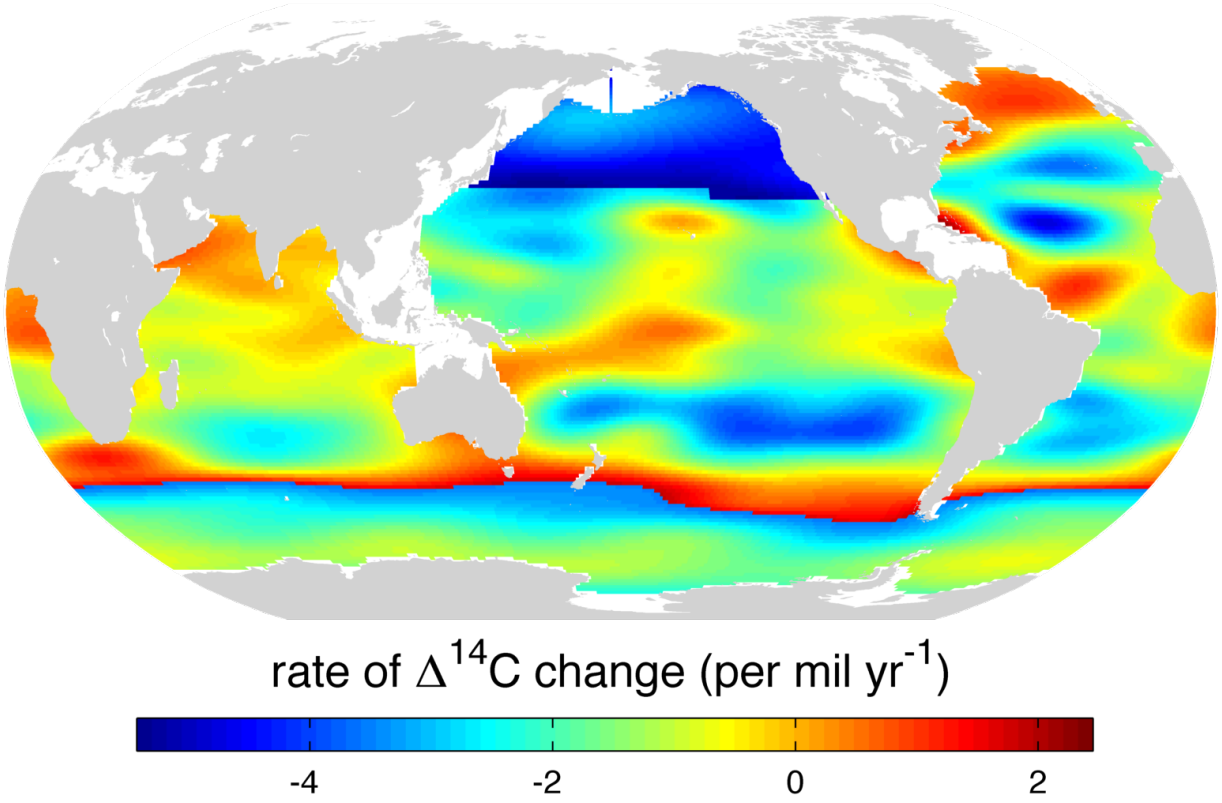

Figure S2: Estimated rates of $\Delta^{14}C$ change since the 1990s, producing using the two relationships shown in Fig. S1 and the GLODAP interpolated surface $\Delta^{14}C$ field.

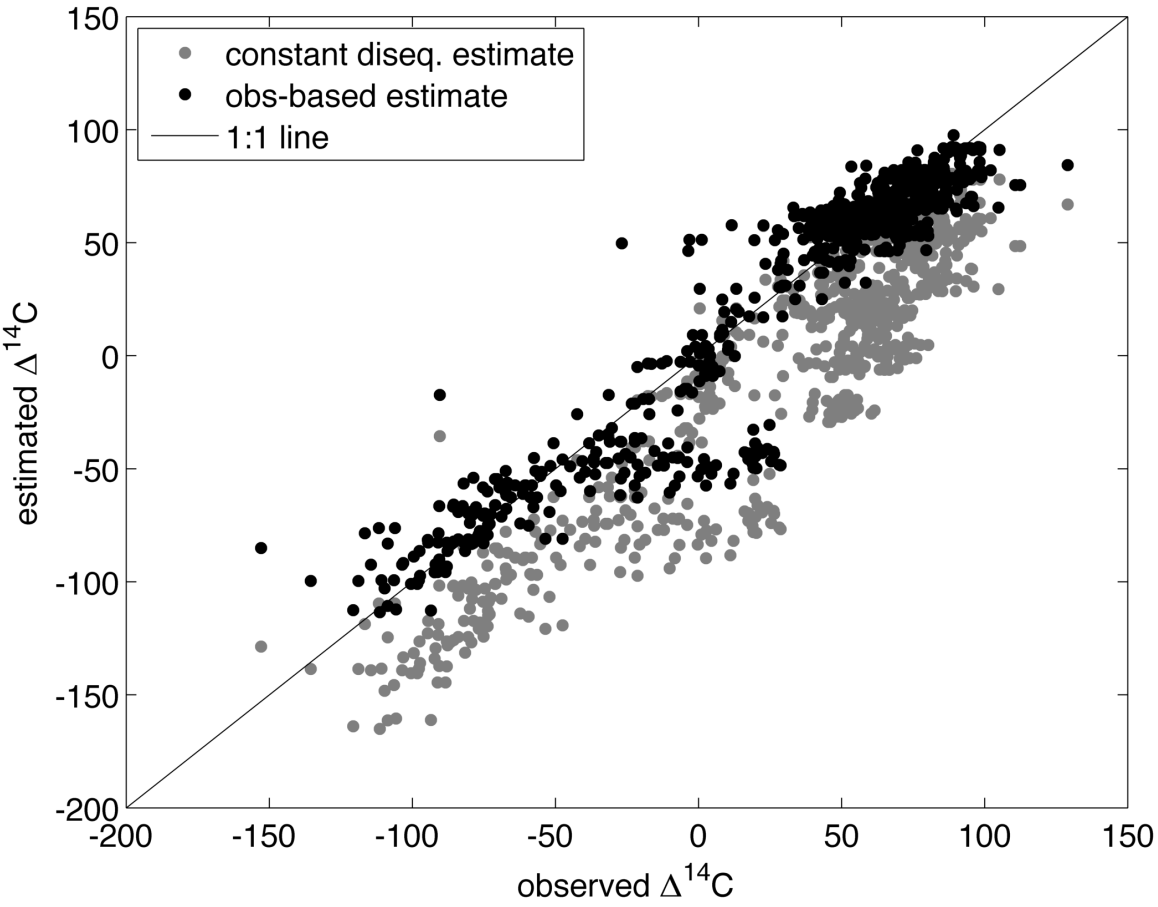

Figure S3: Estimated surface ocean $\Delta^{14}C$ using the method presented in this appendix (black symbols) and a simpler assumption of constant atmosphere-ocean disequilibrium (grey symbols) are plotted versus the compilation of $\Delta^{14}C$ observations for the same months and locations. The results from the observation-based method more faithfully reproduce the underlying observations compared to the simpler method.